DUDLEY KNOX LIBRARY
NAVAL POSTGRADUATE SCHOOL
MONTEREY, CALIFORNIA 93943-5002

Thesis
M36285

CHEMICAL CHARACTERIZATION OF SIMULATED BOILING WATER REACTOR COOLANT

LCDR VerrDon H. Mason

DEPARTMENT OF NUCLEAR ENGINEERING
DEPARTMENT OF CHEMICAL ENGINEERING

MAY 1990

T247950

CHEMICAL CHARACTERIZATION OF SIMULATED BOILING WATER REACTOR COOLANT

by

VERRDON HOLBROOK MASON

B.S., Chemical Engineering,
University of Utah (1980)

SUBMITTED TO THE DEPARTMENT OF
NUCLEAR ENGINEERING
IN PARTIAL FULFILLMENT OF THE REQUIREMENTS
FOR THE DEGREES OF

MASTER OF SCIENCE IN NUCLEAR ENGINEERING

and

MASTER OF SCIENCE IN CHEMICAL ENGINEERING

at the

MASSACHUSETTS INSTITUTE OF TECHNOLOGY

May 1990

© Massachusetts Institute of Technology 1990

Th 313
M36285
C.1

CHEMICAL CHARACTERIZATION OF SIMULATED BOILING WATER REACTOR COOLANT

by

VERRDON HOLBROOK MASON

Submitted to the Department of Nuclear Engineering
on May 9, 1988 in partial fulfillment of the
requirements for the Degrees of
Master of Science in Nuclear Engineering
and
Master of Science in Chemical Engineering

ABSTRACT

An in-pile facility is being constructed at MIT to simulate the thermal-hydraulic, radiation, and coolant-chemistry environment of a Boiling Water Reactor (BWR). The primary purpose of this BWR Coolant Chemistry Loop (BCCL) is to characterize coolant radiolysis chemistry by measurement of O_2, H_2O_2, H_2, electrode potential, pH, etc.. However, H_2O_2, which is highly oxidizing, readily decomposes on system surfaces. Therefore, the measurement of, and computer code prediction of, the concentration of H_2O_2 in the BCCL emerges as the primary challenge to achieving the BCCL project objectives.

The principal objective of this work was to design, build and test a coolant sampling system capable of measuring H_2O_2 to support BCCL operation. This included the requirement to investigate high-temperature H_2O_2 behavior sufficiently, both analytically and experimentally, to develop the design objectives for the sampling system. A computer model was developed, based on previous work, to predict the concentration profiles of the principal chemical species, and to provide a tool for correlating experimental results. Parametric studies were made using the code with different sets of chemical reaction equations and radiolytic source term coefficients (G-values) available in the literature. A laboratory apparatus was constructed to carry out simulated BWR coolant chemistry studies at 280°C. In addition to using this laboratory apparatus for chemistry studies, it was employed to test conceptual designs of high-temperature electrodes for the measurement of corrosion and redox potentials.

The high-temperature experiments on H_2O_2 behavior showed that surface decomposition was the same for the materials tested - titanium, aluminum and stainless steel, and minimal decomposition of H_2O_2 occurred when the sample line tubing wall was cooled. The sampling system constructed for the BCCL performed well during testing: $\geq$60% of inlet H_2O_2 was preserved. Performance of separate elements of the computer model was compared against available bench-marks with good agreement. Parametric studies showed variations in predicted chemical concentrations of more than two orders of magnitude. However, certain combinations of parameters yielded results comparable to available chemistry data for BWRs. Results from the electrode performance study were promising but inconclusive; however, high-temperature electrode performance as a function of H_2O_2 concentration was consistent with reported data.

Thesis Supervisor: Michael J. Driscoll
Title: Professor Emeritus of Nuclear Engineering

Acknowledgments

The author would like to thank Professor Michael J. Driscoll for his patient guidance, encouragement, and considerable help in tieing the pieces of the research and thesis together. The help, guidance and encouragement of Professor Otto K. Harling, Dr. Gordon Kohse, Mr. Mike Ames, and other members of the MIT Coolant Chemistry Loop (CCL) team was also greatly appreciated - particularly Professor Harling's guidance that brought me to the project.

I would also like to thank Professor Jefferson W. Tester for his willingness and interest in my work. I also thank Professor Tester for the tremendous enthusiasm he brings to his profession, including the sometimes mundane role of instructor (Chemical Engineering Thermodynamics).

Special thanks go to John Outwater, who not only was part of the CCL team with the lead on the BCCL project, but also provided extensive help, new ideas and good-humored encouragement throughout the course of the experimental work - and was willing to lend a good set of eyes to the task of proofing the thesis.

I am also indebted to John Chun for his extensive help with computer modeling and, particularly, the debugging process. Also, I would like to thank Dr. Maureen Psaila-Dombrowski for her help in getting me started with both the model development and the programming.

I also wish to express my appreciation to the U.S. Navy, which sponsored me during this two-year experience at MIT.

I'm especially grateful for the love, encouragement and cheerful support provided by my family - particularly my wife, Janet, who has captained the crew of six in my "absence" over the past two years - and was still willing and able to throw me a life-line when needed.

Table of Contents

Abstract 2
Acknowledgments 3
Table of Contents 4
List of Figures 7
List of Tables 9

Chapter 1. Introduction 10
1.1 Foreword 10
1.2 Background 11
1.2.1 Industry Concerns 11
1.2.2 Integration with MIT Reactor Laboratory Efforts 14
1.2.2.1 BCCL Project Objectives 14
1.2.2.2 BCCL In-Pile Experiment 15
1.3 Thesis Organization 19

Chapter 2. Characterization of H_2O_2 Decomposition 22
2.1 Introduction 22
2.2 Bench-Top Test Method 23
2.3 Dependence on Sample Line Material and Sample Flow Rate 25
2.4 Dependence on Sample Cooling Rate 29
2.4.1 Convective Cooling Rate Study 29
2.4.2 Flash Chamber Cooling Study 32
2.5 BCCL Sampling Methodology 34
2.6 Summary 35

Chapter 3. Design and Qualification of BCCL Sampling Device 36
3.1 Introduction 36
3.2 Sampling Design Options 36
3.2.1 Passive Heat Conduction Sample Block 36
3.2.2 Active Cooling Sample Taps 37
3.3 Design and Construction of Sampling Devices 38
3.3.1 Sample Block Design and Fabrication 38
3.3.2 Water-Cooled Sample Probe Design and Fabrication 41
3.3.3 Sample Block Locking Mechanism Design 43
3.4 Out-of-Pile Testing of BCCL Sampling System Components 46
3.4.1 H_2O_2 Measurement Method 46
3.4.2 Sample Line Testing 47
3.4.3 Sample Block Testing 48
3.4.4 Sample Probe Evaluation and Cooling Block Comparison 48
3.5 Summary 49

Chapter 4. Out-of-Pile High-Temperature Electrode Performance 50
4.1 Introduction 50
4.1.1 Background 50
4.1.2 Current Work 52
4.2 Bench-Top Test Method 54
4.2.1 High-Temperature Test Apparatus 54
4.2.2 Electrode Installation 56
4.3 Results of Electrode Performance 57

4.3.1 Electrode Test Procedure 57
4.3.2 Potential Versus Time - Cold 59
4.3.3 Potential Versus Time - High Temperature 64
4.3.4 Potential Versus H_2O_2 Concentration 67
4.3.5 Summary 79

Chapter 5. BCCL Radiolysis Chemistry Computer Code 81
5.1 Introduction 81
5.2 Modification of the Radiolysis Chemistry Computer Model 81
5.2.1 Performance of the Existing Radiolysis Chemistry Code 81
5.2.2 Bench-Mark Comparison 83
5.2.3 BCCL Model Requirements 84
5.2.3.1 Steady-State Mole Balance - Model Constraints 86
5.2.3.2 Steady-State Mole Balance - Model Derivation 88
5.2.3.3 Temperature and Density Compensation 92
5.2.3.4 Two-Phase Stripping Model 96
5.2.3.5 H_2O_2 Surface Decomposition - Model Development 97
5.2.3.6 H_2O_2 Surface Decomposition - Rate Coefficients 102
5.2.4 Computer Code Modifications 103
5.3 BCCLMIT Bench-Mark Calculations 105
5.4 Evaluation of Radiolysis Source Term Data (G-values) 107
5.4.1 MITIRAD Parametric Study 111
5.4.2 BCCLMIT Parametric Study 116
5.5 Evaluation of Chemical Reaction Equation Sets 124
5.5.1 Modified Notre Dame Equation Set 124
5.5.2 Modified Burns and Marsh Equation Set 128
5.5.3 Equation Set Comparison 131
5.6 Summary 137

Chapter 6. Summary and Recommendations for Future Work 139
6.1 Introduction 139
6.2 Summary and Conclusions 139
6.2.1 Characterization of H_2O_2 Decomposition 139
6.2.2 Design and Qualification of BCCL Sampling Device 141
6.2.2.1 BCCL Sampling Device Design 141
6.2.2.2 Qualification of BCCL Sampling Device 144
6.2.3 Out-of-Pile High-Temperature Electrode Performance 144
6.2.4 BCCL Radiolysis Chemistry Computer Code 147
6.3 Recommendations for Future Work 149
6.3.1 Characterization of H_2O_2 Decomposition 149
6.3.2 Reference Electrode Evaluation 150
6.3.3 BCCL Radiolysis Chemistry Modeling 152
6.3.3.1 Recommended Refinements to BCCLMIT 152
6.3.3.2 Additions Required for N^{16} Carryover Studies 154

Appendix A. Data From H_2O_2 Decomposition Experiments 157
A.1 H_2O_2 Decomposition for Different Sample Line Materials 157
A.2 Other H_2O_2 Decomposition Studies 164
A.3 Spectrophotometer/Colorimeter Calibration Curves 169

Appendix B. Sampling Device Calibration Data 172

B.1 Sample Line Calibration 172
B.2 Sample Cooling Block Calibration 176

Appendix C. Electrode Performance Data 178
C.1 Electrode Data: Figures C.1 through C.4 178
C.2 Electrode Data: Tables C.1 through C.10 183

Appendix D. BCCL Radiolysis Chemistry Computer Code 194
D.1 BCCLMIT Program Listing 194
D.2 BCCLMIT Sample Output File 221
D.3 BCCLMIT Sample Input File 236
D.4 Modified Notre Dame Reaction Equation Set 241
D.5 Modified Burns and Marsh Reaction Equation Set 242

Appendix E. References 243

List of Figures

Figure 1.1: Schematic of BWR Coolant Chemistry Loop 18
Figure 1.2: BCCL In-Reactor Components 20
Figure 2.1: Hydrogen Peroxide Decomposition Test Device 24
Figure 2.2: Material Effects on Peroxide Decomposition 28
Figure 2.3: Full-Length Cooled Tubing Test Section 31
Figure 3.1: BCCL Sample Cooling Block 40
Figure 3.2: BCCL Water-Cooled Probe 42
Figure 3.3: BCCL Sample Cooling Block Locking Mechanism 44
Figure 4.1: High-Temperature Electrode Test Section 55
Figure 4.2: Electrode Configuration for Bench-Top Testing 58
Figure 4.3: Cold Reference Run #1 61
Figure 4.4: Cold Reference Comparison 62
Figure 4.5: Passivated - Cold Reference Run #1 63
Figure 4.6: Hot Reference Run #3 65
Figure 4.7: Hot Reference Run Comparison 66
Figure 4.8: E1(Pt-Pd) Potential Versus H2O2 Concentration 68
Figure 4.9: E2(Pt-SScat) Potential Versus H2O2 Concentration 69
Figure 4.10: E3(Pt-SSref Potential Versus H2O2 Concentration 70
Figure 4.11: E4(SScat-Pd Potential Versus H2O2 Concentration 72
Figure 4.12: E5(SSref-SScat)Potential Vs. H2O2 Concentration 73
Figure 4.13: E6(SSref-Pd) Potential Vs. H2O2 Concentration 74
Figure 4.14: Composite Plot of E5(SSref-SScat) Potential 76
Figure 4.15: Composite Plot of E3(SSref-Pt) Potential 77
Figure 4.16: Composite Plot of E6(SSref-Pd) Potential 78
Figure 5.1: MITIRAD Radiolysis Calculation 85
Figure 5.2: BCCLMIT Program Logic 87
Figure 5.3: Examples of Non-Arrhenius Rate Constant Behavior 95
Figure 5.4: Concentration Profile for 2.5cm Uncooled Tube 108
Figure 5.5: BCCL Sample System Concentration Profile 109
Figure 5.6: MITIRAD G-Value Comparison - Set 1 113
Figure 5.7: MITIRAD G-Value Comparison - Set 2 114
Figure 5.8: MITIRAD G-Value Comparison - Set 3 115
Figure 5.9: BCCLMIT G-Value Comparison - Combination #1 119
Figure 5.10: BCCLMIT G-Value Comparison - Combination #2 120
Figure 5.11: BCCLMIT G-Value Comparison - Combination #3 121
Figure 5.12: BCCLMIT G-Value Comparison - Combination #4 122
Figure 5.13: BCCLMIT G-Value Comparison - Combination #5 123
Figure 5.14: Surface Decomposition Study - Notre Dame Set 126
Figure 5.15: Hydrogen Water Chemistry Study-Notre Dame Set 127
Figure 5.16: Surface Decomposition Study - Burns Set 129
Figure 5.17: Hydrogen Water Chemistry Study - Burns Set 130
Figure 5.18: Normal Chemistry - Equation Set Comparison 132
Figure 5.19: Hydrogen Chemistry - Equation Set Comparison 133
Figure 5.20: Revised Equation Set Study - Notre Dame Set 135
Figure 5.21: Revised Equation Set Study - Burns Set 136
Figure 6.1: BCCL Sample Cooling Block 142
Figure A.1: HORIZON Colorimeter Calibration Curve 170
Figure A.2: HACH Spectrophotometer Calibration Curve 171
Figure C.1: Cold Reference Run #2 179

Figure C.2: Cold Reference Run #3 180
Figure C.3: Cold Reference Run #4 181
Figure C.4: Hot Reference Run #4 182

List of Tables

Table 1.1: Range of Conditions Simulated by BCCL 17
Table 2.1: Decomposition Versus Uncooled Tube Length 32
Table 2.2: Flash Chamber & Water-Cooled Probe Comparison 33
Table 3.1: BCCL Sample Block Design Calculations 45
Table 5.1: Gas Absorption / Stripping Coefficients 97
Table 5.2: Gamma Radiolysis Source Term Data 110
Table 5.3: Neutron Radiolysis Source Term Data 111
Table 5.4: Combination of G-Value Sets for Comparison 116
Table 5.5: BCCL Section Descriptions 117
Table 5.6: Updated Reaction Rate Coefficient Data 134
Table A.1: Decomposition Versus Temperature for Titanium 158
Table A.2: Decomposition Versus Temperature for Aluminum 161
Table A.3: Decomposition Versus Temperature for SSteel 162
Table A.4: Decomposition Versus Uncooled Tube Length 164
Table A.5: Sample Calculations 167
Table B.1: Calibration of BCCL Sample System Tubing 173
Table B.2: BCCL Sample Line Decomposition Calculation 174
Table B.3: Calibration of BCCL Sample Cooling Block 177
Table C.1: Run #1 - 225 ppb Hydrogen Peroxide 184
Table C.2: Run #2 - 1900 ppb Hydrogen Peroxide 185
Table C.3: Run #3 - 590 ppb Hydrogen Peroxide 186
Table C.4: Hot Reference Run #6 187
Table C.5: Hot Reference Run #9 188
Table C.6: Hot Reference Run #7 189
Table C.7: Run #5 - 400 ppb Hydrogen Peroxide 190
Table C.8: Run #6 - 249 ppb Hydrogen Peroxide 191
Table C.9: Run #7 - 111 ppb Hydrogen Peroxide 192
Table C.10: Run #8 - 605 ppb Hydrogen Peroxide 193

Chapter 1. Introduction

1.1 Foreword

Much effort has been expended over the last decade by the nuclear power industry to reduce personnel radiation exposure and down-time associated with the operation, maintenance and refueling of Light Water Reactor (LWR) systems. The diversity and complexity of these efforts are reflected in part by the publications of the Electric Power Research Institute (EPRI) and by compilations such as the proceedings from international conferences on the water chemistry of nuclear power plants sponsored by BNES and JAIF. This multifaceted effort to improve the overall economics of nuclear power systems has necessarily been divided by reactor type because of the unique design, operational and maintenance characteristics of Pressurized Water Reactors (PWR) and Boiling Water Reactors (BWR).

In the area of BWR coolant technology and materials research, the problems of intergranular stress corrosion cracking have been the focus of considerable effort, together with concerns about general corrosion, and N^{16} carryover. Efforts to minimize maintenance problems resulting from the stress corrosion cracking have not met with uniform success. This problem is in large part due to an inadequate understanding of the radiolytic and chemical processes involved in the BWR environment.

One of the primary efforts for reducing or eliminating stress corrosion cracking is directed at providing a non-oxidizing environment. There have been substantial efforts over the past decade to suppress radiolytic oxygen production. In the past few years the radiolysis-induced oxidizing conditions of BWR coolant have been extensively studied, and the oxidizing potential of BWR coolant is now considered to be best characterized by radiolytically-produced H_2O_2[1,2,3,4] instead of just dissolved molecular oxygen. Therefore, substantial industry-wide

efforts have more recently been focused on understanding the characteristics of the radiolytic production, and decomposition of H_2O_2: a difficult task complicated by the shortcomings of both data and theory in the area of high-temperature radiolysis and electrochemistry, and by the difficulty in extracting unperturbed coolant samples from actual BWR units.

In recognition of these developments, an inter-disciplinary team at MIT, including participants from the Nuclear Reactor Laboratory, the Chemical Engineering Department and the Nuclear Engineering Department, was formed to construct and operate an in-pile experimental facility to investigate the radiolytic chemistry of the BWR. Conceptual design of the MIT BWR Coolant Chemistry Loop (BCCL) was initially supported by a group of utility participants in the Electric Utility Program of the MIT Energy Laboratory. The project sponsorship was subsequently assumed by the Empire State Electric Energy Research Corporation (ESEERCO) and EPRI for a four-year research program.

The object of this thesis is to design, build and test the coolant sampling system needed to support BCCL operation. This effort includes the requirement to initially characterize high-temperature H_2O_2 behavior sufficiently to confirm sampling system design objectives. Also, this thesis covers the modification of an available radiolysis chemistry computer code, MITIRAD, to support the requirements of BCCL operation. This modified code provides a tool for predicting BCCL primary chemical species concentrations, as well as providing a tool for correlating BCCL experimental results.

1.2 Background

1.2.1 Industry Concerns

Original design and material selection for BWR systems did not fully recognize the importance of radiation-induced effects on the materials of construction, and the corrosive

potential of irradiated high-temperature, high-purity water. Only after a few years of operational experience did detrimental effects such as localized intergranular stress corrosion cracking, and its enhancement by radiolysis products such as H_2O_2 and O_2, become evident. Some BWR materials of construction that are resistant to stress-corrosion cracking in non-reactor applications have been found to be susceptible to stress corrosion cracking after long-term irradiation. Localized corrosion has resulted in premature component failures in BWR systems.

In addition to localized stress corrosion cracking, general corrosion is the principal source of transition metal oxides which deposit on the fuel rods, become activated, and then are released to re-deposit on coolant system components outside of the shielded reactor vessel. This transport of activated corrosion products (crud) provides high out-of-pile radiation fields that in turn result in significant personnel radiation exposure during repair of stress-corrosion cracking damage, general maintenance, and refueling.

Motivated by decreased power plant capacity factors and the increased maintenance costs[5] caused by corrosion (both localized stress corrosion cracking and general), the BWR power industry has invested considerable resources to eliminate this "irradiation-assisted" stress corrosion cracking* (IASCC) problem and minimize general corrosion to reduce personnel exposure and plant maintenance expenses. Industry has embarked on a three-pronged attack on the IASCC problem: (1) correct the material problem, (2) alter design and construction practices to minimize the opportunity for local corrosion attack, and (3) control coolant chemistry to reduce or eliminate the corrosive environment. Unfortunately,

---

*- Irradiation-assisted stress corrosion cracking is intergranular stress corrosion cracking that occurs in a material that is normally not susceptible to stress corrosion cracking were it not for the unique material and environmental effects resulting from γ-ray and neutron irradiation.

the fundamental mechanisms affecting IASCC, activated corrosion product migration, carryover, and, in general, irradiated coolant chemistry, are not well understood. Consequently, initial industry efforts were primarily empirical approaches that yielded diverse, often plant-specific results. For example, the amount of hydrogen added to BWR coolant to scavenge oxygen and thereby reduce the corrosive potential of the coolant has varied widely between power plants. Also, undesirable side effects from hydrogen addition, such as increased N^{16} carryover, has resulted in unacceptably high radiation levels outside of the primary containment.

The mixed results from this empirical approach to eliminate IASCC and minimize personnel radiation exposure has been the driving force behind the rapid expansion of research over the past decade. The efforts have been primarily focused on the following concerns:

1. Identification of material properties that affect susceptibility to IASCC,
2. Calculation and measurement of radiolysis effects on BWR coolant, to understand the corrosive potential of the reactor environment,
3. Control of N^{16} carryover and reducing its contribution to operational personnel radiation exposure,
4. Evaluation of Hydrogen Water Chemistry (HWC) effects on IASCC and N^{16} carryover,
5. Improvement of general BWR coolant chemistry control to minimize general corrosion and crud transport,
6. Improvement of decontamination techniques to remove crud and thereby reduce personnel radiation exposure,

7. Development of the technical basis for current empirical industry radiation exposure reduction techniques and services.

1.2.2 Integration with MIT Reactor Laboratory Efforts

Driscoll et al.[6] have described the research facilities and program at MIT to simulate PWR and BWR reactor coolant chemistry environments. These facilities contribute to the interrelated goals of radiation exposure reduction and general corrosion reduction, as well as furthering the understanding of IASCC fundamentals. The MIT facilities consist of compact in-pile test loops designed for installation in the MIT Research Reactor (MITR-II). Separate facilities are used to simulate PWR coolant chemistry conditions, environmental and material conditions for IASCC, coolant chemistry sensor studies, and BWR coolant chemistry conditions. This thesis involves MIT's BWR Coolant Chemistry Loop (BCCL) project.

1.2.2.1 BCCL Project Objectives

The overall BCCL project objective is to provide a facility that can simulate the coolant chemistry environment of a full-scale operating BWR system. A small scale test facility is required since experimental work in a real BWR would be severely restricted because of the lack of sufficient operational flexibility to characterize the fundamental parameters (due to plant design and licensing constraints). The high temperature and pressure together with the required gamma and neutron radiation fields necessitate the use of a research reactor such as the MITR-II to adequately simulate the BWR environment. The BCCL project at MIT provides an in-pile facility to perform carefully controlled experiments to simulate the thermal-hydraulic and radiolytic

chemistry behavior of a full-scale BWR as closely as possible given the constraints imposed by the MITR-II environment and the loop design described in the next sub-section. The specific goals[7,8,9] of the BCCL project are to:

1. Characterize coolant radiolysis chemistry aspects by measurement of O_2, H_2O_2, H_2, electrode potential, pH and any other chemical species amenable to ion chromatographic analysis.

2. Investigate interrelationships of radiolytic chemistry environment to BWR materials corrosion (such as H_2O_2 concentration and electrochemical corrosion potential*).

3. Investigate methods to suppress N^{16} carryover.

4. Investigate the effects of Hydrogen Water Chemistry on N^{16} carryover and the coolant radiolytic chemistry environment.

1.2.2.2 BCCL In-Pile Experiment

The principal design goal, as discussed by Oliveira[10], for the MIT BCCL was to simulate BWR thermal-hydraulic, radiation, and material parameters as closely as possible. Many parameters can be matched even at a greatly reduced scale. However, it is not always possible to satisfy the scaling criteria without sacrificing similitude for some parameters. Baeza[11] noted that similitude of bulk coolant chemistry was the overriding concern, and compromises were made in other areas, such as Reynolds

---

*- Electrochemical corrosion potential, or electrochemical potential (ECP) as commonly referenced in industry publications, refers to the general corrosive potential of the subject electrochemical environment as measured by electrode potential {referenced against a Standard Hydrogen Electrode (SHE)}. It is not a measure of the thermodynamic quantity of the same name. This thesis will therefore use electrode potential and ECP interchangeably.

number and shear stress, which are more important with respect to radionuclide transport and deposition. Although the BCCL design as modified by Baeza no longer permitted studies of radionuclide transport phenomena, the loop still retained much of the flexibility Oliveira originally envisioned.

Outwater[12,13] and Driscoll, et al., included additional modifications to the BCCL to incorporate technical advisory committee comments as well as lessons-learned from operation of the sister PWR Coolant Chemistry Loop (PCCL). The loop was changed to a once-through system instead of a recirculating loop. Also, the non-core material of construction was changed to titanium to minimize complications resulting from the relatively higher solubilities of the chemical species in stainless steel. Even with the additions and changes, the BCCL is still very flexible and capable of simulating a wide range of BWR conditions. Table 1.1, taken from Ref. 6, shows the broad range of conditions that can be simulated with the BCCL.

A schematic of the current loop is shown in Fig. 1.1 (taken from Ref. 13). Water is drawn from the charging tank, where purity is maintained by a demineralization (and H_2/O_2 recombiner) loop, and He cover gas. The cool, degassed pure water is pumped through a regenerative heat exchanger and then through an electric feedwater heater. The feedwater is heated to the core inlet temperature because there is no internal BCCL recirculation path in the current BCCL configuration to bring the feedwater temperature up to the core inlet temperature (as in a BWR). The chemical injection system (see Fig. 1.1) provides the way to add chemicals to the feedwater, thereby permitting direct control of core inlet water chemistry. The two-phase flow from the U-tube, in-core section is separated in the outlet plenum. The steam flow exits the core tank region and is condensed by the regenerative heat exchanger before being cooled to ambient

temperature and returned to the charging tank. The liquid flow from the outlet plenum goes to the downcomer plenum, and then instead of mixing with the feedwater as in a BWR, the downcomer outlet flow is cooled and returned to the charging tank. The residence time in the charging tank is sufficiently large to ensure feedwater purity is maintained.

Table 1.1

Range of Conditions Simulated by the BCCL

Radiation Dose Rates

Representative Region of Actual BWR	Parameter	Range for BWR (R/hr)	Range Achievable in Loop (R/hr)
Core (in-channel)	Neutron dose rate	$10^8 \rightarrow 10^9$	$10^5 \rightarrow 9.5*10^8$
	Gamma dose rate	$10^8 \rightarrow 10^9$	$3.1*10^6 \rightarrow 10^9$
Core bypass	Neutron dose rate	$10^8 \rightarrow 10^9$	$10^5 \rightarrow 9.5*10^8$
	Gamma dose rate	$10^8 \rightarrow 10^9$	$3.1*10^6 \rightarrow 10^9$
Downcomer	Neutron dose rate	$10^4 \rightarrow 10^8$	$2*10^4 \rightarrow 3.4*10^7$
	Gamma dose rate	$4*10^6 \rightarrow 10^8$	up to $8*10^7$

Thermohydraulic Parameters

Representative Region	Parameter	Range for BWR	Range Achievable in Loop
Core (in-channel)	Transit time	0.7→1.8s	0.7→15s
	Quality	0→10%	0→10%
Core (bypass)	Transit time	5→25s	0.7→25s
Downcomer	Transit time	1→5s	0.9→32s

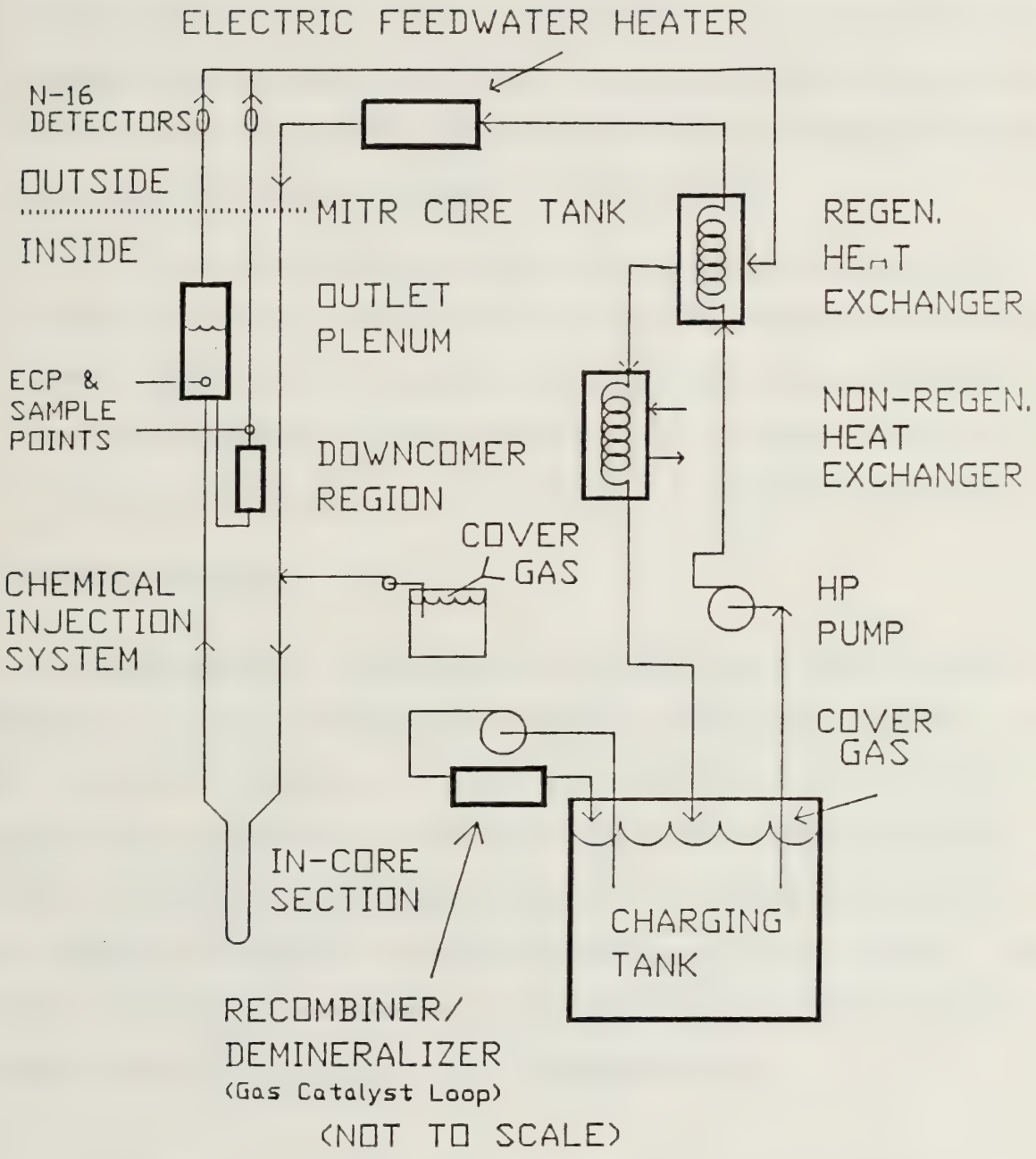

Figure 1.1: Schematic of the BWR Coolant Chemistry Loop (BCCL)

The majority of the BCCL support system is external to the core tank of the MITR-II. The critical portion of the BCCL loop fits within a 8.89 cm (3.5-inch) I.D. aluminum thimble, as depicted in Fig. 1.2 (taken from Ref. 13). This aluminum thimble houses a titanium can, and fits into a dummy (all aluminum) fuel element slot (see Fig. 1.2) of the MITR-II core. The in-core portion of the BCCL is contained in the titanium can in the lower, dummy-fuel-element portion of the thimble.

A major focus of the present thesis is on design, construction and testing of the sampling system which interfaces with the main loop at the stations labeled "ECP and Sample Points" in Fig. 1.1, and shown as "Sample Cooler" in Fig. 1.2. This effort provides the foundation for the first BCCL project objective which is to characterize coolant radiolysis chemistry by measurement of H_2O_2, H_2, O_2, electrode potential, etc..

1.3 Thesis Organization

This thesis is divided into chapters, sections and subsections that describe the design, experimental and computer modeling effort in support of BWR Coolant Chemistry Loop (BCCL) construction and operation. As stated in the foreword (Section 1.1), the objective of this thesis is to design, build and test the coolant sampling system needed to support BCCL operation. Also, this thesis covers the modification of available radiolysis chemistry computer codes (versions of MITIRAD)[14,15] to support the requirements of BCCL operation. This modified code provides a predictive tool for expected BCCL chemistry conditions as well as providing a framework for correlation of BCCL experimental results.

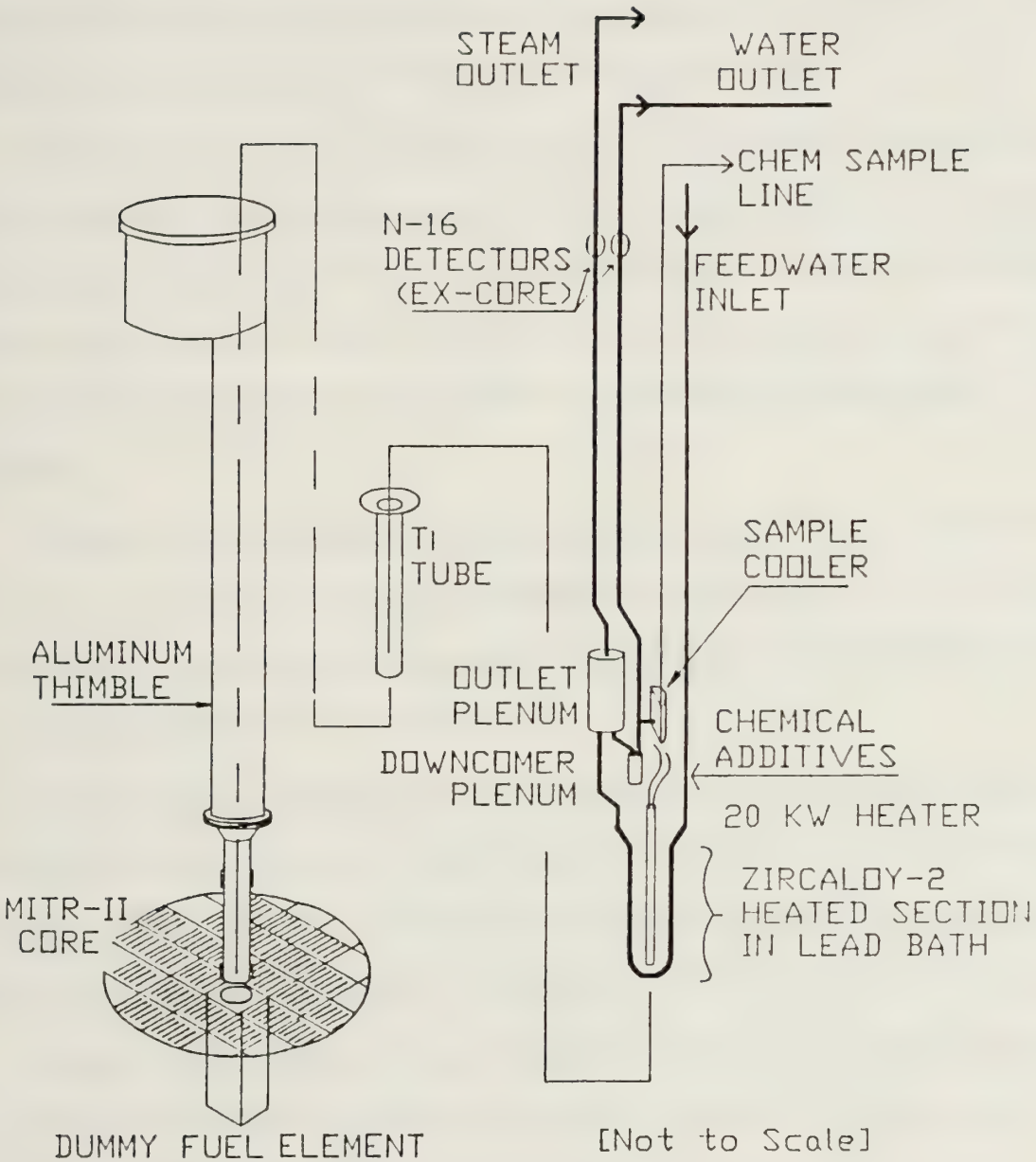

Figure 1.2: BCCL In-Reactor Components

Chapter 2 describes the initial approach and efforts to characterize the decomposition of H_2O_2 in various BCCL coolant sampling configurations. The dependence of H_2O_2 decomposition on sample tube material, flow rates, and temperature was investigated, along with an alternate sampling concept that used flash-cooling of the sample.

Chapter 3 discusses the final design criteria that emerged from the testing described in Chapter 2 along with the two major alternate sampling system designs that evolved: passive sample cooling (heat conduction from the hot BCCL coolant to the relatively cool MITR-II primary coolant), and active sample cooling (heat rejection through a cooler supplied with cooling water) at the sample extraction point. The testing and final design selection is also discussed.

Chapter 4 reviews the efforts to design and qualify high-temperature electrodes for subsequent use in the BCCL to measure electrochemical potential (ECP). The current status of this evaluation process is also documented in this chapter, including efforts to correlate electrode potential and H_2O_2 concentration.

Chapter 5 discusses the radiolysis chemistry computer code BCCLMIT. The radiolysis chemical species source term (G-values) data, and chemical reaction equation sets that are available in the literature are also discussed. In addition, the calculational model for the code is reviewed. The features unique to the code that support the BCCL are discussed.

Chapter 6 summarizes the work described in this thesis. Recommendations for improvements to the BCCL sampling system, and improvements (or alternate approaches) for the computer model are also discussed in this chapter.

Chapter 2. Characterization of H_2O_2 Decomposition

2.1 Introduction

This chapter describes the initial experimental approach to characterize the decomposition of H_2O_2 in prospective BCCL sampling systems. The high-temperature behavior of H_2O_2 was not known with sufficient detail to support the construction of a suitable sampling system that would be capable of preserving and then measuring the low concentration of H_2O_2 (on the order of 100 ppb) that was expected in the BCCL.

To provide the necessary experimental data base on which to design the final BCCL sample system, the following parameters were investigated:

1. Temperature (25°C to 280°C) dependence of H_2O_2 decomposition in tubing fabricated from quartz, aluminum, stainless steel, titanium, and gold.
2. Flow rate (300 to 400 cc/hr) dependence of H_2O_2 decomposition in candidate sample tubing sections.
3. Cooling rate dependence of H_2O_2 decomposition for candidate tubing material as measured by the length of uncooled tubing (0 to 7.6cm) at constant flow rate. This investigation also included evaluation of a flash chamber to quickly cool the sample stream, in addition to conventional heat transfer schemes where the sample remained pressurized until cooled to ambient temperature.

2.2 Bench-Top Test Method

The challenge of providing a high-temperature H_2O_2 solution for testing was met by using a dual-headed metering pump* where one side pumped pure water through a heater section and the second side pumped a cold H_2O_2 solution. Both containers were open to the atmosphere and hence both fluid streams were air-saturated at approximately 20°C. The high-temperature pure water and the cold H_2O_2 solution were then combined in the mixing chamber at the entrance to the test section. Pressures from 10 to 13.8 MPa (1500-2000 psig) were used to ensure that the enthalpy of the heated pure water stream was sufficient to have a final temperature up to 280°C after mixing with the ambient temperature H_2O_2 stream. The schematic for the bench-top H_2O_2 decomposition test device is shown in Fig. 2.1.

The pressure was held constant using a backpressure regulator to ensure the metering pump flow rate was constant throughout a test run. This was required to prevent flow rate changes due to backpressure from altering the proportion of the pure water to H_2O_2 streams sufficiently to interfere with concentration changes due to decomposition. Pressure changes on the order of 10% were sufficient to invalidate decomposition measurements. In addition, the use of high-purity water and pre-cleaning of tubing materials were required to permit accurate measurement of H_2O_2. For example, some tubing materials had residues, such as the manufacturer's mandrel lubricant, etc., that could cause erroneous H_2O_2 measurements. (See Section 3.4.1 for more information on the H_2O_2 measurement technique.)

---

*- Pump Data: Dual-Head Milton-Roy Mini-Pump P/N 92014903 supplied by RAININ Instrument Company, Woburn MA 01801.

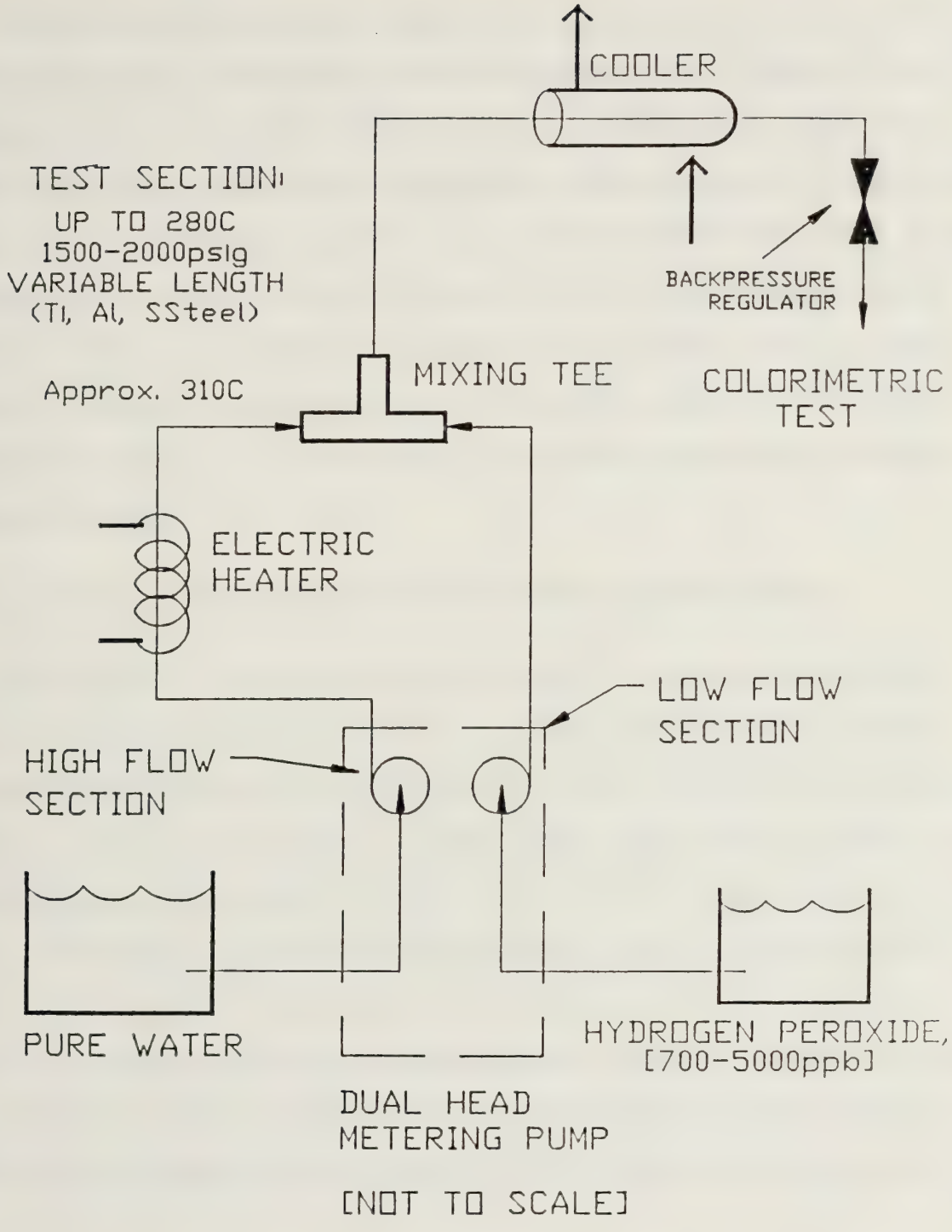

Figure 2.1: H2O2 Decomposition Test Device

The mixing chamber consisted of different components depending on the nature of the testing being conducted. For the initial runs, the mixing chamber was a 1.59mm (1/16-inch) tubing tee and the test section was tubing of various sizes adapted to the tee. The length of tubing between the mixing tee and the cooling jacket varied depending on the test being performed and is subsequently referred to as the "uncooled" length of the test section. The percentage of H_2O_2 that decomposed was determined by mass balance based on cold (approximately 25°C), zero-decomposition test runs with the same flow rates. The mixing chamber was designed, where practicable, to be of minimum volume so that most of the decomposition would occur in the test section. The H_2O_2 concentration measurement technique is described in Section 3.4.

2.3 Dependence on Sample Line Material and Sample Flow Rate

Stainless steel, aluminum, titanium and gold were the first materials investigated. Preliminary bench-top testing of relatively inert non-metallic materials such as quartz demonstrated that any reduction in H_2O_2 decomposition that may have been present was more than offset by the inability to cool the sample sufficiently quick. Stainless steel and titanium were selected because of their compatibility with BCCL materials of construction. Aluminum was selected both because of its high thermal conductivity and because of its good nuclear properties. Gold was initially included because of its relatively inert surface properties (e.g.- resistance to corrosion and hydrogen adsorption); however, preliminary testing of the gold was inconclusive. Therefore, based on satisfactory results from follow-on testing of aluminum, stainless steel and titanium, additional testing of gold tubing and more exotic ceramic materials was not pursued.

The decomposition of H_2O_2 was measured as a function of temperature in 1.59 mm (0.063-inch) O.D. titanium (I.D.=0.108 cm {0.043 in}), stainless steel (I.D.=0.108 cm {0.043 in}) and aluminum (I.D.=0.078 cm {0.030 in}) tubing. Volumetric flow rates were initially held constant at approximately 310 cc/hour. This flow rate corresponds to a Reynolds number of less than 2000 at the high temperature end of the test section. Consequently, the entire length of the test section was maintained in the laminar flow regime. The primary motivation for the low flow rates was to minimize the perturbation on the BCCL coolant caused by sampling. However, based on estimates using a diffusion-limited first-order decomposition model for H_2O_2, coupled with the familiar heat and mass transfer analogies for laminar and turbulent flow, sample flows in the laminar flow regime would result in about one half of the decomposition expected with turbulent sample flow.

The results of this investigation on the temperature dependence of H_2O_2 decomposition are shown in Fig. 2.2. The raw data are included in Appendix A.1. Given a conservative estimate of +/-10% error in the H_2O_2 concentration and +/-5% error in the temperature measurement*, the results for the titanium, aluminum, and stainless steel tubing are essentially the same. Figure 2.2 shows a compilation of a representative number of experimental runs in which the inlet H_2O_2 concentration varied; consequently, the actual H_2O_2 concentrations for each run were normalized by dividing the concentration data by the reference run H_2O_2 concentration.

Flow velocity and hence sample test section residence time was varied by changing the inside diameter of the test section tubing and by changing the volumetric flow rate. Flow velocity had negligible effect on the decomposition rate for the volumetric flow rates of interest

---

*- The precision or reproducibility of the H_2O_2 concentration measurement is dependent on the magnitude of the actual concentration, ranging from +/- 100% in the 30 ppb range to +/- 5% (approximately) in the 1.5-2.0 ppm range.

for the BCCL sampling system. The experimental runs represented in Fig. 2.2 cover a range of residence times from 1.6 to 3.1 seconds corresponding to tubing inside diameters from 0.762 mm (0.030-inches) to 1.09 mm (0.043-inches).

H_2O_2 decomposition in the turbulent flow regime was not investigated. The highest Reynolds number readily achieved with the test device used, was approximately 3000 at the high-temperature end of the test section. Preliminary results indicated that H_2O_2 decomposition may have increased moderately. However, flow rates in the turbulent regime were beyond the range of interest for BCCL sampling requirements as well as beyond the flow capacity of the test device. In addition, if the decomposition reaction was diffusion-limited, instead of reaction kinetics-limited, turbulent mixing would increase H_2O_2 transport to the tubing wall and thereby enhance decomposition. Consequently, turbulent flow H_2O_2 decomposition behavior was not investigated.

The fact that there was negligible difference between the materials tested was consistent with the findings of Lin et al.[16] for titanium and stainless steel. In addition, these results are consistent with the first-order kinetics model for H_2O_2 decomposition reported by Lin et al., in that the H_2O_2 concentration normalization process mentioned above collapsed experimental runs with inlet H_2O_2 concentrations ranging from 100 to 400 ppb to the common curve shown in Fig. 2.2.

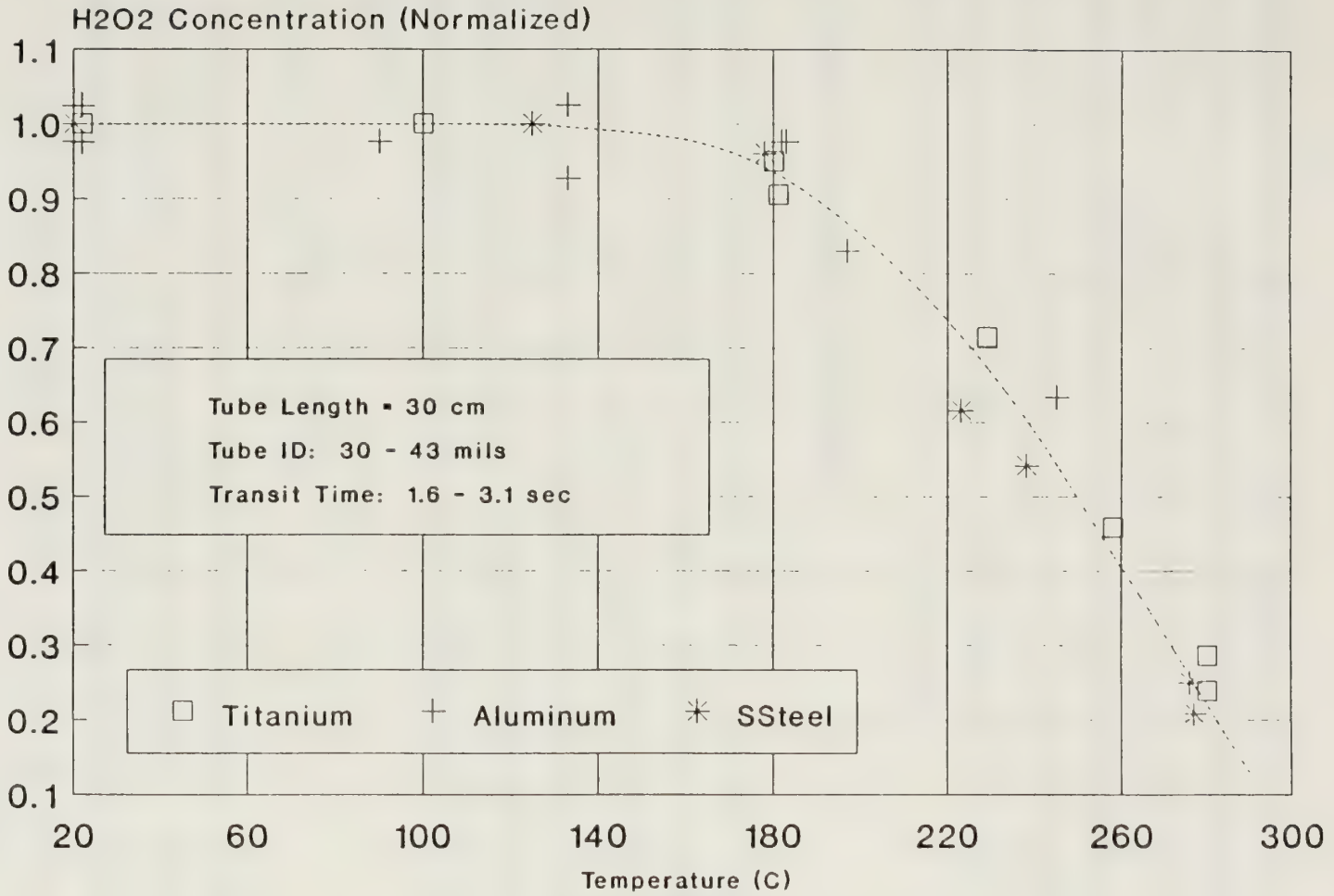

FIGURE 2.2
Material Effects on H2O2 Decomposition

Another pronounced effect shown in Fig. 2.2 is the negligible H_2O_2 decomposition below approximately 140°C. Lin et al.[16] also reported that Teflon tubing had a significantly lower surface decomposition rate coefficient than the metals tested. Unfortunately, because of the low radiation resistance of Teflon, a more radiation resistant material is required for the BCCL sampling system. However, based on the significant decrease in the H_2O_2 decomposition rate below 140°C, we expected to have tolerable levels of H_2O_2 decomposition in metal tubing if we could rapidly cool the sample close to the BCCL sampling points.

2.4 Dependence on Sample Cooling Rate

In order to use proven materials such as stainless steel, aluminum or titanium for the BCCL sampling system, rapid cooling of the sample was required to quench the H_2O_2 decomposition process. Two schemes were used to explore the dependence of H_2O_2 decomposition on the cooling rate. The main approach was to modify the test section and cooler test apparatus depicted in Fig. 2.1; however, a modified testing apparatus was also used to investigate the use of flash cooling to rapidly cool the sample below the 140°C threshold shown on Fig. 2.2.

2.4.1 Convective Cooling Rate Study

Initial parametric studies with the cooling rate involved changing the cooling water flow rate and temperature with the configuration depicted in Fig. 2.1. Cooling water temperatures were varied from 0°C to 95°C, with statistically insignificant differences in the measured H_2O_2 outlet concentrations. The next study varied the length of tubing between the mixing chamber and the cooler along with cooling water temperatures. Significant decreases in the H_2O_2 decomposition were measured as the uncooled length of the test section was reduced.

The results of these experiments indicate that tubing wall temperature was more important than bulk fluid temperature. However, the minimum uncooled length achieved with the tubing arrangement used for testing up to this point was approximately 2.5 cm; therefore, the apparatus shown in Fig. 2.3 was built to measure H_2O_2 decomposition, where the full-length of the sample tubing was cooled. Also, because of the large mixing chamber of the apparatus shown in Fig. 2.3, the cold H_2O_2 solution was also cooled up to the point of injection into the mixing chamber.

The results shown in Table 2.1 identify the importance of cooling the sample tubing wall (as opposed to rapidly cooling the entire sample stream). The raw data is included in Appendix A.2. Furthermore, it was only necessary to cool the sample line to below the high decomposition rate threshold depicted in Fig. 2.2. Correction of these data for homogeneous, or thermal, decomposition of H_2O_2 was not required. Published studies such as those reported by Takagi et al.[17] indicate surface decomposition is dominant over thermal decomposition, and the high-temperature thermal decomposition half-life reported by Lin et al.[16] of approximately 30 seconds, confirms that thermal decomposition of H_2O_2 is negligible in the small diameter tubing used in these studies.

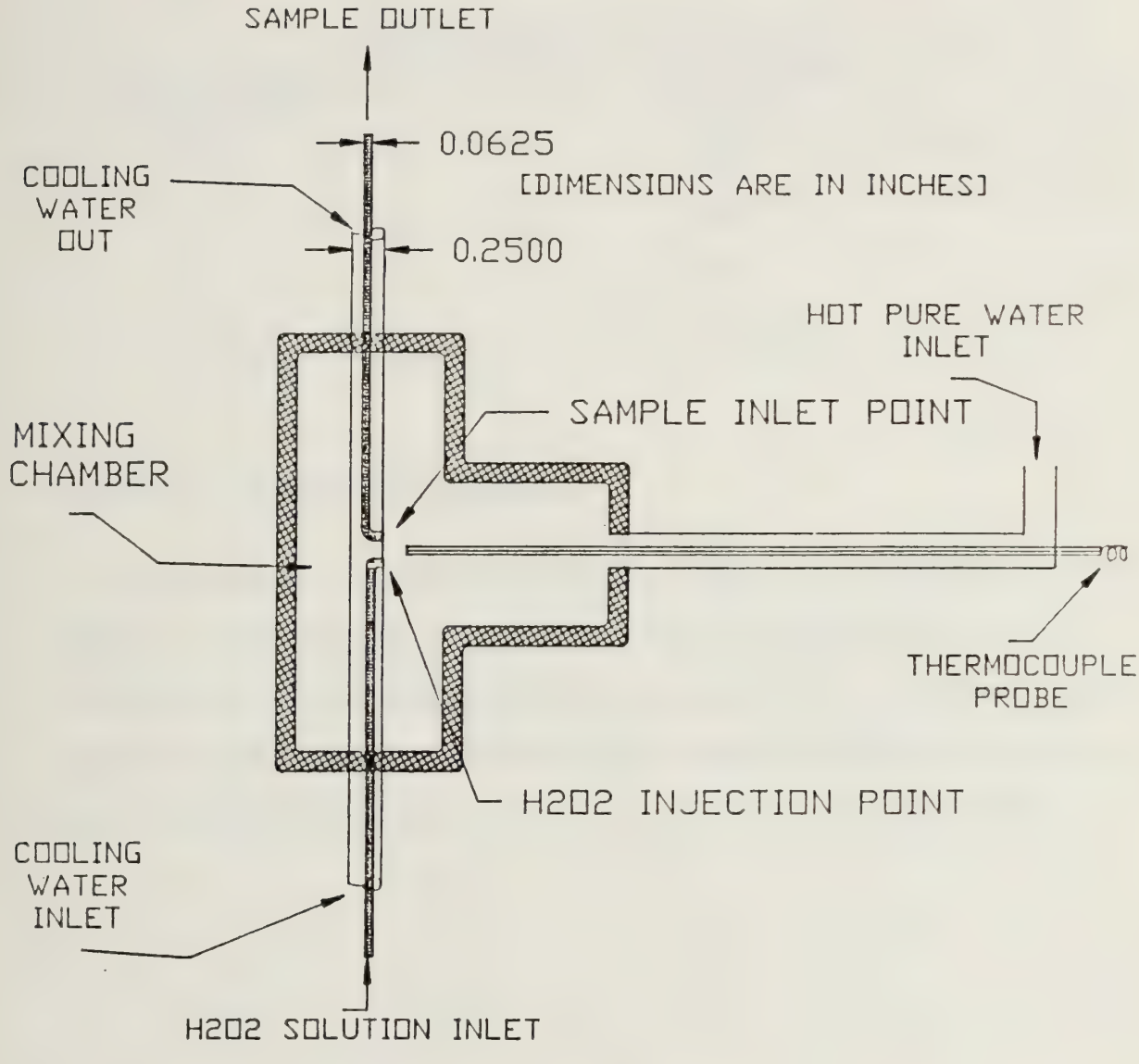

Figure 2.3: Full-Length Cooled Tubing Test Section

Table 2.1 H_2O_2 Decomposition Dependence on Uncooled Test Section Tubing Length	
Uncooled Tubing Length (cm)	**Percent Decomposition* of H_2O_2**
7.6	80%
3.8	75%
2.5	50%
< 0.5	< 10%

2.4.2 Flash Chamber Cooling Study

A flash chamber was devised for attachment to the mixing chamber. The output from the flash chamber was compared with that from a water-cooled sample probe (see Fig. 3.2 of Section 3.3.2). The operating conditions for the mixing chamber are the same as previously used, with pressure control effected from the sample line that exits through the water-cooled probe. The test fluid entered the flash chamber through a small orifice** sized

---

*- Percent decomposition is the percentage of H_2O_2 lost in the test section. The uncooled lengths were estimates, typically ±0.5 cm, and the percentage decomposition was approximately ±10%. Also, no corrections were made for H_2O_2 losses due to decomposition within the test chamber.

**- The orifice was made by inserting a scored, tapered pin into a larger hole. The resulting ultra-fine flowpath along the scored pin readily plugged. To minimize errors due to irregular flow, the performance of the flash-chamber was evaluated relative to the water-cooled probe instead of calibrating decomposition using the time consuming mass-balance approach.

to provide a flow rate in the range of 100-300 cc/hr. The chamber downstream of the orifice was at ambient pressure. The results of this comparison are shown in Table 2.2 below.

No effort was made to improve the flash chamber concept. In addition to the relatively high surface decomposition caused by the stainless steel orifice components, orifice clogging and an irregular flow rate created problems which constituted a formidable challenge. A quartz or ceramic orifice was considered as a candidate material to be evaluated to possibly reduce the H_2O_2 decomposition. However, these materials offered little promise of minimizing the clogging problem, or of fine tuning orifice size to achieve the necessary flow rate, given the minimal flexibility available in adjusting the pressure drop across the orifice.

Table 2.2

Flash Chamber and Water-Cooled Probe Comparison

	Flash-Chamber	Water-Cooled Probe
H_2O_2 Concentration: (±20%)	50 ppb	105 ppb
Percent Decomposition* : (±5%)	60%	20%

*- Percent decomposition was determined for the water-cooled probe using cold mass-balance calibration. The percent decomposition for the flash-chamber is then based on the comparative results and the water-cooled probe calibration:

$$\text{FLASH\%} = 100\% \times \left\{1 - \frac{50}{105} \times \left(1 - \frac{\text{PROBE\%}}{100\%}\right)\right\}$$

2.5 BCCL Sampling Methodology

The preceding series of experimental investigations provided some engineering guidelines for design and development of candidate sampling systems for the BCCL. The maximum tolerable BCCL sample line decomposition of H_2O_2 was fixed by the resolution of the H_2O_2 measurements and the expected BCCL H_2O_2 concentrations, which are on the order of approximately 100 ppb. The colorimetric H_2O_2 measurement technique has a low-end resolution of about 10 ppb. Consequently, sample line outlet H_2O_2 concentration should not be below approximately 50 ppb. This in turn dictates a maximum BCCL sample line decomposition factor of approximately 0.5 (so that 100 ppb x 0.5 $\geq$ ~50 ppb).

The BCCL sampling system methodology design guidance that resulted from the parametric evaluations discussed in this chapter is as follows:

1. Minimize the length of tubing the sample passes through with wall temperatures above about 140°C.
2. Size tubing such that sample flow remains in the laminar flow regime.
3. Use aluminum and stainless steel as materials of construction (as well as titanium, if desired) within the constraints of (a) and (b) above.
4. Maintain a pressurized sampling system to ensure stable single-phase behavior (ensures reproducibility of bench-top calibration) and to provide positive control over sample flow rate.
5. BCCL sampling system decomposition factor should be less than 0.5 to ensure adequate resolution in measuring H_2O_2 concentrations at the sampling system outlet.

2.6 Summary

This chapter has discussed the experimental approach taken to characterize the high-temperature behavior of H_2O_2 in prospective BCCL sampling system flow configurations. The sampling system wall temperature was ascertained to be the principal consideration for minimizing the decomposition of H_2O_2. A pressurized single-phase, laminar flow sampling system emerged as the most satisfactory candidate. Also, aluminum and stainless steel were determined to be satisfactory materials of construction provided the overall (from inlet to outlet) BCCL sampling system H_2O_2 decomposition was less than about 50%.

Chapter 3. Design and Qualification of BCCL Sampling Device

3.1 Introduction

In Chapter 2, the decomposition of H_2O_2 was evaluated with respect to the need to develop a sampling system to support BCCL operations. This chapter discusses the final design objectives that emerged from that testing. Two alternate sampling system designs emerged from the parametric studies: a passive sample cooling system (heat conduction from the hot BCCL sample to the relatively cool MITR-II primary coolant), and an active sample cooling system (heat rejection to an independent cooling water system).

This chapter also compares the performance of the two systems. The criteria used to select the final sampling system design are detailed as well as the calibration of the sampling system with respect to the amount of H_2O_2 in the sample that will decompose during transit through the sampling system.

3.2 Sampling Design Options

Our primary design objective was to maintain the sample-wetted surfaces below about 140°C to minimize the surface decomposition of H_2O_2. Based on the measurement capabilities of the colorimetric technique used, the maximum permissible decomposition would then be approximately 50%.

3.2.1 Passive Heat Conduction Sample Block

As shown in Fig. 1.2, the BCCL assembly fits within an aluminum thimble that is in turn inserted in the core tank of the MITR-II with the lower portion actually occupying a dummy fuel element location within the core. The MITR-II coolant temperature during

full power operation is nominally about 56°C. The BCCL as well as the sister PWR loop both utilize passive heat rejection to the MITR-II primary coolant in place of independent secondary system cooling loops.

That same concept can be extended to cooling the BCCL sample stream. The passive sample cooling block would by necessity be connected to the BCCL as well as to the thimble wall. Since the heat sink temperature is 56°C, the sample cooling device would necessarily need high thermal conductivity. Of the metals of interest, only aluminum is also compatible with the BCCL coolant (i.e. - copper solubility and the catalytic effect of copper ions on H_2O_2 decomposition would be detrimental to measuring H_2O_2 concentrations).

Another design constraint that complicates the passive design is that the heat conduction path from the BCCL assembly to the MITR-II coolant must permit the BCCL assembly to slide into and later be removed from the thimble. Therefore, the cooling block could not be integral with, or welded to the thimble wall. Also, the helium-filled atmosphere within the thimble does not provide sufficient conductivity to give an acceptable temperature drop across an appreciable thimble-wall to cooling block gap. Consequently, the sample cooling block must be pressed tightly against the thimble wall remotely, and later retracted away from the thimble wall to permit subsequent removal of the BCCL assembly from the thimble.

3.2.2 Active Cooling Sample Taps

During the preliminary bench-top testing to characterize the decomposition of H_2O_2, active cooling (e.g. - the heat sink is an independent cooling water supply through a heat exchanger) was normally used for the experiments. In fact, the full-length cooled tubing

test section shown in Fig. 2.3 was shown to be quite effective in cooling the simulated BCCL coolant sample with no more than 10% decomposition of H_2O_2. Also, the single-entry variant of the cooled test section, or the water-cooled sample probe, performed well with no more than 25% (20% +/- 5%) decomposition of H_2O_2.

Aside from their good performance, the active cooling sampling probes, or sample taps, require extensive (by comparison to the passive sample cooling system) support systems. An independent cooling water supply, along with the pumps, heat sink, alarm systems and additional plumbing, would all be required to support BCCL sampling operations. Also, fit-up requirements within the confines of the thimble of the water-cooled sample taps would provide a substantial engineering complication.

3.3 Design and Construction of Sampling Devices

3.3.1 Sample Block Design and Fabrication

Aluminum was selected for the sample cooling block because of its high thermal-conductivity, compatibility with the coolant, and satisfactory performance in the H_2O_2 decomposition studies. To meet the design criteria of minimizing sample residence time while staying in the laminar flow regime, 0.101 cm (0.040 inch) diameter sample water-ways were bored through the sample block using aircraft drill bits. The relative weakness of aluminum in the high-temperature BCCL coolant environment was compensated for by machining the sample cooling block out of one block of aluminum with integral 0.635 cm (0.25 inch) mechanical tubing attachment nipples.

The sample cooling block schematic is shown in Fig. 3.1. The sample cooling block is situated immediately below the outlet plenum so that both BCCL sampling points (one

at the plenum outlet and the second at the downcomer outlet) can be serviced by one common cooling block. The large diameter tubing nipples, together with the small 0.101 cm diameter water-way, provide sufficient mechanical integrity to permit leak-tight mechanical tubing connections* to (1) the titanium BCCL tubing at the sampling point, and (2) the 0.159 cm (0.063 inch) O.D. stainless steel sample lines that carry the sample up out of the thimble. The large diameter tubing nipples also provide additional heat transfer area, thereby decreasing the wall temperature of the tubing nipples where they attach to the BCCL tubing. The "L"-shaped sample flow path (the sample exits the BCCL in the horizontal plane and then turns upward) was required to fit the device within the available space envelope inside the thimble.

The vertical water-ways of the cooling block were extended completely through the block to permit alignment for subsequent boring of the horizontal water-ways. The vertical water-way extensions were then counter-bored and plugged, and the plugs seal-welded in place. The radius of curvature of the back side of the cooling block matches the I.D. of the aluminum thimble. Figure 3.1 also shows a thimble cross-section depicting the orientation of the tubing nipples with respect to BCCL internals.

The lower end of the cooling block was bored to accept a thermocouple (not shown in Fig. 3.1). The temperature readout from the thermocouple is needed to ensure the applicability and validity of the bench-top calibrations (the block temperature at the thermocouple location is an important reference temperature, together with the BCCL coolant temperature).

---

*- Compression tubing fittings such as those manufactured by PARKER CPI and SWAGELOCK are used. Larger mechanical tubing connectors such as ULTRA-SEAL O-ring connectors are too large to fit within the space envelope.

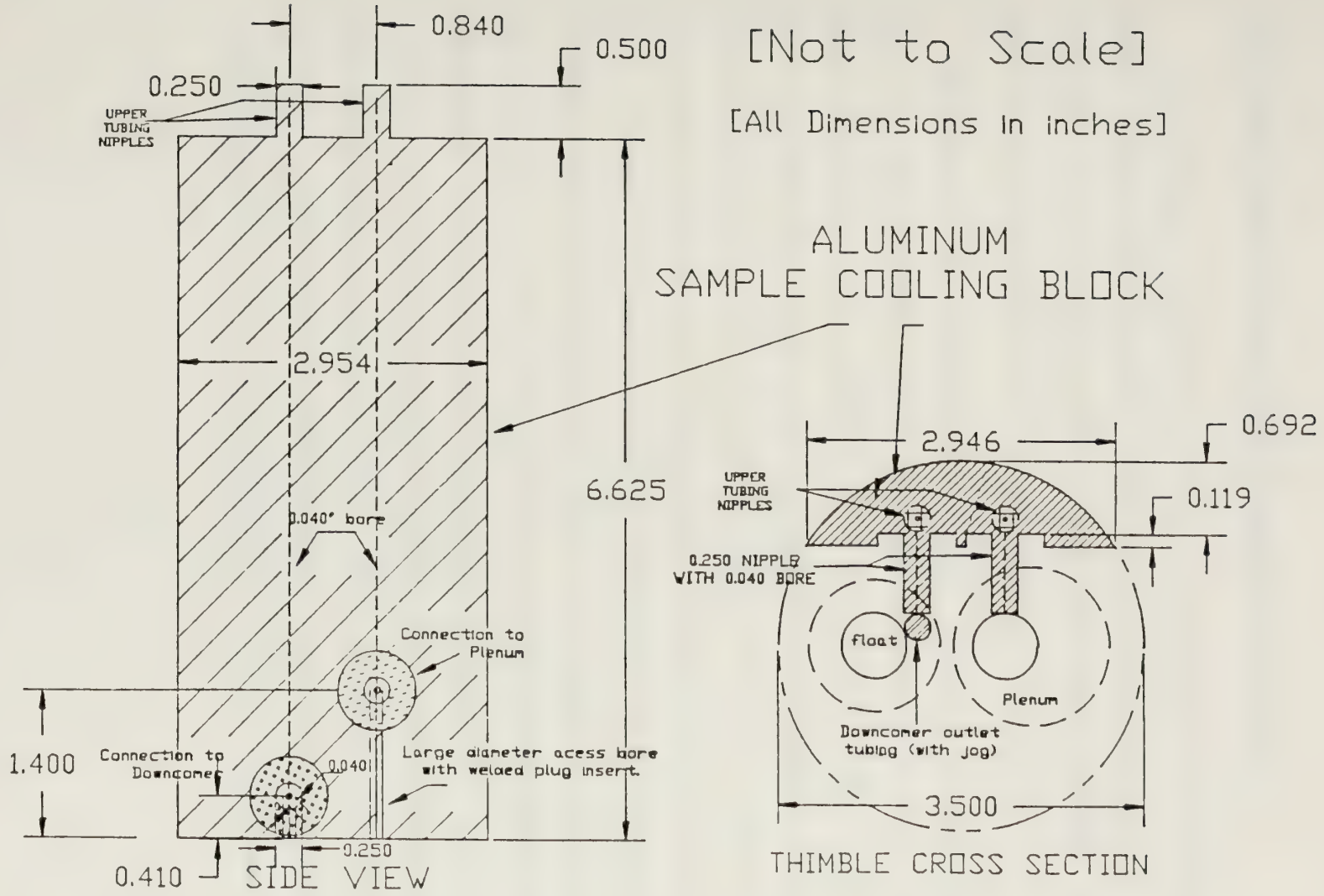

FIGURE 3.1: BCCL SAMPLE COOLING BLOCK

3.3.2 Water-Cooled Sample Probe Design and Fabrication

The sample tap, or water-cooled sample probe, used a 0.159 cm (0.063 inch) O.D. stainless steel tube for the sample flow. The water-way of the tubing was then 0.109 cm (0.043 inch), which was the same as the water-way of the sample cooling block. Consequently, the flow characteristics were identical between the two designs.

The schematic of the water-cooled probe is shown in Fig. 3.2. The bench-top prototype used copper-free silver solder for the sample inlet end of the probe. In-reactor models would require welded or high-temperature silver-free solder. Also, in order to fit within the limited thimble space envelope, the sample probe would require the use of a tee, instead of a straight, concentric tubing configuration. With the tee configuration, the cooling water would flow up into the tee, and the cooling water out-flow would exit out the top of the tee, with the sample line inside the cooling water tubing. The sample lines could then remain in their respective cooling water lines out through the top of the thimble. Alternatively, the two cooling water return and sample lines could be joined within the thimble and one water return line could contain both sample lines. Either way, the sample line could remain within the cooling water return lines, which provides thermal isolation, thereby minimizing the decomposition of H_2O_2. In addition, putting the sample lines within the cooling water return tubing simplifies the tubing connection and sealing problem at the thimble lid which would result from the addition of an active cooling system.

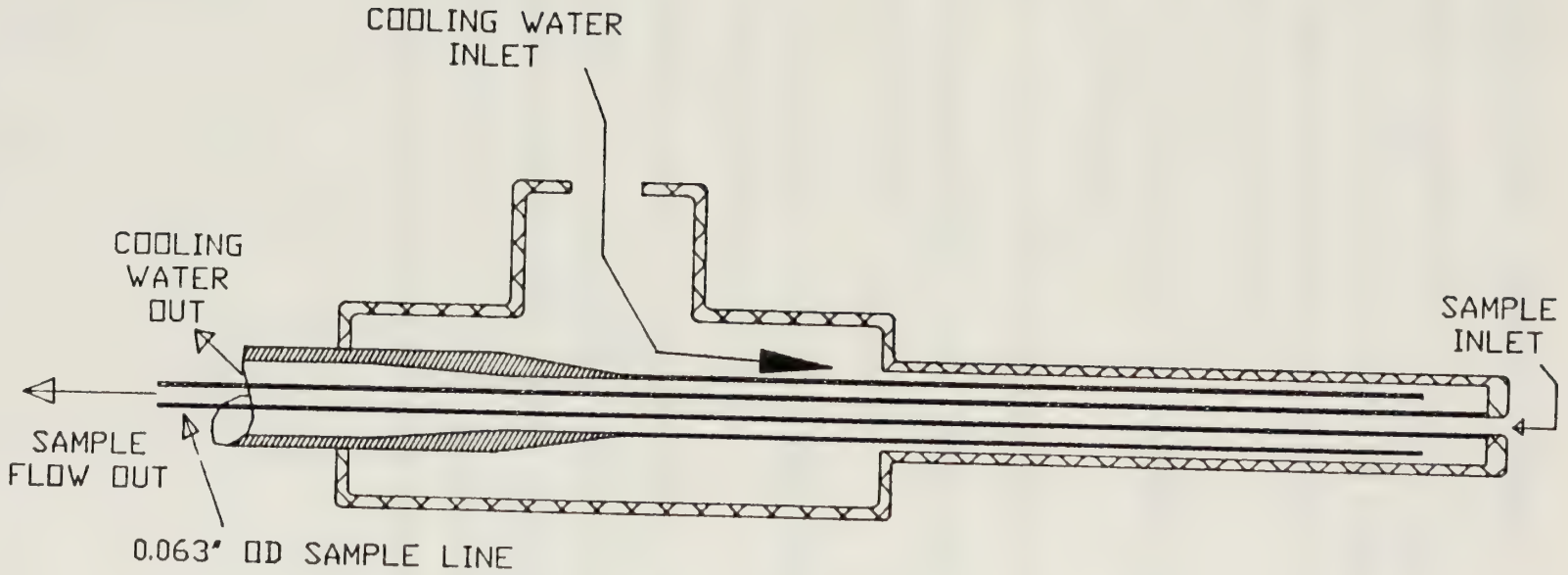

[NOT TO SCALE]

FIGURE 3.2: BCCL WATER-COOLED PROBE

3.3.3 Sample Block Locking Mechanism Design

As discussed in the previous sections, the use of a passive BCCL sample cooling system would necessarily include a way to press the sample cooling block against the thimble wall to provide the passive heat conduction path. This device must satisfy the following design objectives and constraints:

1. Must be remotely actuated from the top of the thimble (about 3 m above the location of the sample cooling block).
2. Must securely lock the cooling block in place during BCCL operation.
3. Must provide sufficient force (e.g. >400 N {>90lb$_f$}) to ensure good gap conductance at the sample block to thimble wall interface.
4. Must be remotely retractable to provide adequate clearance for sliding the BCCL assembly from the thimble when necessary.

The final design for the sample cooling block locking mechanism is shown in Fig. 3.3. The locking mechanism is fabricated from stainless steel except for the attachment blocks on the sample cooling block and the vertical restraint bracket that attaches to the vertical pebble bed support leg. The latter two components are fabricated from aluminum and are welded to the sample cooling block, and the pebble bed support leg, respectively.

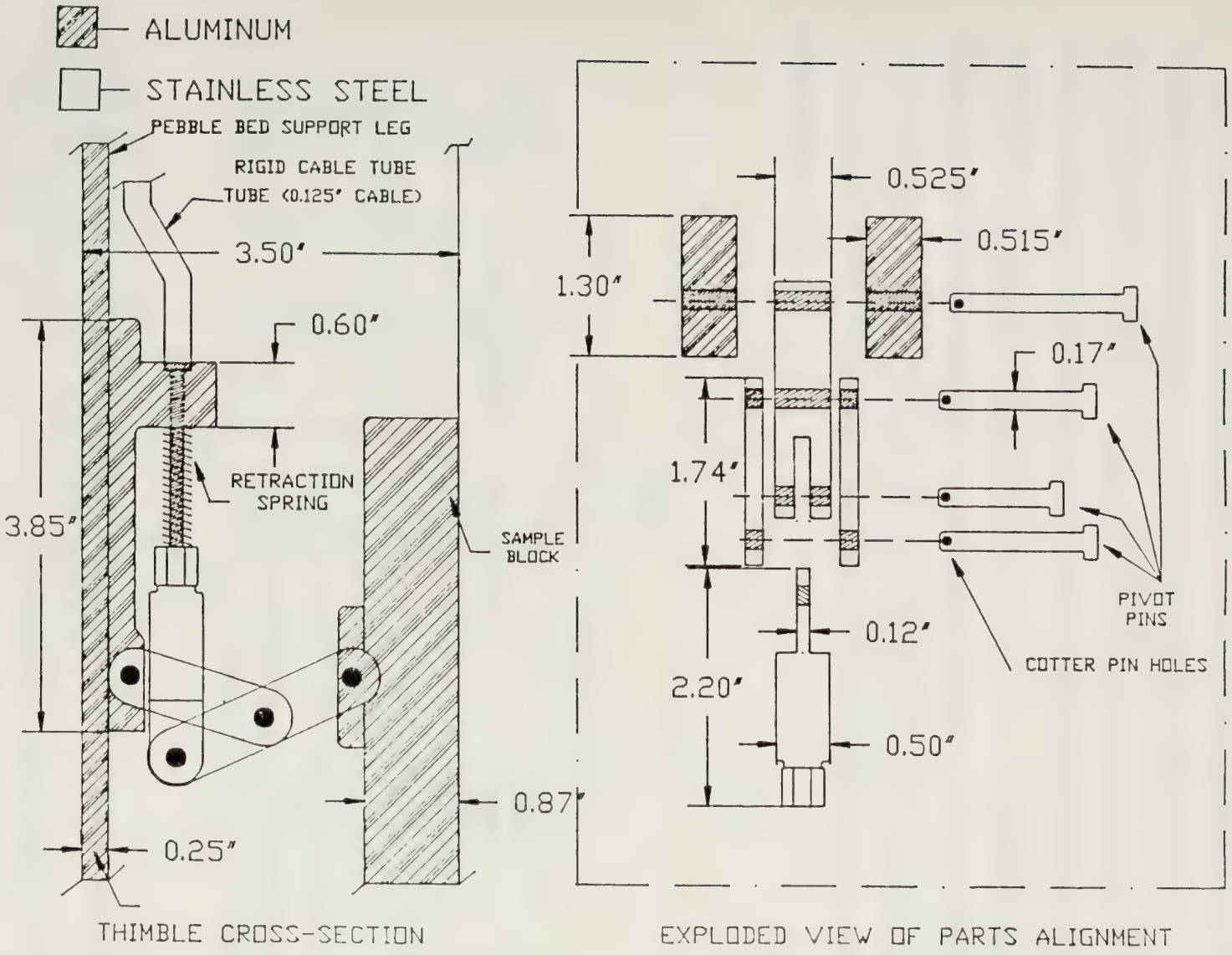

FIGURE 3.3: BCCL SAMPLE COOLING BLOCK LOCKING MECHANISM

The locking force is exerted through the 0.318 cm (0.125 inch) diameter stainless steel cable to the mechanism shown in Fig. 3.3. The cable's tensile force is exerted by a spring and threaded rod (attached to the upper cable end) assembly (not shown in Fig. 3.3) in the top section of the thimble. The spring shown in Fig. 3.3 provides sufficient counter-force to ensure that the locking mechanism retracts when the operator releases the tensile load on the cable. The range of motion of the locking device provides approximately 0.15 cm (0.063 inch) of clearance on the radius between BCCL internal components and the thimble wall. Table 3.1 shows the range of the calculated mechanical advantage for the locking mechanism.

Table 3.1

BCCL Sample Cooling Block Design Calculations

Extended Length [cm]	Block Compression Factor*	Restraint Factor**	Vertical Block Factor***
8.89	2.12	0.78	0.22
8.64	1.65	0.76	0.24
8.38	1.35	0.73	0.27
8.13	1.14	0.70	0.30
7.87	0.97	0.66	0.34

*- **Block Compression Factor** is the horizontal force pressing the sample cooling block against the thimble wall, divided by the active cable load.

- **Restraint Factor is the upward force exerted on the pebble bed support leg, divided by the active cable load.

***- **Vertical Block Factor** is the downward force exerted by the locking mechanism, divided by the active cable load. Based on bench-top testing, friction forces resulting from the compressive load were more than sufficient to prevent vertical sample cooling block motion.

An additional consideration resulting from locking the sample cooling block in place was that relative motion between components within the thimble due to thermal expansion could put excessive shear stresses on the tubing nipples. To compensate for thermal expansion, the tubing lines attached to the cooling block have offsets to reduce the force. Also, the downcomer and plenum will not be rigidly fixed, to permit their movement to compensate for relative expansion.

3.4 Out-of-Pile Testing of BCCL Sampling System Components

In order to quantify the extent of H_2O_2 decomposition in the sample system, both the sample tubing and sample cooling block required calibration. The design goal, as previously mentioned, was to limit sampling system decomposition to less than 50%.

3.4.1 H_2O_2 Measurement Method

H_2O_2 concentration measurements were made using a colorimetry technique on the cool (approximately 25°C), depressurized BCCL coolant. A colorimetry system was used that is commercially available from CHEMetrics[18], Inc. (K-5503 Vacu-vial system for H_2O_2 concentrations in the range 0.001-2.00 mg/liter (ppm)). The CHEMetrics' Vacu-vials were read with a HACH 2000 Spectrophotometer or a HORIZON model 50 colorimeter. Both the Spectrophotometer and the colorimeter were calibrated using CHEMetrics' calibration kit A-5503. The calibration curves are shown in Figs. A.1 and A.2 in Appendix A.3.

The CHEMetrics system employs a methyl-substituted form of DPN (N,N-diethyl-p-phenylene diamine) which develops a blue-violet color in the presence of iodine. The

sample is first reacted with an acidic solution of potassium iodide. Any H_2O_2 present in the sample liberates free iodine which in turn reacts with the reagent to produce a color that is proportional to the H_2O_2 content of the sample.

CHEMetrics reports that various oxidizing agents such as halogens, ozone, ferric ions and cupric ions will produce high results. Also, highly alkaline or buffered samples must be neutralized prior to performing the test procedure.

3.4.2 Sample Line Testing

The BCCL sampling system tubing must carry the two sample streams up out of the radiation environment of the thimble before less reactive tubing materials such as Nylon or Teflon can be used. About 4 meters of stainless steel tubing was tested at different temperatures; however, only at the highest temperature, 90°C, did a measurable amount of decomposition occur. The measured decomposition of 4% was within the accuracy of high-temperature (>200°C) H_2O_2 decomposition measurements. The raw data for this calibration is included in Appendix B.1.

The sample line calibration was performed isothermally at the worst case temperature of 90°C. Therefore, actual system performance should have less H_2O_2 decomposition. Also, this isothermal test provided an opportunity to compare this result with that reported by Lin et al.[16]. Table B.2 in Appendix B.1 compares the calculated decomposition with the experimental value. The experimental H_2O_2 decomposition result of 4.2% compared well with the value of 3.9% calculated from Lin's data.

3.4.3 Sample Block Testing

The BCCL sample cooling block was tested in a constant temperature bath. Several different experimental runs were performed to compare the two sample flow paths through the sample block. The sensitivity of the block was also evaluated with respect to sample flow rate and cooling block temperature.* Two methods were used to compare H_2O_2 decomposition for these experimental runs. The primary method involved measurement of the percent decomposition in the sample cooling block against the H_2O_2 concentration as measured by the water-cooled sample probe. The second method is much more difficult, but it measures the absolute level of decomposition by using zero-decomposition, or mass-balance, reference runs.

The absolute, mass-balance calibration result is 35% (+/- 5%) for the plenum sample tap side of the sample cooling block. The data are included in Appendix B.2. All other sample block evaluations were done by relative comparisons with the sample probe.

3.4.4 Sample Probe Evaluation and Cooling Block Comparison

The amount of H_2O_2 decomposition in the water-cooled sample probe was estimated at 20% (+/- 5%). The determination was made using the absolute decomposition measurement for the cooling block and comparing that against the relative H_2O_2 decomposition performance of the probe versus the cooling block.

The results of the relative comparison between the water-cooled probe and the sample cooling block are as follows:

---

*- The simulated BCCL coolant was held at about 280°C for the experimental runs. However, the block temperature, as determined by a thermocouple inserted into the hole centered between the two sample water-ways within the sample cooling block, was varied.

1. There was no measurable difference in H_2O_2 decomposition between the plenum sample side and the downcomer sample side of the sample cooling block.
2. The percent H_2O_2 decomposition (approximately 4%) was essentially constant for sample cooling block reference temperatures from 70 to 95°C.
3. With sample flow in the laminar flow regime, the percent H_2O_2 decomposition was constant at approximately 35% for sample flow rates from 300 to 400 cc/hr.

3.5 Summary

This chapter discussed the design of BCCL sampling system components, including a comparative assessment of the water-cooled sample probe and the sample cooling block. The sample cooling block emerged as the most viable option given the support system requirements of the water-cooled sample probe. Also, the sample cooling block was found to have negligible variation in the measured H_2O_2 decomposition factor with flow rates from 300-400 cc/hr and for reference block temperatures from 70-95°C. These flow rate and temperature ranges cover the expected ranges needed to support BCCL operations.

The calibration of the sample cooling block with respect to the decomposition of H_2O_2 in the sample flow path resulted in 35% (+/- 5%) decomposition (e.g. - Sample Outlet Concentration = (1-0.35) x Sample Inlet Concentration). The sample line that transports the sample from the sample cooling block to the top of the core tank showed 4% decomposition as the worst case (entire length of tubing at 90°C). Therefore, the overall BCCL sampling system using the sample cooling block is expected to decompose $\leq$40% of the inlet H_2O_2, which just meets the design objective of decomposing less than 50% of the inlet H_2O_2.

Chapter 4. Out-of-Pile High-Temperature Electrode Performance

4.1 Introduction

4.1.1 Background

As has been previously discussed, H_2O_2 is considered to be the most oxidizing species present in BWR coolant. However, the role of H_2O_2 in BWR radiolysis chemistry is not sufficiently understood to be able to use H_2O_2 concentration alone (even assuming the technical problems associated with measuring H_2O_2 concentration within a BWR are solvable) as a measure of the local coolant environment to induce IASCC in stainless steel. Moreover, when H_2O_2 is present, so is O_2 - which is also a promoter of IASCC. Research has shown that the measurement of the ECP of BWR coolant is a good indicator of the ability of the environment to crack susceptible stainless steel[3,16]. In addition, given the current technology for monitoring H_2O_2 concentration, the measurement of ECP is not only the best monitor of environmental aggressiveness, but it also holds the greatest promise for future in-reactor measurements.

Much research has been done evaluating various types of electrodes for measurement of pH, H_2 concentration and ECP[19]. The nuclear reactor environment poses substantial problems for the electrode designer. The common high-temperature electrical insulators and construction materials used in non-reactor applications (i.e. - Teflon) are not suitable for long-term exposure in a gamma or neutron radiation environment. Also, the relative aggressiveness of the coolant due to irradiation effects makes non-disruptive measurement of the actual environment difficult. A principal complication with ECP measurements is that the active electrode potential must be measured against a standard reference electrode (e.g. - Standard Hydrogen Electrode {SHE}) to provide a useful indication. Development

of a high-temperature standard reference electrode system is by itself very challenging, and the challenge increases markedly considering the effects of irradiation and potential chemical incompatibility between the standard reference electrode system and the reactor coolant. For example, the introduction of Ag^+, Cl^- or Cu^{2+} ions into the coolant from a standard reference electrode may be considered unacceptable depending on the reactor type, chemistry and radionuclide control requirements, etc..

Standard reference electrode designs using a metal/salt combination (e.g. - silver/silver chloride) involve all of the aforementioned problems. A substantial advantage could be realized if a simple metal electrode could be used for the SHE reference electrode. Investigations have been made using palladium (Pd) metal as a reference electrode for measuring pH, hydrogen concentration and as a SHE[20,21,22,23]. The use of Pd for a SHE reference takes advantage of palladium's extraordinary hydriding ability. The Pd hydride would provide the H_2 environment required for the SHE reference junction. Most standard reference electrode systems have a limited lifetime due to either salt depletion, loss of electrolyte or structural failure, etc. that necessitate their replacement. The Pd SHE would have the added benefit of being able to be "replenished", or recharged with H_2, without physically removing the electrode, by electrolytic production of H_2 at the electrode surface, and taking advantage of Pd's hydriding ability. Therefore, even though the Pd SHE may have a relatively short "lifetime" based on an initial charge of hydride, periodic recharging could extend the lifetime indefinitely.

Unfortunately, the Pd electrode has some disadvantages. EPRI[19] researchers reported that Pd electrodes were problematic as high-temperature H_2 monitors. In general, Pd electrodes respond to variations in pH, H_2 concentration in solution and redox potential.

Also, the ideal surface current density necessary to recharge the Pd electrode is temperature dependent, as are other properties such as the H_2 diffusion rate and Pd's chemical affinity for H_2.

4.1.2 Current Work

This chapter discusses the design and bench-top evaluation of electrodes for possible use in the BCCL to measure electrochemical potential (ECP). The high-temperature Ag/AgCl reference electrodes built and tested by GE will support BCCL operations. GE's electrodes were not included in this evaluation. This work was an extension of considerable work by Driscoll[20,24,25] to develop a suitable alternate reference electrode system for measuring ECP in the BCCL. The motivation for an alternate ECP measurement scheme was to provide a smaller, more durable reference electrode that will not introduce Ag^+ and Cl^- into the BCCL coolant, and will permit more flexibility in localized measurement of ECP within the BCCL.

Based on tests of Pd electrodes performed at room temperature, Driscoll reported that (1) low-voltage (9V) electrolytic recharging of the Pd electrode in high-purity water (e.g. - simulated unirradiated BWR coolant) was feasible with charging times as short as 30 minutes, (2) the extent of charging was sufficient to produce stable SHE performance for several hours, (3) Pd electrode performance relative to a commercial standard reference electrode (Ag/AgCl) was consistent with literature values, and (4) Pd electroplated on different metal wires cracked and flaked after several electrochemical cycles. In addition, Driscoll noted that the disadvantages of the Pd reference electrode (i.e. - measured potential is dependent on pH, H_2 concentration, etc.) should not disqualify it for use in the BCCL where chemical additives and radiolytic species concentrations are dilute.

The work described in this chapter provided a preliminary high-temperature extension of Driscoll's work. The primary objectives of this testing were to (1) qualify a suitable electrode feedthrough design, (2) provide data on the high-temperature behavior of the Pd electrode in a more prototypical environment, and (3) provide comparative high-temperature data on stainless steel, platinum (Pt) and Pd electrodes. This work also provides the basis for additional high-temperature testing and/or qualification of an alternate standard reference electrode for use in the BCCL.

The comparative potential data for stainless steel, Pt and Pd provided a preliminary investigation of the possible use of a electrode potential "comparator" described by Driscoll[25]. The potential comparator involves three electrodes: one each as cathode and anode in an electrolysis cell and the third as an unperturbed test electrode monitoring the actual coolant environment. The cathode electrode would be exposed to a highly localized H_2 environment and would therefore be "fully protected", while the anode would be in a localized O_2 environment and would therefore by "fully vulnerable". By switching off the electrolysis voltage and then measuring the potential difference between the test electrode and the two electrolysis electrodes, we can interpolate to find how close the test electrode is to being protected. Driscoll reported the feasibility of this concept at room temperature. However, he also noted that diffusion coefficients are an order of magnitude larger at 300°C, consequently, the electrolysis electrode potential drift rate may be excessive at 300°C.

4.2 Bench-Top Test Method

4.2.1 High-Temperature Test Apparatus

High-temperature testing of the electrodes was done with the same basic bench-top test device used for the H_2O_2 decomposition studies (see Fig. 2.1). The test device was modified by building a special test section, as shown in Fig. 4.1. The test section consisted of a 1.27cm (0.5in) SS316 stainless steel tee with compression fittings (SWAGELOCK) on the straight run and 1.27cm (0.5in) pipe threads on the branch-run of the tee. A CONAX* PL-18-4 feedthrough gland was screwed into the branch-run of the tee.

The critical aspect of this installation was the use of the proper sealant for the CONAX feedthrough. The use of bare wire electrodes necessitated a non-conducting sealant that would withstand the temperature, pressure and radiation environment in which the BCCL was exposed. Previous project experience with Teflon and Lava sealants was unsatisfactory. The Teflon sealant deformed excessively and failed after temperature cycling (the coolant temperature in the test section was 280°C, which is above the manufacturer's high temperature limit for the Teflon).

The Lava sealant was initially non-conducting; however, the sealant apparently absorbed sufficient water that its electrical resistance dropped enough to short out the electrodes after several hours of exposure. The final installation used a Grafoil sealant which exceeds the temperature, pressure and irradiation requirements. However, use of Grafoil, which is electrically conductive, requires the use of an insulated electrode.

---

*- CONAX Corp., 2300 Walden Ave., Buffalo NY 14225.

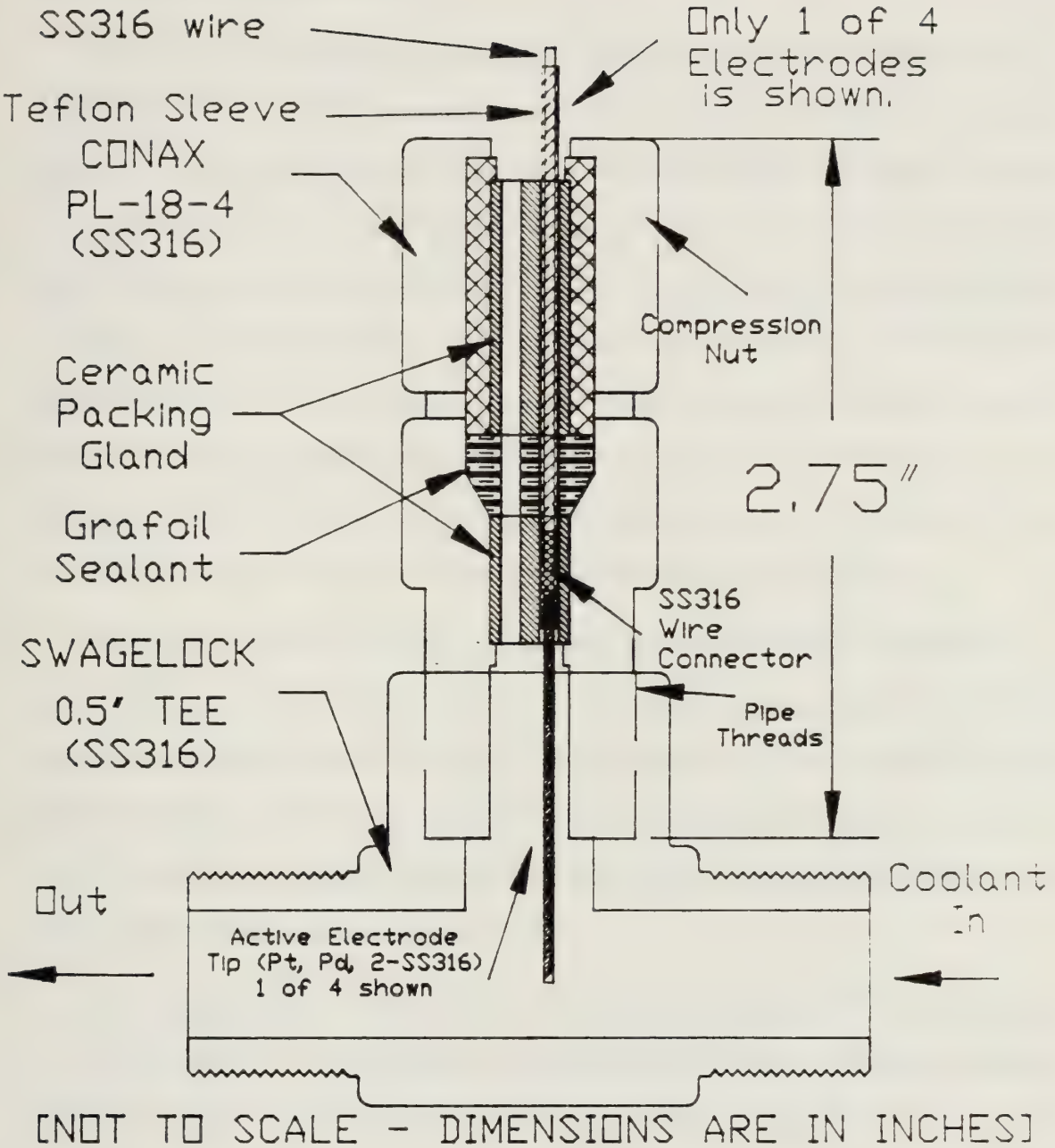

Figure 4.1: High-Temperature Electrode Test Section

4.2.2 Electrode Installation

The use of the CONAX feedthrough provided flexibility in the total number of electrode wires that could be accommodated. In order to meet the objectives set forth in Section 4.1.2, four electrodes were to be used. A major concern for the electrode design was to avoid errors in the electrode potential measurements due to temperature gradients and material interactions that would be unique to each electrode material as it passes through a feedthrough into the coolant environment of interest. In order to avoid undesirable electrode interactions, the configuration shown in Fig. 4.2 was used. The main electrode sections are 1mm O.D. SS316 wires*. Within the lower ceramic insulator section on the pressure side of the sealant, the stainless wire was adapted to the active electrode tip, which extended out of the ceramic into the simulated coolant within the test section.

Four active electrode tips were crimped onto the stainless wires: One palladium**, one platinum and two SS316 tips. Stainless steel tips were crimped onto the ends of the stainless wires instead of using a continuous stainless steel wire to ensure that the exposure area and transition was directly comparable for the four electrodes. Potential measurement error caused by thermocouple effects at the Pt and Pd joints were negligible compared to the magnitude of the potentials to be measured.

Electrical insulation of the electrodes was achieved by using 0.168 cm (0.066 in) O.D. Teflon tubing***. At the temperature and pressure of interest, the tubing provided negligible strength. Initial tests resulted in the electrodes ejecting from the test section.

---

*- Supplied by GOODFELLOW, Malvern PA 19355.

**- Palladium and Platinum wires, CAS#7440-05-3 and 7440-06-4, respectively, were supplied by ALFA PRODUCTS, Danvers MA 01923.

***- Supplied by COLE-PARMER INSTRUMENT CO., Chicago IL 60648 (P/N 6417-41).

After several modifications, the design shown in Fig. 4.2 was successful. This design relied on the Grafoil sealant extruding into the rounded groove in the side of the electrode to capture the electrode. This groove was created by filing one side of the electrode with a small, half-round file. Maximum torque values on the feedthrough were used, such that the final compressed Teflon wall thickness was a small fraction of its original thickness of 0.031 cm (0.012 in). This feedthrough design is also expected to withstand moderate in-pile irradiation before insulating properties deteriorate to the point replacement is required.

4.3 Results of Electrode Performance

4.3.1 Electrode Test Procedure

In order to characterize basic electrode performance, several reference runs were made without adding H_2O_2. Both cold (25°C) and hot (280°C) reference runs were performed. All runs were started with an electrode charging period where the Pd electrode and one stainless steel (SS) electrode, hereafter referred to as the stainless steel cathode, were made approximately 18V negative with respect to the test section wall. This charging period ensured that the stainless steel cathode was "fully protected" by a localized reducing environment, and provided time for the Pd electrode to adsorb H_2 for subsequent evaluation as a SHE reference. The charging period was varied to evaluate the sensitivity of the Pd electrode behavior to H_2 pickup.

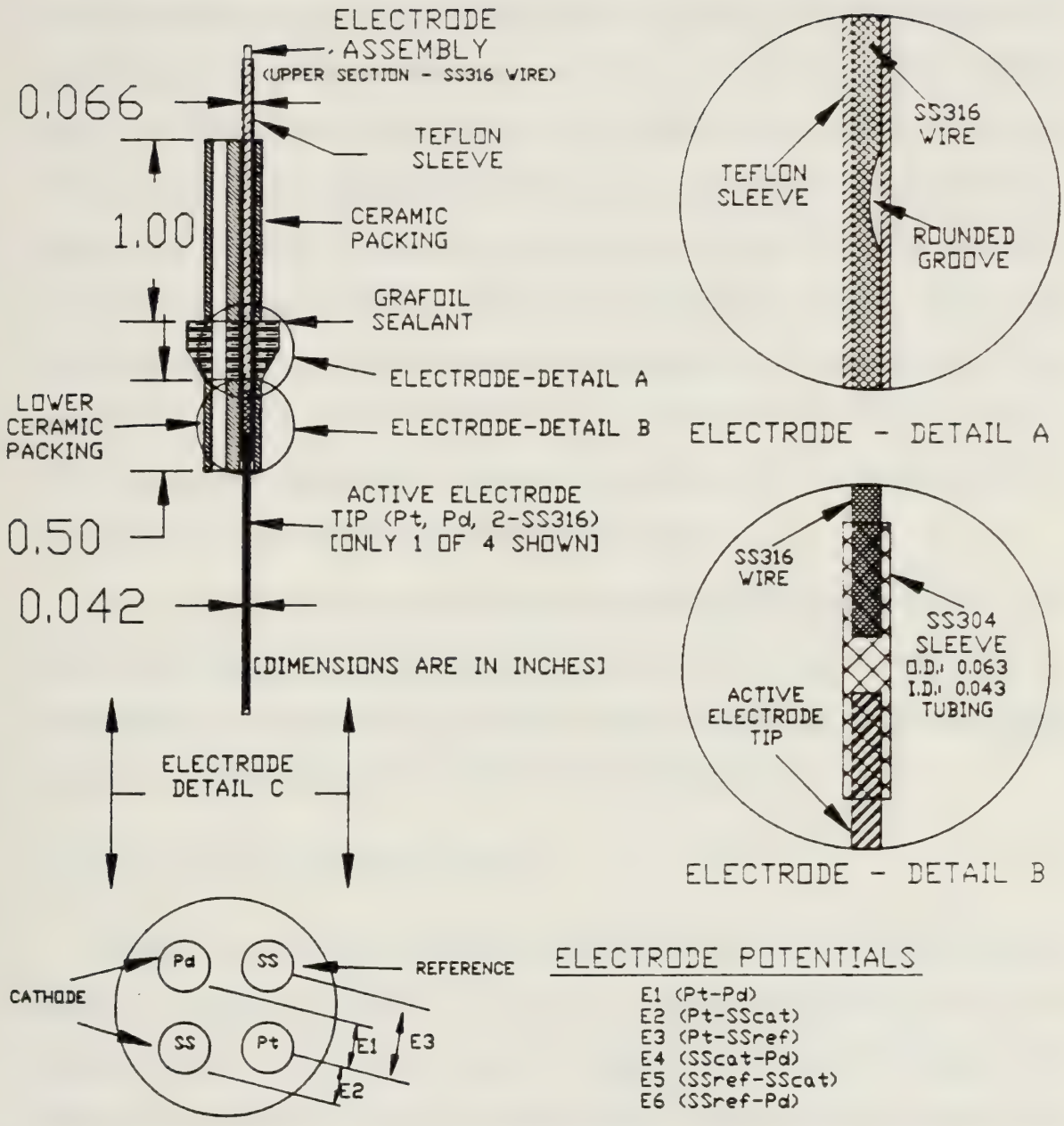

FIGURE 4.2: ELECTRODE CONFIGURATION FOR BENCH-TOP TESTING

The end of the charging period started the data collection sequence, during which the three basic differential voltages, shown in Fig. 4.2; E1 (Pt-Pd), E2 (Pt-SScat) and E3 (Pt-SSref) (actually -(E3) was measured for most runs); were measured versus elapsed time. The voltages were measured using a FLUKE 2200B DATALOGGER*. The three differential voltages {E4 (SScat-Pd), E5 (SSref-SScat) and E6 (SSref-Pd)} are calculated from the three measured voltages. Experimental runs made prior to 21 March 1990 used an electrode configuration with the positions of the SS reference electrode (same as the "test electrode" of the potential comparator concept) and the Pt electrode reversed. The reported voltages have all been converted to the convention shown on Fig. 4.2; however, some anomalies are evident in the initial slopes (immediately following charging) of some data curves because of the electrode configuration change.

H_2O_2 concentrations were measured using the water-cooled probe (see Fig. 3.2). This probe decomposes approximately 20% of the H_2O_2 at the probe inlet. Consequently, the reported H_2O_2 concentrations are the measured values divided by 0.8, to provide the best estimate of the H_2O_2 concentration within the electrode test section.

4.3.2 Potential Versus Time - Cold

Figure 4.3 shows the electrode potential behavior for the first cold reference run. The electrodes have not been exposed to H_2O_2 or to elevated temperatures for the first 4 experimental runs. The behavior of run #1 was also duplicated by the first 4 runs. The charging time for the first 3 runs was 15 minutes, and 10 minutes for the fourth run. The data for runs #2 through #4 are shown in Figs. C.1 through C.3, respectively, of Appendix C. Although the basic behavior was the same in the first 4 runs, a distinct trend was

*- Made by JOHN FLUKE MFG., CO., INC., Mountlake Terrace, WA 98043.

evident. Figure 4.4 shows E4 (SScat-Pd) and E5 (SSref-SScat) curves for the first 3 cold reference runs. The measured potentials decreased in magnitude as a function of exposure. These E4 (SScat-Pd) and E5 (SSref-SScat) traces are indicative of the other curves. This aging effect was also noted by Driscoll.

Electrode behavior changed markedly after high-temperature exposure. Figure 4.5 shows the data for the first cold reference run following operation of the test apparatus at high-temperature (but no H_2O_2). This change was most likely indicative of the passivation of the SS electrodes. Of the six reported differential voltages, all, except for E1 (Pt-Pd), involved a stainless steel electrode. The behavior of E1 (Pt-Pd) changed very little between the passivated and the pre-passivated reference runs (Fig. 4.4).

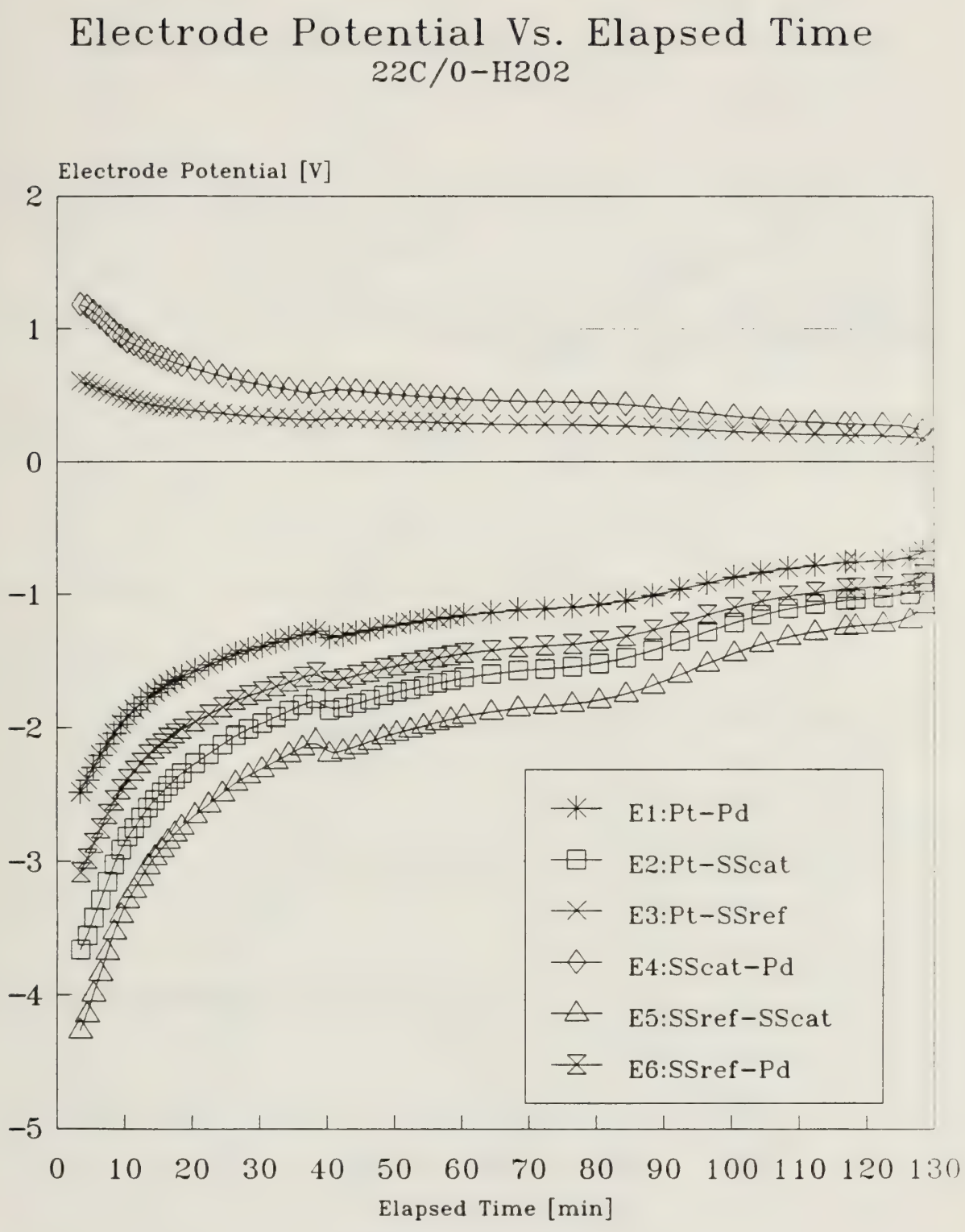

Figure 4.3:
Cold Reference Run #1

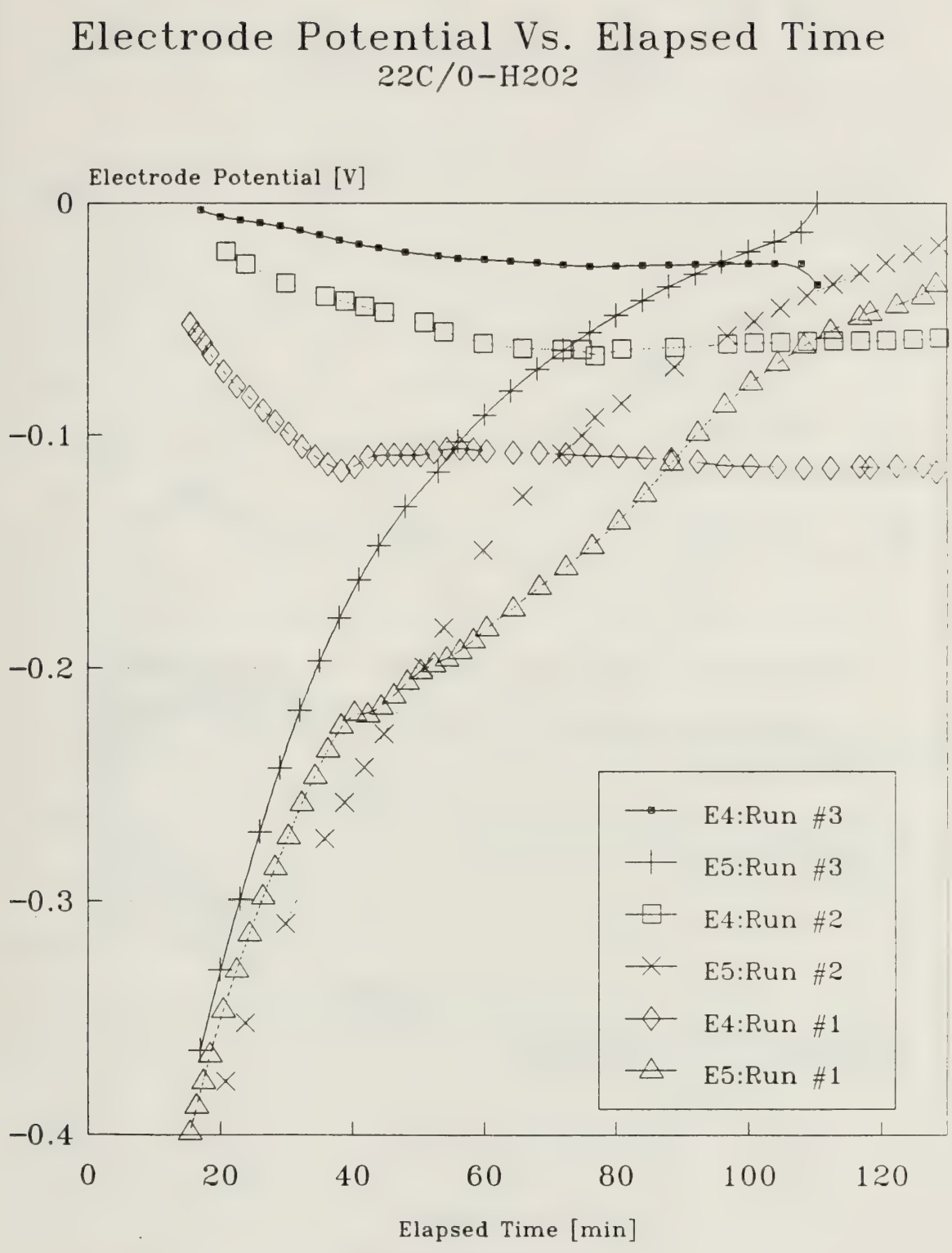

Figure 4.4:
Cold Reference Comparison

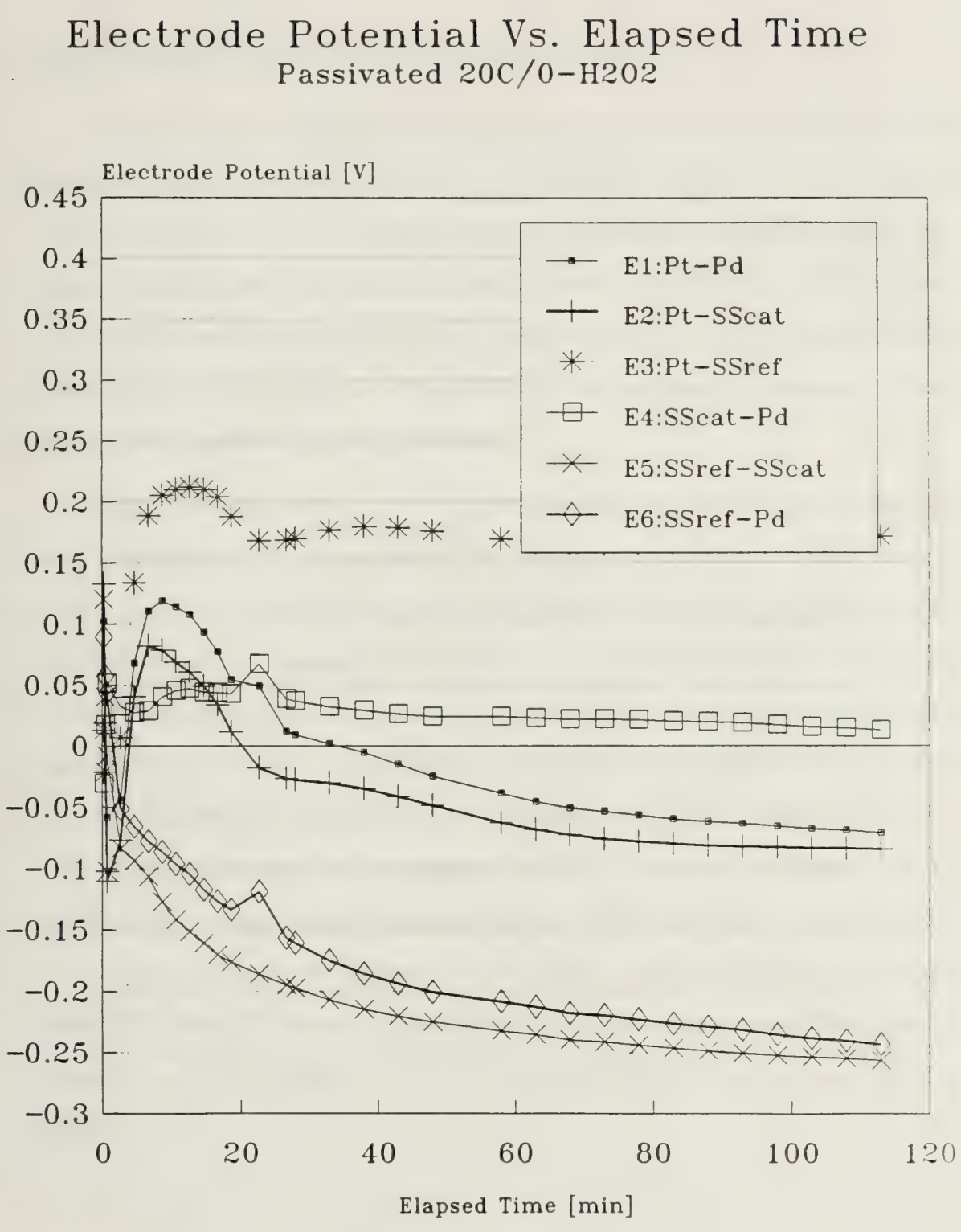

Figure 4.5:
Passivated-Cold Reference Run #1

4.3.3 Potential Versus Time - High Temperature

The basic behavior of the high-temperature reference runs was characteristic of the passivated electrode behavior shown in Fig. 4.5. Figure 4.6 shows electrode potential as a function of elapsed time for hot reference run #3. Based on preliminary high-temperature testing, a charging time of 10 minutes produced relatively stable behavior. Hot reference run #4 mirrored run #3 very closely with no evidence of electrode aging. The hot reference run #4 data are shown in Fig. C.4 of Appendix C. The raw data for subsequent runs are included in the applicable tables in Appendix C.

Following hot reference run #4, a high-temperature run, with H_2O_2 concentrations up to approximately 2 ppm, was made. Following that run, another zero H_2O_2 run (run #9) was made. The enhanced oxidation effect of the H_2O_2 solution substantially aged the electrodes. Figure 4.7 compares E3 (Pt-SSref), E4 (SScat-Pd), E5 (SSref-SScat) and E6 (SSref-Pd) potentials for reference run #3 (preceding the H_2O_2 run) with the corresponding potentials for hot reference run #9. The effects of the hot H_2O_2 run were more complicated and could not readily be attributed to passivation alone. Charging times were progressively increased from 10 minutes for hot reference run #4, to 27 minutes for reference run #9. Additional runs would be required to conclusively validate the adequacy of the charging cycle; however, the potential difference between the two cathodically charged electrodes (Pd and SS cathode), E4, was essentially the same for the two reference runs. Other potential differences involving stainless steel and Pd electrodes varied considerably, as shown in Figure 4.7.

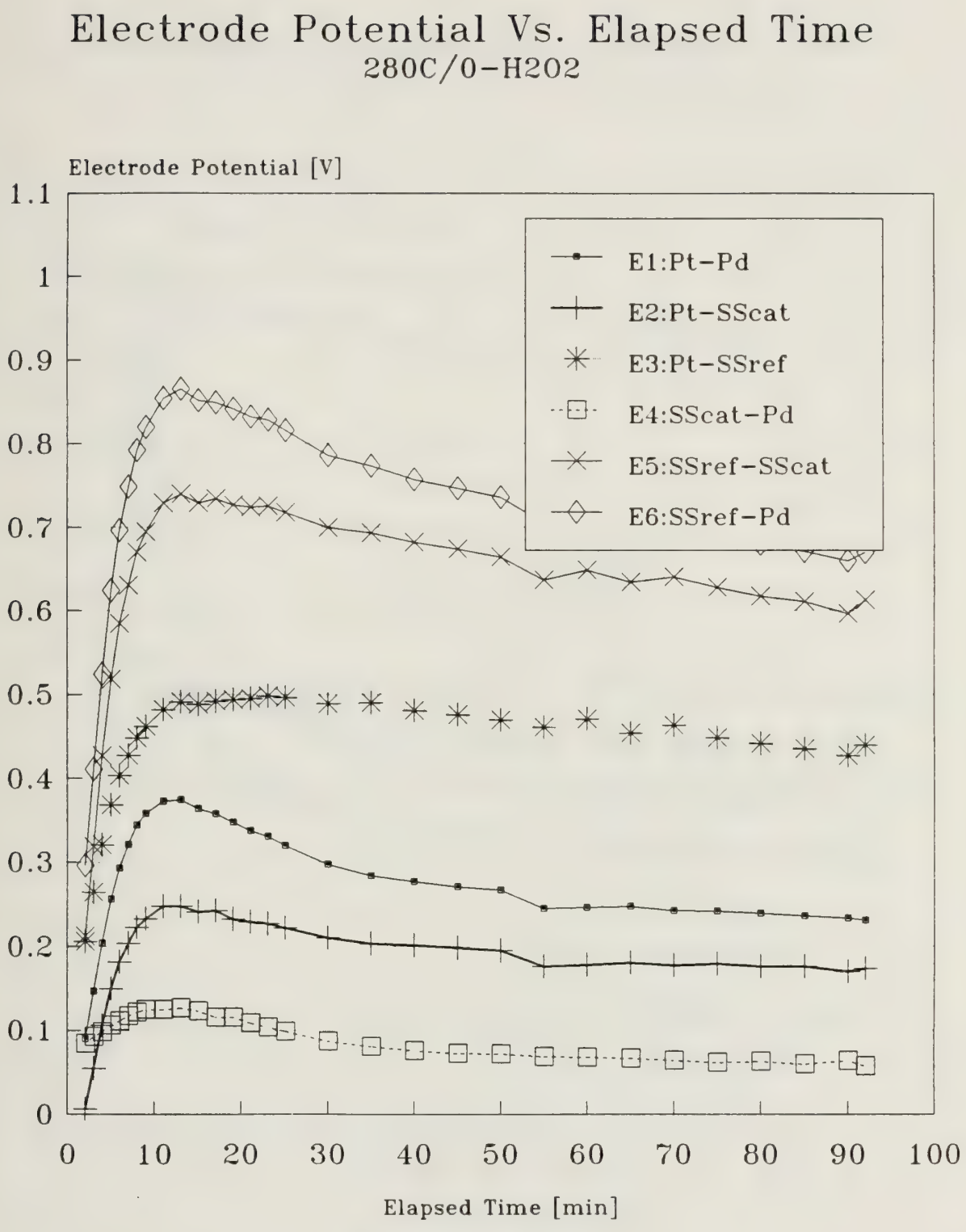

Figure 4.6:
Hot Reference Run #3

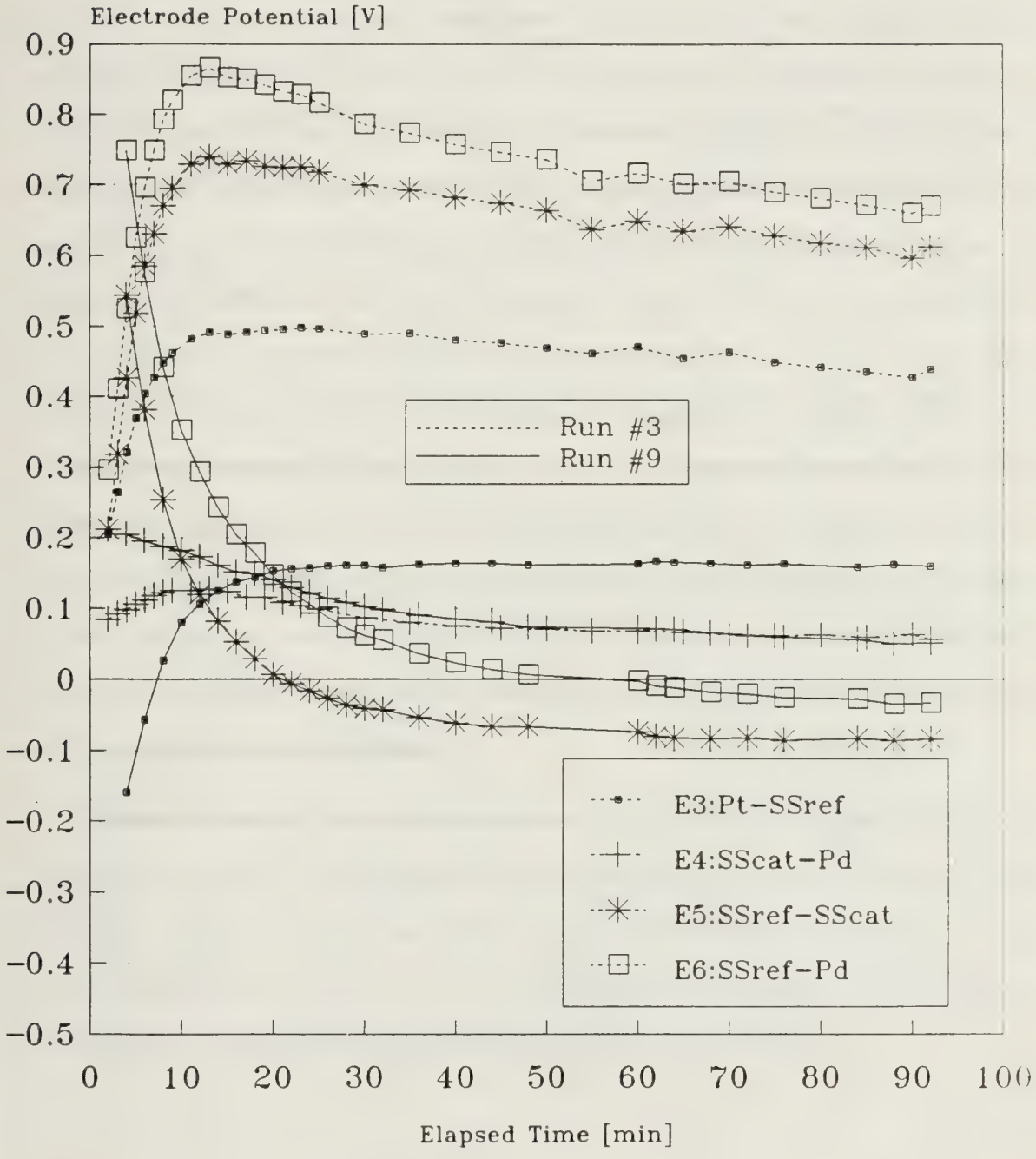

Figure 4.7:
Hot Reference Run Comparison

4.3.4 Potential Versus H_2O_2 Concentration

Two independent sets of high-temperature runs were made, varying the concentration of H_2O_2. The H_2O_2 concentrations were varied within the range currently expected to be achieved within the BCCL, based on BWR plant data and the computer modeling predictions discussed in Chapter 5. Several high-temperature reference runs were performed between these two H_2O_2 runs. To aid in the comparison of these two runs, the applicable potential curve from hot reference run #9 (zero H_2O_2) is included with each set of curves. Figure 4.8 shows the E1 (Pt-Pd) potential behavior for both H_2O_2 sets. Case A of Fig. 4.8 shows the first hot H_2O_2 run and Case B the second hot H_2O_2 run. Two important characteristics in evidence are that (1) electrode aging suppresses the potential differences caused by the different H_2O_2 concentrations, and (2) the more oxidizing the environment (higher H_2O_2 concentration) the lower the measured potential. For Case B of Fig. 4.8, the lines are sufficiently compressed that experimental variations between runs are of the same order of magnitude as the actual potential differences. The raw data for these and subsequent runs, involving potential measurements as a function of H_2O_2 concentration, are included in the applicable tables of Appendix C.

Figures 4.9 and 4.10 show similar comparisons for E2 (Pt-SScat) and E3 (Pt-SSref) potentials, respectively. The characteristics are comparable to that of E1 (Pt-Pd) even though the enlarged scale for Case B of Fig. 4.10 gives the appearance that the curves are not compressed more than in Case A. The enlarged scale for Case B of Fig. 4.10 does show that the potential decreased with increasing H_2O_2 concentration.

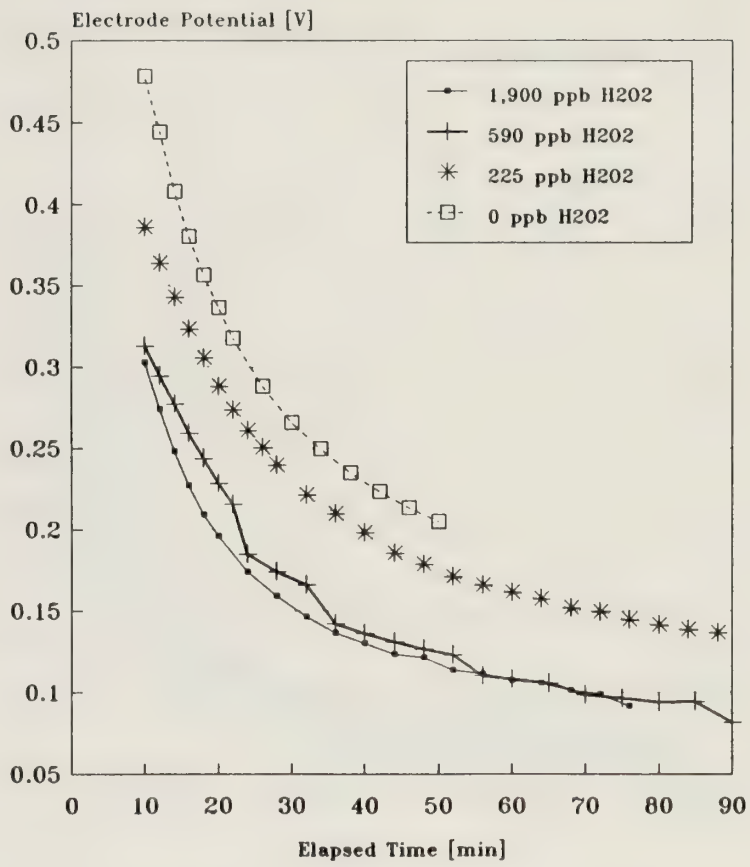

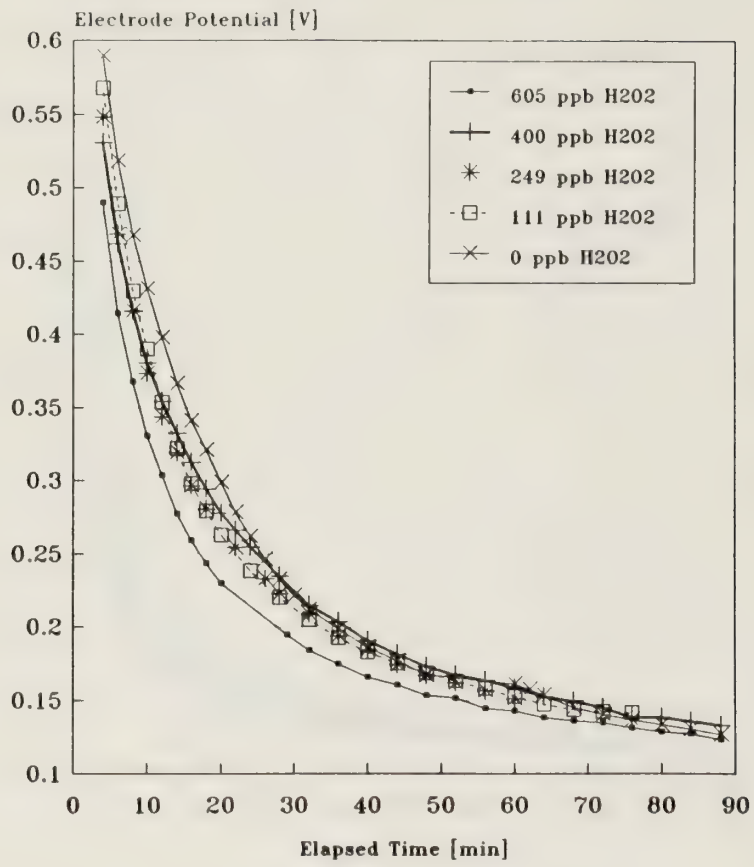

Figure 4.8: E1(Pt-Pd) Potential Vs. H202 Concentration

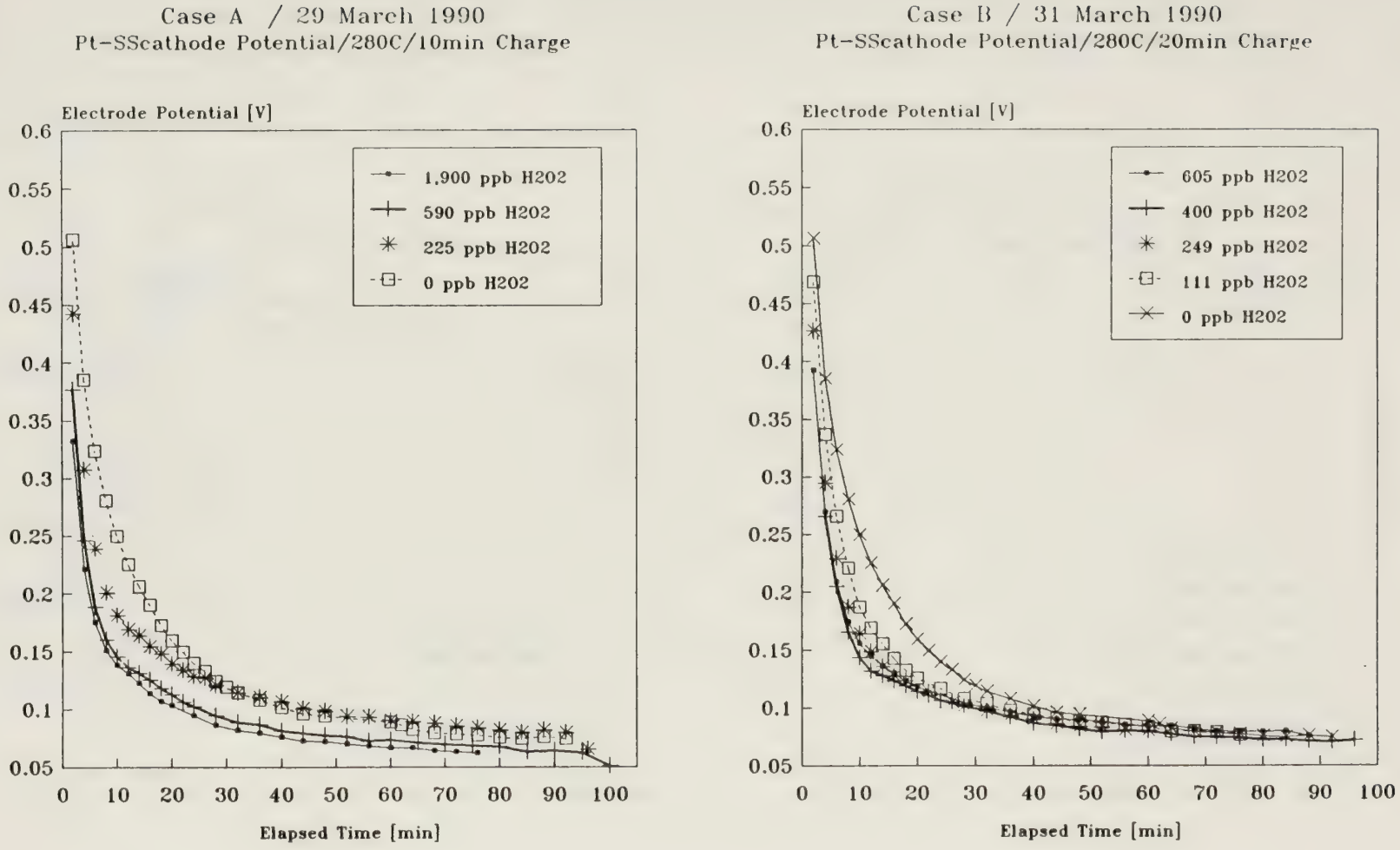

Figure 4.9: E2 (Pt-SScat) Potential Vs. H202 Concentration

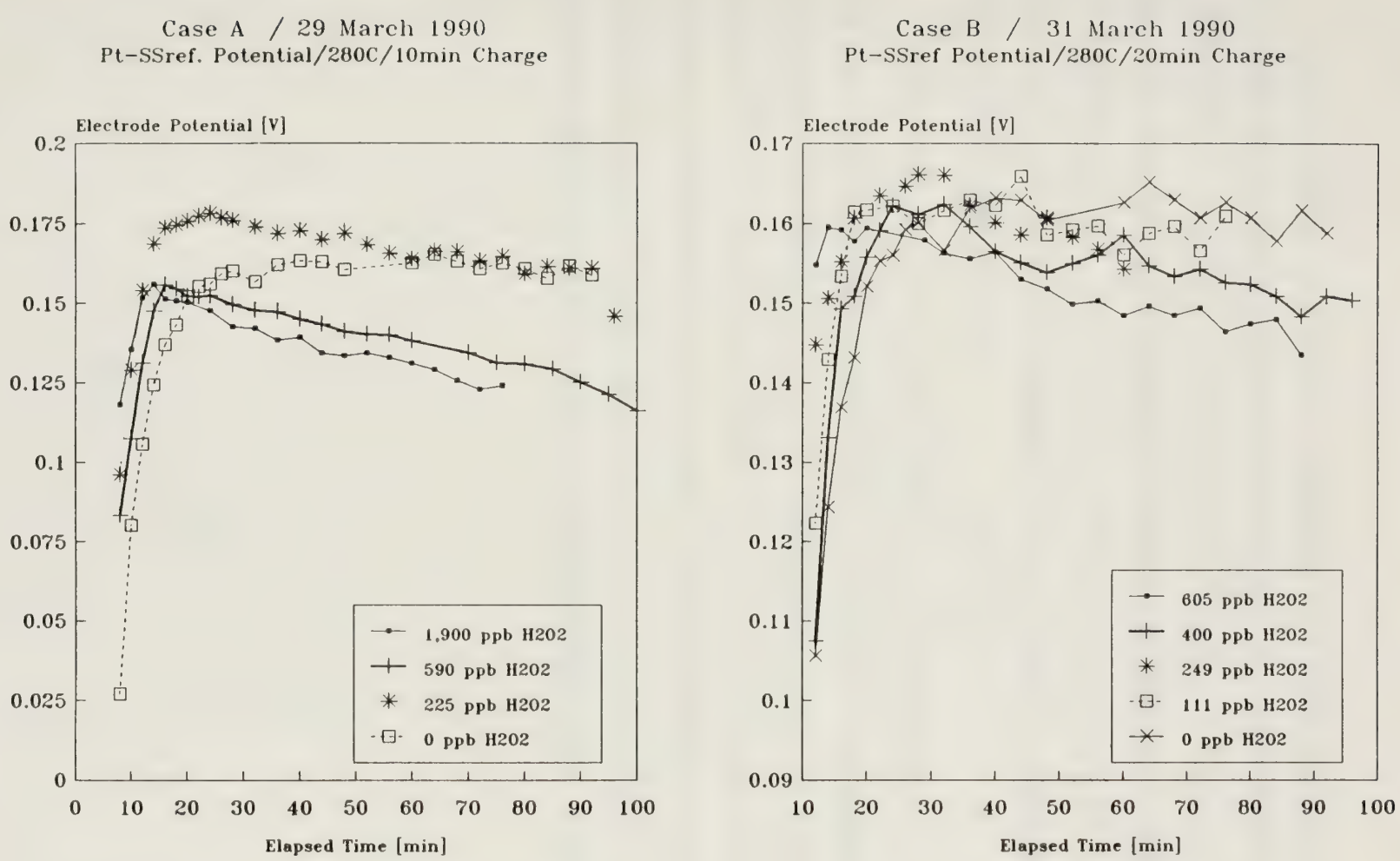

Figure 4.10: E3(Pt-SSref) Potential Vs. H202 Concentration

Figure 4.11 shows the hot H_2O_2 run comparison for potential E4 (SScat-Pd). The compression due to aging, and the ordering based on H_2O_2 concentration, are not consistently evident as in previous cases. The inconsistent behavior with respect to H_2O_2 concentration is also true for the E5 (SSref-SScat) and E6 (SSref-Pd) potentials shown in Figs. 4.12 and 4.13, respectively. The compression with aging is clearly depicted in both Figs. 4.12 and 4.13. Also, higher H_2O_2 concentrations clearly decrease the magnitude of the E5 (SSref-SScat) potential (Fig. 4.12).

Another interesting feature shown in Figs. 4.11 - 4.13 for the first H_2O_2 run (Case A) is that a limit apparently exists on the effects of higher H_2O_2 concentrations on the electrode potential. Specifically, there was negligible difference in the potential measurements for the 590ppb and the 1,900ppb cases. However, H_2O_2 concentrations below approximately 500ppb showed more variation. This limiting behavior is qualitatively consistent with the ECP behavior reported by Takagi[26] for stainless steel and platinum. Quantitative comparisons would require potential measurements relative to a SHE.

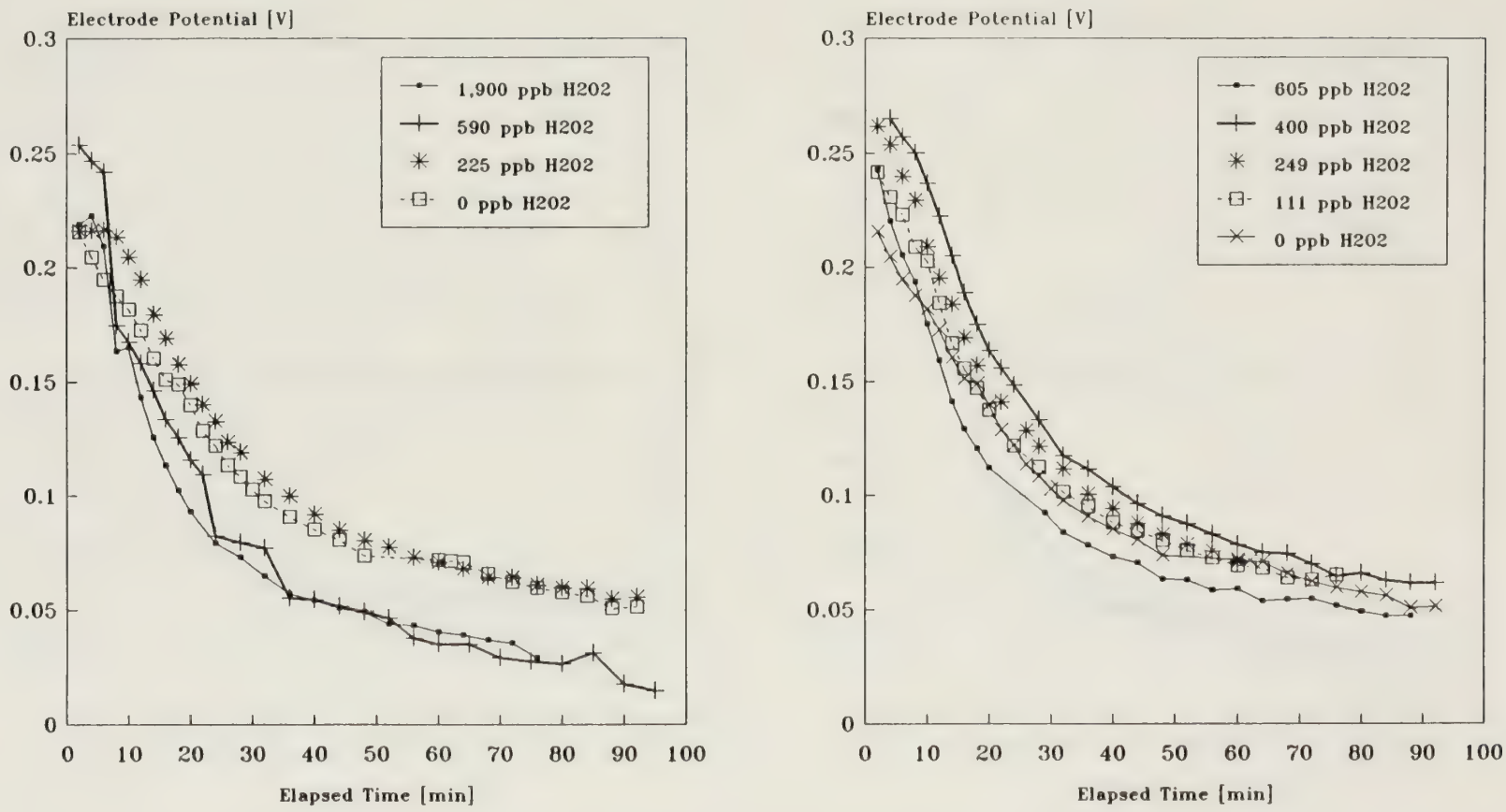

Figure 4.11: E4(SScat-Pd) Potential Vs. H202 Concentration

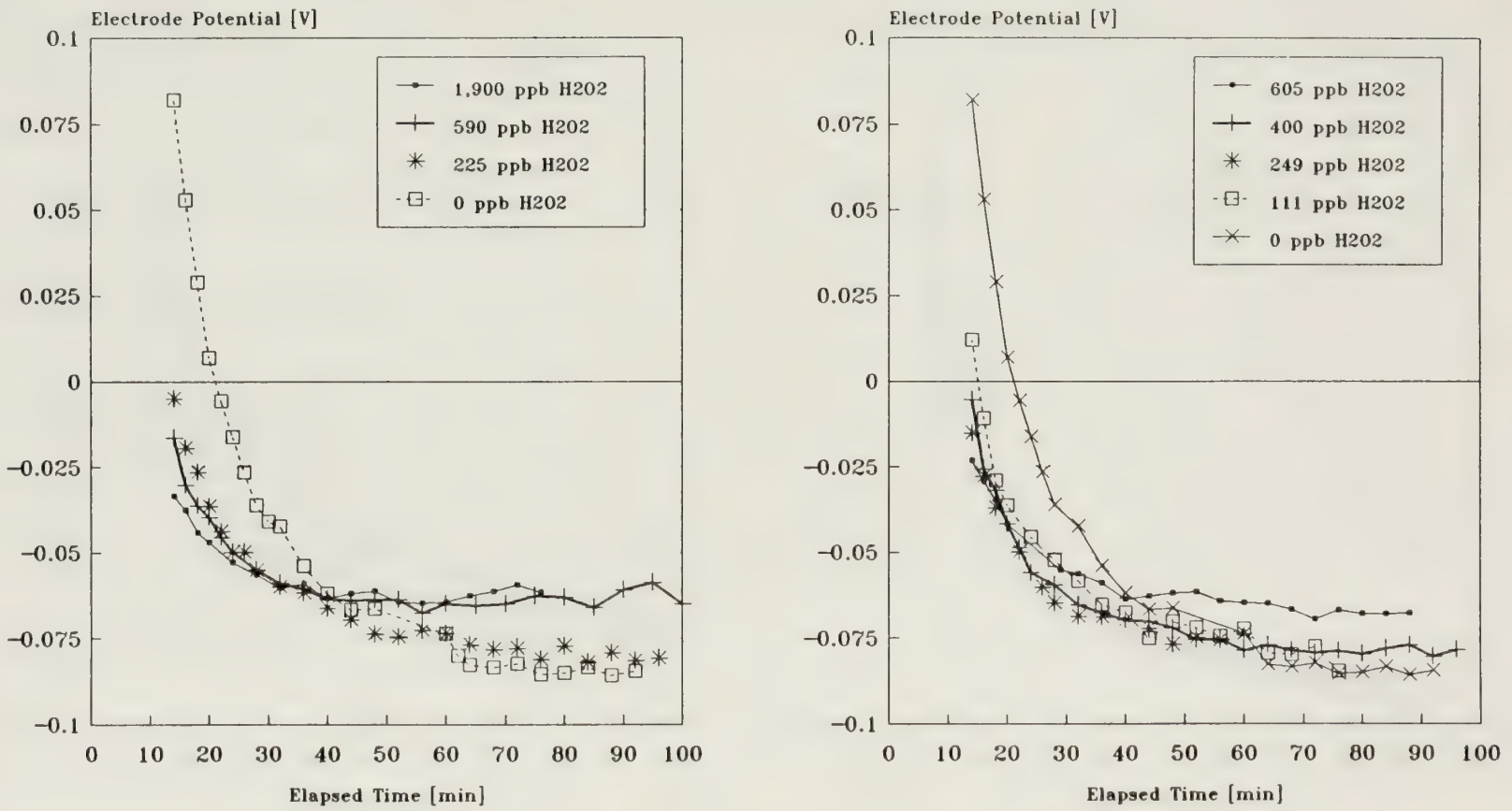

Figure 4.12: E5(SSref-SScat) Potential Vs H202 Concentration

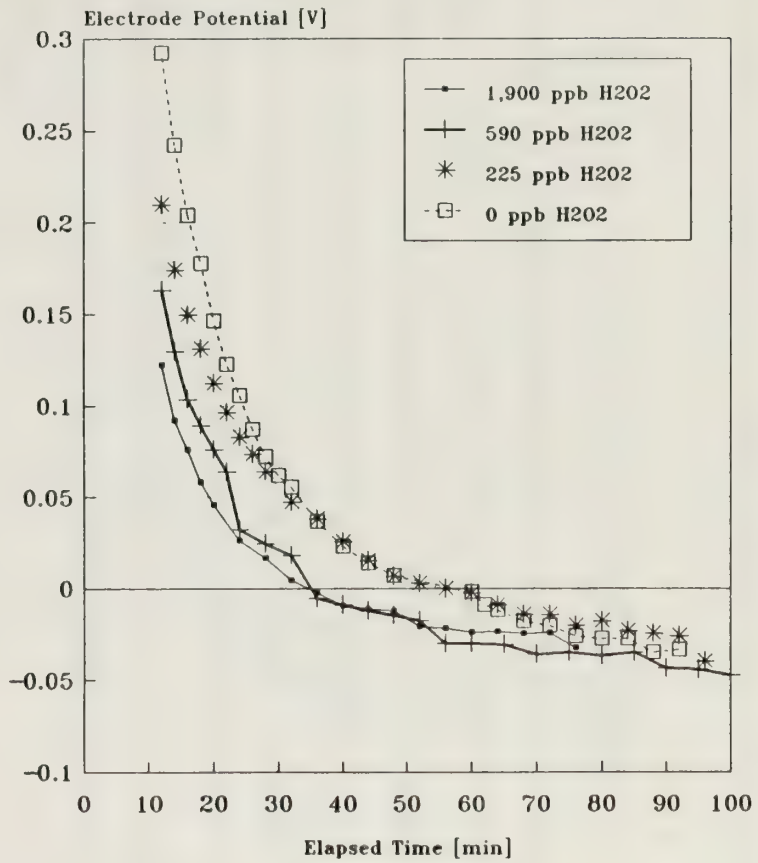

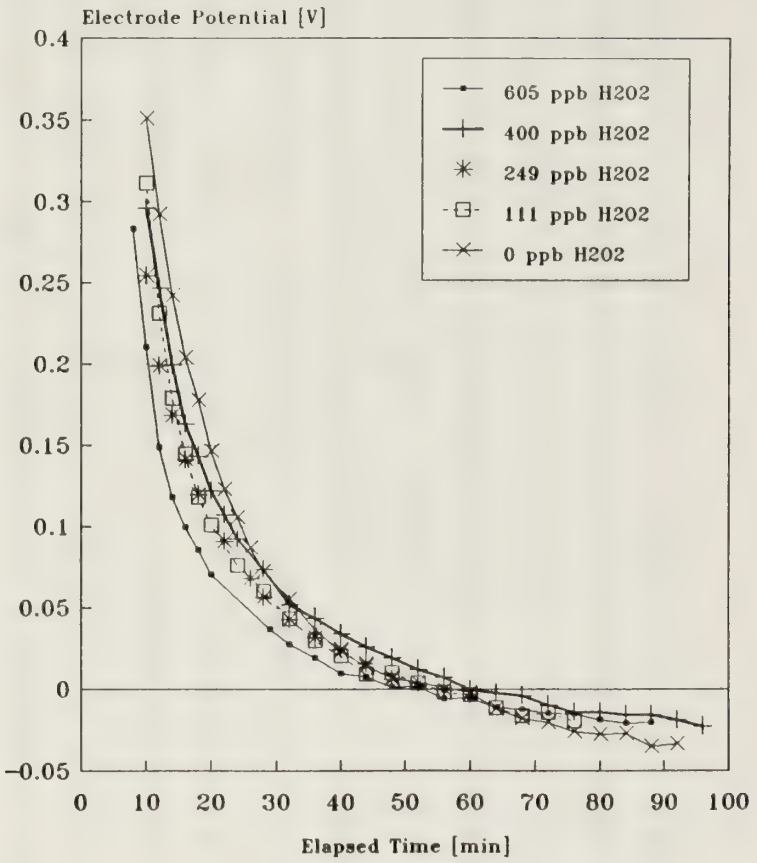

Figure 4.13: E6(SSref-Pd) Potential Vs. H2O2 Concentration

An original motivation for this electrode investigation was, in part, to find suitable electrode configurations that can act as, or substitute for, a standard reference electrode. Starting with the assumption that the true ECP within the test section was independent of the presence and nature of the measurement electrodes, and constant over the duration of the test run, a potential that quickly reached a constant equilibrium value would be an obvious candidate for possible future correlation and calibration. Only two potentials, E5 (SSref-SScat) and E3 (SSref-Pt), achieved a relatively stable reading within the time frame of these initial tests. Figures 4.14 and 4.15 show the data for all H_2O_2 runs on a common axis (Case A) for E5 (SSref-SScat) and E3 (SSref-Pt), respectively. In order to see the fine structure, or sequence, of the sets of curves, an enlarged view of the relatively horizontal section of the curves is included in each figure as Case B. It is interesting to note that the charging of the SS cathode sufficiently altered its surface oxide layers to sustain a significant potential difference over the experimental run (100 minutes) as seen by the E5 (SSref-SScat) potential, shown in Fig. 4.14.

Unfortunately, the E5 (SSref-SScat) and E3 (Pt-SSref) potentials did not involve the Pd electrode, which was the prime candidate for use as a SHE reference electrode. The best candidate for a suitable ECP bench-mark electrode was the E6 (SSref-Pd) potential. Figure 4.16 shows E6 (SSref-Pd) potential curves in the same format as Figs. 4.14 and 4.15. Within the relatively short time span of these preliminary tests, the E6 (SSref-Pd) potential did not level sufficiently relative to the spacing of the curves (spacing is a function of H_2O_2 concentration) to be useful. One conclusion that can be drawn from these results is that additional evaluation is warranted to determine if the electrode charging step was sufficient to load the Pd matrix with sufficient hydride to provide the assumed constant local H_2 environment.

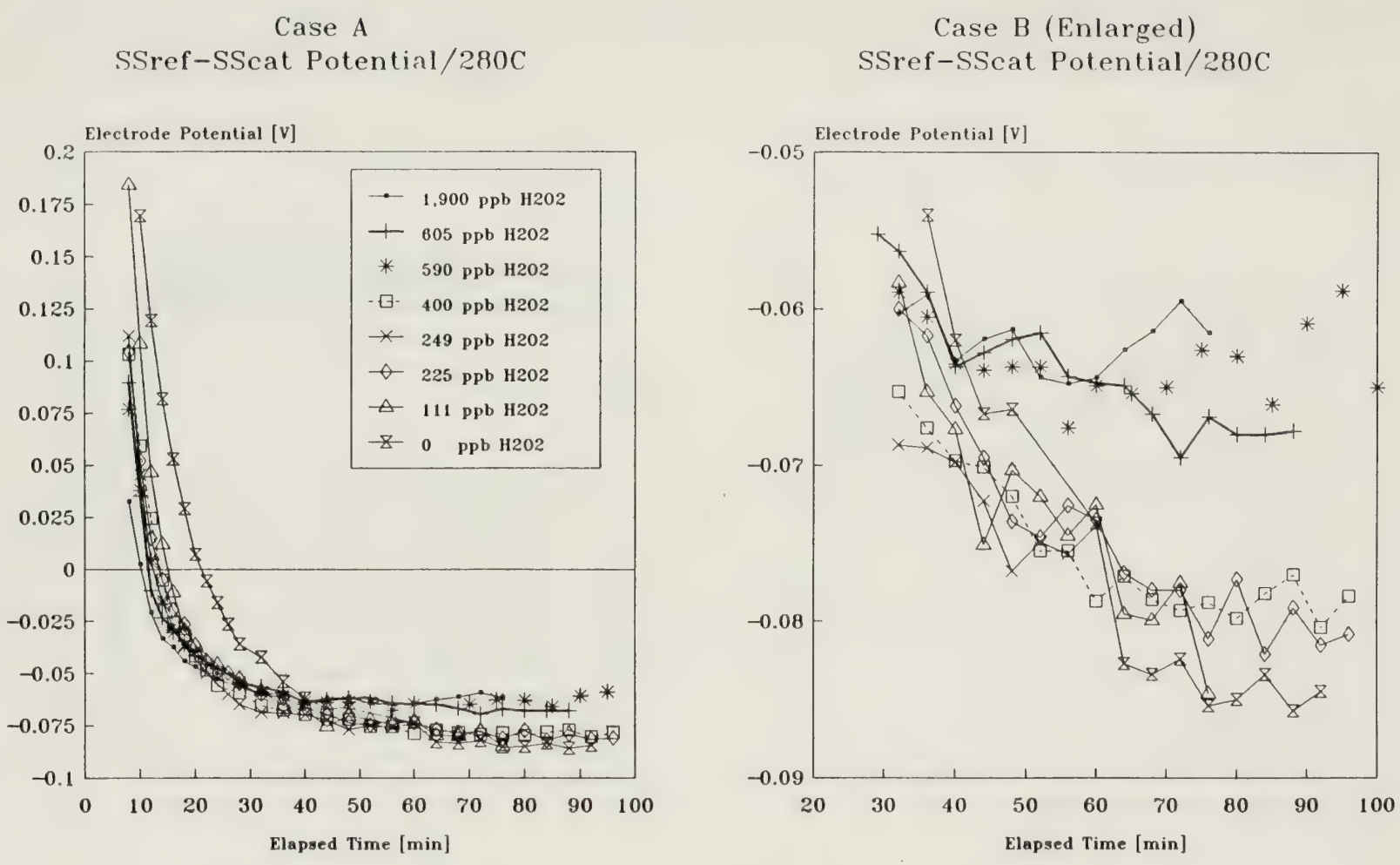

Figure 4.14: Composite Plot of E5(SSref-SScat) Potential

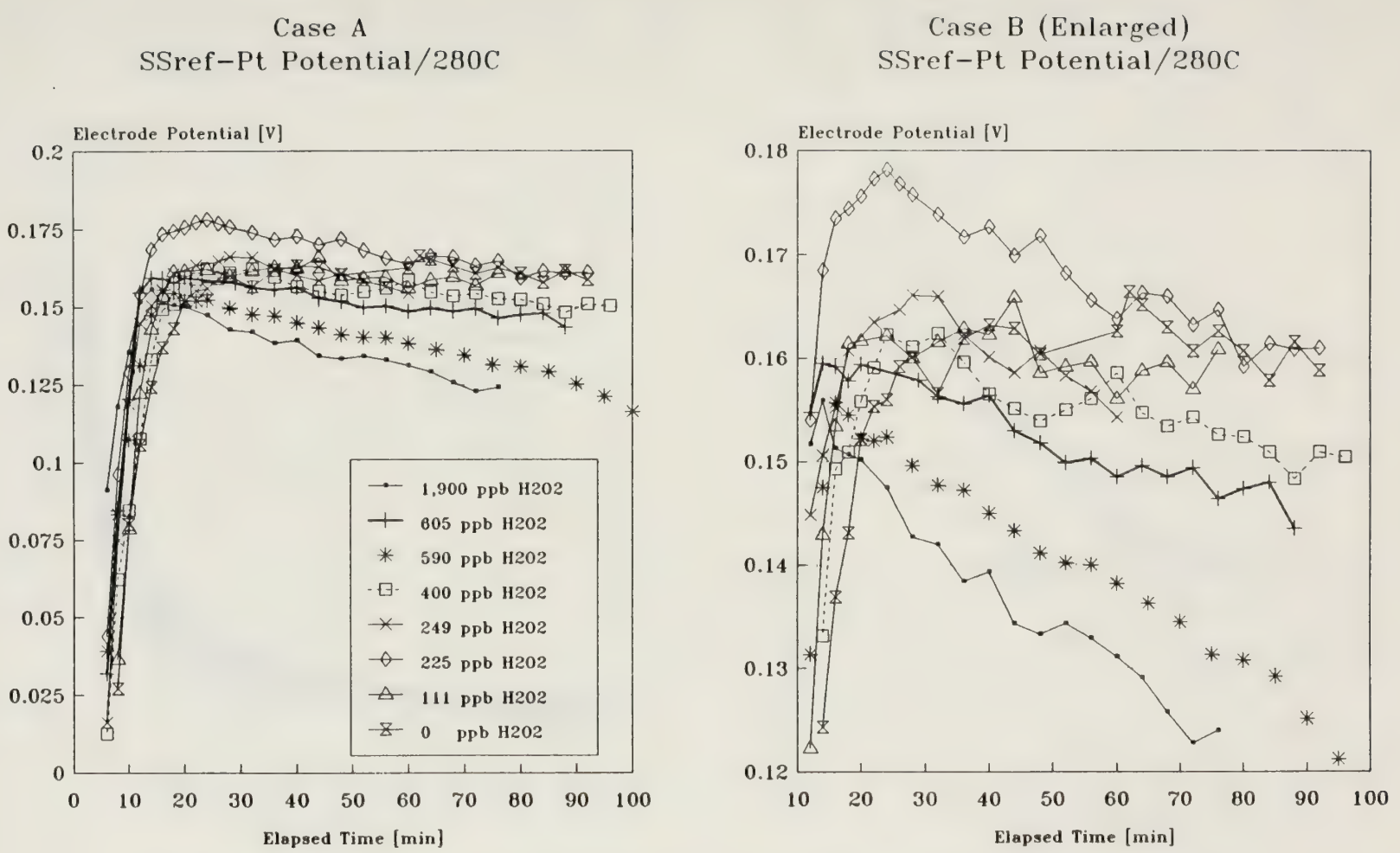

Figure 4.15: Composite Plot of E3(SSref-Pt) Potential

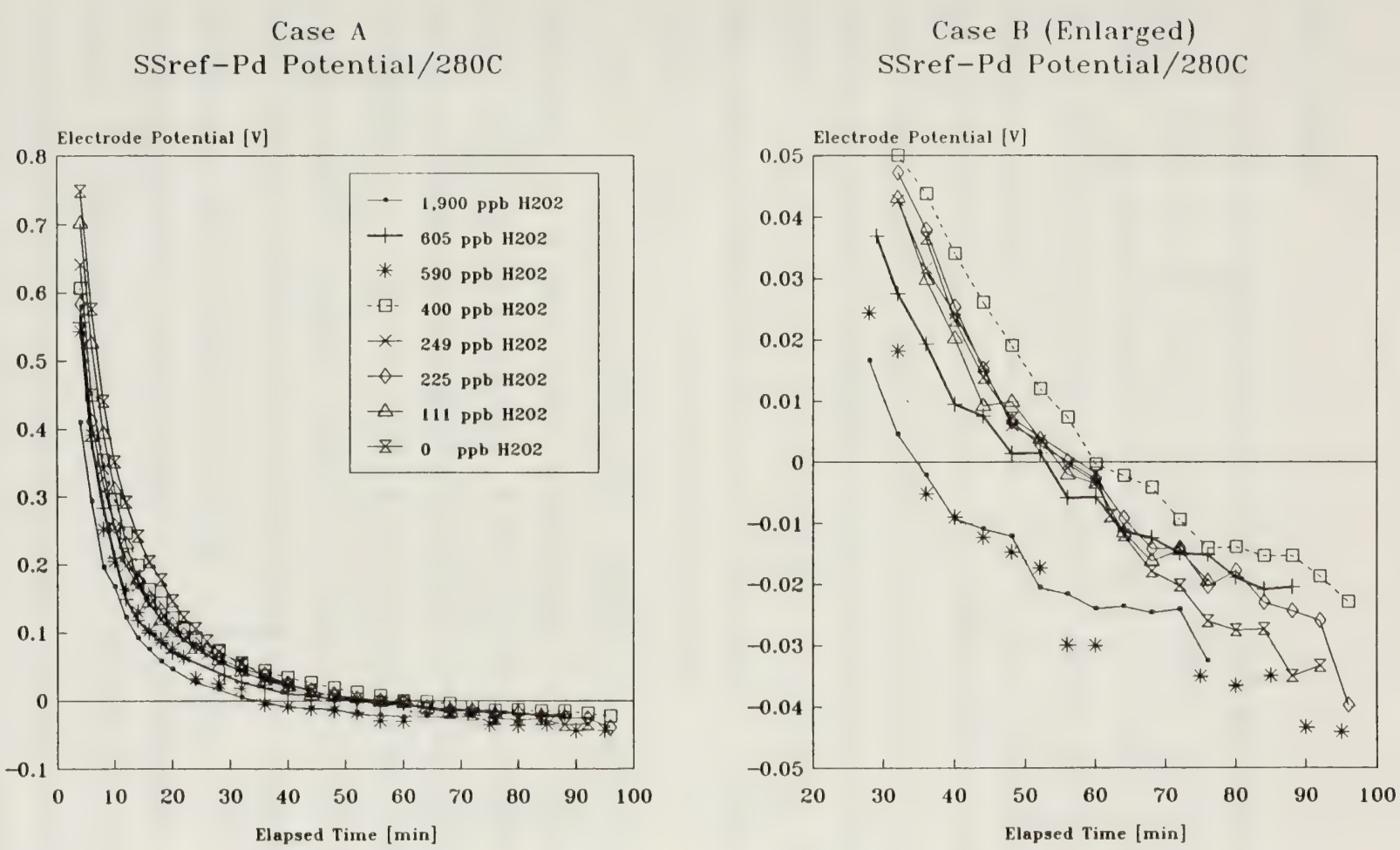

Figure 4.16: Composite Plot of E6(SSref-Pd) Potential

4.3.5 Summary

This chapter discussed the basic motivation for investigating alternate reference electrode configurations that would provide greater flexibility in measuring ECP within the BCCL. This electrode testing was an extension of work started by Driscoll[24]. In addition, this chapter discussed a high-temperature, high-pressure electrode feedthrough scheme that was built and tested successfully. A total of approximately 40 hours of successful high-temperature (280°C), high-pressure {10.3MPa (1500 psig)} operation were logged. This feedthrough configuration will permit short duration in-reactor support of BCCL operations using alternate electrode arrangements involving the separate, or paired, use of Pt, stainless steel, and Pd electrodes. Bench-top electrode testing involved cold reference runs (no added H_2O_2), hot reference runs and two sets of high-temperature experimental runs where the concentration of H_2O_2 was varied.

In the cold reference runs, the "aging" of the electrodes made the runs unreproducible. Cold stainless steel electrode behavior changed significantly after high-temperature operation, presumably due to passivation. Initial high-temperature behavior (no added H_2O_2) was reproducible. However, after exposure to high-temperature H_2O_2-doped coolant (concentrations up to 2 ppm) the electrode behavior (not just stainless steel electrodes) once again changed dramatically. Electrode H_2 charging times were progressively increased throughout the course of the testing to compensate for the apparent effects of electrode aging. However, complete, reproducible recovery was not achieved for either stainless steel or palladium. A charging period of 10 minutes, which produced satisfactory behavior at the beginning of the test series, appeared to be insufficient toward the end of the test series. Insufficient charging resulted in potential measurement behavior that lacked the extreme initial potential drift, and did not level out. In general, high-temperature

electrode potentials also exhibited an aging effect, in that the electrode potential spread, that was a function of H_2O_2 concentration, decreased with time (i.e. - the electrode potential range covered by the family of curves in Case B of Fig. 4.11 is less than the range of potentials covered by the curves in Case A of Fig. 4.11). However, in general, the higher the H_2O_2 concentration, the lower the magnitude of the measured potential relative to the zero H_2O_2 reference case. Comparison of this reported behavior with literature values is not meaningful at this point without electrode potentials measured relative to a SHE standard.

These preliminary high-temperature tests were inconclusive in determining the suitability of Pd as a SHE reference for possible future use in the BCCL. These tests were limited to approximately 100 minutes per run. Consequently, it is unknown whether or not the Pd potential will eventually reach equilibrium. Achieving equilibrium is important not only to permit use of Pd-relative potentials for analytic purposes, but it is also an important check on the adequacy of the Pd electrode's internal hydride inventory in supplying the necessary localized environment. Another concern was that the charging current density was inadequate to maximize the hydrogenation of the palladium. (A current density of approximately 1 milliamp/cm^2 was used.) Further testing is clearly in order. Other reference systems should be investigated such as tungsten[27], for example. Cathodic restoration of the Pt electrode should also be evaluated.

Chapter 5. BCCL Radiolysis Chemistry Computer Code

5.1 Introduction

Simonson[14] developed a radiolysis chemistry computer code, MITIRAD, to support his work, which was focused on the transient behavior of nuclear waste package corrosion. In order to provide a model for predicting the steady-state behavior of coolant chemistry in the BCCL, significant changes were required to accommodate the non-isothermal and two-phase flow aspects of the BCCL. In addition, as noted by Lin et al.[16], Ibe and Uchida,[28,29] Takagi et al.[17,26], and others[1,30], the heterogeneous decomposition of H_2O_2 on reactor surfaces is important. Consequently, the computer model must also be altered to include surface decomposition of H_2O_2.

The main features retained from MITIRAD were the chemical reaction handling routines, and the numerical method for solving systems of stiff, ordinary differential equations (developed by Hindmarsh[31]). The modified mathematical model was developed in parallel by the author, for adaptation to the BCCL, and by Chun[15], for adaptation to BWR power plants.

Parametric studies, involving the radiolytic source terms (G-values) and the chemical reaction equation sets, were done with a version of MITIRAD and with the author's code, BCCLMIT. The salient features of both sets of parametric studies are also discussed in this chapter.

5.2 Modification of the Radiolysis Chemistry Computer Model

5.2.1 Performance of the Existing Radiolysis Chemistry Code

According to Simonson[14], the main contributions of his radiolysis chemistry code were the ability to handle large sets of chemical reaction equations, and the ability to

perform sensitivity analyses (differential adjoint, or "importance" approach). The chemical reaction handling technique permits rapid (minimal conditional branching) matrix manipulation of large equation sets. The sensitivity analysis part of the code provides a tool for evaluating equation sets, both to identify equations containing possible errors and to identify which chemical equations (or radiolysis parameters) have the most significant effect. The intent was that those equations or parameters, which were most important to the code calculation could be flagged for priority research and refinement.

Although the subject equation handling technique is powerful, there are several significant limitations that the user must be aware of. First, the chemical reaction equation input format of the code uses an implicit reaction order representation. For example, the simple H_2O_2 decomposition expression,

$$H_2O_2 \rightarrow H_2O + \frac{1}{2}O_2 \qquad \text{Eq. 5.1}$$

and the following expression,

$$2H_2O_2 \rightarrow 2H_2O + O_2, \qquad \text{Eq. 5.2}$$

represent the same reaction. However, Eq. 5.2 would be interpreted as a second-order reaction whereas Eq. 5.1 would correctly be interpreted as the first-order reaction. The code implicitly assumes that the product of all reactants, even duplicated ones such as in Eq. 5.2, is multiplied by the rate coefficient, instead of explicitly entering the reaction order.

The second limitation of the chemical reaction equation format causes problems for non-mechanistic expressions and reaction products. For example, the correct interpretation of the above reactions is that 1 mole of O_2 is produced for every 2 moles of H_2O_2 consumed. The use of Eq. 5.1 would lead to the accumulation of a new species, "$\frac{1}{2}O_2$". Another

chemical reaction equation must be added to complete the chemical species balance by explicitly including the relation between "$\frac{1}{2}O_2$" and O_2. In general, the format only permits the direct input of integer (≤3 total for reactants and ≤ 4 total for products) stoichiometric coefficients. Overall reaction expressions that contain fractional stoichiometric coefficients must be partitioned into fundamental (or mechanistic), or pseudo-fundamental expressions with integer coefficients (using, for example, a "pseudo" species such as "$\frac{1}{2}O_2$"). The majority of equation sets were already in a form compatible with this equation set format. Therefore, adding reaction equations to compensate for the limitations in the equation set input format was not a significant handicap, and the benefits of this formatting approach outweighed the disadvantages.

5.2.2 Bench-Mark Comparison

The accuracy of MITIRAD (only the homogeneous, isothermal point kinetics part of the code was considered for this and subsequent discussions) was verified using the classical Bateman[32] equations and using a Cesium-Flare bench-mark calculation prepared by Edelson[33].

Figure 5.1 shows typical radiolytic chemical species concentration curves calculated by MITIRAD. For this calculation, gamma and neutron radiation dose rates were both 10^8 Rad/hr and all initial concentrations were set to zero. Gordon's[34] fast neutron (high LET*) radiolysis source term constants (G-values**) and Pikeav's[35] gamma (low LET) G-values

---

*- Linear Energy Transfer: The rate of energy deposition per unit track length from ionizing radiation. Typical units are keV/micrometer.

**- The number of chemical species (e.g. OH, H^+, etc.) produced per 100ev of absorbed dose from incident radiation. The quantity of species produced is a function of both the amount of, and the rate of, energy deposition.

were used for these calculations. Numerous case studies were run using MITIRAD to determine the most significant parameters. These studies provided the basis on which the BCCL model was developed.

5.2.3 BCCL Model Requirements

An integral approach was required to model the BCCL, instead of the homogeneous, point kinetics-type model employed in MITIRAD. This BCCL model must include the following items:

(1) Heterogeneous effects of H_2O_2 decomposition at the tube wall,

(2) Stripping of gaseous (principally O_2 and H_2) from the liquid phase by the steam bubbles,

(3) Temperature changes of the BCCL coolant from the inlet up to the point of inception of boiling,

(4) Coolant density changes corresponding to the temperature changes, and the effects of density change on the flow velocities and radiolysis source term calculations.

(5) Convective transport of chemical species in both phases, and

(6) Tracking of mass and mole balances through the different flow sections of the BCCL.

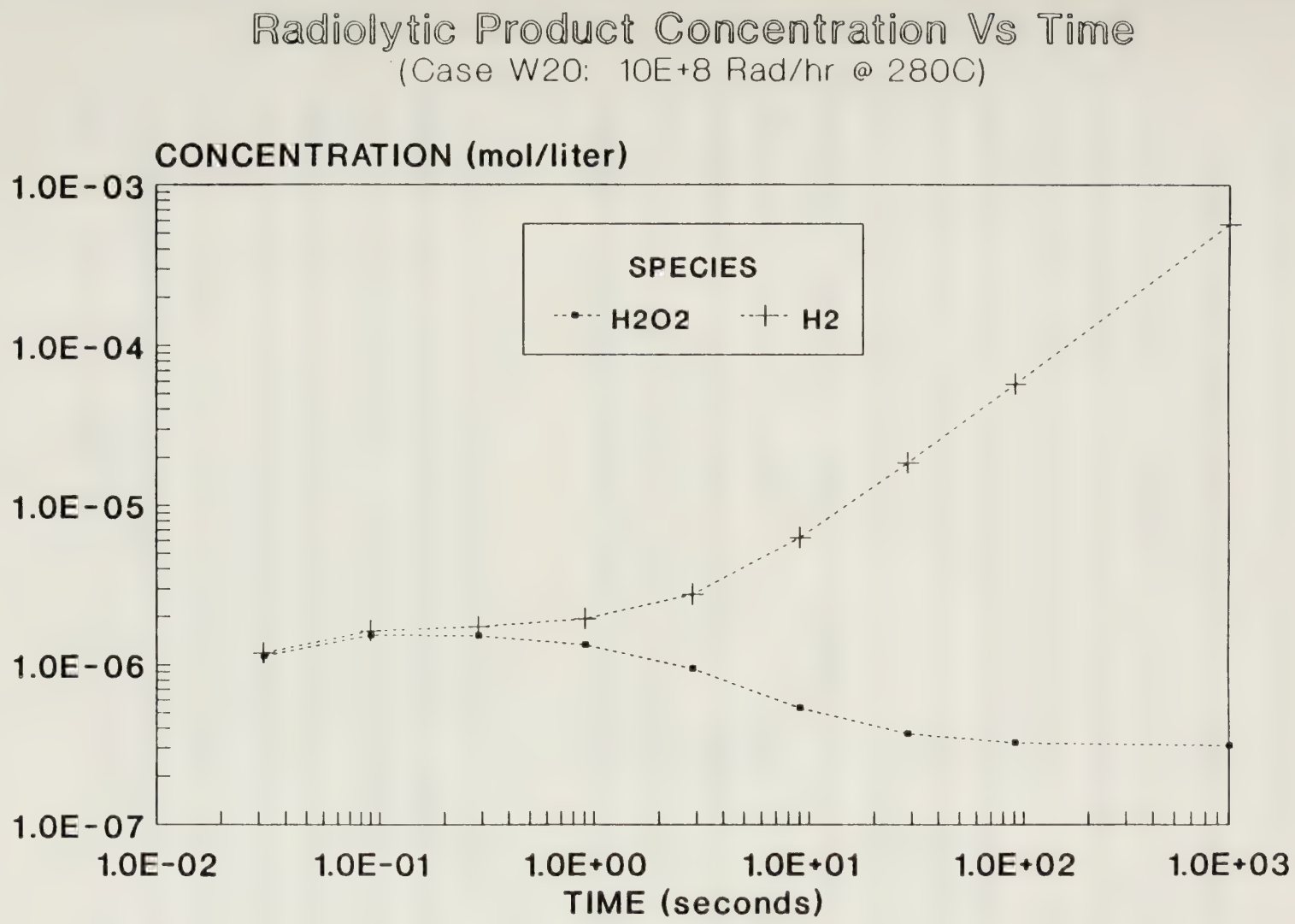

Figure 5.1
MITIRAD Radiolysis Calculation

5.2.3.1 Steady-State Mole Balance - Model Constraints

Different approaches have been taken for the modeling of radiolysis chemistry in a reactor environment. Ibe[28] developed a time-based water radiolysis model using a control-mass approach on the liquid phase. The vapor-phase species were tracked using an integral accumulation term to avoid the problem due to vapor velocity and liquid velocity differences. Takagi[26] used an approach based on a position-based (or spatial) control volume across the flow channel. Parallel liquid and vapor phase balances were then written describing each phase with a mass transfer intertie between the two phases at each spatial meshpoint. The approach used in BCCLMIT (same basic approach used by Chun[15]) is similar to that used by Takagi; however, the species concentration was explicitly solved for in the differential equation. The overall layout of BCCLMIT is similar to MITIRAD; however, the computational models within the subroutines are substantially different. The BCCLMIT program logic is shown in Fig. 5.2.

Several compromises and approximations are required to produce a workable computer model. The BCCLMIT model uses a simplistic one dimensional flow model which neglects axial dispersion. Axial dispersion and diffusion are assumed to be negligible with respect to the convective flow terms. Also, the generalized homogeneous reactions are assumed to be unaffected by surface reactions with the exception of the decomposition of H_2O_2, which is included in the model. The two-phase flow, gas absorption/stripping, surface decomposition and temperature dependence models, along with the applicable assumptions, are included in their respective sub-sections.

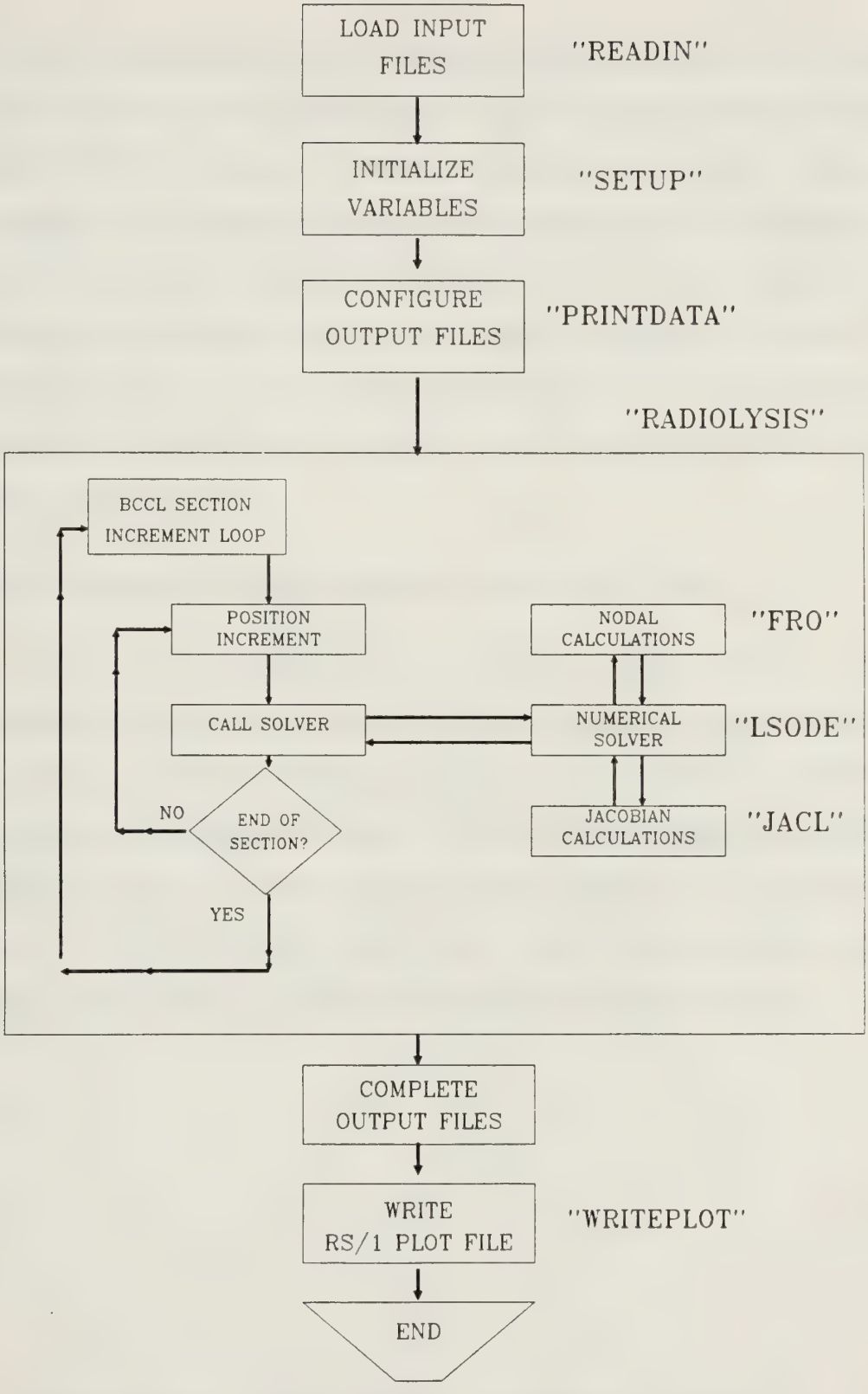

Figure 5.2: BCCLMIT Program Logic

Because of the complexities and uncertainties associated with the radiolysis source terms and the associated chemical reaction set, the macroscopic approach to the flow model (even the two-phase flow model) is considered to be justified. Subsequent refinement of the flow model should be carried out after comparison of predicted versus experimental results. For example, if radiolysis water chemistry at a location within a boiling channel is driven by the stripping of dissolved gases from the coolant, with negligible dependence on inlet conditions, the developmental focus should be on models that better characterize stripping and not on models, for example, that focus on quantifying axial dispersion.

5.2.3.2 Steady-State Mole Balance - Model Derivation

The following development is for the arbitrary species of interest, **i**, which is assumed to be present in both phases. Also, the details of temperature and density corrections are left out for clarity and simplicity. Parameters that are a function of temperature and density are assumed to be implicitly adjusted as described later in this chapter. The species, or mole balance provides the framework of the computational model. To derive it, we start with an arbitrary control volume of length **dx** across a boiling section of tubing. The species balance for the liquid phase is then

$$\frac{\partial(A^l C_i^l)}{\partial t} = -\left\{\frac{\partial(A^l C_i^l v^l)}{\partial x}\right\} \Leftarrow \{\text{Convection term}\}$$

$$+A^l\{G'_{i,\gamma}D_\gamma + G'_{i,nt}D_{nt}\}_{Rad} \Leftarrow \{\text{Radiolysis source term}\}$$

$$+A^l \sum_j^J k_j \mu_{i,j} \prod_n^N (C_n^l)^{|\mu_{i,n}|} \Leftarrow \{\text{Generalized reaction term}\}$$

$$-A^l\left(\frac{k_i^{ref} d^{ref}}{d^{section}}\right)C_i^l \Leftarrow \{\text{Surface decomposition term}\}$$

$$+A^g\{\eta^* C_i^g - \eta C_i^l\}_{Abs}; \Leftarrow \{\text{Gas absorption term}\} \qquad \text{Eq. 5.3}$$

where ***l*** = liquid phase,

g = vapor phase,

i = species of interest,

A = cross sectional area,

C = molar concentration of species,

v = fluid velocity,

x = axial position in tube,

G' = G-value in converted units,

D = dose rate,

k = rate coefficient,

η^* = gas absorption coefficient,

η = gas stripping coefficient,

μ = reaction stoichiometric coefficient,

$\frac{d^{ref}}{d^{section}}$ = ratio of tubing I.D. to scale k^{ref},

J = # of reactions involving species,

N = # of reactants for reaction #***j***, and

n = one of the ***N*** reactants whose numerical value corresponds to the appropriate reactant species.

Next, since this is for steady flow conditions, the time derivative in Eq. 5.3 is equal to zero. The convective term in Eq. 5.3 is then expanded using the chain rule and rearranged yielding

$$\frac{\partial C_i^l}{\partial x} = \frac{1}{v^l}\left\{ \quad \right\}_{Rad} + \sum_j^J k_j \mu_{i,j} \prod_n^N (C_n^l)^{|\mu_{i,n}|} - \left(\frac{k_i^{ref} d^{ref}}{d^{section}}\right) C_i^l \Bigg\}_I$$

$$+\frac{1}{v^l}\left\{\frac{v_f}{1-v_f}\right\}\{\eta^* C_i^g - \eta C_i^l\}_{Abs} - \frac{C_i^l}{A^l}\left\{\frac{\partial A^l}{\partial x}\right\} - \frac{C_i^l}{v^l}\left\{\frac{\partial v^l}{\partial x}\right\}; \qquad \text{Eq. 5.4}$$

where v_f = void fraction (ratio of vapor phase cross-sectional area to total cross sectional area).

To complete Eq. 5.4, the partial derivatives of A and v with respect to x are evaluated using the respective defining relations. First,

$$A^l = (1 - v_f) A^{total}; \qquad \text{Eq. 5.5}$$

therefore,

$$\left\{\frac{\partial A^l}{\partial x}\right\} = -A^{total}\left\{\frac{\partial v_f}{\partial x}\right\}. \qquad \text{Eq. 5.6}$$

This partial derivative is further resolved using Bankoff's[36] relations for v_f, etc.,

$$v_f = \frac{K}{1 - \frac{\rho^g}{\rho^l}\left\{1 - \frac{1}{q}\right\}}; \qquad \text{Eq. 5.7}$$

where K = 0.71 + 0.00143P [atm],

$\frac{\rho^g}{\rho^l}$ = density ratio, and

q = steam quality (fractional).

The derivative is then

$$\left\{\frac{\partial v_f}{\partial x}\right\} = \frac{v_f^2 \rho^g}{K q^2 \rho^l}\left\{\frac{dq}{dx}\right\}, \qquad \text{Eq. 5.8}$$

and

$$\left\{\frac{dq}{dx}\right\} = \text{Constant} = \left\{\frac{q_{exit}}{Boiling\ \ Length}\right\}. \qquad \text{Eq. 5.9}$$

The second step is to determine $\{\partial v^l/\partial x\}$. We start with the basic expression

$$v^l = \frac{v_o}{1 - v_f\left\{1 - S_L\frac{\rho^g}{\rho^l}\right\}}, \qquad \text{Eq. 5.10}$$

where v_o = reference liquid velocity at onset of boiling, and

S_L = slip ratio (velocity of vapor stream divided by the velocity of the liquid stream).

Taking the derivative of Eq. 5.10, and then rearranging terms, yields

$$\left\{\frac{\partial v^l}{\partial x}\right\} = -\frac{(v^l)^2}{v_o}\left[\left\{\frac{\partial v_f}{\partial x}\right\}\left\{S_L\frac{\rho^g}{\rho^l} - 1\right\} + v_f\frac{\rho^g}{\rho^l}\left\{\frac{dS_L}{dx}\right\}\right]. \qquad \text{Eq. 5.11}$$

Finally, the derivative of the slip ratio is required. Once again starting with the basic relation (Bankoff's formulation)

$$S_L = \frac{1 - v_f}{K - v_f}, \qquad \text{Eq. 5.12}$$

and taking its derivative, yields

$$\left\{\frac{dS_L}{dx}\right\} = \left\{\frac{\partial v_f}{\partial x}\right\}\frac{S_L - 1}{K - v_f}. \qquad \text{Eq. 5.13}$$

A parallel expression to Eq. 5.4 is then developed for the vapor phase. The most significant differences are (1) the vapor phase velocity is a function of the slip ratio and liquid phase velocity, (2) vapor phase radiolysis is neglected, and (3) vapor phase chemical reactions are neglected. Therefore,

$$\left\{\frac{\partial v^g}{\partial x}\right\} = v^l\left\{\frac{dS_L}{dx}\right\} + S_L\left\{\frac{\partial v^l}{\partial x}\right\}, \qquad \text{Eq. 5.14}$$

and the vapor phase relation parallel to Eq. 5.4 is then

$$\left\{\frac{\partial C_i^g}{\partial x}\right\} = \frac{1}{v^g}\left\{[\eta C_i^l - \eta^* C_i^g]_{\text{Abs}} - \frac{C_i^g v^g}{A^g}\left\{\frac{\partial A^g}{\partial x}\right\} - C_i^g\left\{\frac{\partial v^g}{\partial x}\right\}\right\}. \qquad \text{Eq. 5.15}$$

The bases for neglecting the vapor phase radiolysis source and chemical reactions are twofold. First, since the vapor density is much less than the liquid density, the concentration of reactants and their residence time is small compared to those in the liquid phase. Second, the primary species of interest in the gas phase, O_2 and H_2, are primarily characterized by the mass transfer (stripping and absorption) reactions[28] which are retained in Eq. 5.15. More-detailed descriptions of the mass transfer model and the surface decomposition model are included in the following sections of this chapter.

5.2.3.3 Temperature and Density Compensation

Temperature and density compensation must be compatible with both the model and the chemical reaction kinetics data. An Arrhenius exponential model is the primary one used to correlate the temperature dependence of reaction rate coefficients. However, based on work by Elliot et al.[37], large errors can result by assuming an Arrhenius model over a large temperature range. Figure 5.3 (from Elliot's Fig.6) shows an Arrhenius plot and non-linear rate coefficient curves. Although an Arrhenius model is a good temperature correction model for kinetics-limited reactions, the chemical

reactions of interest may be diffusion-limited, or combined (as in series resistances). Consequently, an effective overall rate coefficient does not correlate well over a large temperature range using an Arrhenius model. An accurate temperature scaling model would need to include the temperature correction model for diffusion-limited reactions, in addition to the Arrhenius model for the reaction-limited component. The overall rate coefficient for each chemical reaction would then be calculated from the two separate component reaction coefficients.

There are two additional options for providing adequate temperature compensation in the code, short of the aforementioned more rigorous approach. First, since BCCL operation would cover a temperature range of less than 20°C between the BCCL feedwater (simulated downcomer outlet conditions) and saturation temperature, an effective activation energy (slope of the rate coefficient curve multiplied by the universal gas constant) can be taken from a plot such as Fig. 5.3. The rate coefficient curves shown in Fig. 5.3 cover a wide temperature range, and using a linear segment for a narrow temperature band would not normally introduce significant error. This effective activation energy would then provide a valid temperature correction using an Arrhenius model for those reactions that have some degree of diffusion-controlled effects. The second option available to provide temperature compensation without separate diffusion- and kinetics-limited reaction models is to use parallel forward and reverse reactions with the respective rate coefficients and activation energies adjusted to fit the non-linear rate coefficient curves.

Given the options available to subsequent users of the code to accommodate future high-temperature rate coefficient data, the author kept the basic Arrhenius model in MITIRAD. In MITIRAD, temperature compensation occurred in the equivalent

SET-UP subroutine (see Fig. 5.2). To provide the desired temperature compensation in BCCLMIT, the temperature control logic and temperature correction were built into the subroutine FRO, which updates parameters for each spatial meshpoint.

Three user-specified parameters control temperature variations: inlet temperature, outlet temperature and the presence or absence of boiling. In all cases inlet flow is assumed isothermal up to the point the flow enters the core region. For the boiling case, the temperature is assumed to increase linearly from the core inlet up to the saturation temperature at the point corresponding to the inception of boiling. This linear relationship is based on an assumed constant heat flux into the core tubing, and negligible variation in the coolant heat capacity. For the non-boiling case, the temperature varies linearly from the inlet temperature at the core inlet to the outlet temperature at the core exit. All BCCL sections downstream of the core are assumed to be isothermal at the outlet temperature.

Rate Coefficients for Hydrated Electron Reactions with Nitrogenous Species

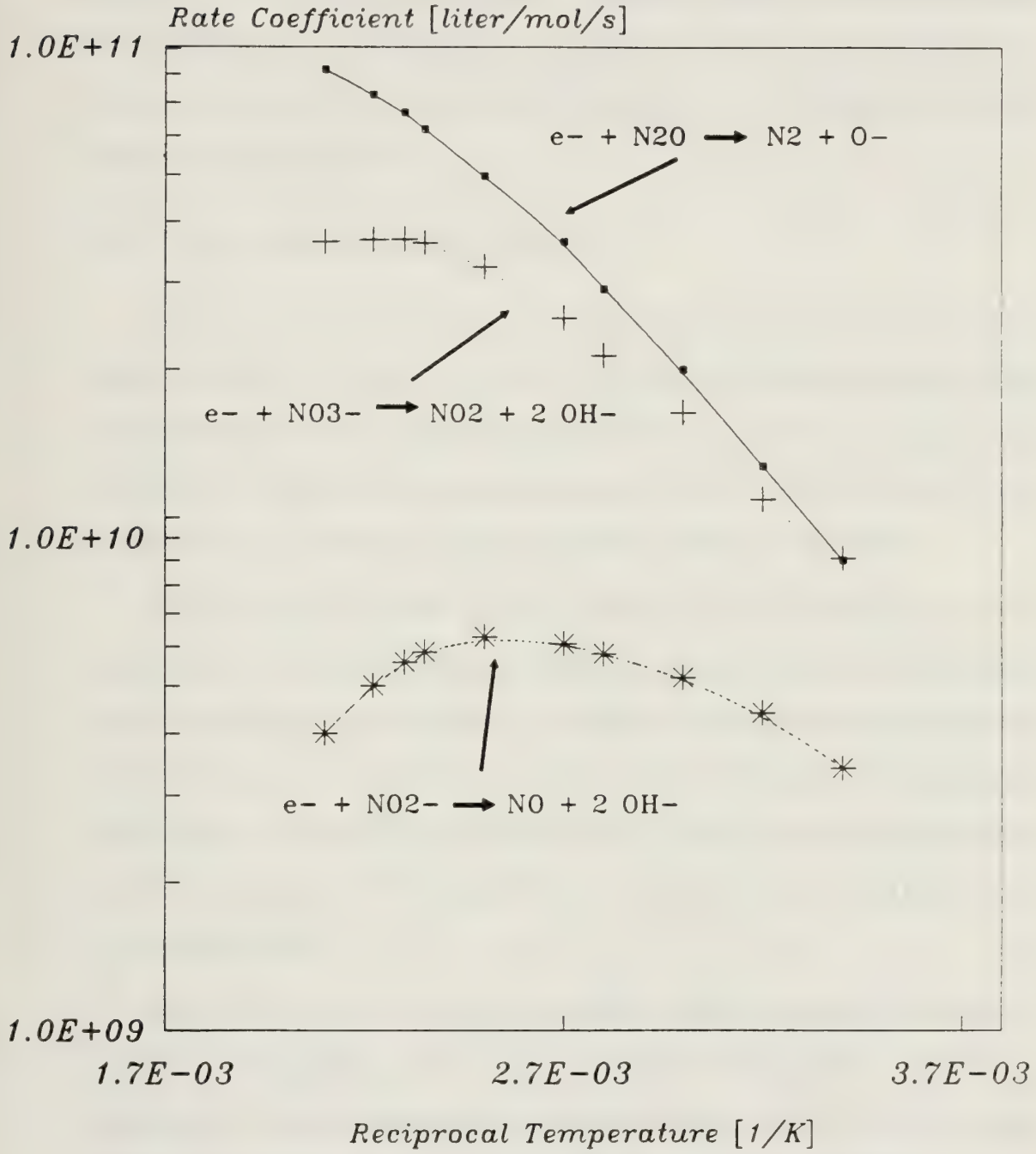

Figure 5.3: Examples of Non-Arrhenius Rate Coefficient Behavior

The density compensation parallels that of the temperature compensation in the computer code. A rudimentary approach is to interpolate linearly between the inlet and outlet densities over the same spatial span as the temperature interpolation. Errors due to the non-linear temperature dependence of density are small over the relatively narrow temperature range of interest.

5.2.3.4 Two-Phase Stripping Model

Ibe[28,29] and Takagi[26] both use the same model for interphase mass transfer in their respective radiolysis models. Ibe developed his model from fundamental local mass transfer coefficients for each species diffusing from the liquid to the vapor phase. These coefficients were calculated using a penetration theory model. The reverse mass transfer coefficient was then determined using an equilibrium Henry's Law constant.

After presenting this model for vapor phase stripping, Ibe introduced correction factors to account for non-equilibrium conditions. These correction factors were then determined by fitting experimental data. Takagi arrived at the same final model directly using the concept of forward and reverse mass transfer coefficients. With the current limited ability to characterize two-phase bubble dynamics and other fundamental variables, Ibe's approach does not at present provide additional precision in modeling the stripping process.

Ibe made parametric studies of the importance of the mass transfer coefficients as well as to what numerical values best approximated BWR performance. Given the high degree of channel similitude between the BCCL and a BWR, the following values from Table VII of Ref. 29 are the basis for the values used in BCCLMIT:

Table 5.1 Gas Absorption / Stripping Coefficients		
Coefficient	**Hydrogen [s^{-1}]**	**Oxygen [s^{-1}]**
Gas Stripping	30	23
Gas Absorption	9.9	12.4

Lukac[30] reported hydrogen (and deuterium) stripping data which indicate that the vapor phase gas concentrations are approximately three times the equilibrium values predicted by Henry's Law. His results are consistent with the ratio of stripping rate coefficients to absorption rate coefficients in Table 5.1.

5.2.3.5 H_2O_2 Surface Decomposition - Model Development

Based on reports in the literature (e.g. - Lin et al.[16] and Ullberg et al.[1]), the heterogeneous surface decomposition of H_2O_2 follows a first-order kinetics-limited rate model. The data discussed in Chapter 2 also supports first-order rate law dependence. Lin et al. performed H_2O_2 decomposition rate measurements using different materials. They also considered surface catalyzed, homogeneously catalyzed (i.e. - dissolved ions), and thermal decomposition. For the high surface-to-volume ratios typical of the core region of a BWR (and in the absence of significant dissolved catalytic species), H_2O_2 is sufficiently stable so that decomposition is dominated by surface decomposition. The BCCL uses titanium for high-temperature ex-core fluid boundaries to minimize H_2O_2 decomposition by dissolved chemical species. Consequently, the program BCCLMIT only considers surface and thermal decomposition.

The surface decomposition term in Eq. 5.3 is derived from a basic mole balance. Therefore, we start with a control volume across a single-phase (liquid), constant flow area tube of length Δx (x is distance along radial axis of tube). Next, making the assumptions that there are no radial concentration and velocity gradients, and the reaction is kinetics-limited, a simple steady-flow mole balance for this differential control volume yields

$$C_x \cdot A_f \cdot v \;=\; C_{x+\Delta x} \cdot A_f \cdot v \;+\; k_s \cdot A_s \cdot \overline{C}, \qquad \text{Eq. 5.16}$$

where $\mathbf{C}$ = Concentration of the species of interest [moles/liter],

$\mathbf{A_f}$ = Cross-section flow area [cm^2],

$\mathbf{v}$ = average flow velocity [cm/s],

$\mathbf{A_s}$ = $\pi \cdot D \cdot \Delta x$,

$\mathbf{D}$ = tube inside diameter [cm],

$\mathbf{k_s}$ = surface rate constant [cm/s], and

$\overline{C}$ = "average" concentration at the surface.

Equation 5.14 is then rearranged to yield

$$\left\{\frac{C_{x+\Delta x} - C_x}{\Delta x}\right\} \;=\; -\left\{\frac{4 \cdot k_s}{v \cdot D}\right\}\overline{C}. \qquad \text{Eq. 5.17}$$

We now take the limit of Eq. 5.17 as Δx goes to zero. In the limit, $\overline{C} \approx C$ and Eq. 5.17 becomes

$$\left\{\frac{dC}{dx}\right\} \;=\; -\frac{k'}{v}C, \qquad \text{Eq. 5.18}$$

where k' = $4k_s/D$.

k' is the actual rate constant which is experimentally determined. To find k'_2 for a tube of diameter D_2, we first solve for k_s in terms of the k' measured for the reference tube of D_1

$$k_s = \frac{D_1 \cdot k'_1}{4}. \qquad \text{Eq. 5.19}$$

k'_2 can then be expressed in terms of k_s, and then substitute Eq. 5.19 in to yield k'_2 in terms of k':

$$k'_2 = \frac{4k_s}{D_2} = \frac{4}{D_2}\left(\frac{D_1 k'}{4}\right) = \frac{D_1}{D_2}k'. \qquad \text{Eq. 5.20}$$

Equation 5.20 forms the basis for the surface decomposition rate coefficient scaling for the different diameter BCCL sections. This surface decomposition rate coefficient model together with Eq. 5.18 constitute the surface decomposition term in Eq. 5.4.

The above mole balance was for a single-phase system; the problem is complicated significantly when the second phase is added. However, there are two limiting cases that bound the expected surface decomposition behavior. The first case assumes both phases are homogeneously mixed, and, therefore, the liquid fraction (fraction of the total cross-sectional area not occupied by the vapor phase) would be a valid indicator of the fraction of the surface area contacted by the liquid phase. Consequently, the cross-sectional area term and the surface area term of Eq. 5.16 would be multiplied by $(1\text{-}v_f)$. These void fraction correction terms would then cancel and the result would be the same as the single-phase derivation. The other two-phase case is annular flow. With perfect annular flow, only the liquid phase contacts the surface. Therefore, the

$(1-v_f)$ term only multiplies the cross-sectional area term. Consequently, for the annular flow case, Eq. 5.18 becomes

$$\left\{\frac{dC}{dx}\right\} = -\frac{k'}{(1-v_f)v}C. \qquad \text{Eq. 5.21}$$

The homogeneous case and the annular flow case are both readily adapted to the computer model. Unfortunately, the expected two-phase flow dynamics for the BCCL are neither homogeneous nor annular in behavior. To ascertain what the best two-phase surface decomposition model is for the BCCL, the two-phase flow must first be analyzed. Based on the two-phase flow analysis in Todreas and Kazimi[38], the total mass flux (G) and phase velocities (j_v and j_l) are calculated first. Two different diameter tubes are evaluated: D_c is the I.D. of the Zircaloy core tubing (0.645 cm), and D_t is the I.D. of the ex-core titanium tubing (0.460 cm). The mass flux for the core tubing is

$$G_c = \frac{\left(27\frac{g}{s}\right)\left(\frac{1kg}{1000g}\right)}{\left(\frac{\pi}{4}D^2\right)\left(\frac{1m^2}{10000cm^2}\right)} = 826\frac{kg}{m^2\cdot s}. \qquad \text{Eq. 5.22}$$

Similarly, G_t equals 1625 kg/(m^2 s).

The liquid phase velocity for the core tubing is

$$j_{l,c} = \frac{G_c(1-q)}{\rho^l} = \frac{826(1-0.1)}{741} = 1.00\frac{m}{s}, \qquad \text{Eq. 5.23}$$

and, similarly, the other phase velocities are:

$j_{l,t}$ = 1.97 m/s,

$j_{v,c}$ = 2.28 m/s, and

$j_{v,t}$ = 4.49 m/s.

Using these parameters, the RELAP-5[39] flow regime map suggests slug flow exists for both BCCL tube sizes. The Hewitt and Roberts[40] flow regime map puts the smaller diameter titanium tubing more into the wispy-annular regime; however, Hewitt and Roberts flow map is based on air-water studies at 25°C. Based on the RELAP-5 predictions, the void fraction (estimated to be 56% when steam quality is 10%) is too low for annular flow to develop. In either case, BCCL flow dynamics are between the two limiting cases previously discussed.

Another complication is that the governing mole balance does not account for the enhanced axial dispersion (i.e. - entrainment) resulting from non-homogeneous two-phase flow. This enhanced axial dispersion would tend to reduce surface decomposition, whereas non-homogeneous two-phase flow would tend to increase the effects of surface decomposition by effectively increasing the surface-to-volume (liquid volume) ratio. If surface decomposition was the only mechanism, or even the principal mechanism, controlling the concentration of H_2O_2, Eq. 5.21 could be modified by replacing $(1-v_f)$ with $(1-v_f)^n$ where **n** would be fitted to experimental results. Theoretically, this added parameter **n** would be a measure of the heterogeneity of the two-phase flow; **n** equal to zero corresponding to homogeneous two-phase flow (and single phase flow), and **n** equal to 1 corresponding to annular flow. However, depending on the relative importance of the surface decomposition mechanism, as compared to the total H_2O_2 balance within a two-phase flow region, the effects of two-phase axial dispersion (currently considered by the author to be second-order effects) may be more significant than the $(1-v_f)$ factor in Eq. 5.21. Consequently, **n** could take on values greater than one, and values less than zero.

Based on initial BCCLMIT calculations, surface decomposition is not the dominant mechanism controlling the concentration of H_2O_2 in the core region. However, the relative importance of surface decomposition increases as the radiolytic source of H_2O_2 decreases with distance above the core region. In any case, without a priori knowledge of the relative importance of enhanced axial dispersion as compared to enhanced surface decomposition (included in Eq. 5.21), the author chose n equal to zero, which corresponds to the surface decomposition model of Eq. 5.18 (homogeneous case). The heterogeneous model of Eq. 5.21 can be added later as a second-order refinement when the principal two-phase flow approximations, such as the gas absorption/stripping correlations and the slip-flow model based on upward flow through vertical tubing*, are validated by BCCL operation.

5.2.3.6 H_2O_2 Surface Decomposition - Rate Coefficients

Lin et al.[16] reported negligible difference between the H_2O_2 decomposition rate coefficients for stainless steel and titanium. Their data are consistent with the present author's findings, as discussed in Chapter 2. Although BCCLMIT includes provisions for different rate expressions for the different materials of construction (i.e. - Zircaloy in-core and titanium elsewhere), data for Zircaloy are not available. Consequently, the same surface decomposition rate data were used for all BCCL sections (but corrected for section diameter changes).

As discussed in the previous section, the H_2O_2 surface decomposition model must take into account the variation in the surface-to-volume ratio. Lin et al.[16] performed

---

*- The BCCL in-core boiling section starts on the down-flow side of the U-tube section (see Fig. 1.2) before passing through the U-bend and flowing up through the remaining half of the in-core section.

some parallel tests using 0.635 cm (0.25 in) and 1.27 cm (0.5 in) O.D. tubing. Scaling these experimental data for two different tube sizes using estimated I.D. values, gave results which agreed well with the ratio of their I.D.s, as predicted by the analytic model (single-phase) described in the preceding section. In addition, as discussed in Section 5.3, this surface-to-volume scaling technique worked well for comparing Lin's data with data reported in Chapter 2.

5.2.4 Computer Code Modifications

The computational model described in section 5.2.3 is significantly different from the model used by Simonson in MITIRAD. However, the general equation handling methods and subroutine layout of MITIRAD provided the framework for the present work. MITIRAD was modified by Chun[15] (MITIRAD Version MIT5.0) to model a BWR core region using a computational model comparable to the model discussed in Section 5.2.3 above. This computational model was tailored by the present author for the BCCL, to include appropriate two-phase flow parameters and to include provisions for mass balances between the various sections of the BCCL. This code modification (MITIRAD Version MIT5.1) for the BCCL is named BCCLMIT. The overall BCCLMIT program logic is shown in Fig. 5.2.

BCCLMIT is written to run on a DIGITAL Micro-Vax computer using MICROVMS version 5.0 and Vax FORTRAN compiler version 4.2. The BCCLMIT code is listed in Appendix D.1. Input and output format and BCCL section descriptions are included in the Version 5.1 Note at the front of the program listing. In addition, all code variables and logic control flags are defined in this description section of the listed code. The program is organized into documented logic or function blocks to facilitate future modification or expansion.

All code calculations are done on a concentration basis (moles/liter) at the actual temperature (and therefore fluid density) of the position (spatial) meshpoint. User-specified initial conditions must be in moles/liter referenced to water at 25°C. The output format is either in moles/liter or ppb (mass basis) normalized to water at 25°C.

The code produces two output files. The first type of output file is formatted in tabular form for each section and position increment*. A sample output file of this type is included in Appendix D.2. The second type of output file is optional. This second type of file is called the plot file since it is a serial listing of the same data included in the other output file format. This plot file format is easily read by graphics packages such as RS/1 on the Micro-Vax.

When running the program, the user must specify the input file name. The input file provides the user-specified options as well as the reaction equation set, chemical species data, initial concentrations and loop section geometry information. A sample input file, which corresponds to the sample output file, is included in Appendix D.3. BCCLMIT currently has a 12 section default; however, the user can explicitly define the control variable "ID4" in the "$CONTROL" namelist of the input file. The value specified for "ID4" will be the number of Section descriptions the code reads into the code. (However, if "ID4" is set to a value less than 8, two-phase calculations will give error messages.)

---

*- The position increment step size within BCCL sections is user-specified and does not affect the accuracy of the calculation. The actual computational meshpoint spacing is internally calculated by LSODE (see Fig. 5.2); the size depends on the stiffness of the equation set at the position of interest.

5.3 BCCLMIT Bench-Mark Calculations

Prior to using BCCLMIT for predictive calculations, the code was used to reproduce an analytic calculation, and was compared with available experimental results to verify proper program execution. BCCLMIT reproduced the simple Bateman equation calculation, as did Simonson's MITIRAD. However, the best available evaluation of the validity of the BCCLMIT model at this time was comparison with bench-top experimental data.

The most significant comparisons are (1) the isothermal sample line calibration data reported in Chapter 2, and (2) the H_2O_2 decomposition tests (non-isothermal), also reported in Chapter 2. A plot of the BCCLMIT calculated H_2O_2 concentration profile is shown in Fig. 5.4. Figure 5.4 shows an approximate 49% H_2O_2 decomposition between the inlet and outlet H_2O_2 concentrations for the case with 2.5cm uncooled tube length. The calculated value for the percent decomposition of H_2O_2 agrees closely with the experimental value of 50% shown in Table 2.1. This comparison, however, is for a case which has one of the best matches between predicted and measured values. The code does not, for example, accurately predict the experimental result for the water-cooled probe runs (Fig. 2.3 and Fig. 3.2). There are two assumptions that are violated in attempting to reproduce this latter category of runs. First, in this instance the code was set up for spatial mesh sizes 1 cm and greater (the numerical solver, LSODE, is capable of much smaller step sizes with proper initialization), which is smaller than would typically be needed for BCCL calculations. Second, the model assumes no temperature or concentration gradients in the radial (as referenced from the tubing axis) direction. These assumptions, however, are considered to be valid for modeling BCCL behavior.

To calculate the curve shown in Fig. 5.4, the inlet temperature was held constant at 280°C for 2.5cm (the uncooled tube length), after which the temperature drops to 30°C over a 1 cm distance. Consequently, from position 3.5 in Fig. 5.4 to the end of the tubing, negligible

decomposition occurs. An interesting feature of Fig. 5.4 is the more negative slope in the H_2O_2 concentration curve from the point cooling starts (2.5cm) to the point at which the sample is estimated to be cool (3.5cm). If no cooling occurred, the H_2O_2 concentration at 3.5cm would be 132ppb instead of 152ppb; therefore, cooling did indeed slow the decomposition. The slope variation is mainly an artifact of the rapid water density change (the concentrations are normalized to the density of water at 25°C).

The predicted concentrations shown in Fig. 5.4 are sensitive to small variations in the uncooled length of sample tubing (2.5cm). However, the length over which the sample is assumed to be cooled (1cm in the above case) also influences the predicted H_2O_2 concentration, and the flowrate affects the predicted value. These latter two variables have a second-order effect, however. Experimentally, as reported in Chapters 2 and 3, varying flow rates within the laminar flow range of about 300 to 400 cc/hr had an insignificant effect on measured H_2O_2 decomposition. For the calculated result, decreasing the flow rate 10% resulted in a 2% increase in decomposition, which was within the accuracy of the experimental results. The selected value (1cm) of the other variable, the length over which the sample flow is estimated to be cooled, is more subjective. However, doubling this length to 2cm increased the predicted H_2O_2 decomposition by less than 5%.

Figure 5.5 shows the predicted H_2O_2 concentration profile through the BCCL sample system. Temperature gradients along the sample cooling block's inlet tubing nipples (see Fig. 3.1) have only been estimated. Based on the experimental result of 35% H_2O_2 decomposition through the sample cooling block, a cooling length of 5 cm (the distance over which the sample temperature drops from 280°C to the estimated final 85°C) yielded the corresponding predicted decomposition from the code. The 5 cm cooling length is a physically realistic value since it corresponds to the approximate distance from the sampling point to the main section of the

cooling block. To obtain a conservatively high limit, the sample is assumed to remain at the sample block reference temperature as it flows through the remaining length of the sample cooling block and sample system tubing. Using the 5 cm cooling length, the H_2O_2 concentration profile in Fig. 5.5 correlates well with both the measured sample block percent decomposition and the isothermal sample line calibrations.

5.4 Evaluation of Radiolysis Source Term Data (G-values)

Considerable research has been performed to quantify the radiolysis source coefficients, or the G-values, for gamma irradiation, and to a lesser extent, neutron irradiation of water. In general the G-values are a function of the energy deposition rate of the incident radiation and the temperature of the medium. The G-values specify the number of chemical species produced per 100 ergs of absorbed energy. The numerical values for these coefficients are usually categorized by whether it is gamma or neutron radiation, and, particularly for neutrons, the energy of the incident radiation. There are some inconsistencies in the literature as to the temperature dependence of the G-values. For example, the gamma G-values reported by Burns and Marsh[41] for high temperature vary considerably from those at 25°C, whereas the values reported by Elliot[42,43] show only a very modest temperature dependence. Indeed, this modest temperature dependence is also consistent with some EPRI[44] work, and Ibe's work[28,29], where the 25°C G-values reported by Burns and Marsh are used at BWR operating temperatures.

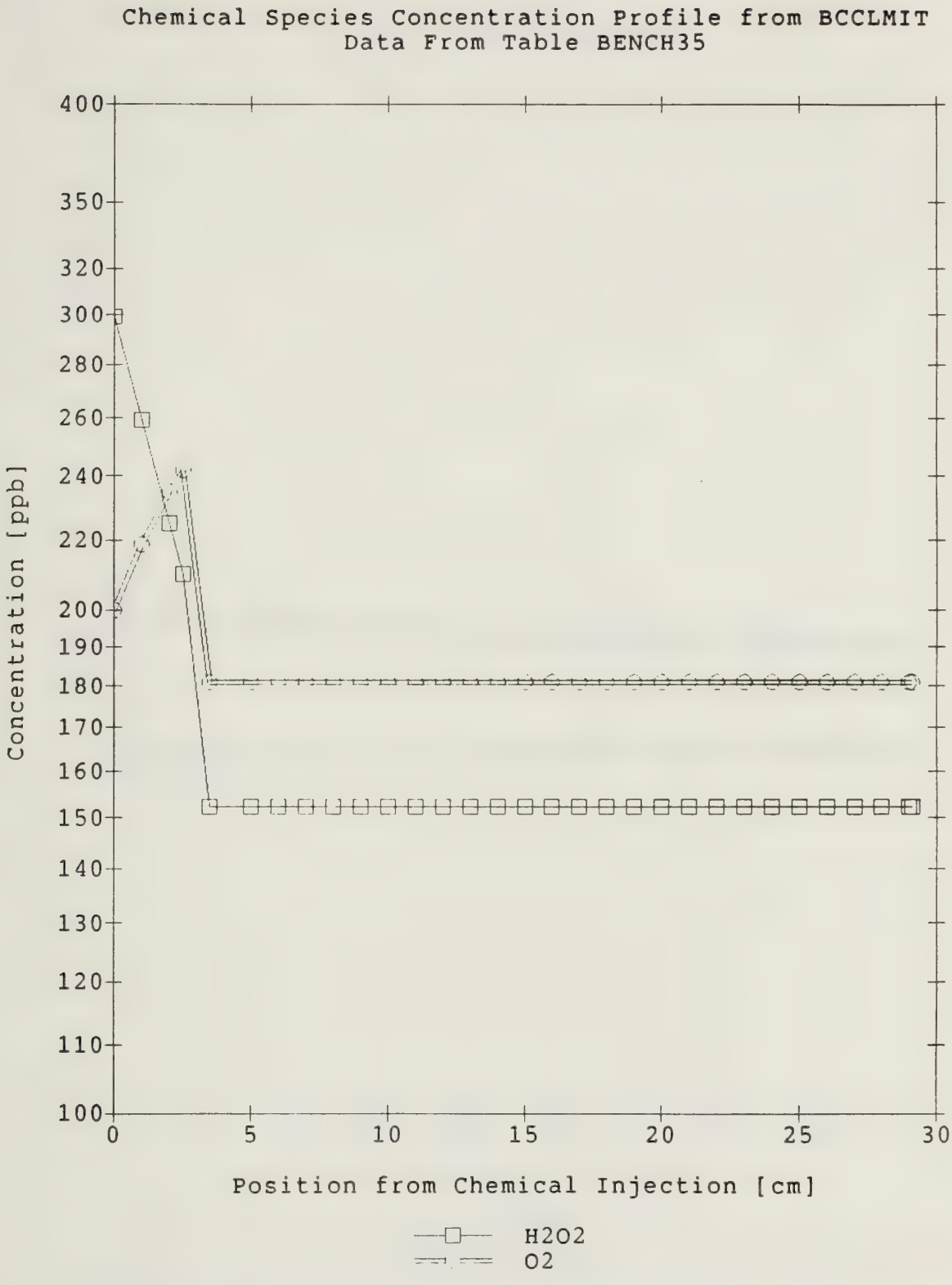

FIGURE 5.4: CONCENTRATION PROFILE FOR 2.5CM UNCOOLED TUBE

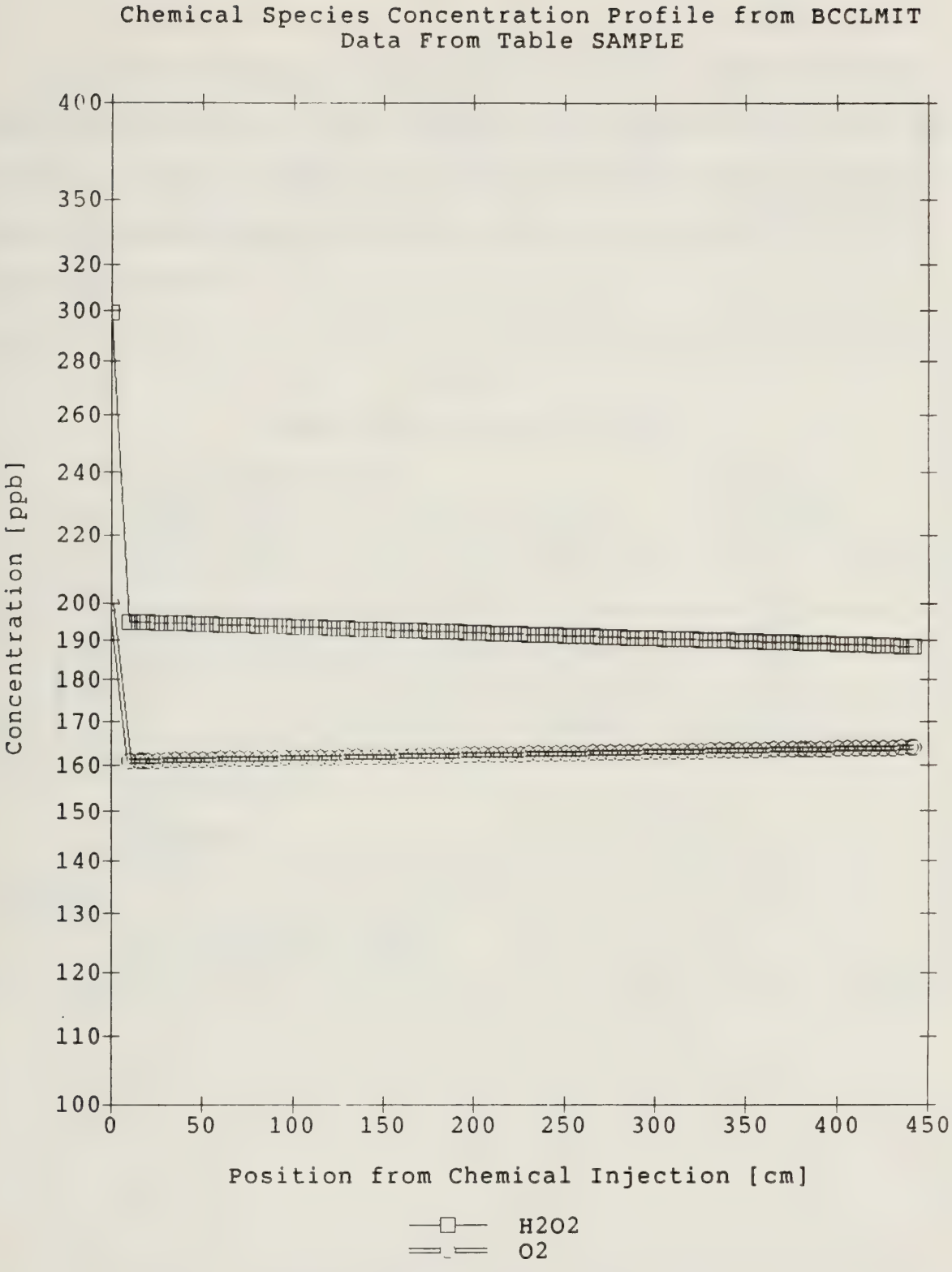

FIGURE 5.5: BCCL SAMPLE SYSTEM CONCENTRATION PROFILE

Several sets of G-values were compiled for parametric studies. Table 5.2 lists the gamma irradiation G-values surveyed. Table 5.3 lists the neutron irradiation G-values surveyed. Not all combinations from these tables were evaluated, only combinations that were notably different, or combinations commonly used by others, such as Burns and Marsh, EPRI researchers, and Ibe and co-workers.

Table 5.2

Gamma Radiolysis Source Term Data

G(Chemical Species)								Source / Comments
e-	H+	H_2O_2	OH	O	H	H_2	HO_2	
2.7	2.7	0.61	2.87	0.0	0.61	0.43	0.03	1 / 1
0.4	0.4	0.0	0.7	2.0	0.3	2.0	0.0	1 / 2
3.2	3.2	0.57	5.3	0.0	2.4	0.44	0.0	2 / 2
3.2	3.2	0.6	4.7	0.0	3.4	1.2	0.0	3 / 2
4.0	0.0	1.2	3.9	0.0	1.0	0.5	0.0	4 / 2

Source Information:

1. Burns and Marsh[41]
2. Pikeav[35]
3. Katsumura[45]
4. Elliot[43]

Comments:

1. Low temperature (25 - 90°C)
2. High temperature (100 - 400°C)

Table 5.3

Neutron Radiolysis Source Term Data

G(Chemical Species)							Source / Comments
e-	H+	H_2O_2	OH	H	H_2	HO_2	
0.93	0.93	0.99	1.09	0.5	0.88	0.04	1 / 1
0.15	0.15	0.95	0.37	0.41	0.855	0.0	2 / 2
1.48	1.48	0.91	1.66	0.64	0.68	0.0	3 / 3
0.8	0.8	1.27	0.68	0.45	0.99	0.0	4 / 4

Source Information:

1. Burns[41]
2. Gordon[34]
3. Appleby[46]
4. Katsumura[45]

Comments:

1. LET: 4ev/A
2. 2 Mev / high temperature (T > 100°C)
3. 18 Mev
4. Fission

5.4.1 MITIRAD Parametric Study

The first parametric studies were made using the homogeneous, isothermal, transient point-kinetics model of MITIRAD. In these initial comparisons the same neutron G-values are used (Gordon's) and the same equation set is used (an updated Burns and Marsh set). Also, three sets of gamma G-values are compared: High-Temperature Burns', Pikeav's, and Katsumura's G-values. The predicted chemical concentration profiles show a strong dependence on the selected G-value set. Figure 5.6 shows profiles for H_2O_2 and H_2 concentrations. All three sets predict the attainment of equilibrium concentrations of H_2O_2, but two orders of magnitude separate the two equilibrium levels. Pikeav's and Katsumura's sets are identical except for hydrogen production. The effects of that difference is shown by the two parallel, monotonically increasing concentrations of H_2 for both sets. Burns'

$G(H_2)$ is significantly larger than the other $G(H_2)$ values, yet Burns' set predicts that H_2 concentration reaches equilibrium. Consequently, the "buffering" effect of the large equation sets can be significantly changed by the relative magnitudes, and not just the absolute magnitudes, of the G-value sets. Given the experimental process of elimination and mass balances used to calculate G-values from experimental data, more weight should be given to those sets that were experimentally determined using the same experimental approach, rather than selective compilation of individual G-values from various researchers.

Figure 5.7 shows concentration profiles for H^+ and OH^-. The most significant feature is that Burns' set predicts a low pH radiolysis environment whereas the other two sets predict essentially neutral pH water. This is particularly interesting considering that the Burns' $G(H^+)$ value is 8 times lower than the corresponding values in the other two sets. Apparently the G(O) value, which is unique to the Burns' set, is the predominant scavenger of H_2. This in turn results in an equilibrium H_2 concentration, whereas the high G(OH) values in the Pikeav and Katsumura sets (which is their mass-balance way of putting radiolysis oxygen species back into the reaction) buffer the pH but are ineffective in scavenging the excess H_2, which continues to increase with time as shown in Fig. 5.6. Figure 5.8 shows concentration profiles for $e^-_{(aq)}$ and OH. The trends for OH are inversely proportional to the H_2 concentration trends shown in Fig. 5.6 (i.e. - OH concentration steadily decreases when H_2 concentration steadily increases).

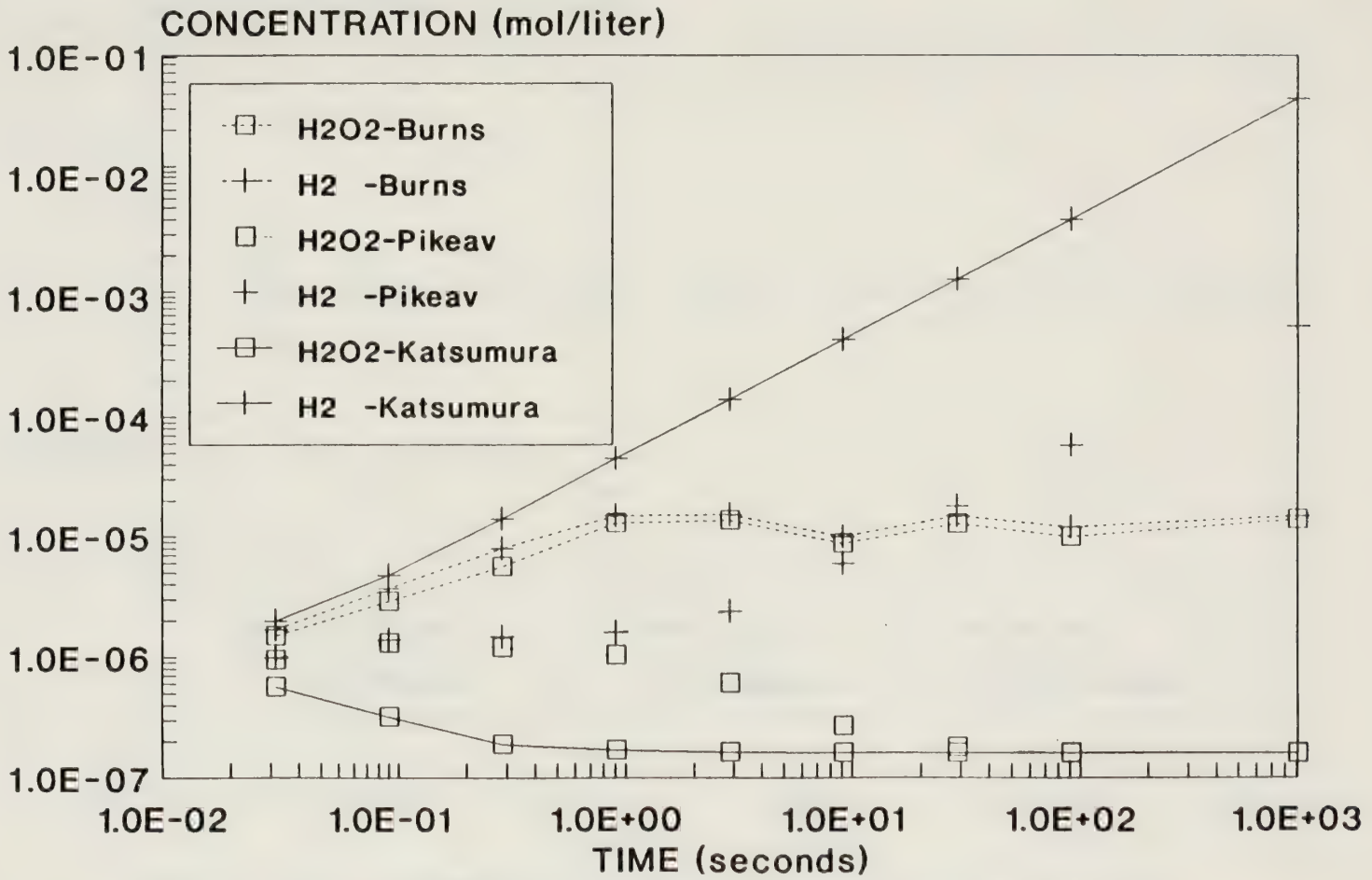

Figure 5.6: MITIRAD G-Value Comparison - Set 1

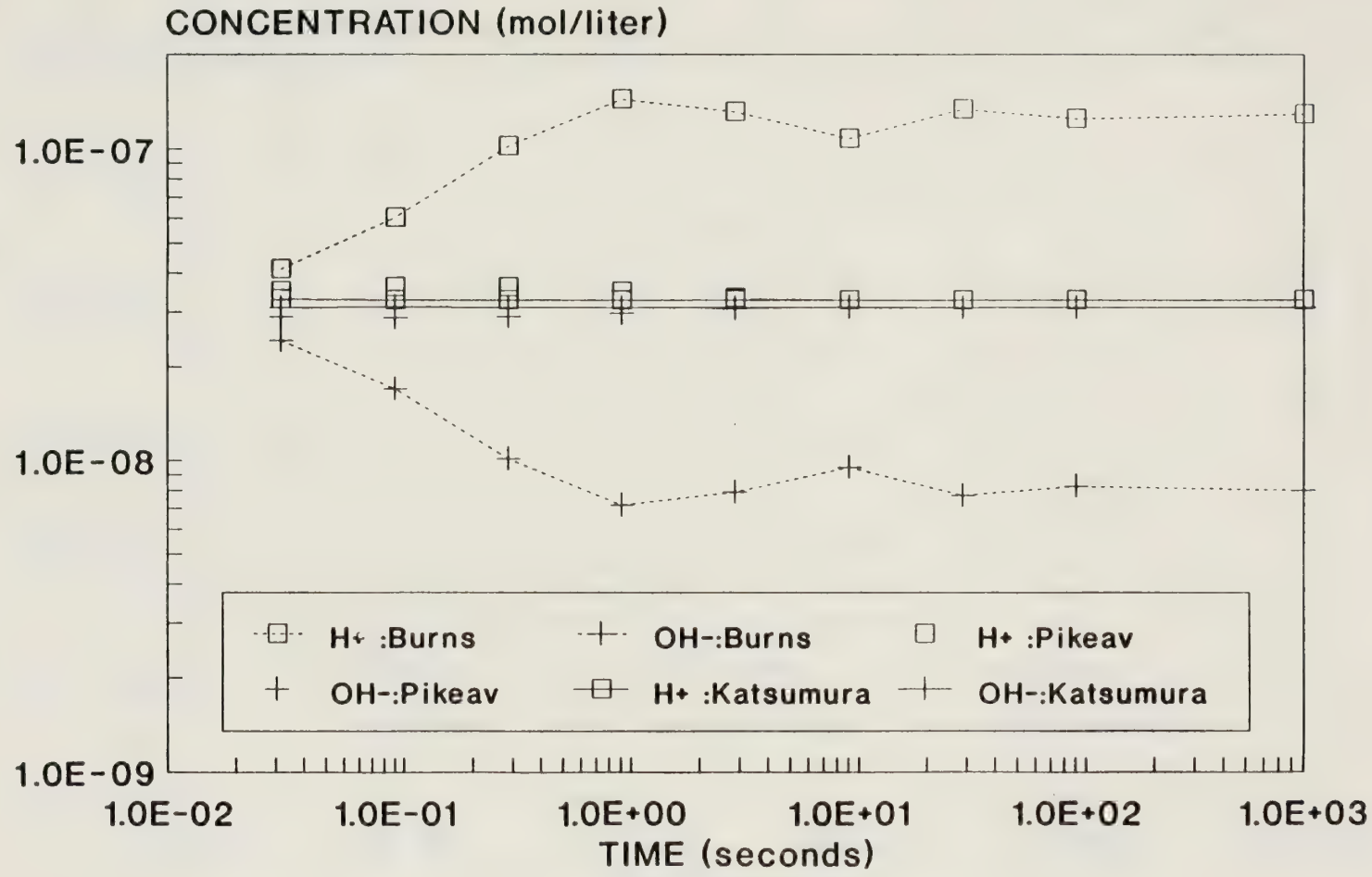

Figure 5.7: MITIRAD G-Value Comparison - Set 2

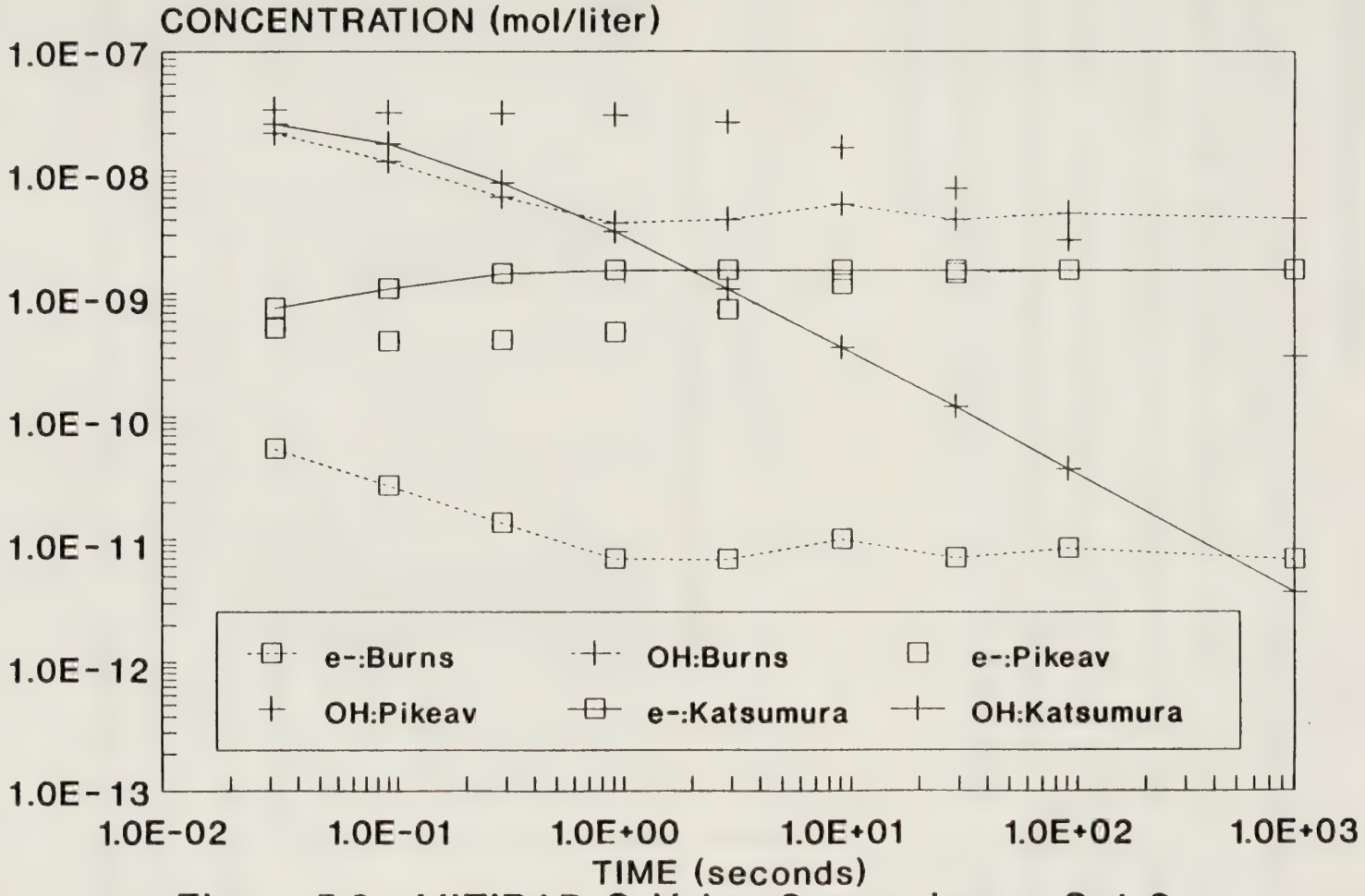

Figure 5.8: MITIRAD G-Value Comparison - Set 3

5.4.2 BCCLMIT Parametric Study

The six different combinations of G-value sets listed in Tables 5.2 and 5.3 were evaluated using BCCLMIT. The chemical reaction equation set used for these runs was the Notre Dame set (see the following section for equation set descriptions). Also, a value of 200ppb was used for both the H_2 and O_2 initial concentrations. These initial concentrations were used to accentuate the effects of the G-value sets. For comparison purposes, one of the six combinations was used as the reference case. Table 5.4 below lists the G-value set combinations used.

Table 5.4

Combination of G-Value Sets for Comparison

Combination #	Gamma G-Value Set*	Neutron G-Value Set
1	Pikeav	Gordon
2	Burns(Low T)	Burns
3	Burns(Hot)	Burns
4	Katsumura	Katsumura
5	Elliot	Katsumura
Reference	Pikeav	Katsumura

Figures 5.9 and 5.10 show the BCCLMIT output for combinations #1 and #2, respectively. These figures plot chemical species concentration as a function of position along the BCCL flowpath. Table 5.5 lists the BCCL section positions and descriptions.

*- Only the first member of each research team is listed. See Tables 5.2 and 5.3 for references and additional information.

Position measurements start at the chemical injection point and are measured linearly along the direction of coolant flow. Figure 5.9 also has position labels to aid in identifying the location of the BCCL section transitions.

Table 5.5

BCCL Section Descriptions

Position (cm)	Section Descriptions
0.0	Chemical Injection Point
0.0 - 5.0	0.635cm Ti tubing to Zircaloy Joint
5.0 - 36.0	0.794cm Zircaloy tubing to Core Inlet
36.0 - 42.4	Core Inlet to Boiling Inception
42.4 -178.3	Boiling Length (in-core)
178.3-209.3	Core Outlet to Zircaloy Joint
209.3-261.5	Ti tubing from Zircaloy Joint to Plenum
261.5-276.7	Outlet Plenum
276.7-306.5	Ti tubing from Outlet Plenum to Sample Tap
306.5-318.9	Sample Tap to Downcomer Plenum Inlet
318.9-332.8	Downcomer Plenum
332.8-344.9	Ti tubing from Downcomer Plenum to 2nd Tap

The only significant difference between the sets compared in Fig. 5.9 is in the neutron $G(e^-)$ and $G(H^+)$ values. The major difference observed in Fig. 5.10 occurs between the start of the core tubing and the core inlet. Prior to this point the gamma/neutron ratio is 10, which, with the other conditions given, favors rapid formation of H_2O_2 from the initial

O_2. At the start of the core tubing (approximately 30.5 cm above the core), the gamma/neutron ratio is 3.3. At the core inlet the gamma/neutron ratio is 1.0 for MITR-II; however, the absolute magnitudes of the radiation doses are sufficiently large that the radiolysis source term dominates and, therefore, drives the H_2O_2 concentration, whereas decomposition mechanisms dominated in the previous section.

Figures 5.11 and 5.12 show increasingly divergent behavior. One unusual difference in O_2 behavior is shown in Fig. 5.11. The O_2 concentration in the downcomer region increases (i.e. - changes inversely to H_2O_2 concentration) instead of decreasing as it does for the other cases. Figure 5.12 adds yet another dimension to the downcomer profile behavior for H_2. Of all the comparison combinations, only the Katsumura set in Fig. 5.12 shows H_2 concentration significantly increasing at the end of the loop. Also, very low O_2 levels were predicted.

The most dramatic variation is shown in Fig. 5.13. The Elliot set appears to be the most sensitive to the gamma/neutron ratio. H_2O_2 concentration spikes rapidly in the region where the ratio is 10 and drops as soon as the ratio drops. Even the high core dose rates are unable (with the given conditions/equation set) to increase H_2O_2 concentrations to significant levels. Predicted O_2 levels rapidly fall below the 1 ppb level (predicted O_2 concentrations level off in the 0.1 to 0.01 ppb range). The comparison in Fig. 5.13 is probably more indicative of the need for a integrated approach for coupling compatible equation and G-value sets, rather than an indictment of the validity of Elliot's data.

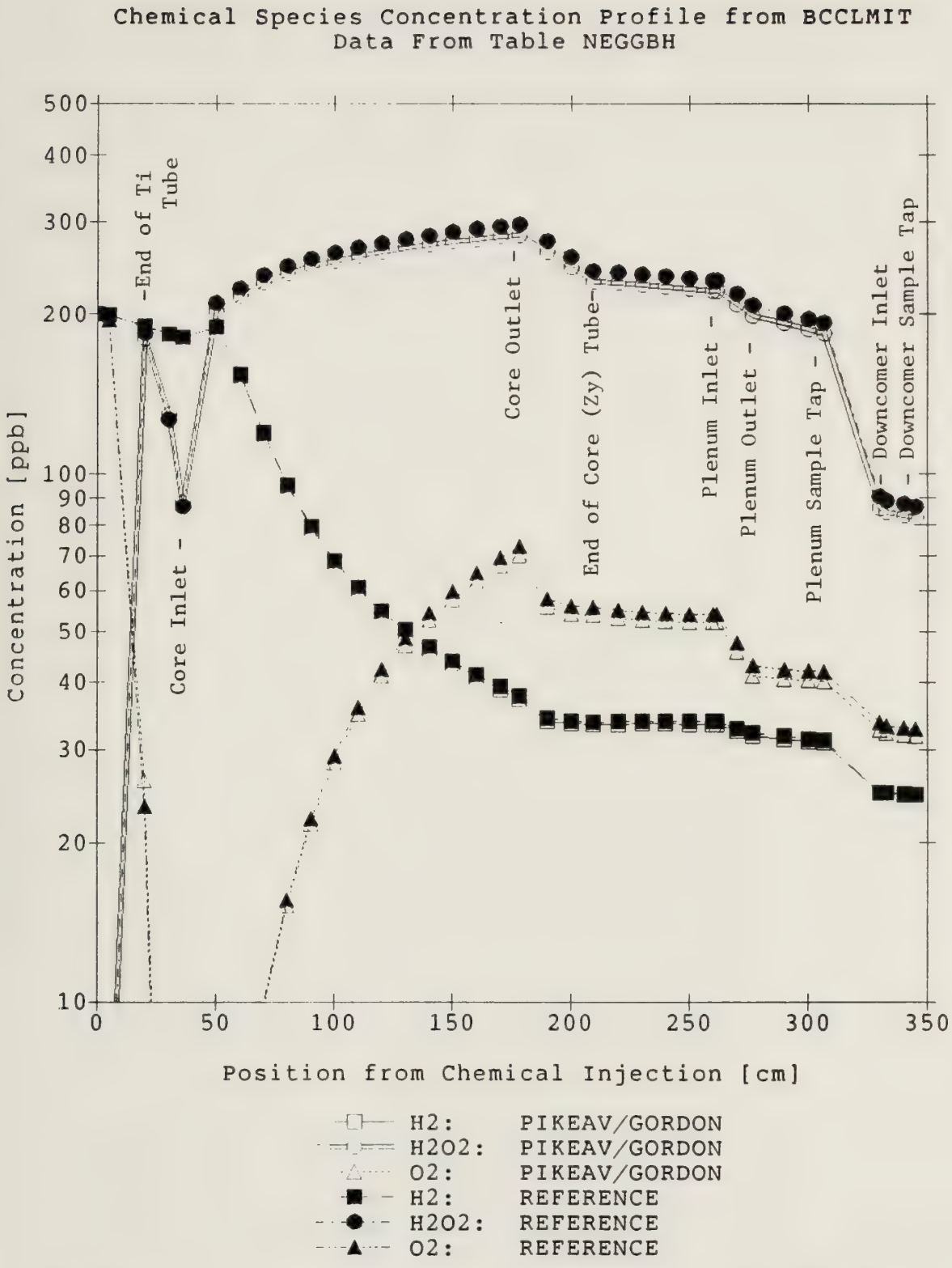

FIGURE 5.9: BCCLMIT G-VALUE COMPARISON - COMBINATION #1

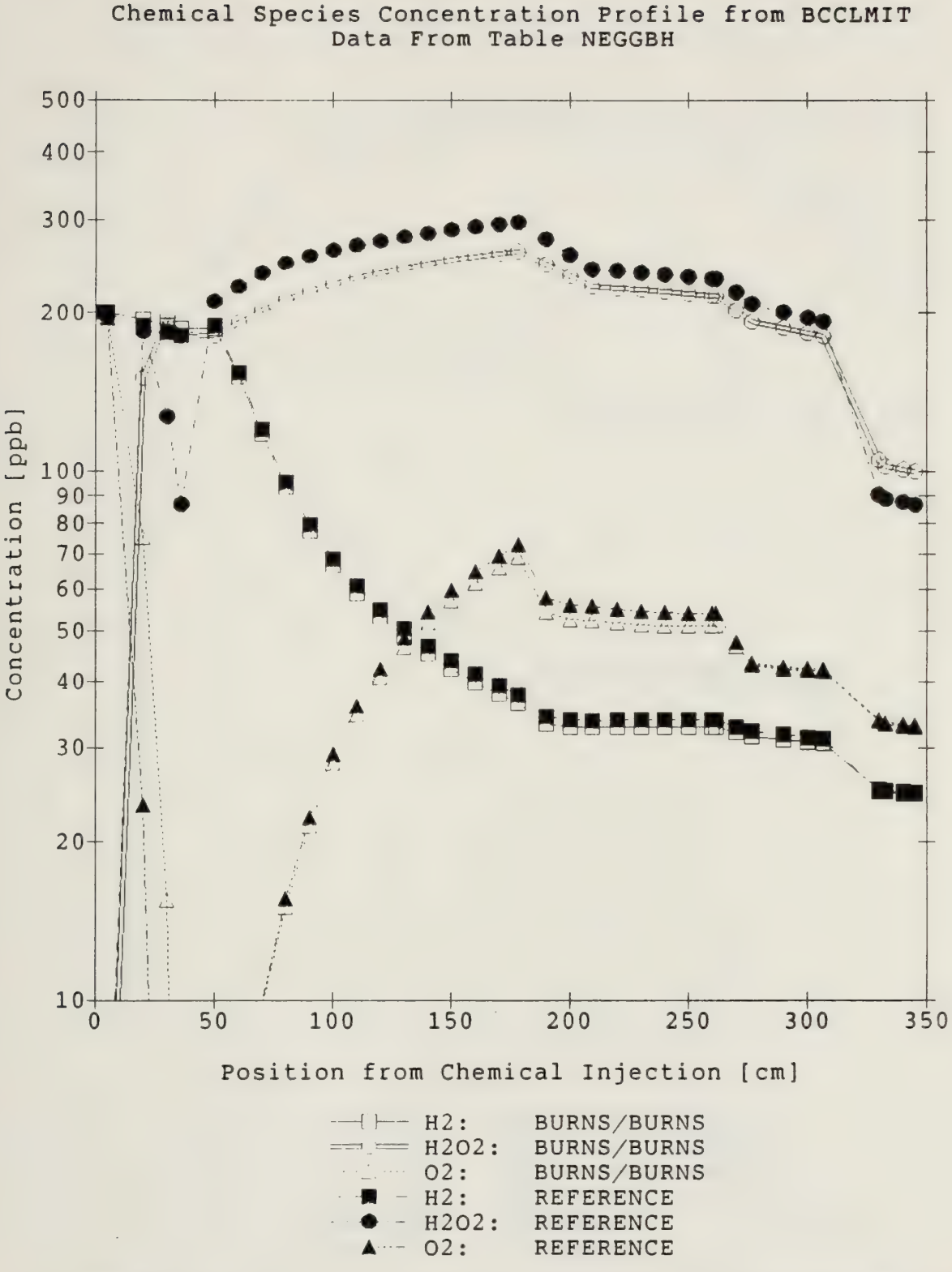

FIGURE 5.10: BCCLMIT G-VALUE COMPARISON - COMBINATION #2

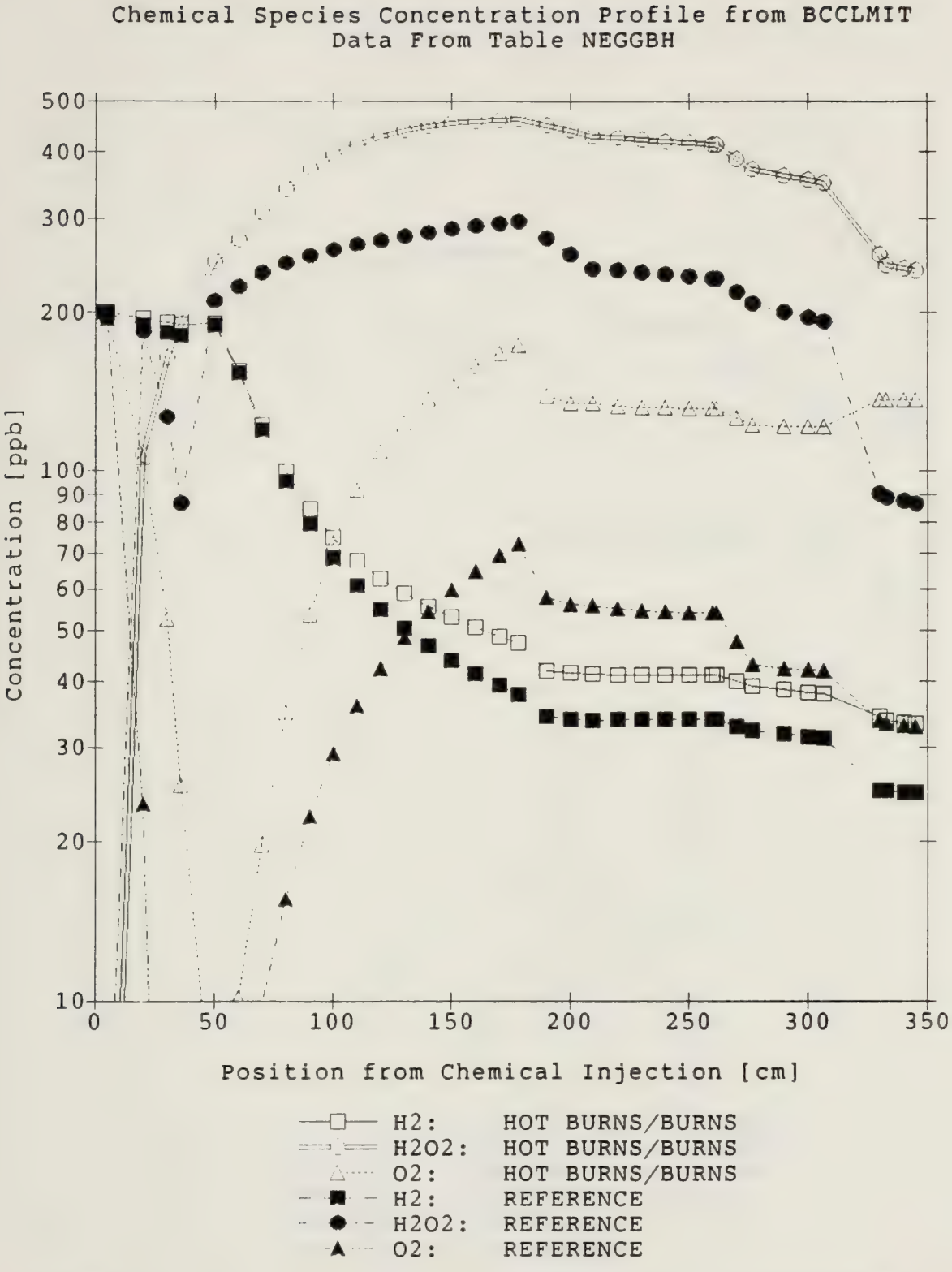

FIGURE 5.11: BCCLMIT G-VALUE COMPARISON - COMBINATION #3

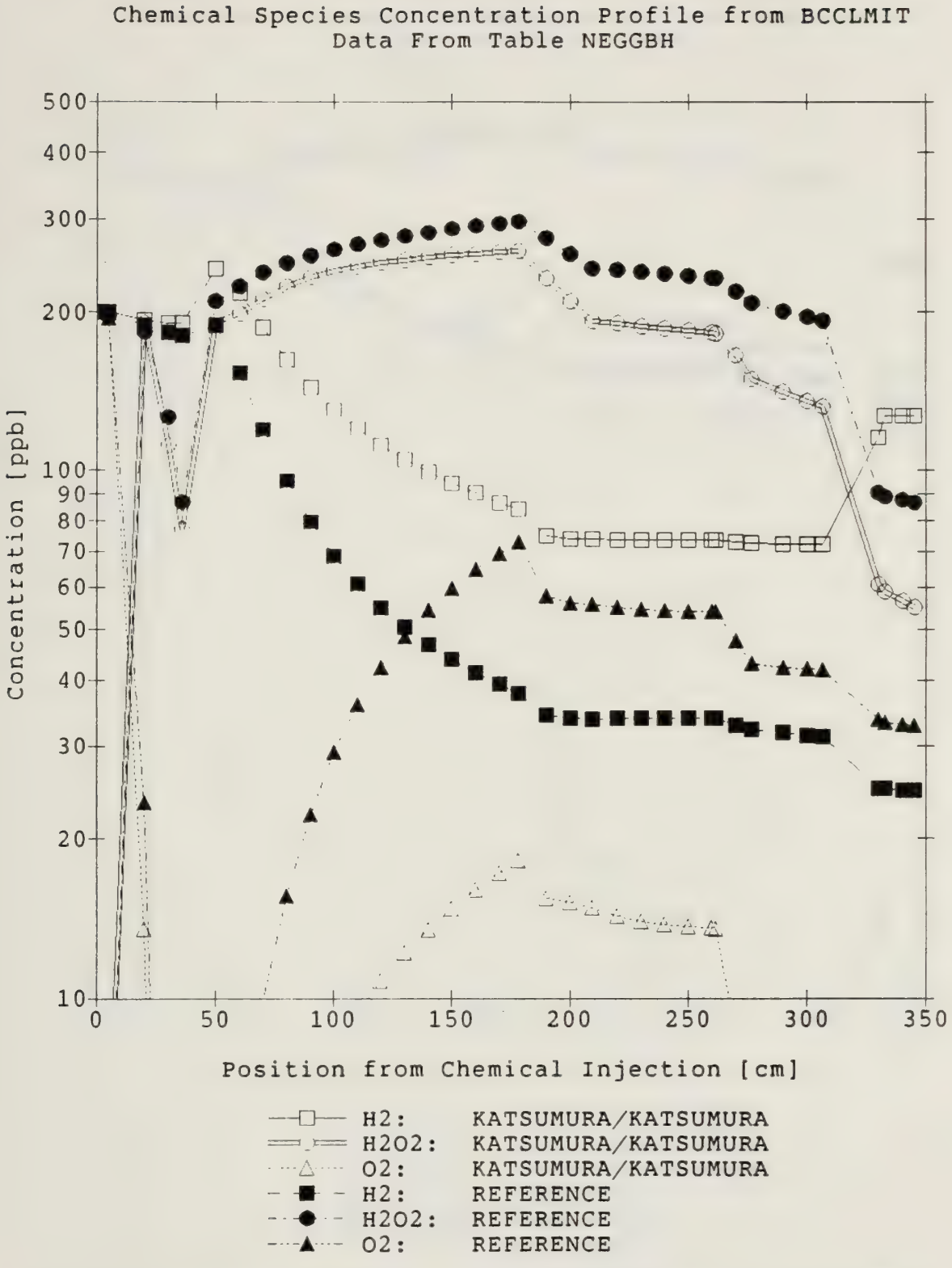

FIGURE 5.12: BCCLMIT G-VALUE COMPARISON - COMBINATION #4

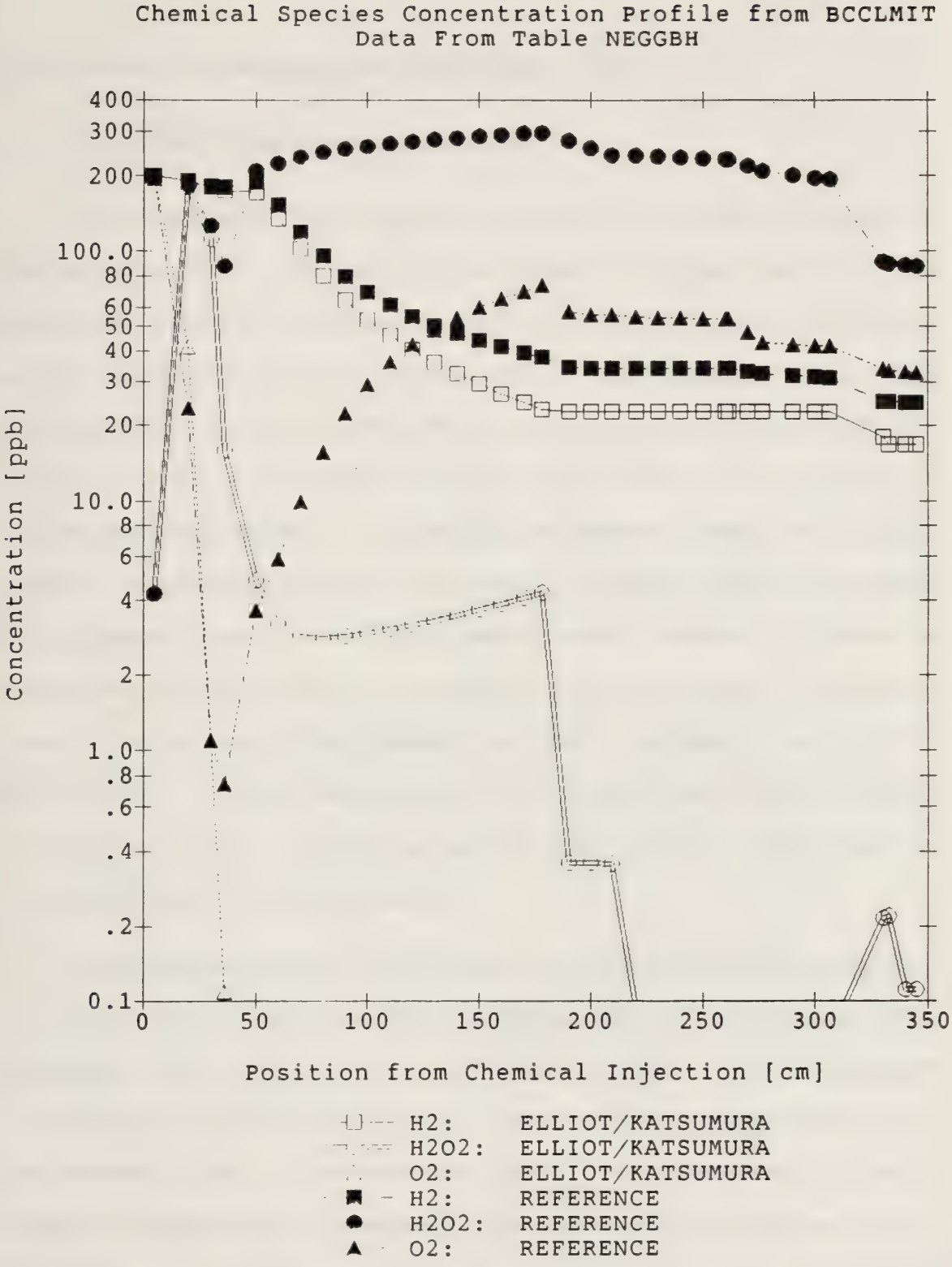

FIGURE 5.13: BCCLMIT G-VALUE COMPARISON - COMBINATION #5

5.5 Evaluation of Chemical Reaction Equation Sets

5.5.1 Modified Notre Dame Equation Set

The modified Notre Dame equation set is based on the equation set obtained by Simonson[14] from the University of Notre Dame's Radiation Chemistry Data Center[47]. The equation set reported by Simonson was already in a water-implicit format. This format assumes the concentration of water to be unchanged by those reactions involving water as either a reactant or a product; therefore, the concentration of water is included in the rate constant and water is deleted from the reactant list. MITIRAD and BCCLMIT can accommodate water-implicit or water-explicit sets; however, neither code implicitly adjusts the concentration of water with temperature. If the rate coefficients were known to a high degree of precision (at the temperatures of interest), a water-explicit equation set can be used and water concentration adjusted over the approximate 10°C temperature range. The current water-implicit equation set was based on the density of water at 280°C. FRO (see Fig. 5.2) already interpolates the water density at each spatial meshpoint; therefore, it would be a straightforward addition to BCCLMIT to accommodate large temperature changes with greater precision.

Three changes were made by the present author to the basic Notre Dame equation set. The first change was the use of new forward and reverse rate coefficients for the dissociation of water. These revised rate coefficients are based on the high-temperature values of K_w reported by EPRI[48] researchers. The rate coefficients and associated activation energies were adjusted to give a linear best fit for K_w versus temperature. The second change was the addition of a set of reactions involving the species O. These reactions were taken from another Notre Dame equation set (see Ref. 14) for air/water reactions and also from Burns and Marsh[41]. These reactions were included to support parametric studies

where G(O) was non-zero. Also, these reactions supported the format of the surface H_2O_2 decomposition equation used. The addition of the surface decomposition reactions was the third modification to the Notre Dame equation set. The modified equation set is listed in Appendix D.4.

The performance of the equation set was contrasted against predicted chemical concentration profiles with and without the effects of surface decomposition, and with the effects of Hydrogen Water Chemistry (HWC). The reference G-value combination discussed in the previous section was used for these studies. Figure 5.14 compares the case with no surface H_2O_2 decomposition with the reference case which includes surface decomposition. The most pronounced effect occurs downstream of the core exit, where the H_2O_2 concentration is high and the radiolysis source for the H_2O_2 falls off with the decrease in radiation level.

Figure 5.15 shows the effects of HWC on predicted concentration profiles. This study shows that the addition of 200 ppb of H_2 has a marked effect on H_2O_2 and O_2 levels. However, also evident is the ability of in-core radiolysis to generate high concentrations of oxidizing species even with the addition of H_2. Another feature that warrants future investigation is that the initial H_2O_2 concentration spike at the start of the Zircaloy tubing only happens with HWC. Both cases assume a 200 ppb initial O_2 concentration. If the G-value and equation set indicate the correct trends, the addition of H_2 greatly exaggerates the effects of the gamma/neutron dose rate ratio.

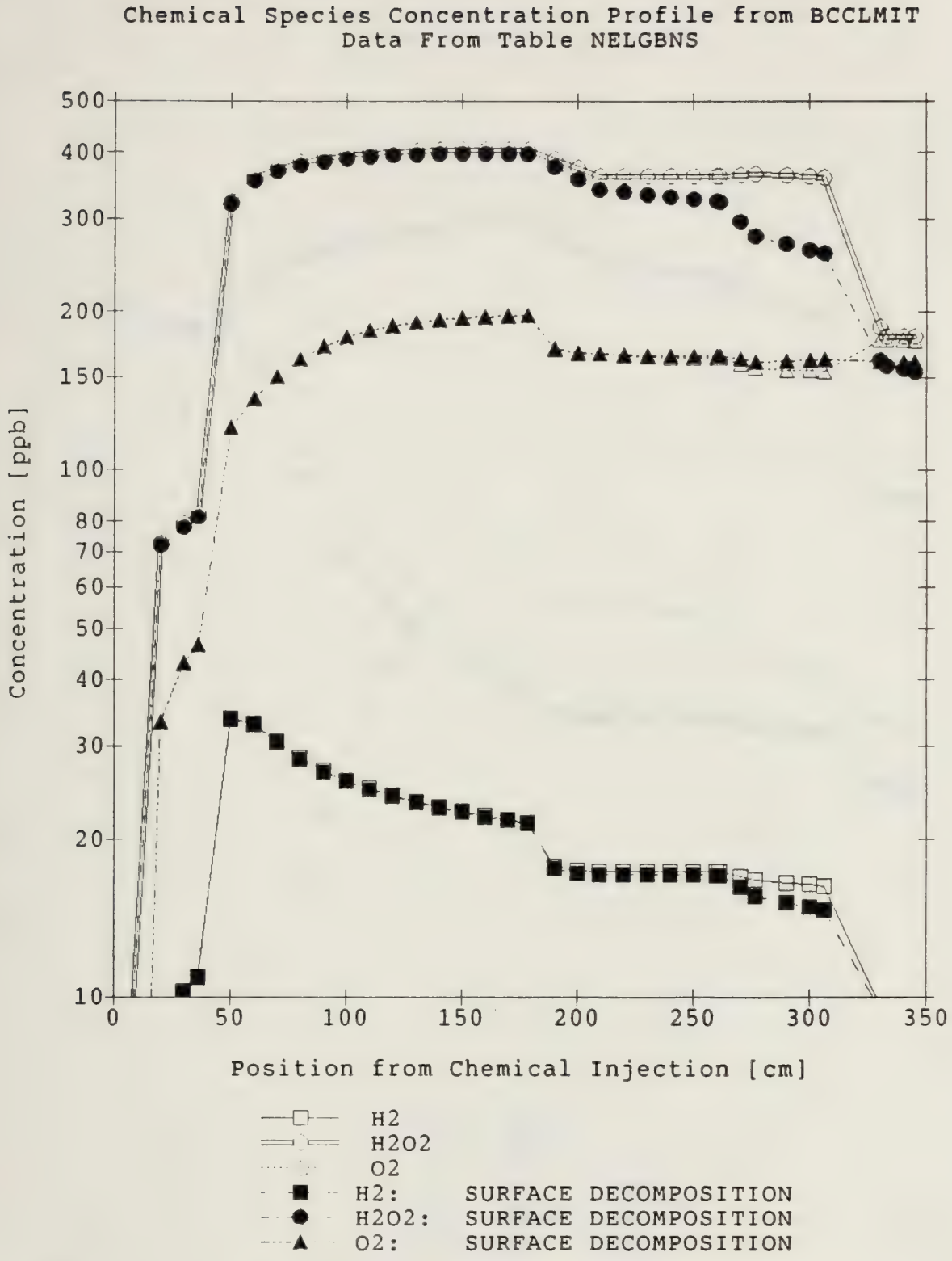

FIGURE 5.14: SURFACE DECOMPOSITION STUDY - NOTRE DAME SET

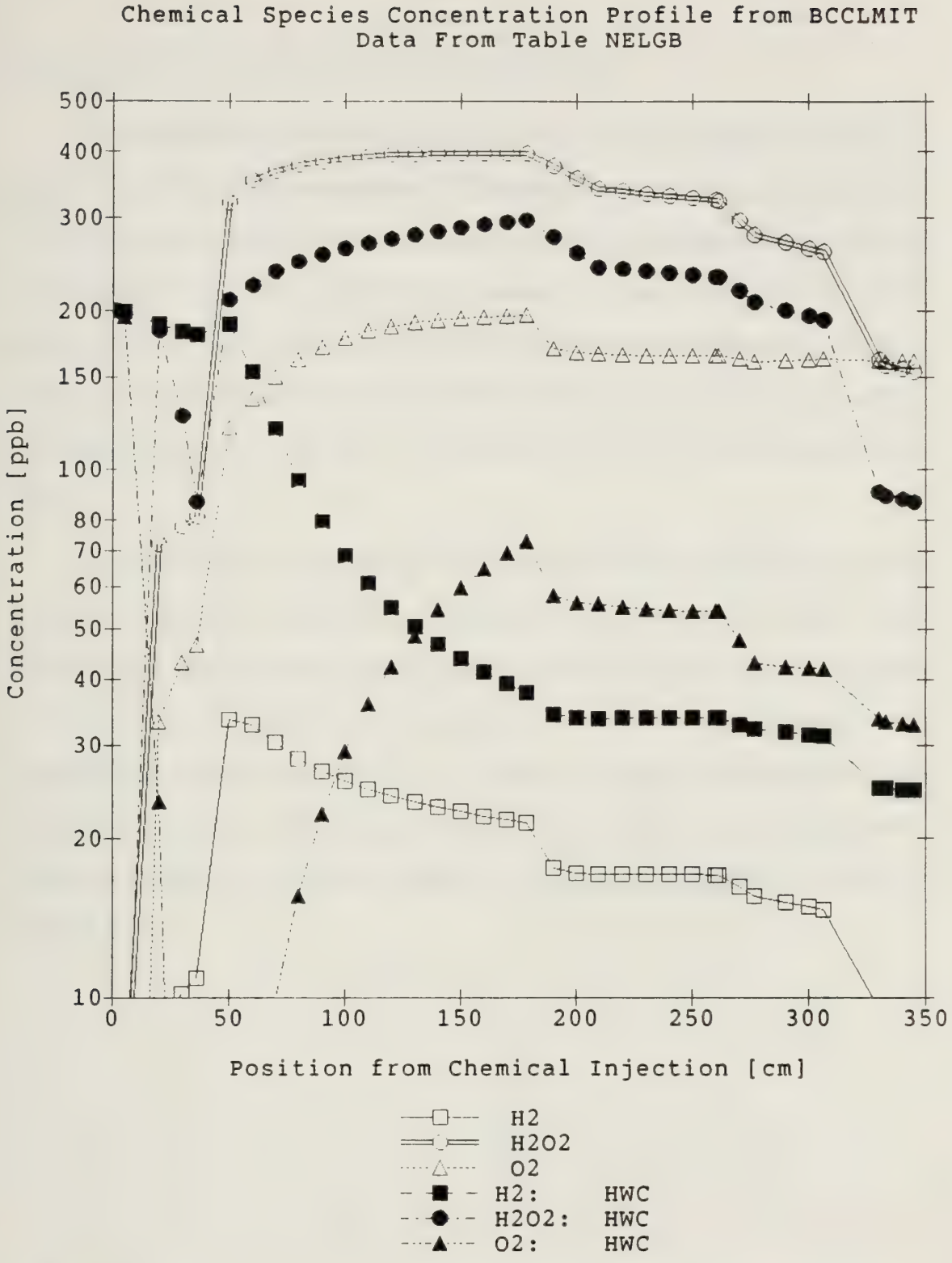

FIGURE 5.15: HYDROGEN WATER CHEMISTRY STUDY - NOTRE DAME SET

5.5.2 Modified Burns and Marsh Equation Set

The modified Burns and Marsh equation set was taken from Table 1 of Ref. 41. As was done for the Notre Dame equation set[14,47], the water dissociation reactions were adjusted to reflect the correct high-temperature behavior, and the H_2O_2 surface decomposition rate equations were added. The modified Burns equation set is listed in Appendix D.5. A few updates were also included in this equation set (even though the subsequent calculations were not significantly altered by these updates). Reaction equations (see Appendix D.5 for applicable reactions) W8, W14, W21 and W23 were revised based on more recent data[30,49].

The performance of the Burns equation set was evaluated using the same variations as for the Notre Dame equation set. Figure 5.16 shows the effects of H_2O_2 surface decomposition. The resultant variation parallels the behavior shown in Fig. 5.14 for the first equation set. However, an outstanding feature is the extremely high predicted O_2 concentrations with the Burns equation set. Figure 5.17 shows the effects of HWC using the Burns equation set. For this equation set, only the initial H_2 concentrations show a significant difference, and there is virtually no difference in predicted H_2O_2 or O_2 concentrations.

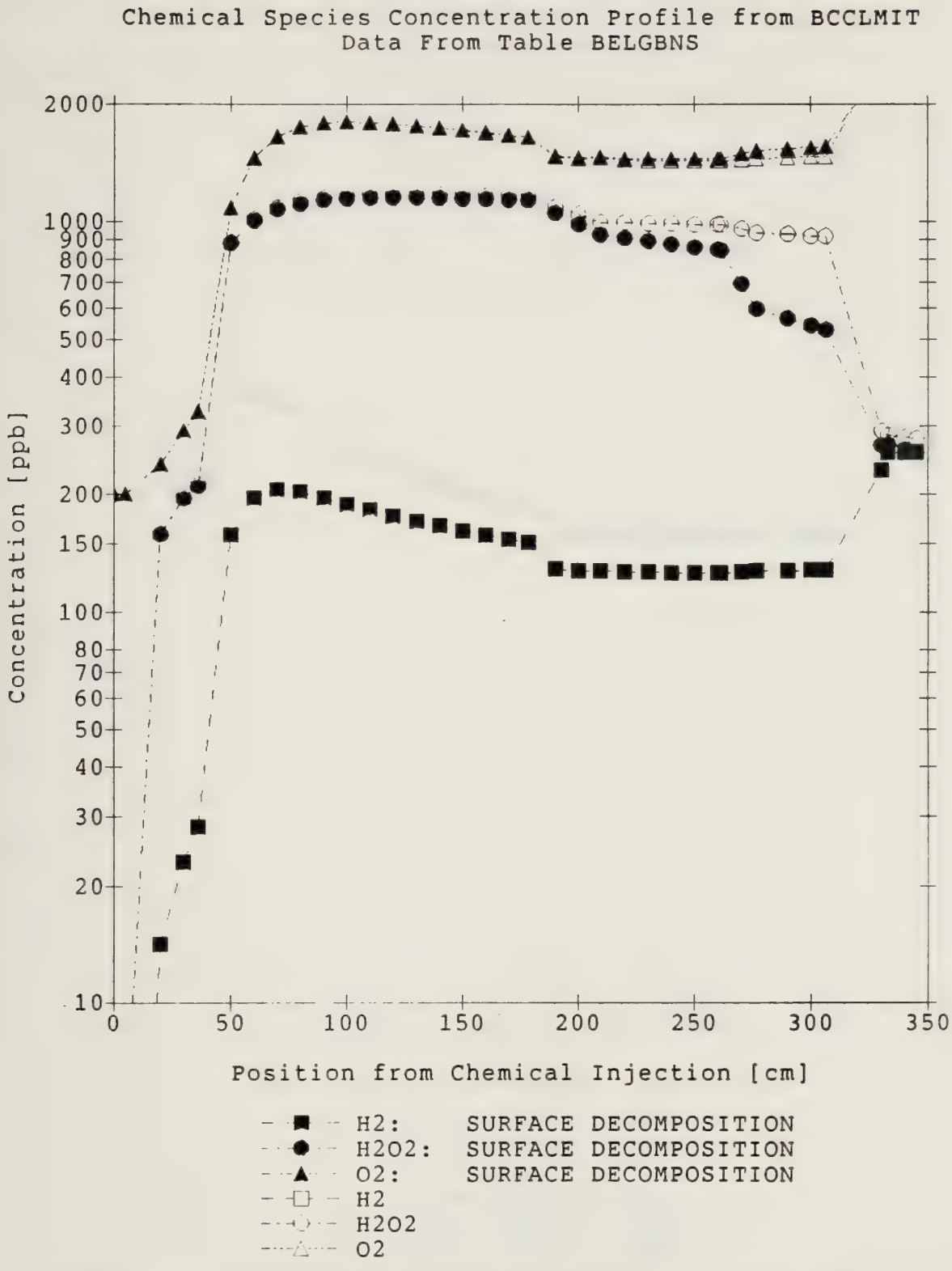

FIGURE 5.16: SURFACE DECOMPOSITION STUDY - BURNS SET

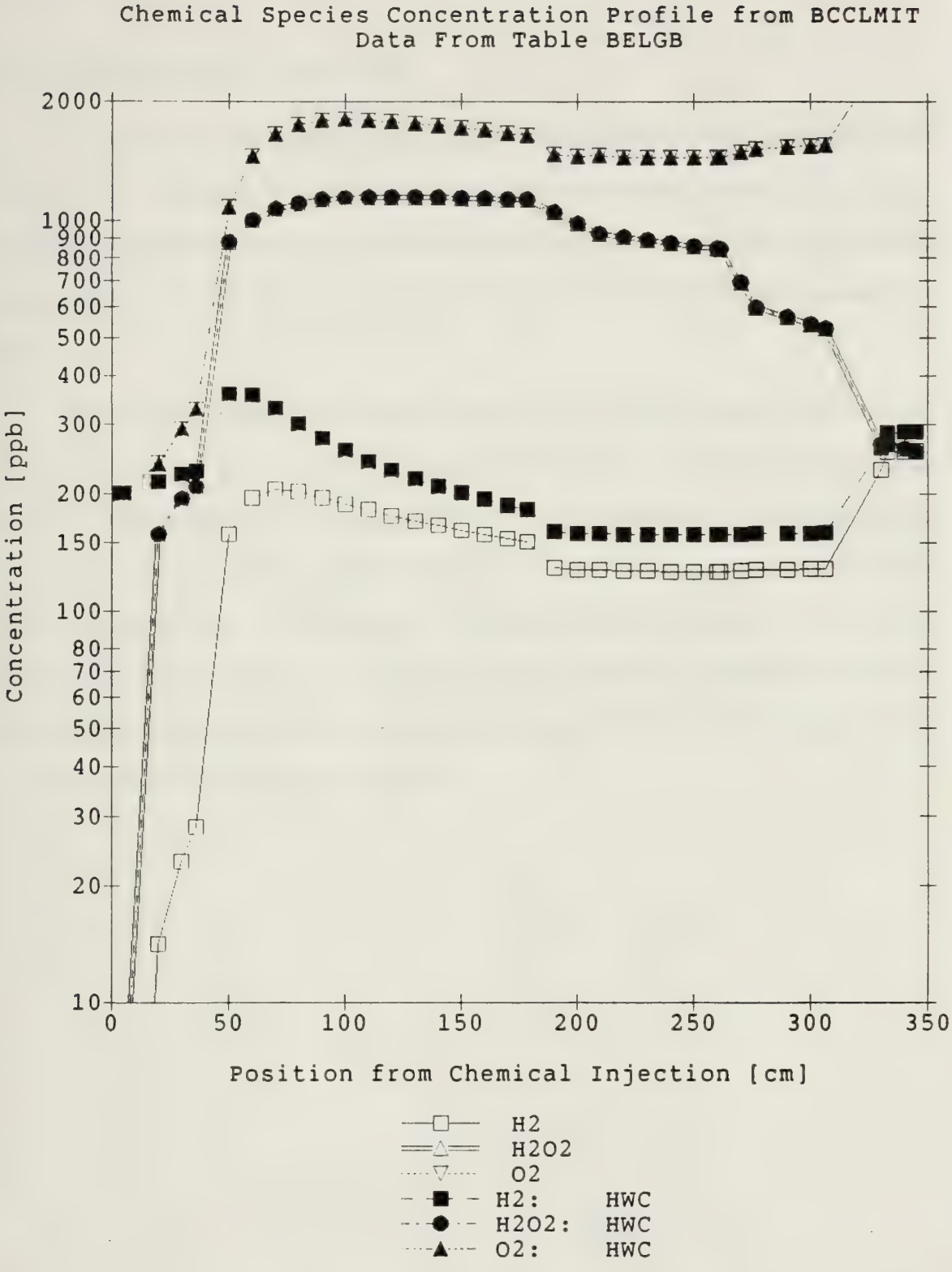

FIGURE 5.17: HYDROGEN WATER CHEMISTRY STUDY - BURNS SET

5.5.3 Equation Set Comparison

The distinguishing features unique to the two equation sets are most apparent in direct comparison. Figures 5.18 and 5.19 compare the two equation sets for normal water chemistry and HWC, respectively. The Burns equation set was insensitive to significant perturbations. Also, the Burns set predicted substantially higher H_2O_2 and O_2 concentrations.

An additional equation set perturbation was evaluated. Elliot[37] reported new reaction rate coefficient data for a number of reactions, some of which are applicable for this case. Table 5.6 lists the new rate coefficient data for the reaction equations evaluated by Elliot. The new rate coefficient data reported in Table 5.6 are the Arrhenius model best-fit values for the data in the 200 to 300°C range. Consequently, the coefficient at 25°C is not the true rate coefficient at 25°C, but rather the value needed to provide the best high temperature-range rate coefficient. The equation numbers in Table 5.6 correspond to the reaction equations listed in Appendix D.4.

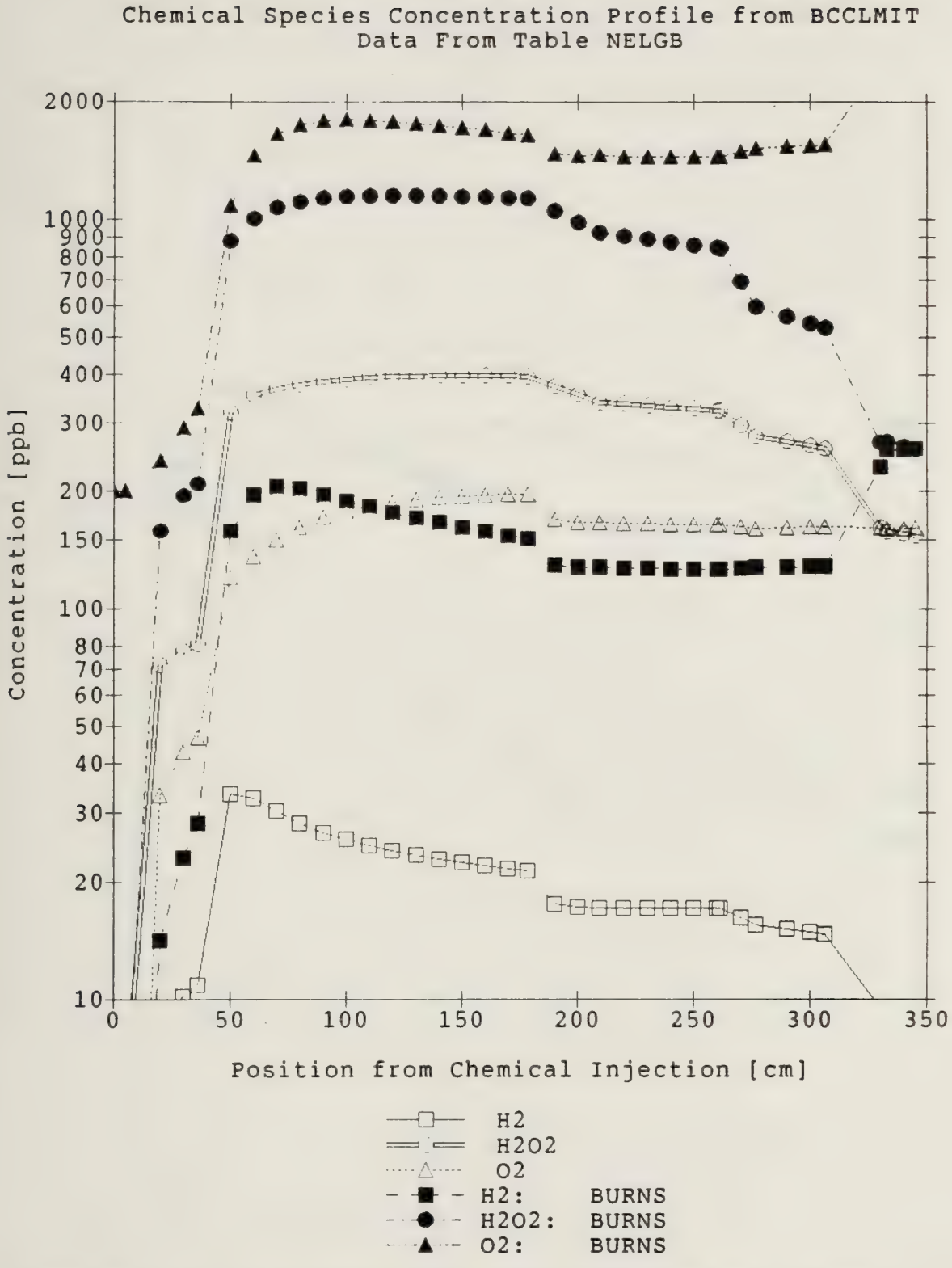

FIGURE 5.18: NORMAL CHEMISTRY - EQUATION SET COMPARISON

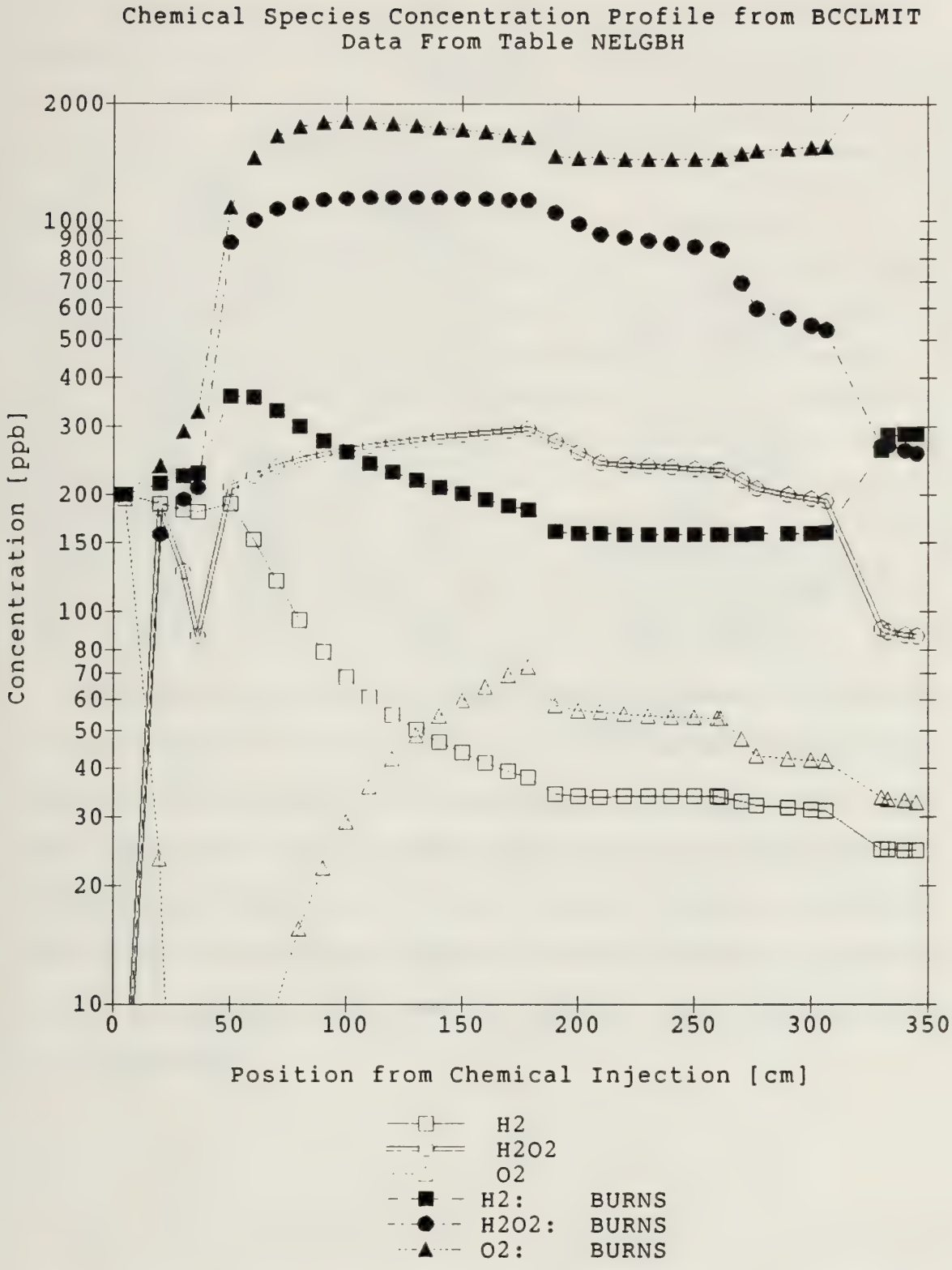

FIGURE 5.19: HYDROGEN CHEMISTRY - EQUATION SET COMPARISON

Table 5.6

Updated Reaction Rate Coefficient Data

Eq. #	Rate Constant [l/mol/s]		Activation Energy [kJ/mol]		Reactions
	Old	New	Old	New	
W2	6.0E10	2.3E10	12.6	13.9	$e^- + H^+ > H + H_2O$
W4	3.2E10	1.3E10	12.6	11.9	$e^- + H_2O_2 > OH + OH^-$
W7	4.7E10	1.6E10	12.6	15.3	$e^- + O_2 > O_2^-$
W9	1.1E10	6.3E9	12.6	5.4	$2(OH) > H_2O_2$
W14	1.1E8	4.0E7	12.6	18	$OH + H_2 > H + H_2O$
W16	4.7E10	1.6E10	12.6	8.6	$H + O_2 > HO_2$
W20	2.4E8	5.0E7	14	16.6	$H + H_2O_2 > OH + H_2O$
W21	4.1E7	3.0E7	14	13	$OH + H_2O_2 > HO_2 + H_2O$
W29	1.1E7	8.0E5	19	22.8	$2(HO_2) > H_2O_2 + O_2$

Both the Burns and Notre Dame equation sets were revised next to include the data of Table 5.6. Figures 5.20 and 5.21 show the impact of these revised reaction sets on the calculated concentration profiles. The reference case for Figs. 5.20 and 5.21 are, respectively, the Notre Dame and Burns equation sets listed in Appendix D.4 and Appendix D.5. HWC conditions were used for both the revised set, and the reference equation set, in Figs. 5.20 and 5.21. The most significant impact of the revised equations is the substantial decrease in predicted H_2O_2 concentrations, with only minor changes to the calculated H_2 and O_2 concentrations.

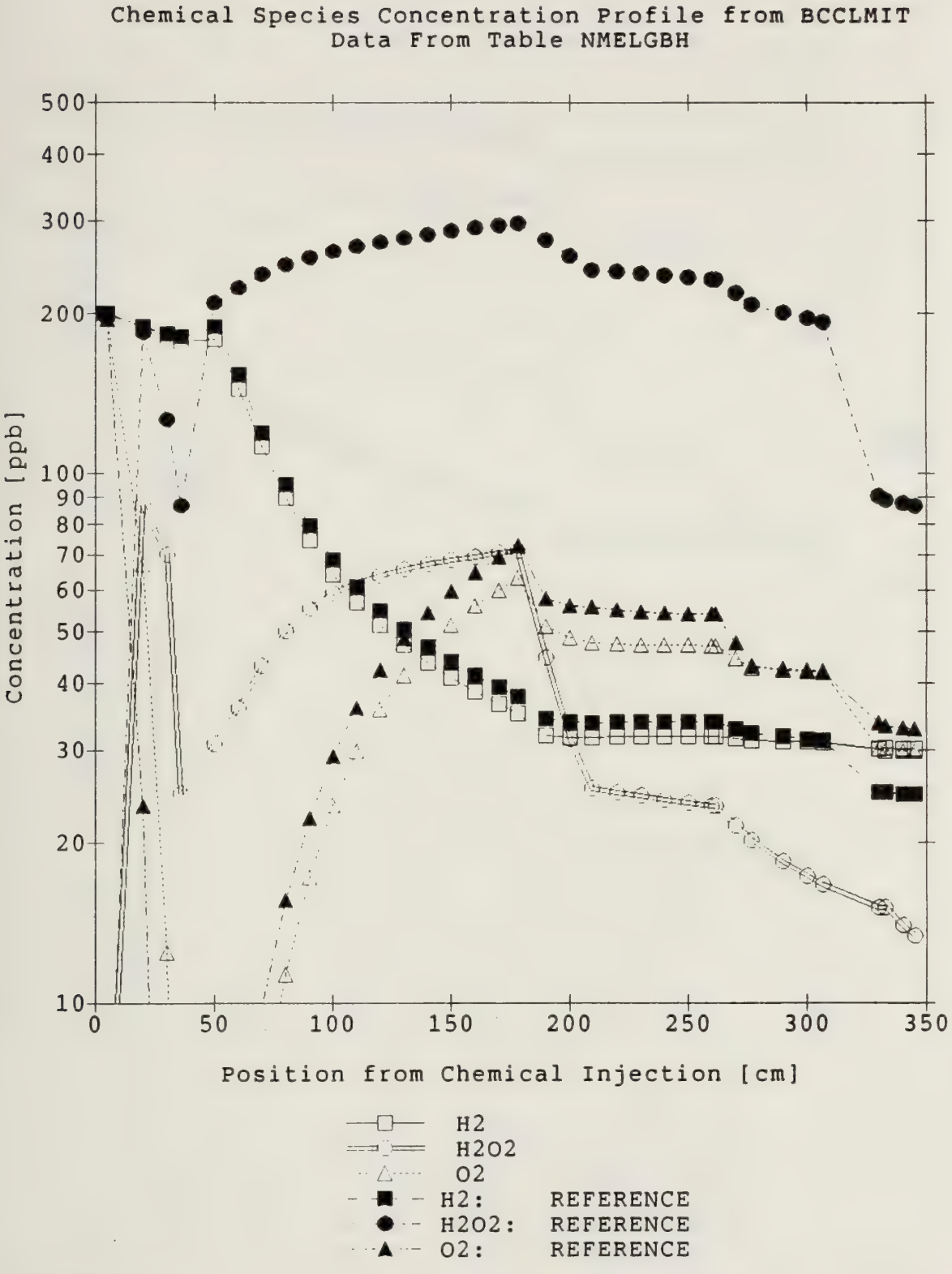

FIGURE 5.20: REVISED EQUATION SET STUDY - NOTRE DAME SET

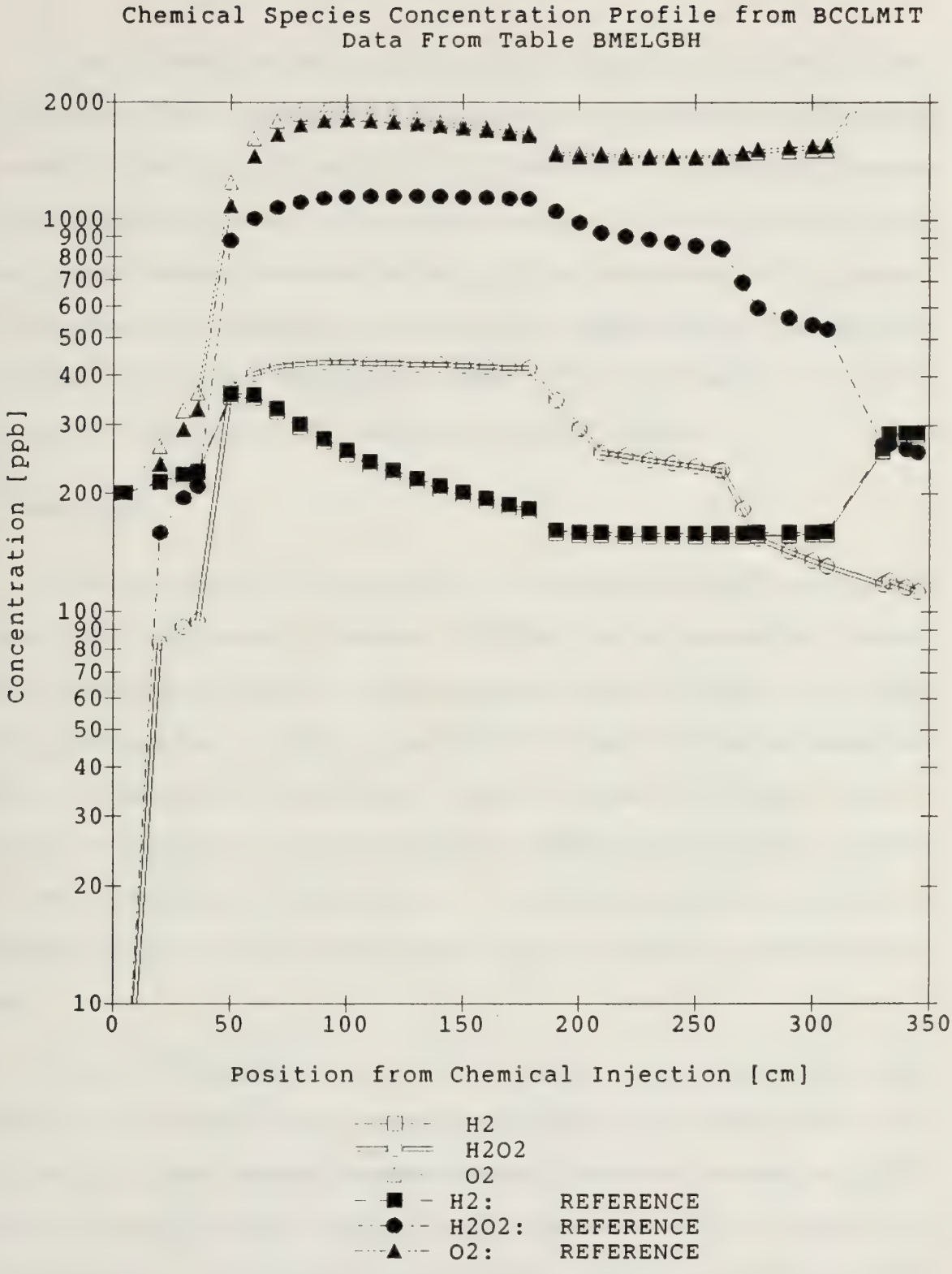

FIGURE 5.21: REVISED EQUATION SET STUDY - BURNS SET

The H_2O_2 surface decomposition reaction product wasn't a critical selection for either equation set. Three different product combinations were evaluated, where the products were (1) $H_2O + O$, (2) 2(OH), and (3) $1/2(O_2)$. There was no difference in the three cases; the product oxygen ended up as O_2 with all the equation sets used. Consequently, when any gamma G-value set, other than the high-temperature Burns set (where G(O) is nonzero) is used, the group of equations that contain the species O can be deleted without measurable change in the predicted concentration profiles. (The surface decomposition reaction products would also have to be changed to either OH or $1/2(O_2)$.)

5.6 Summary

This chapter presented the computational model on which BCCLMIT was based. The original source code prepared by Simonson[14], MITIRAD, was also discussed and contrasted against the calculation requirements needed to support modeling of the BCCL. Until actual BCCL operational data are compared against BCCLMIT predicted chemical concentration profiles, only subsets of the model can be validated on a case-by-case basis. Only a few bench-top experimental runs were in close agreement with BCCLMIT calculations. However, for those cases that did not closely agree (i.e. - the water-cooled probe experiments), the applicability of the BCCLMIT model was suspect; therefore, those cases do not invalidate the model.

Given the BWR plant data reported for H_2O_2 and O_2 concentrations, the Notre Dame equation set[14,47] is the more promising starting point for future BCCL studies and evaluations. Also, until experimental validation of an entire reaction equation set is accomplished for BWR conditions, apparently the best combinations of G-value sets for the Notre Dame equations are combinations 1, 2, and "Reference" given in Table 5.1. More work is needed to couple a complete set of equations with the updated values reported by Elliot et al.[37] (listed in Table

5.6). In addition, the G-values reported by Elliot et al. apparently must also be tailored to an appropriate equation set in order to predict concentration profiles on the order of those reported from operating BWR plants. Coupling Elliot's G-value set[42,43] with his modified reaction equations[37] still predicted H_2O_2 and O_2 concentrations orders of magnitude lower than concentrations predicted by other researchers such as Ibe[28,29], Lin[16], Ullberg[1], and Takagi[26].

The various data sets predict large (often as much as two orders of magnitude) differences in the concentrations of principal species (e.g. - H_2, O_2 and H_2O_2), all of which will be measured in BCCL experiments. Hence the test program planned with this loop should go a long way toward sorting out the best combinations of parameters for the relevant reactions.

Chapter 6. Summary and Recommendations for Future Work

6.1 Introduction

The principal objective of this thesis was to design, build and test the coolant sampling system needed to support the operation of the MIT BWR Coolant Chemistry Loop (BCCL). This effort included the requirement to characterize high-temperature H_2O_2 behavior sufficiently to develop sampling system design requirements. This characterization and design work also provides the foundation for the first BCCL overall project objective, which is to characterize coolant radiolysis chemistry by measurement of H_2O_2, H_2, O_2, electrode potential, etc.. In addition, a preliminary investigation of high-temperature electrode performance was also made.

A secondary objective of this thesis was the modification of the radiolysis chemistry computer code, MITIRAD. This modified code provides a tool for predicting BCCL chemical concentration profiles, and will, therefore, also provides a tool for correlating BCCL experimental data.

6.2 Summary and Conclusions

6.2.1 Characterization of H_2O_2 Decomposition

An initial series of experiments were carried out to characterize the decomposition of H_2O_2, to support the design of a BCCL sampling system. The high-temperature behavior of H_2O_2 was not known in sufficient detail to support the construction of a suitable sampling system capable of preserving, and then measuring, the low concentrations (on the order of 100 ppb) of H_2O_2 expected within the BCCL. The investigation of H_2O_2 decomposition

included measurement of the effect of: (1) temperature dependence (25°C to 280°C); (2) flow rate dependence (300 to 400 cc/hr); and (3) cooling rate dependence, as measured by the residence time of the sample in uncooled sample tubing.

The principal conclusions that were drawn from these studies are:

1. H_2O_2 decomposition behavior as a function of coolant temperature was the same (within experimental error) for flow through aluminum, titanium and stainless steel tubing (Fig. 2.2). This finding is consistent with results published by Lin et al.[16].

2. H_2O_2 decomposition was not significantly affected by changing the flow rate over the range of interest for BCCL operations (300 to 400cc/hr), which is in the laminar flow regime with Reynolds numbers ranging from approximately 200 to 2000. Laminar flow is expected to minimize H_2O_2 decomposition, because a larger temperature difference between the bulk coolant and the wall is sustainable; therefore, everything else being equal, a lower wall temperature is achievable. Furthermore, if the H_2O_2 decomposition is diffusion-limited, turbulent mixing would increase H_2O_2 decomposition. Lin et al. and Ullberg[1] reported surface decomposition of H_2O_2 to be first-order, kinetics-limited for the small diameter (0.635 - 1.27 cm O.D.) tubing used for much of their experimental work.

3. H_2O_2 decomposition was more dependent on the tubing wall temperature than on the bulk coolant temperature, which is consistent with thermal decomposition and surface decomposition rates reported by Lin et al.[16]. Under similar flow conditions, quartz tubing showed more H_2O_2 decomposition (>80%) in comparison with the metal tubes tested. Because of the low thermal conductivity of the quartz, wall temperatures at the sample inlet were approximately 100°C higher than the wall temperature of the

metal tubing, resulting in higher decomposition rates. Therefore, the surface reactivity of the quartz would have to be several orders of magnitude lower than the surface reactivity of the metals tested in order to cause less overall H_2O_2 decomposition. Consequently, the high thermal-conductivity of the metal tubing permits lower wall temperatures, which compensates for the high surface decomposition rate of the metal tubing.

These conclusions defined the design goals for construction of the BCCL sampling device: (1) minimize the length of the water-way in the sampling device that is above approximately 140°C, and (2) maintain pressurized single-phase sample flow in the laminar flow regime. Based on these H_2O_2 decomposition characterization studies, the use of convenient materials of construction (such as aluminum, stainless steel and titanium) was possible, while still meeting the basic objective, which was to build a sampling system that would preserve more than 50% of the inlet H_2O_2 for subsequent measurement.

6.2.2 Design and Qualification of BCCL Sampling Device

6.2.2.1 BCCL Sampling Device Design

Two sampling devices were considered based on the BCCL sampling system design goals. One system used an independent cooling water system to provide forced cooling at the sampling site of the BCCL coolant. The second system provided passive cooling of the sample at the BCCL sampling site via heat conduction through the sampling device to the MITR-II reactor coolant (at about 56°C). This sample cooling block, which is shown in Fig. 6.1, was ultimately selected because of its compactness and its independence of an external support system.

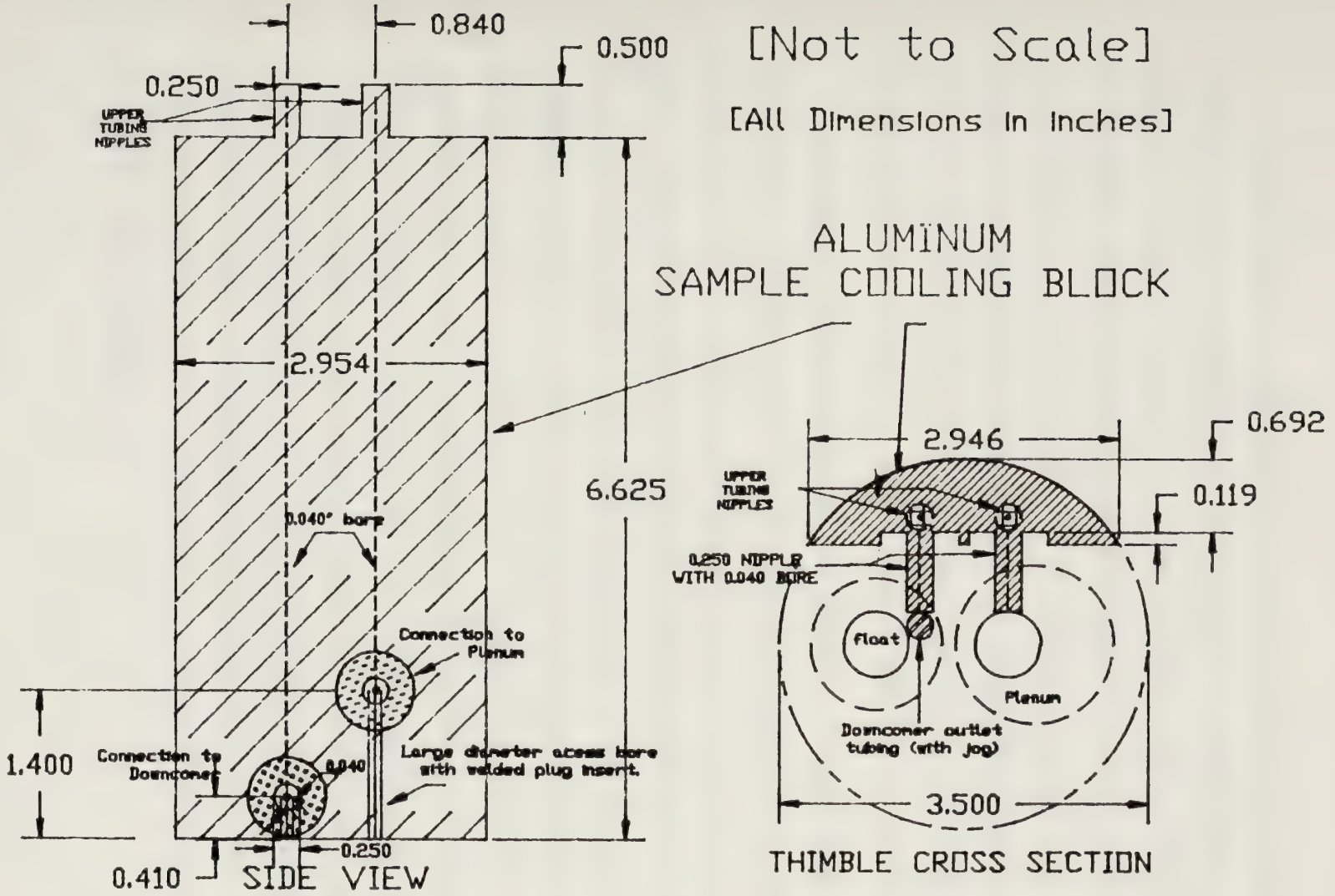

FIGURE 6.1: BCCL SAMPLE COOLING BLOCK

Aluminum was selected as the material of construction because of its high thermal conductivity, and its comparable H_2O_2 decomposition performance relative to BCCL materials of construction: titanium and stainless steel. The sample cooling block has two independent sample flow paths: one path for sampling the coolant at the outlet of the Outlet Plenum, and the second flow path for sampling the coolant at the outlet of the Downcomer Plenum. The samples flow from the sample cooling block to a sample measurement station through approximately 5 m of 0.108 cm I.D. stainless steel tubing, and then through approximately 7 m of inert plastic tubing external to the thimble.

The internal components of the BCCL are housed within an aluminum thimble. Consequently, in order to provide a good heat conduction path from the sample cooling block to the MITR-II reactor coolant (which is external to the thimble), the sample block must be pressed tightly against the interior wall of the thimble, to minimize the temperature drop across the gap between the thimble and the sample block. A remotely operated locking mechanism (not shown in Fig. 6.1) was designed to secure the block against the thimble wall. Based on the MITR-II core tank temperature (56°C) and the internal loop configuration, the sample cooling block is expected to cool the sample to below 90°C. In order to remotely check the function of the locking mechanism, as well as to provide a sample calibration reference temperature, a thermocouple is positioned in the lower section of the sample block. High temperature readings will indicate an excessive temperature drop across the gap between the sample block and the thimble wall, an indication that the locking mechanism is not pressing the sample block against the thimble wall with sufficient force.

6.2.2.2 Qualification of BCCL Sampling Device

Following fabrication of the sample cooling block and a prototypical water-cooled sampling probe (forced-circulation cooling), both devices were tested. Both devices were found to give a negligible variation in the measured H_2O_2 decomposition with flow rates from 300 to 425 cc/hr, and, in the case of the sample block, for reference sample block temperatures of 70 to 90°C. These flow rate and temperature ranges cover the expected ranges needed to support BCCL operations. However, the sample cooling block emerged as the most viable option, given the support system requirements of the water-cooled sample probe.

Testing of the water-cooled probe, with respect to the decomposition of H_2O_2 in the sample flow path, resulted in 20% (+/- 5%) sample decomposition. Testing of the sample cooling block resulted in 35% (+/- 5%) decomposition of H_2O_2. (The better performance of the probe was outweighed by its added system complexity.) The sample line that transports the sample from the sample cooling block to the top of the core tank was found to induce 4% decomposition for the worst case (entire length of tubing at 90°C). Therefore, the overall BCCL sampling system using the sample cooling block is expected to decompose ≤40% of the inlet H_2O_2, which exceeds the design objective of having a sampling system that decomposes less than 50% of the inlet H_2O_2. Also important is that the fractional decomposition is stable, reproducible and readily calibrated.

6.2.3 Out-of-Pile High-Temperature Electrode Performance

The electrode testing described in this thesis provided a preliminary high-temperature extension of Driscoll's[20,24,25] work at MIT. The primary objectives of these tests were to

(1) qualify a suitable electrode feedthrough design, (2) provide data on the high-temperature behavior of the palladium (Pd) electrode (a candidate Standard Hydrogen Electrode {SHE} reference electrode) in a more prototypical environment, and (3) provide comparative high-temperature data on stainless steel, platinum (Pt) and Pd electrodes. This work also provides the basis for additional high-temperature testing and/or qualification of an alternate standard reference electrode for use in the BCCL. The motivation for investigating alternate reference electrode configurations is to provide greater flexibility in measuring ECP within the BCCL, beyond what currently exists with the available high-temperature Ag/AgCl reference electrode provided by GE.

A high-temperature, high-pressure electrode feedthrough scheme using bare electrode wires was built and tested successfully. The feedthrough arrangement used a CONAX feedthrough with a Grafoil sealant gland (Figs. 4.1 and 4.2). Electrical insulation of the bare wire electrodes was provided by a thin Teflon tubing sleeve. The key to the successful design was found to be filing a rounded groove in the side of the wire in the gland region so that the Grafoil could extrude into the groove and thereby lock the wire in place, preventing its extrusion from the fitting under high differential pressure. The wire electrodes used a SS316 upper section with an active electrode tips (one each of Pt and Pd, and two SS316) mechanically connected by a crimped-on sleeve to the ends of the SS316 upper sections. Approximately 40 hours of high temperature (280°C), high-pressure {10.3MPa (1500 psig)} operation were logged. This feedthrough configuration will also permit short-duration in-reactor support of BCCL operations using alternate electrode arrangements involving the separate or paired use of Pt, stainless steel, and Pd electrodes.

In the cold reference runs with no added H_2O_2, the "aging" of the electrodes made the runs unreproducible. Cold stainless steel electrode behavior changed significantly after

high-temperature operation, presumably due to oxidation and passivation. This electrode behavior is similar to problems reported by Wikmark[50]. Initial high-temperature behavior (no added H_2O_2) was reproducible. However, after exposure to high-temperature H_2O_2-doped coolant with concentrations of H_2O_2 up to 2 ppm, the electrode behavior again changed dramatically. Cathodic charging of electrodes with H_2 was investigated and electrode H_2 charging times were progressively increased throughout the course of the testing to compensate for the apparent effects of electrode aging. However, complete, reproducible recovery was not achieved for the either stainless steel or palladium. In general, high-temperature electrode potentials also exhibited an aging effect, in that the electrode potential spread, that was a function of H_2O_2 concentration, decreased with time. However, in general, the higher the H_2O_2 concentration, the lower the magnitude of the measured potential relative to the zero H_2O_2 reference case. Comparison of this reported behavior with literature values is not meaningful at this point without the measurement of electrode potentials relative to a SHE standard. However, a threshold effect was noted for several of the potentials measured as a function of increasing H_2O_2 concentration. Specifically, increasing H_2O_2 concentration above approximately 500 ppb had negligible affect on measured electrode potentials. This threshold behavior is consistent with data reported by Takagi[17] for H_2O_2 and similar to behavior reported by Ford and Andresen[51] for O_2.

These preliminary high-temperature tests were inconclusive in determining the suitability of Pd as a SHE reference for possible future use in the BCCL. These tests were limited to approximately 100 minutes per run. Consequently, it is unknown whether or not the Pd potential will eventually reach equilibrium. Achieving equilibrium is important not only to permit use of Pd-relative potentials for analytic purposes, but it is also an important check on the adequacy of the Pd electrode's internal hydride inventory in supplying the necessary localized environment, which is required to sustain the Pd electrode

as a SHE reference. Another concern was that the charging current density was inadequate to maximize the hydrogenation of the palladium. (A current density of approximately 1 milliamp/cm^2 was used.) Further testing is clearly in order.

6.2.4 BCCL Radiolysis Chemistry Computer Code

The radiolysis chemistry computer model developed for the BCCL, BCCLMIT, was developed based on similar work by Takagi[26] and Ibe[28] for BWRs. The basic structure and operation of the code was based on the radiolysis chemistry computer code, MITIRAD, developed by Simonson[14] at MIT. BCCLMIT includes the calculation of two-phase gas absorption and stripping effects on coolant chemistry, and includes surface decomposition of H_2O_2. The basic flow model of the code assumes simple one-dimensional flow with no temperature and concentration gradients in the radial direction. This simple model provides a starting point for predicting BCCL radiolysis chemistry behavior, and provides a tool for correlating BCCL experimental measurements.

The main features retained from MITIRAD were the chemical reaction handling routines and the numerical method for solving systems of stiff, ordinary differential equations. The basic mathematical model used in the computer model was developed in parallel by the author, for adaptation to the BCCL, and by Chun[15], for adaptation to BWRs.

Bench-mark calculations were performed to validate the computational accuracy of the mathematical model. However, until actual BCCL operational data are compared with BCCLMIT's predicted chemical concentration profiles, only the validity of portions of the model can be checked on a case-by-case basis. Some bench-top experimental runs were in close agreement with BCCLMIT calculations, others differed by as much as a factor of 3. However, for those cases that did not closely agree (e.g. - the water-cooled probe

experiments), the applicability of the BCCLMIT model was suspect; therefore, such cases do not invalidate the model. For example, the water-cooled probe has very large radial and axial temperature gradients (on the order of 1000°C/cm and 200°C/cm, respectively), whereas BCCLMIT assumes no radial gradient, and is limited as to the size of the axial temperature gradient that can be accommodated.

Parametric studies involving different sets of radiolytic source term values (G-values) and reaction rate equation sets were performed with a version of MITIRAD and with BCCLMIT. The various combinations of sets predict large (often as much as two orders of magnitude) differences in concentrations of principal species (e.g. - H_2, O_2 and H_2O_2), all of which will be measured in BCCL experiments. Hence, the test program planned with this loop should go a long way toward sorting out the best combinations of parameters for the relevant reactions.

Given the BWR plant data reported for H_2O_2 and O_2 concentrations, the Notre Dame equation set[14,47] is the more promising starting point for future BCCL studies. Also, until experimental validation of an entire reaction equation set is accomplished for BWR conditions, the best combinations of G-value sets for the Notre Dame equation set appear to be: Pikeav's[35] gamma irradiation G-values coupled with either Gordon's[34] or Katsumura's[45] neutron irradiation G-values, or Burns'[41] low-temperature gamma-irradiation G-values and his neutron-irradiation G-values. These combinations of G-values, coupled with the Notre Dame water radiolysis equation set, predicted principal species concentrations for BWRs in the range expected by other researchers such as Ibe[28,29], Lin[16], Ullberg[1], and Takagi[26]. More important, the best-current-estimate results predict that the BCCL will generate H_2, O_2 and H_2O_2 concentrations well within the measurable range (several hundred ppb) by available methods: ORBISPHERE H_2 and O_2 meters and CHEMetrics H_2O_2 colorimetry.

6.3 Recommendations for Future Work

The work described in this thesis provides a framework for the characterization of simulated BWR coolant in the BCCL. Additional work is required to support the full-range of experimental work that is currently planned for the BCCL, such as the prediction and measurement of nitrogenous species to support N^{16} carryover studies during later experiments. The following recommendations for future work are made with this additional work in mind, as well as providing recommendations for future work based on a logical extension of the work described in this thesis.

6.3.1 Characterization of H_2O_2 Decomposition

The extent of testing to characterize the surface decomposition of H_2O_2 at high-temperature was limited to the flow rates and prototypical configurations needed to develop a sampling system for the BCCL. Consequently, the bench-top test apparatus used was not ideally suited for determining the flow rate dependence of H_2O_2 decomposition in the turbulent flow regime. Although the BCCL sampling system operates in the laminar flow range, the BCCL coolant flows are all turbulent. Elliot et al.[37] emphasizes the importance of properly characterizing the rate coefficient for a given chemical reaction as to whether the reaction is diffusion-limited, kinetics-limited, or a combination of the two. For example, data reported by Lin et al.[16] for H_2O_2 decomposition in stainless steel tubes (0.635cm O.D.) show a well-defined change of slope (a factor of two) at about 200°C in the Arrhenius plot of the decomposition rate coefficient. A well-defined change of slope of that magnitude is characteristic of a first-order reaction that changes from kinetics-limited behavior at lower temperatures to diffusion-limited behavior at high temperature[52]. For first-order

kinetics, the temperature dependence of both limiting cases scale with an Arrhenius relation; however, the effective activation energies (the slopes on the Arrhenius plot) typically differ by a factor of two.

The BCCLMIT model assumes surface decomposition of H_2O_2 is kinetics-limited, as reported by Lin et al.[16]. Even if the correct activation energy is used for temperature scaling, a diffusion-limited rate coefficient would scale differently than the kinetics-limited case, for surface-to-volume ratios typical of the different diameters in the various sections of the BCCL. The largest diameter BCCL sections, such as the Outlet Plenum and the Downcomer Plenum, would be the most affected sections, since they are most likely to be diffusion limited (since they are the least turbulent, and have the lowest surface-to-volume ratio).

In addition to the recommended work to evaluate the possible diffusion-dependence of the H_2O_2 surface decomposition rate coefficient, the surface decomposition performance of Zircaloy should also be evaluated. At present, the H_2O_2 surface decomposition rate coefficient for Zircaloy is assumed to be equal to that measured for stainless steel and titanium. If Zircaloy tubing is more reactive than the other metals tested, then the code may overestimate the H_2O_2 concentrations by underestimating the surface decomposition rate within the core region.

6.3.2 Reference Electrode Evaluation

The electrode work discussed in this thesis was a preliminary extension of work performed at room temperature. Consequently, a lot of work is still required to achieve the objective of qualifying an alternate SHE reference electrode, such as Pd, or qualifying an alternate ECP measurement electrode combination.

In order to determine the suitability of Pd as a SHE reference standard, two items should be investigated. First, the electrolysis cell electrode current density should be increased by an order of magnitude from approximately 1 milliamp/cm^2 to approximately 20 milliamp/cm^2 as suggested by Hwang[53]. The higher current density would be more effective at producing H_2 in sufficient concentration to ensure the Pd has absorbed the maximum quantity of H_2 at high temperatures. The second issue is that testing periods should be extended (> 100 minutes) to evaluate if Pd electrode equilibrium is achieved. Charging times could also be increased to attempt to increase the hydride content of the Pd electrode; however, at high-temperature, with its attendant high diffusion rates and Pd dehydrogenation rates, the equilibrium hydride concentration using low current density charging may always be inadequate.

Other reference systems should also be investigated, such as tungsten, based on work reported by Ashraf-Knorassami and Braun[27]. They reported some disadvantages to using tungsten as a reference electrode because of its response to changing hydrogen concentration, pH, etc.. However, this should not disqualify tungsten from possible use as a standard reference electrode for the BCCL. Another alternate worth evaluating is cathodic restoration of the Pt electrode. Including Pt as an electrolysis cathode may provide a reproducible electrode potential measurement for calibration against a SHE reference standard.

In addition to testing of the active electrode element, evaluation of alternate electrode feedthrough designs is also warranted. CERAMASEAL* has glass-ceramic feedthroughs that can handle both the pressure and temperature requirements of the BCCL, but of

---

*- CERAMASEAL INC., New Lebanon, New York.

unproven resistance to radiation and high-temperature irradiated water. Also, CERAMASEAL is developing glass-ceramic sealing techniques for mineral-insulated cable, which would provide considerable flexibility in the fabrication of devices for measuring electrode potentials in the BCCL. However, this feedthrough flexibility is lost on the reference electrode unless the above efforts are successful in qualifying a reference electrode that can use a metal tip (i.e. - Pd, W or Pt) instead of the metal/salt systems currently available.

6.3.3 BCCL Radiolysis Chemistry Modeling

Recommended future modifications of the computer code BCCLMIT are grouped into two categories. The first category includes those refinements that were identified using BCCLMIT for the parametric studies described in this thesis. The second category is for the additions required to support future N^{16} carryover studies.

6.3.3.1 Recommended Refinements to BCCLMIT

The changes in the first category are (1) change the Notre Dame equation set from a water-implicit form to a water-explicit form, and (2) change the method for specifying dose-rate for a given BCCL section from a constant level to a linearly-varying level. The water-implicit equation set does not explicitly include water as either a reactant or product, even though it is involved in the stoichiometry of several reactions. The assumption is that the concentration of water, which is several orders of magnitude greater than other species, is unchanged by the reactions. For the water-implicit form, the rate coefficients for those reactions with water as a reactant are multiplied by the concentration of water. The reactant water species is then deleted from the list of reactants. Although the assumption that the reactions do not change the concentration

of the water is valid, the concentration does change as a function of density. If a density corresponding to 280°C is used for BCCL simulations, the error introduced by using a constant water density for the reaction set over the small temperature range encompassed between loop inlet and outlet, is within the accuracy of the high-temperature rate coefficients. However, the equation set, and therefore the code, are significantly less flexible, because the equation set is now temperature-dependent. Assuming the effective temperature range is not already limited because of non-Arrhenius rate coefficient behavior, explicitly including water as a reactant restores considerable flexibility. With an explicit equation set, the water concentration could be calculated at each meshpoint in the subroutine FRO (in BCCLMIT) from the density which is already calculated at each meshpoint. A branching flag would be required in the reaction control loop to identify each time water came up as a reactant, and then set the concentration of water to the value previously calculated.

BCCLMIT currently specifies a separate gamma and neutron dose rate for each of the twelve sections of the BCCL. These dose rates are held constant over the entire length of the section. The parametric studies indicate that the ratio of gamma dose rate to neutron dose rate can be as important as the magnitude of the appropriately averaged sectional dose rate. Given the differences between the slope of the fast-neutron flux and the slope of the gamma flux, the gamma-to-neutron dose ratio can change rapidly over a 30 to 50 cm length. In addition, the large step changes in dose rate from one section to another challenged the numerical solver, although no convergence errors were flagged. Considering the importance of the dose rate to the calculated concentration of principal chemical species, the input list for each section should be expanded to include two gamma and two neutron dose rate values for each section instead of one value for each. An inlet and an outlet value would then be specified for each section.

Even though the actual flux shapes are non-linear, a linear approximation is superior to the constant value case in that it (1) permits a smooth dose rate transition at section boundaries, (2) permits variation of the gamma-to-neutron ratio along the length of a section, and (3) provides a better approximation of the actual dose rate for the section of interest.

In addition to the two dose rate parameters added to the input list, the dose rate evaluation step in the subroutine RADIOLYSIS must be moved to FRO, where the linear interpolation can be made at each meshpoint. Similar linear interpolations are already performed in FRO to support temperature and density changes.

6.3.3.2 Additions Required for N^{16} Carryover Studies

The changes required to support N^{16} carryover studies include the addition of the applicable nitrogenous species reactions, and the addition of gas absorption and stripping mass transfer coefficients for gaseous species used in the two-phase mole balance. In addition to the Notre Dame water radiolysis equation set[47] listed by Simonson[14], a set involving nitrogen-containing species was also included. However, some of the chemical species of interest for N^{16} carryover studies are not included in the Notre Dame set. More recent compilations of chemical reaction equation sets would provide a more complete set of equations for nitrogenous species. Ibe et al.[54,55], for example, reported the results of recent N^{16} carryover studies, including the applicable chemical reaction equations involving nitrogenous species.

In this regard, and also with reference to water radiolysis, it may be of some benefit to exercise the sensitivity computation features of Chun's code[15], to reduce the equation sets to the minimum array needed to generate important and measurable data.

Some reaction equation sensitivity work carried out by the present author indicate that only approximately 25% of the equation set are "important", or controlling, for any given set of parameters. However, the group of controlling equations vary depending on the G-value set combination being used, or, for example, on added H_2 concentrations. Furthermore, the controlling group of equations can vary through different BCCL sections, due to changes in radiation dose rates, etc.. This variation within the BCCL necessitates a cautious approach when using differential ("importance") sensitivity analysis, so that, for example, a reaction that is important in-core with high dose rates is not deleted from the reaction equation set based on a sensitivity analysis focused on a section of the BCCL dominated by surface decomposition. In general, an equation set can be reduced by roughly 30% for a given set of G-values and environmental constraints. However, the modeler should always check the validity of a reduced equation set before proceeding with calculations for different chemistry conditions, power levels, etc..

Mass transfer coefficients for the rate at which gaseous species dissolve in the liquid-phase, and for the rate at which gaseous species enter the vapor phase, are included in the code input file using the same format as the applicable chemical reaction equation set. A matched pair of stripping/absorption mass transfer coefficients are required for each volatile chemical species whose concentration in the vapor-phase is important, or whose absence in the liquid-phase, due to stripping, is important. Any number of combinations can be added to the input file. The mass transfer coefficients are distinguished from the reaction rate coefficients, because the former includes a suffix "G" for each chemical species that exists in the gas phase. The only constraint

is that the last two equations in the equation set of the input file must always be the two surface decomposition equations, and these two equations must remain in the specified order.

An assumption made in the BCCLMIT model is that vapor-phase reactions are negligible, except for the absorption and stripping mass transfer rates. This is a valid assumption for the water radiolysis modeling performed thus far. However, if any carryover study involves important vapor-phase reactions, the appropriate addition to the vapor-phase differential equation in FRO would have to be made (to parallel the expression in the liquid-phase differential equation). This addition would also be required if the radioactive decay of N^{16} was to be factored into the studies.

In conclusion, an experimental capability has been provided for the measurement of H_2O_2 (and other less sensitive species such as H_2 and O_2) in a simulated BWR coolant chemistry environment, together with a radiolysis code to calculate the amount of these products. The resulting components should be extremely useful in reconciling and amending the shortcomings of present data and equation sets, which now often predict differences in concentrations of one or even two orders of magnitude.

Appendix A. Data From H_2O_2 Decomposition Experiments

A.1 H_2O_2 Decomposition for Different Sample Line Materials

The following tables summarize the H_2O_2 concentration measurements made to characterize the high-temperature behavior of H_2O_2 in candidate materials for proposed BCCL sample system configurations. Only experimental runs that were free of colorimetric interferences and had reproducible cold mass-balance calibrations are included. All H_2O_2 concentration data below are from the outlet of the test device.

Table A.5 provides sample calculations for (1) normalizing the data from Table A.1, Titanium Part 2: 14 July 1989, and (2) determining percent decomposition from runs #3 and #4 of Table A.4, Part 3. Although these data were not included with the representative data set shown in Fig. 2.2, they are in good agreement with the trend shown in Fig. 2.2.

Table A.1

H_2O_2 Decomposition Versus Temperature for Titanium*

Titanium Part 1: 27 June 1989**

RUN#	SAMPLE#	PERCENT TRANSMIS.	H_2O_2 [ppb]	MIXING TEMP[°C]	COMMENT***
1	1	89	50	26	#1
2	1	88	60	38	#2
3	1	88	60	81	
4	1	90	40	121	
5	1	89	50	187	
6	1	90	40	222	
7	1	92	20	241	
8	1	93	10	253	

COMMENTS:

#1. This sample was used as the reference sample for subsequent normalization.

#2. Early experimental runs used H_2O_2 inlet concentrations on the order expected for the BCCL. After verification of the first-order behavior of H_2O_2 decomposition, higher H_2O_2 concentrations were used to reduce measurement error due to the resolution of the colorimetric technique used.

---

*- The material of construction for the bench-top testing apparatus is stainless steel. Only the high temperature test section material was changed for these experiments.

**- Titanium tubing I.D. was 0.108 cm (0.043 in).

***- Run number is used to identify the sample(s) taken to measure the H_2O_2 concentration at the unique temperature and flow combination identified by the run number.

Table A.1 (Continued)

H_2O_2 Decomposition Versus Temperature for Titanium

Titanium Part 2: 14 July 1989

RUN#	SAMPLE#	PERCENT TRANSMIS.	H_2O_2 [ppb]	MIXING TEMP[°C]	COMMENT
1	1	84	110	28	#1
	2	84	110	28	
	3	84	110	28	
2	1	86	80	185	
	2	85	100	185	
3	1	90	40	266	
	2	90	40	266	

COMMENT: #1. This sample run was used as the reference run.

Table A.1 (Continued)

H_2O_2 Decomposition Versus Temperature for Titanium*

Titanium Part 3: 12 July 1989

RUN#	SAMPLE#	PERCENT TRANSMIS.	H_2O_2 [ppb]	MIXING TEMP[°C]	COMMENT
1	1	76	200	22	#1
	2	77	190	22	
	3	74	220	21	
	4	74	220	20	
	5	74	220	20	
2	1	74	220	100	
	2	74	220	100	
3	1	76	200	181	#2
	2	79	160	187	
	3	77	190	180	
4	1	80	150	227	#2
	2	80	150	227	
	3	82	130	233	
5	1	89	50	277	#2
	2	88	60	277	
	3	87	70	276	
	4	87	70	276	
6	1	90	40	285	
	2	90	40	285	

COMMENTS:

#1. This sample run was used as the reference run.
#2. Sample groups include measurements made at different times, including increasing and decreasing temperature step changes to ensure that any non-equilibrium effects would become evident.

*- The material of construction for the bench-top testing apparatus is stainless steel. Only the high temperature test section material was changed for these experiments.

Table A.2

H_2O_2 Decomposition Versus Temperature for Aluminum*

RUN#	SAMPLE#	PERCENT TRANSMIS.	H_2O_2 [ppb]	MIXING TEMP[°C]	COMMENT
1	1	75	210	22	#1
	2	76	200	21	
	3	75	210	22	
	4	76	200	22	
2	1	76	200	90	
3	1	75	210	133	
	2	77	190	133	
4	1	76	200	183	
		76	200	182	
5	1	78	170	197	
6	1	82	130	245	#2

COMMENTS:

#1. This sample run was used as the reference run.
#2. The thin-wall aluminum tubing failed at higher temperatures.

*- Aluminum tubing I.D. was 0.078 cm (0.030 in).

Table A.3

H_2O_2 Decomposition Versus Temperature for Stainless Steel

Stainless Steel* Part 1: 28 June 1989					
RUN#	**SAMPLE#**	**PERCENT TRANSMIS.**	**H_2O_2 [ppb]**	**MIXING TEMP[°C]**	**COMMENT**
1	1	73	240	22	#1
	2	73	240	21	
2	1	76	200	181	
3	1	80	150	229	
4	1	83	120	250	
5	1	84	110	258	
	2	86	80	258	
6	1	83	120	268	
7	1	85	100	280	#2
	2	86	80	280	

COMMENT: #1. This sample run was used as the reference run.

*- Stainless steel tubing I.D. was 0.108 cm (0.043 in).

Table A.3 (Continued)

H_2O_2 Decomposition Versus Temperature for Stainless Steel

Stainless Steel Part 2: 11 July 1989					
RUN#	SAMPLE#	PERCENT TRANSMIS.	H_2O_2 [ppb]	MIXING TEMP[°C]	COMMENT
1	1	70	270	22	#1
	2	70	270	21	
	3	69	290	20	
2	1	70	270	125	
3	1	72	250	178	
4	1	79	160	223	
1A	1	73	240	20	#1,2
	2	73	240	20	
2A	1	82	130	238	
3A	1	88	60	277	
	2	89	50	277	

COMMENTS:

#1. This sample run was used as the reference run.
#2. A flow rate change required renormalization for the subsequent samples.

A.2 Other H_2O_2 Decomposition Studies

The following table summarizes the raw data collected to characterize the decomposition of H_2O_2 as a function of the length of the uncooled test section. The standard bench-top test apparatus used an uncooled length of 3.8 cm; therefore, only data for 2.5 cm, 7.6 cm and <0.5 cm are included here. Data for variation in flow rates and cooling water temperature are not included since, as discussed in Chapter 2, there was no observable variation in H_2O_2 concentration. A percent H_2O_2 decomposition sample calculation is included in Table A.5.

Table A.4

H_2O_2 Decomposition Versus Uncooled Tube Length*

Part 1: 2.5cm

RUN#	SAMPLE#	PERCENT TRANSMIS.	H_2O_2 [ppb]	MIXING TEMP[°C]	COMMENT
1	1	76	200	20	#1
	2	77	190	20	
	3	76	200	20	
	4	76	200	20	
	5	76	200	20	
	6	76	200	20	
2	1	85	100	282	#2
	2	86	80	284	
	3	86	80	282	
	4	85	100	283	
	5	85	100	282	

COMMENTS:

#1. This sample run was used as the reference run.
#2. Only one temperature datum is required along with its respective reference run for comparison.

*- The uncooled test section tubing length is discussed in Chapter 2. It is the length of tubing between the mixing tee and the cooler.

Table A.4 (Continued)

H_2O_2 Decomposition Versus Uncooled Tube Length

Part 2: 7.6 cm

RUN#	SAMPLE#	PERCENT TRANSMIS.	H_2O_2 [ppb]	MIXING TEMP[°C]	COMMENT
1	1	75	210	27	#1
	2	74	220	27	
	3	75	210	27	
	4	74	220	27	
2	1	88	60	281	#2
	2	87	70	281	
	3	88	60	283	
3	1	72	250	20	#1
	2	73	240	20	
	3	73	240	20	
	4	73	240	20	
	5	73	240	20	
4	1	88	60	275	#2
	2	89	50	276	
	3	89	50	276	
	4	88	60	276	
	5	89	50	276	

COMMENTS:

#1. This sample run was used as the reference run.
#2. Only one temperature datum is required along with its respective reference run for comparison.

Table A.4 (Continued)

H_2O_2 Decomposition Versus Uncooled Tube Length

Part 3: <0.5 cm

RUN#	SAMPLE#	PERCENT TRANSMIS.	H_2O_2 [ppb]	MIXING TEMP[°C]	COMMENT
1	1	73	240	21	#1
	2	73	240	21	
2	1	76	200	280	#2
	2	73	240	280	
	3	73	240	280	
	4	72	250	280	
	5	73	240	280	
3	1	85	100	21	#1
	2	86	80	21	
	3	86	80	21	
	4	86	80	21	
4	1	87	70	280	#2
	2	86	80	280	
	3	86	80	280	
5	1	83	120	25	#1
	2	83	120	23	
	3	83	120	23	
6	1	83	120	214	#2
	2	81	140	214	
	3	82	130	212	
	4	83	120	212	

COMMENTS:

#1. This sample run was used as the reference run.
#2. Only one temperature datum is required along with its respective reference run for comparison.

Table A.5: Sample Calculations
Part 1: H_2O_2 Decomposition Normalization

The data for this part are taken from Table A.1, Titanium Part 2: 14 July 1989.

1. The average reference run (run #1) H_2O_2 concentration is determined first. The high temperature runs will be compared against the following average H_2O_2 concentration:

$$\overline{C}_{H_2O_2} = 110 ppb$$

2. Each of the H_2O_2 measurements from runs #1, #2 and #3 are now divided by the average H_2O_2 concentration from step 1:

Run#	Sample#	H_2O_2 [ppb]	H_2O_2 Normalized
1	1	110	1.0
	2	110	1.0
	3	110	1.0
2	1	80	0.73
	2	100	0.91
3	1	40	0.36
	2	40	0.36

Part 2: Percent H_2O_2 Decomposition

The data for this part are taken from runs #3 and #4 of Table A.4, Part 3.

1. As in Part 1 above, the first step is to average the H_2O_2 concentrations for the reference run, run #3. The average reference H_2O_2 concentration is then

$$\overline{C}^{ref}_{H_2O_2} = \frac{100+80+80+80}{4} = 85ppb. \qquad \text{Eq. A.1}$$

2. The next step is to average the H_2O_2 data for run #4. The average H_2O_2 concentration is

$$\overline{C}_{H_2O_2} = \frac{70+80+80}{3} = 76.7ppb. \qquad \text{Eq. A.2}$$

3. Finally, the percent decomposition is determined as follows:

$$\%\ Decomposition = 100\% \times \left\{1 - \frac{\overline{C}_{H_2O_2}}{\overline{C}^{ref}_{H_2O_2}}\right\} = 9.8\%. \qquad \text{Eq. A.3}$$

A.3 Spectrophotometer/Colorimeter Calibration Curves

The following figures show the calibration curves for the HORIZON 5965-50 Colorimeter and HACH DR/2000 Spectrophotometer. The calibration curves were provided by CHEMetrics based on measurements using standards provided by CHEMetrics. The curves are each based on four measurements. These data points are also plotted on their respective plots.

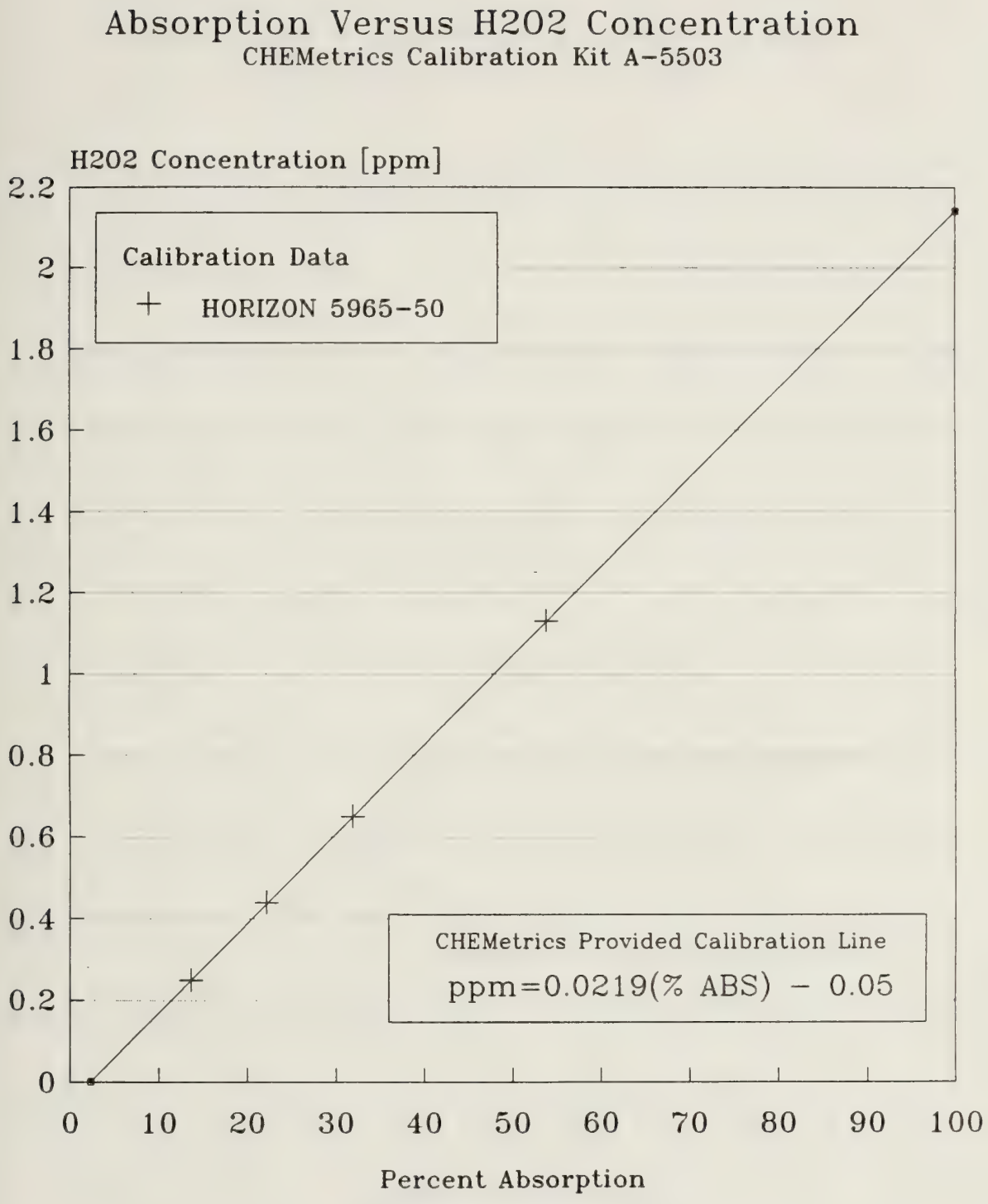

Figure A.1:
HORIZON Colorimeter Calibration Curve

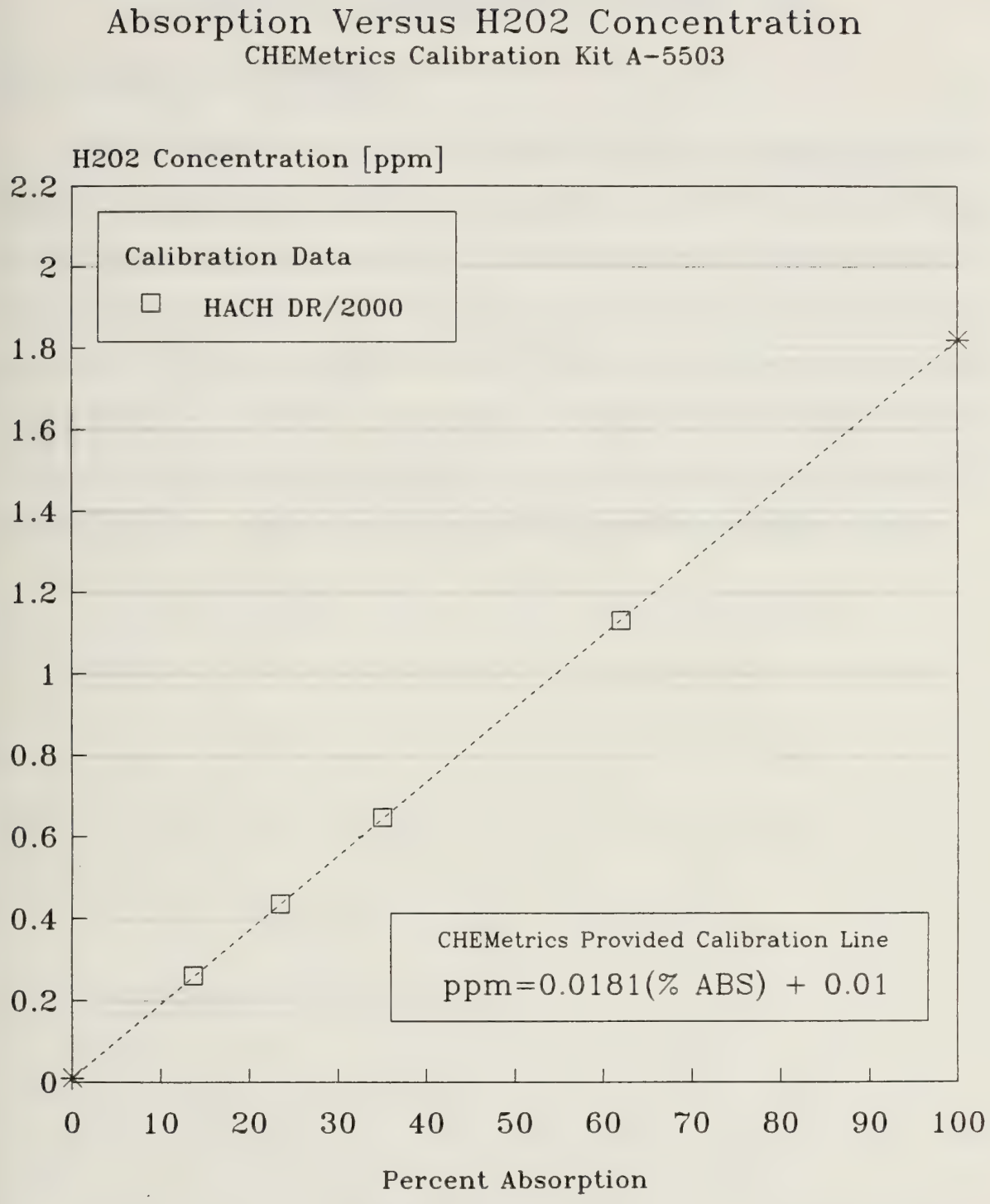

Figure A.2:
HACH Spectrophotometer Calibration Curve

Appendix B. Sampling Device Calibration Data

B.1 Sample Line Calibration

Table B.1 contains the raw data for calibration of the BCCL sampling system tubing which leads from the sample cooling block. The tested length was 487.7 cm, which is sufficient to take the sample line out of the MITR-II core tank, where plastic tubing can be used to transport the sample to the analysis bench. More measurements were not made because (1) the fraction of H_2O_2 that decomposes is within the tolerance of the calibration for the sample cooling block (see Appendix B.2), and (2) as shown in the calculation in Table B.2, the calibration measurements correlate well with H_2O_2 decomposition rates reported by Lin et al.[16]. Table B.2 provides a sample calculation for the BCCL sample system tubing calibration.

Table B.1

Calibration of BCCL Sample System Tubing*

RUN#	SAMPLE#	PERCENT TRANSMIS.	H_2O_2 [ppb]	TEMP** [°C]	COMMENT
1	1	54	510	22	#1
	2	53	530	22	
	3	57	460	22	#1,2
	4	57	460	22	
	5	57	460	22	
	6	57	460	22	
2	1	57	460	92	#3
	2	57	460	92	

COMMENTS:

#1. This sample run was used as the reference run.
#2. Because of the long time required to reach equilibrium at the specific test conditions for this calibration, cold reference runs were run before and after the elevated temperature conditions.
#3. The maximum expected sample line temperature of approximately 90°C was used.

---

*- Calibration of sample tubing is with respect to hydrogen peroxide decomposition. A 0.318 cm (0.125-inch) O.D. stainless steel tube was used (I.D. was 0.236 cm {0.093 in}).

**- The entire test section was maintained at the specified temperature.

Table B.2

BCCL Sample Line H_2O_2 Decomposition Calculation

Experimental result:

1. The average reference H_2O_2 concentration, using the data from Run#1 of Table B.1, is:

$$\overline{C}_{H_2O_2} = \left\{ \frac{510 + 530 + (4 \times 460)}{6} \right\} = \quad 480\text{ppb}. \qquad \text{Eq. B.1}$$

2. The percent decomposition is then:

$$\%\ \ Decomposition = \left\{ 1 - \frac{460\ \text{ppb}}{\overline{C}_{H_2O_2}} \right\} \times 100\% = \quad 4.2\%. \qquad \text{Eq. B.2}$$

Calculated Result:

1. Tubing length = 365.8 cm (12 feet).
2. Tubing inside diameter = 0.236 cm (0.093 inches).
3. Volumetric flow rate = 425 cc/hr = 0.12 cc/s.
4. Cross-sectional flow area = 0.0438 cm^2.
5. Velocity (Volumetric flowrate/cross-sectional area) = 2.694 cm/s.
6. Reynolds number equals

$$Re = \left\{ \frac{965.3 \frac{kg}{m^3} \times 2.694 \frac{cm}{s} \times 0.236 cm \times 10^{-6} \frac{m^3}{cm^3}}{0.3147 \times 10^{-2} \frac{gm}{cm \cdot s} \quad \times \quad 10^{-3} \frac{kg}{gm}} \right\} = 195. \qquad \text{Eq. B.3}$$

7. Average residence time equals

$$\tau = \left\{ \frac{365.8cm}{2.694 \frac{cm}{s}} \right\} = \quad 136 \quad s. \qquad \text{Eq. B.4}$$

8. From data reported by Lin et al.[16], the H_2O_2 surface decomposition rate coefficient at 90°C is $3 \times 10^{-4} \quad s^{-1}$. This rate coefficient includes a correction that scales the rate coefficient by multiplying it by the ratio of the surface-to-volume ratios (i.e. - scaling inversely proportional to diameter).

9. Therefore, using a first-order decomposition model, the predicted percent decomposition equals

$$100\% \times \left\{ 1 - e^{-(3 \times 10^{-4})(136s)} \right\} = \quad 4\%, \qquad \text{Eq. B.5}$$

which is consistent with the experimentally measured value.

B.2 Sample Cooling Block Calibration

Sample cooling block bench-top calibration was done in two ways. The first was a series of parametric evaluations, measuring the percent decomposition of H_2O_2 with respect to the water-cooled, single entry probe (described in Chapter 2). The second way was by the cold, zero-decomposition mass balance approach. The latter method is much more difficult and time consuming. The results from this "absolute", mass-balance approach are included as Table B.3. The results of the "relative" comparison are discussed in Chapter 2.

Table B.3

Calibration of BCCL Sampling System Cooling Block*

RUN#	SAMPLE#	PERCENT TRANSMIS.	H_2O_2 [ppb]	MIXING TEMP[°C]	COMMENT
1	1	48	620	18	#1
	2	45	680	18	
	3	46	660	18	
2	1	61	400	280	#2
	2	60	420	280	
3	1	49	600	28	#1
	2	51	570	24	
	3	50	590	22	
	4	51	570	20	
	5	49	600	20	
4	1	62	390	280	#2
	2	62	390	280	
	3	62	390	280	

COMMENTS:

#1. This sample run was used as the reference run.
#2. Sample cooling block temperature was held at 77°C.

*- Calibration of sample cooling block was with respect to hydrogen peroxide decomposition. The sample cooling block has two independent sample taps. Both were tested against the water-cooled probe (relative, not absolute comparison) and no difference in performance was identified within the accuracy of the colorimetric measurements used.

Appendix C. Electrode Performance Data

C.1 Electrode Data: Figures C.1 through C.4

Figures C.1 through C.4 are discussed in Chapter 4. The electrode potentials (corrosion and redox) listed on these figures are also listed in Fig. 4.2, along with the experimental electrode configurations.

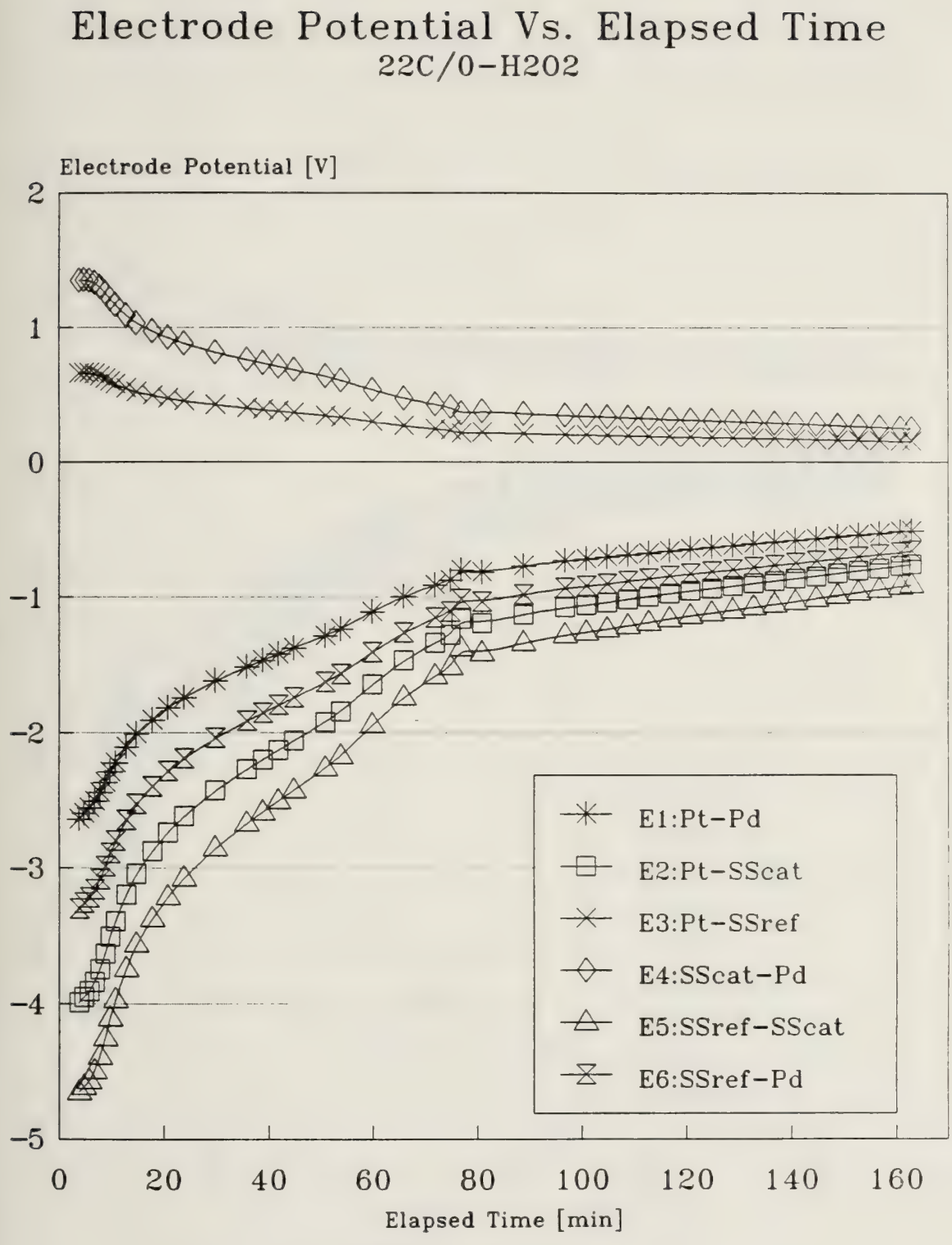

Figure C.1:
Cold Reference Run #2

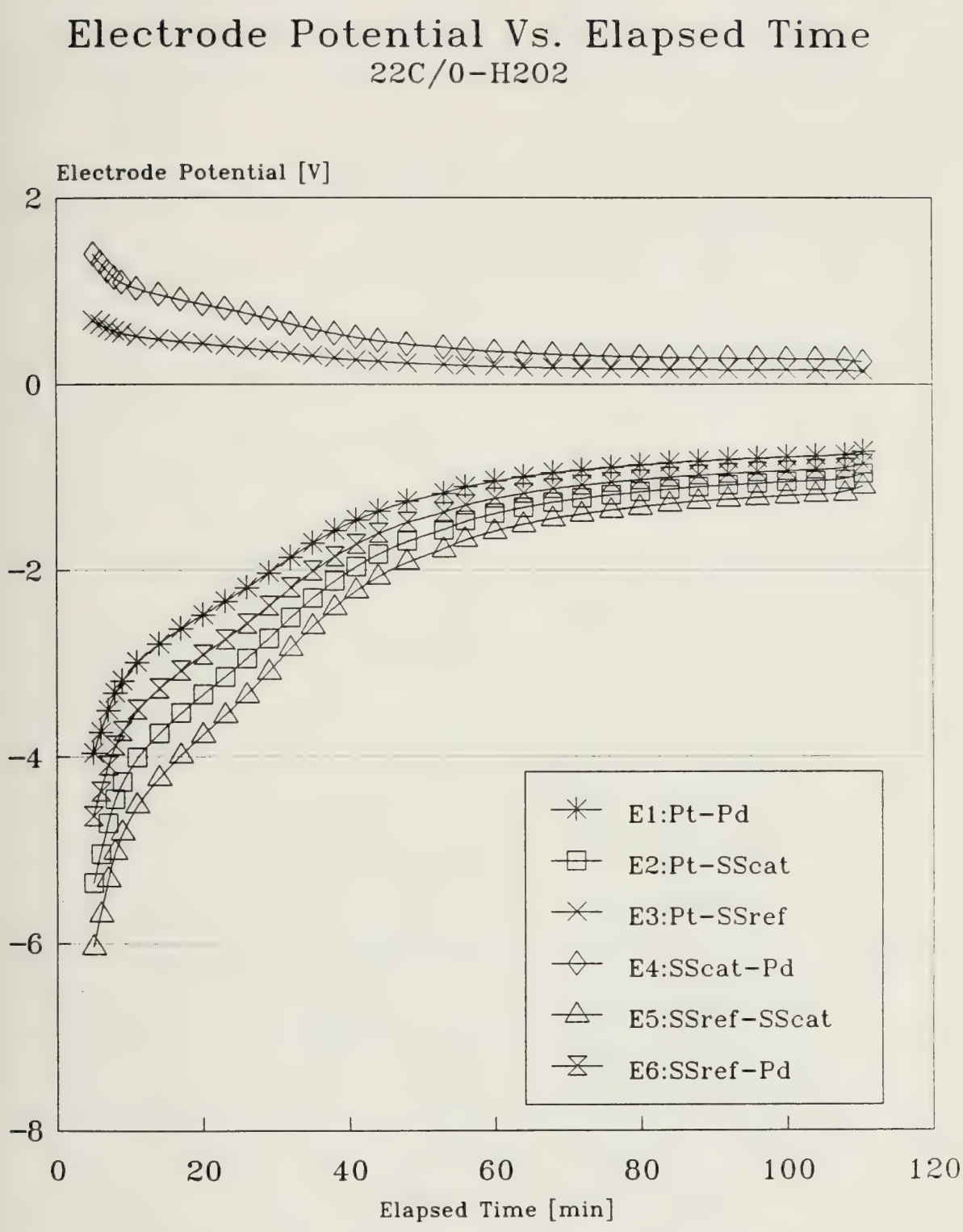

Figure C.2:
Cold Reference Run #3

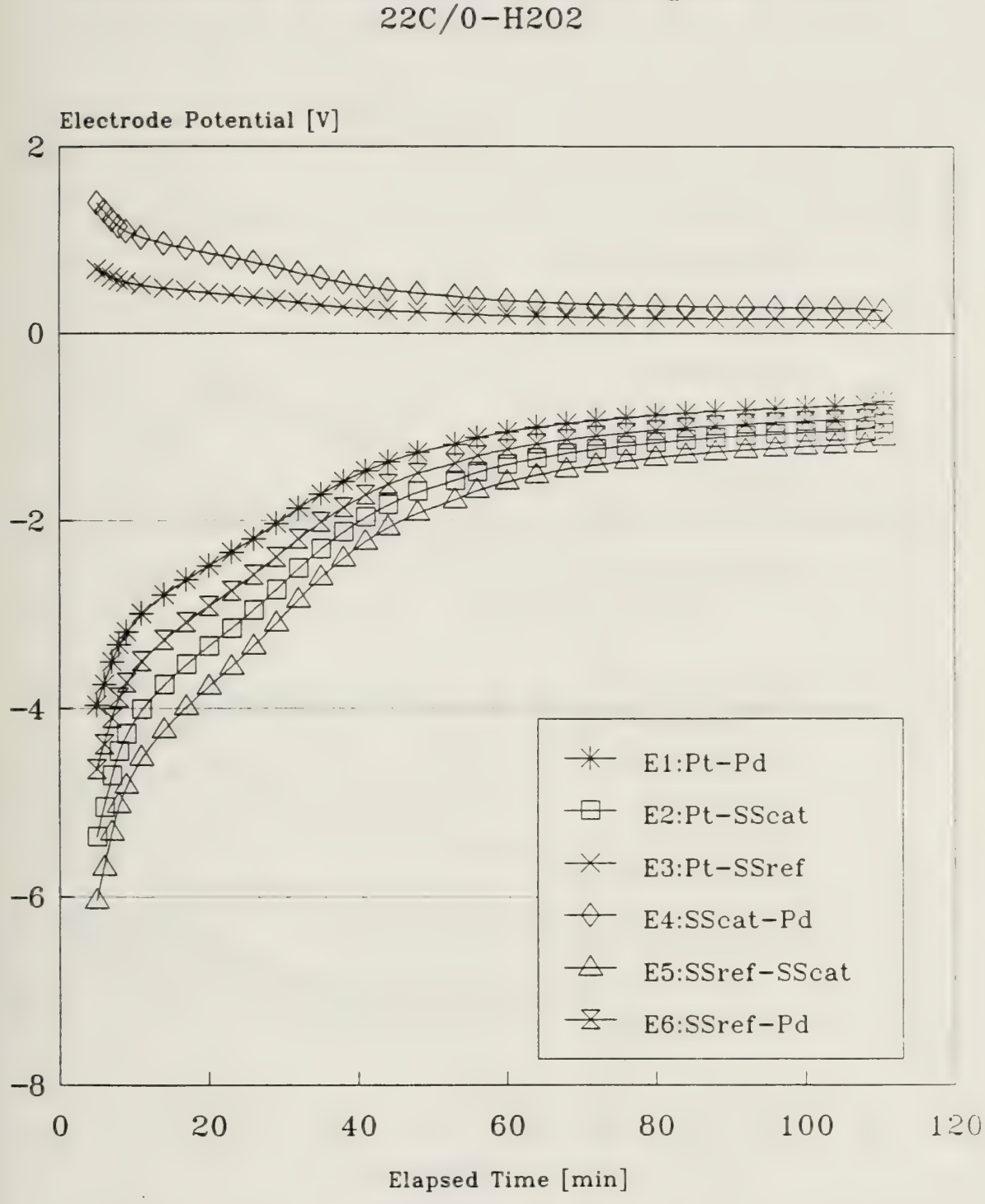

Figure C.3
Cold Reference Run #4

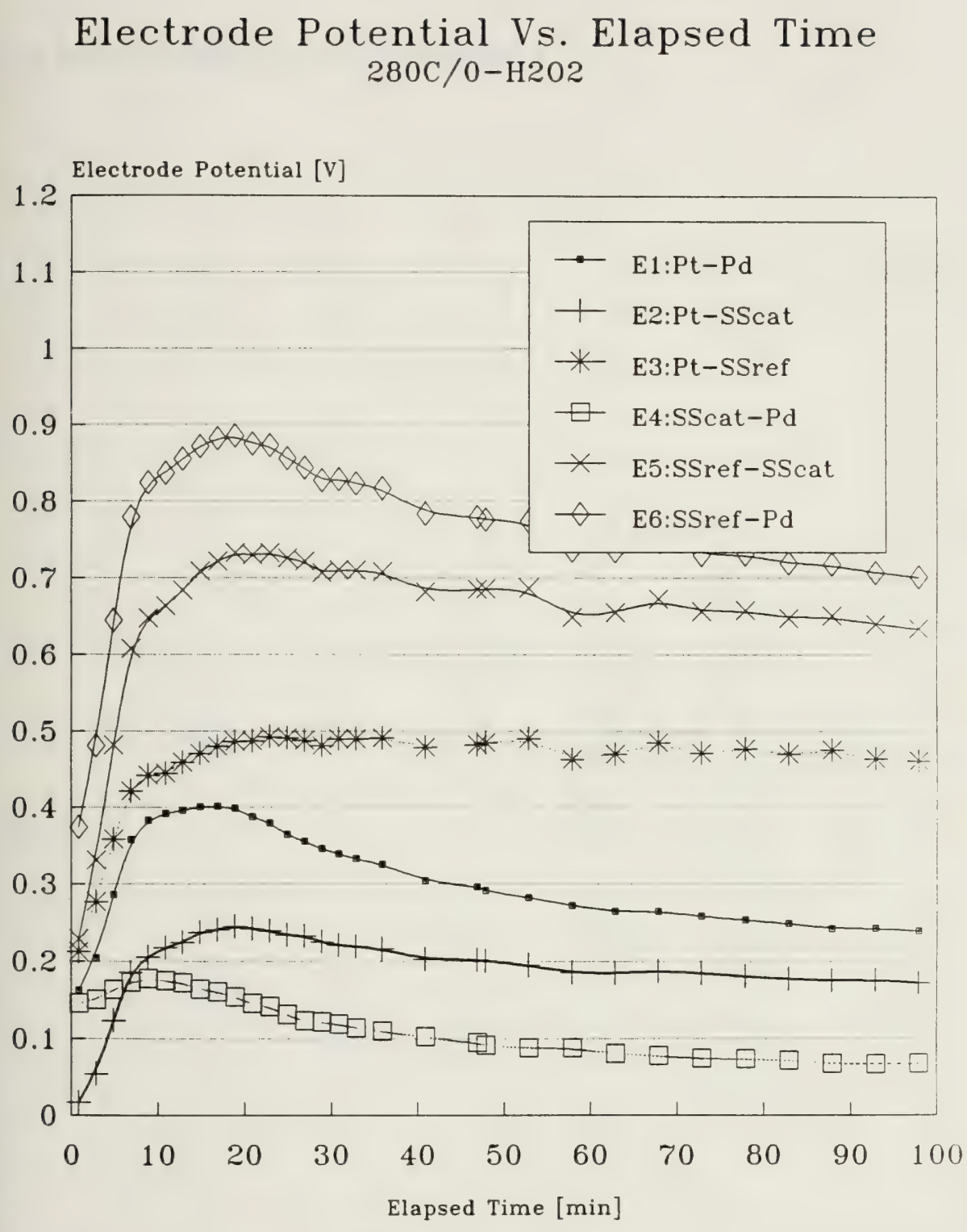

Figure C.4:
Hot Reference Run #4

C.2 Electrode Data: Tables C.1 through C.10

Table C.1

Run #1 - 225 ppb H_2O_2

Electrode Potential (V) Versus Elapsed Time

Elapsed Time [min]	E1 Pt-Pd	E2 Pt-Cat	E3 Pt-Ref	E4 Cat-Pd	E5 Ref-Cat	E6 Ref-Pd
2	0.658	0.442	-0.2475	0.216	0.6895	0.9055
4	0.5232	0.3071	-0.0604	0.2161	0.3675	0.5836
6	0.4553	0.2389	0.0439	0.2164	0.195	0.4114
8	0.4137	0.2004	0.0961	0.2133	0.1043	0.3176
10	0.3855	0.181	0.1289	0.2045	0.0521	0.2566
12	0.3636	0.1689	0.154	0.1947	0.0149	0.2096
14	0.3428	0.1634	0.1685	0.1794	-0.0051	0.1743
16	0.3232	0.1541	0.1735	0.1691	-0.0194	0.1497
18	0.3056	0.1479	0.1744	0.1577	-0.0265	0.1312
20	0.2881	0.1391	0.1756	0.149	-0.0365	0.1125
22	0.2735	0.1335	0.1773	0.14	-0.0438	0.0962
24	0.2609	0.1284	0.1782	0.1325	-0.0498	0.0827
26	0.2504	0.1269	0.1768	0.1235	-0.0499	0.0736
28	0.2396	0.1206	0.1758	0.119	-0.0552	0.0638
32	0.2212	0.1139	0.1739	0.1073	-0.06	0.0473
36	0.2097	0.11	0.1717	0.0997	-0.0617	0.038
40	0.1982	0.1065	0.1727	0.0917	-0.0662	0.0255
44	0.1852	0.1004	0.1699	0.0848	-0.0695	0.0153
48	0.1784	0.0982	0.1718	0.0802	-0.0736	0.0066
52	0.171	0.0936	0.1682	0.0774	-0.0746	0.0028
56	0.1657	0.093	0.1656	0.0727	-0.0726	0.0001
60	0.1611	0.0903	0.1638	0.0708	-0.0735	-0.0027
64	0.1572	0.0894	0.1663	0.0678	-0.0769	-0.0091
68	0.1518	0.0877	0.166	0.0641	-0.0783	-0.0142
72	0.1491	0.0852	0.1632	0.0639	-0.078	-0.0141
76	0.1443	0.0836	0.1647	0.0607	-0.0811	-0.0204
80	0.1414	0.0819	0.1592	0.0595	-0.0773	-0.0178
84	0.1384	0.0793	0.1614	0.0591	-0.0821	-0.023
88	0.1365	0.0818	0.1609	0.0547	-0.0791	-0.0244
92	0.1351	0.0795	0.161	0.0556	-0.0815	-0.0259
96	0.106	0.065	0.1458		-0.0808	-0.0398

Table C.2

Run #2 - 1900 ppb H_2O_2

Electrode Potential (V) Versus Elapsed Time

Elapsed Time [min]	E1 Pt-Pd	E2 Pt-Cat	E3 Pt-Ref	E4 Cat-Pd	E5 Ref-Cat	E6 Ref-Pd
2	0.5514	0.3323	-0.1351	0.2191	0.4674	0.6865
4	0.444	0.2213	0.034	0.2227	0.1873	0.41
6	0.3846	0.1751	0.0911	0.2095	0.084	0.2935
8	0.314	0.1506	0.118	0.1634	0.0326	0.196
10	0.3029	0.1379	0.1355	0.165	0.0024	0.1674
12	0.2741	0.1309	0.1517	0.1432	-0.0208	0.1224
14	0.2481	0.1225	0.1559	0.1256	-0.0334	0.0922
16	0.2272	0.1138	0.1513	0.1134	-0.0375	0.0759
18	0.2091	0.1066	0.1507	0.1025	-0.0441	0.0584
20	0.1962	0.1032	0.1502	0.093	-0.047	0.046
24	0.1739	0.0947	0.1475	0.0792	-0.0528	0.0264
28	0.1593	0.0863	0.1427	0.073	-0.0564	0.0166
32	0.1466	0.0817	0.142	0.0649	-0.0603	0.0046
36	0.1363	0.0793	0.1384	0.057	-0.0591	-0.0021
40	0.1301	0.076	0.1393	0.0541	-0.0633	-0.0092
44	0.1234	0.0724	0.1343	0.051	-0.0619	-0.0109
48	0.1212	0.072	0.1333	0.0492	-0.0613	-0.0121
52	0.1137	0.0699	0.1343	0.0438	-0.0644	-0.0206
56	0.1113	0.0681	0.1329	0.0432	-0.0648	-0.0216
60	0.1071	0.0667	0.1311	0.0404	-0.0644	-0.024
64	0.1055	0.0665	0.1291	0.039	-0.0626	-0.0236
68	0.1012	0.0644	0.1258	0.0368	-0.0614	-0.0246
72	0.0987	0.0633	0.1228	0.0354	-0.0595	-0.0241
76	0.0915	0.0625	0.124	0.029	-0.0615	-0.0325

Table C.3

Run #3 - 590 ppb H_2O_2

Electrode Potential (V) Versus Elapsed Time

Elapsed Time [min]	E1 Pt-Pd	E2 Pt-Cat	E3 Pt-Ref	E4 Cat-Pd	E5 Ref-Cat	E6 Ref-Pd
2	0.6306	0.3769	-0.216	0.2537	0.5929	0.8466
4	0.4928	0.2462	-0.0508	0.2466	0.297	0.5436
6	0.4302	0.1882	0.0392	0.242	0.149	0.391
8	0.335	0.1602	0.0833	0.1748	0.0769	0.2517
10	0.3127	0.1453	0.1074	0.1674	0.0379	0.2053
12	0.2945	0.1362	0.1313	0.1583	0.0049	0.1632
14	0.2774	0.1311	0.1475	0.1463	-0.0164	0.1299
16	0.2592	0.1255	0.1557	0.1337	-0.0302	0.1035
18	0.2437	0.1181	0.1545	0.1256	-0.0364	0.0892
20	0.2283	0.1125	0.1522	0.1158	-0.0397	0.0761
22	0.2158	0.1064	0.152	0.1094	-0.0456	0.0638
24	0.1848	0.1025	0.1524	0.0823	-0.0499	0.0324
28	0.174	0.0946	0.1496	0.0794	-0.055	0.0244
32	0.1659	0.0888	0.1477	0.0771	-0.0589	0.0182
36	0.142	0.0867	0.1472	0.0553	-0.0605	-0.0052
40	0.136	0.0815	0.145	0.0545	-0.0635	-0.009
44	0.131	0.0794	0.1433	0.0516	-0.0639	-0.0123
48	0.1264	0.0774	0.1411	0.049	-0.0637	-0.0147
52	0.1229	0.0765	0.1402	0.0464	-0.0637	-0.0173
56	0.1101	0.0724	0.14	0.0377	-0.0676	-0.0299
60	0.1082	0.0733	0.1382	0.0349	-0.0649	-0.03
65	0.1058	0.0709	0.1363	0.0349	-0.0654	-0.0305
70	0.0986	0.0695	0.1345	0.0291	-0.065	-0.0359
75	0.0963	0.0687	0.1313	0.0276	-0.0626	-0.035
80	0.0942	0.0678	0.1308	0.0264	-0.063	-0.0366
85	0.0943	0.0631	0.1292	0.0312	-0.0661	-0.0349
90	0.0817	0.0642	0.1251	0.0175	-0.0609	-0.0434
95	0.0771	0.0624	0.1212	0.0147	-0.0588	-0.0441
100	0.0687	0.0512	0.1162		-0.065	-0.0475

Table C.4

Hot Reference Run #6 (0 ppb H_2O_2)

Electrode Potential (V) Versus Elapsed Time

Elapsed Time [min]	E1 Pt-Pd	E2 Pt-Cat	E3 Pt-Ref	E4 Cat-Pd	E5 Ref-Cat	E6 Ref-Pd
2	0.7294	0.4919	-0.3009	0.2375	0.7928	1.0303
4	0.635	0.4532	-0.1086	0.1818	0.5618	0.7436
6	0.5692	0.4263	-0.0628	0.1429	0.4891	0.632
8	0.5152	0.3838	0.0043	0.1314	0.3795	0.5109
10	0.4782	0.3351	0.0584	0.1431	0.2767	0.4198
12	0.444	0.2794	0.1222	0.1646	0.1572	0.3218
14	0.4078	0.2316	0.155	0.1762	0.0766	0.2528
16	0.38	0.1985	0.1727	0.1815	0.0258	0.2073
18	0.3563	0.1769	0.1785	0.1794	-0.0016	0.1778
20	0.3363	0.1604	0.1812	0.1759	-0.0208	0.1551
22	0.3175	0.152	0.1814	0.1655	-0.0294	0.1361
26	0.2881	0.1354	0.18	0.1527	-0.0446	0.1081
30	0.2655	0.1271	0.1859	0.1384	-0.0588	0.0796
34	0.2497	0.1191	0.1857	0.1306	-0.0666	0.064
38	0.2347	0.1135	0.1793	0.1212	-0.0658	0.0554
42	0.2231	0.1095	0.1784	0.1136	-0.0689	0.0447
46	0.2134	0.1052	0.1733	0.1082	-0.0681	0.0401
50	0.2047	0.1014	0.1777	0.1033	-0.0763	0.027

Table C.5

Hot Reference Run #9 (0 ppb H_2O_2)

Electrode Potential (V) Versus Elapsed Time

Elapsed Time [min]	E1 Pt-Pd	E2 Pt-Cat	E3 Pt-Ref	E4 Cat-Pd	E5 Ref-Cat	E6 Ref-Pd
2	0.7216	0.5061	-0.343	0.2155	0.8491	1.0646
4	0.5894	0.3848	-0.159	0.2046	0.5438	0.7484
6	0.5183	0.3235	-0.0572	0.1948	0.3807	0.5755
8	0.4678	0.2804	0.0271	0.1874	0.2533	0.4407
10	0.4311	0.2494	0.08	0.1817	0.1694	0.3511
12	0.3977	0.225	0.1056	0.1727	0.1194	0.2921
14	0.3665	0.2062	0.1243	0.1603	0.0819	0.2422
16	0.3409	0.1899	0.1369	0.151	0.053	0.204
18	0.3209	0.1721	0.1431	0.1488	0.029	0.1778
20	0.2987	0.159	0.1521	0.1397	0.0069	0.1466
22	0.2781	0.1495	0.1553	0.1286	-0.0058	0.1228
24	0.2617	0.1397	0.156	0.122	-0.0163	0.1057
26	0.2462	0.1327	0.1592	0.1135	-0.0265	0.087
28	0.2324	0.124	0.1601	0.1084	-0.0361	0.0723
30	0.2216	0.1189	0.1599	0.1027	-0.041	0.0617
32	0.2119	0.1142	0.1566	0.0977	-0.0424	0.0553
36	0.1985	0.1079	0.1619	0.0906	-0.054	0.0366
40	0.1864	0.1012	0.1632	0.0852	-0.062	0.0232
44	0.1768	0.0962	0.1629	0.0806	-0.0667	0.0139
48	0.1676	0.094	0.1604	0.0736	-0.0664	0.0072
60	0.1608	0.0889	0.1626	0.0719	-0.0737	-0.0018
62	0.1576	0.0863	0.1664	0.0713	-0.0801	-0.0088
64	0.1533	0.0825	0.1652	0.0708	-0.0827	-0.0119
68	0.1451	0.0796	0.163	0.0655	-0.0834	-0.0179
72	0.1405	0.0783	0.1607	0.0622	-0.0824	-0.0202
76	0.1366	0.0772	0.1626	0.0594	-0.0854	-0.026
80	0.1332	0.0757	0.1607	0.0575	-0.085	-0.0275
84	0.1305	0.0744	0.1578	0.0561	-0.0834	-0.0273
88	0.1266	0.0759	0.1616	0.0507	-0.0857	-0.035
92	0.1254	0.0743	0.1588	0.0511	-0.0845	-0.0334

Table C.6

Hot Reference Run #7 (0 ppb H_2O_2)

Electrode Potential (V) Versus Elapsed Time

Elapsed Time [min]	E1 Pt-Pd	E2 Pt-Cat	E3 Pt-Ref	E4 Cat-Pd	E5 Ref-Cat	E6 Ref-Pd
2			-0.3625		0.3625	0.3625
4		0.3474	-0.1958	-0.3474	0.5432	0.1958
6		0.281	-0.07294	-0.281	0.35394	0.07294
8	0.416	0.2331	0.00509	0.1829	0.22801	0.41091
10	0.3803	0.19851	0.05461	0.18179	0.1439	0.32569
12	0.35151	0.17283	0.09634	0.17868	0.07649	0.25517
14	0.32432	0.15876	0.13643	0.16556	0.02233	0.18789
16	0.29926	0.14518	0.15789	0.15408	-0.01271	0.14137
18	0.276	0.1311	0.16232	0.1449	-0.03122	0.11368
20	0.256	0.1192	0.16281	0.1368	-0.04361	0.09319
24	0.2271	0.10464	0.1647	0.12246	-0.06006	0.0624
28	0.2075	0.0951	0.1688	0.1124	-0.0737	0.0387
32	0.1939	0.0864	0.1667	0.1075	-0.0803	0.0272
36	0.182	0.0834	0.1666	0.0986	-0.0832	0.0154
38	0.1765	0.0792	0.1671	0.0973	-0.0879	0.0094

Table C.7

Run #5 - 400 ppb H_2O_2

Electrode Potential (V) Versus Elapsed Time

Elapsed Time [min]	E1 Pt-Pd	E2 Pt-Cat	E3 Pt-Ref	E4 Cat-Pd	E5 Ref-Cat	E6 Ref-Pd
4	0.5308	0.2658	-0.0762	0.265	0.342	0.607
6	0.462	0.2049	0.0125	0.2571	0.1924	0.4495
8	0.4157	0.1655	0.0622	0.2502	0.1033	0.3535
10	0.3804	0.1436	0.0845	0.2368	0.0591	0.2959
12	0.3543	0.1318	0.1075	0.2225	0.0243	0.2468
14	0.3327	0.1277	0.1331	0.205	-0.0054	0.1996
16	0.3124	0.1236	0.1493	0.1888	-0.0257	0.1631
18	0.2942	0.1191	0.1509	0.1751	-0.0318	0.1433
20	0.2777	0.1141	0.1558	0.1636	-0.0417	0.1219
22	0.2663	0.1105	0.1591	0.1558	-0.0486	0.1072
24	0.2549	0.1065	0.1623	0.1484	-0.0558	0.0926
28	0.2347	0.1016	0.1611	0.1331	-0.0595	0.0736
32	0.2146	0.0971	0.1624	0.1175	-0.0653	0.0522
36	0.2034	0.092	0.1596	0.1114	-0.0676	0.0438
40	0.1906	0.0868	0.1565	0.1038	-0.0697	0.0341
44	0.1812	0.085	0.1551	0.0962	-0.0701	0.0261
48	0.173	0.0819	0.1539	0.0911	-0.072	0.0191
52	0.167	0.0795	0.155	0.0875	-0.0755	0.012
56	0.1635	0.0806	0.1561	0.0829	-0.0755	0.0074
60	0.1583	0.0799	0.1586	0.0784	-0.0787	-0.0003
64	0.1525	0.0776	0.1547	0.0749	-0.0771	-0.0022
68	0.1493	0.0748	0.1534	0.0745	-0.0786	-0.0041
72	0.1449	0.075	0.1543	0.0699	-0.0793	-0.0094
76	0.1385	0.0738	0.1526	0.0647	-0.0788	-0.0141
80	0.1385	0.0726	0.1524	0.0659	-0.0798	-0.0139
84	0.1355	0.0727	0.1509	0.0628	-0.0782	-0.0154
88	0.1329	0.0713	0.1483	0.0616	-0.077	-0.0154
92	0.1322	0.0705	0.1509	0.0617	-0.0804	-0.0187
96	0.1275	0.072	0.1504		-0.0784	-0.0229

Table C.8

Run #6 - 249 ppb H_2O_2

Electrode Potential (V) Versus Elapsed Time

Elapsed Time [min]	E1 Pt-Pd	E2 Pt-Cat	E3 Pt-Ref	E4 Cat-Pd	E5 Ref-Cat	E6 Ref-Pd
2	0.6882	0.4266	-0.2689	0.2616	0.6955	0.9571
4	0.5482	0.2946	-0.0929	0.2536	0.3875	0.6411
6	0.4687	0.2289	0.0161	0.2398	0.2128	0.4526
8	0.4161	0.1867	0.0747	0.2294	0.112	0.3414
10	0.3732	0.1642	0.1188	0.209	0.0454	0.2544
12	0.3435	0.1482	0.1448	0.1953	0.0034	0.1987
14	0.3191	0.1354	0.1506	0.1837	-0.0152	0.1685
16	0.2966	0.1274	0.1552	0.1692	-0.0278	0.1414
18	0.2805	0.1236	0.1607	0.1569	-0.0371	0.1198
22	0.2545	0.1136	0.1635	0.1409	-0.0499	0.091
26	0.2328	0.1046	0.1647	0.1282	-0.0601	0.0681
28	0.2227	0.1013	0.1661	0.1214	-0.0648	0.0566
32	0.2087	0.0973	0.166	0.1114	-0.0687	0.0427
36	0.194	0.0934	0.1623	0.1006	-0.0689	0.0317
40	0.1844	0.0903	0.1601	0.0941	-0.0698	0.0243
44	0.1742	0.0863	0.1586	0.0879	-0.0723	0.0156
48	0.1667	0.0839	0.1607	0.0828	-0.0768	0.006
52	0.1619	0.0834	0.1583	0.0785	-0.0749	0.0036
56	0.1566	0.0811	0.1568	0.0755	-0.0757	-0.0002
60	0.151	0.0804	0.1543	0.0706	-0.0739	-0.0033

Table C.9

Run #7 - 111 ppb H_2O_2

Electrode Potential (V) Versus Elapsed Time

Elapsed Time [min]	E1 Pt-Pd	E2 Pt-Cat	E3 Pt-Ref	E4 Cat-Pd	E5 Ref-Cat	E6 Ref-Pd
2	0.7102	0.4686	-0.3013	0.2416	0.7699	1.0115
4	0.5675	0.3368	-0.134	0.2307	0.4708	0.7015
6	0.4888	0.2659	-0.0371	0.2229	0.303	0.5259
8	0.4296	0.2207	0.0364	0.2089	0.1843	0.3932
10	0.3898	0.187	0.0786	0.2028	0.1084	0.3112
12	0.3535	0.1691	0.1223	0.1844	0.0468	0.2312
14	0.3218	0.155	0.1429	0.1668	0.0121	0.1789
16	0.298	0.1425	0.1534	0.1555	-0.0109	0.1446
18	0.2793	0.1323	0.1614	0.147	-0.0291	0.1179
20	0.2626	0.1253	0.1617	0.1373	-0.0364	0.1009
24	0.2384	0.1167	0.1622	0.1217	-0.0455	0.0762
28	0.22	0.1077	0.16	0.1123	-0.0523	0.06
32	0.2048	0.1033	0.1616	0.1015	-0.0583	0.0432
36	0.1927	0.0976	0.1629	0.0951	-0.0653	0.0298
40	0.1826	0.0946	0.1623	0.088	-0.0677	0.0203
44	0.1751	0.0908	0.1659	0.0843	-0.0751	0.0092
48	0.1685	0.0883	0.1586	0.0802	-0.0703	0.0099
52	0.163	0.0872	0.1592	0.0758	-0.072	0.0038
56	0.1577	0.0852	0.1597	0.0725	-0.0745	-0.002
60	0.1526	0.0836	0.1561	0.069	-0.0725	-0.0035
64	0.1473	0.0793	0.1588	0.068	-0.0795	-0.0115
68	0.1434	0.0797	0.1596	0.0637	-0.0799	-0.0162
72	0.1422	0.0791	0.1566	0.0631	-0.0775	-0.0144
76	0.1415	0.0763	0.1609	0.0652	-0.0846	-0.0194

Table C.10

Run #8 - 605 ppb H_2O_2

Electrode Potential (V) Versus Elapsed Time

Elapsed Time [min]	E1 Pt-Pd	E2 Pt-Cat	E3 Pt-Ref	E4 Cat-Pd	E5 Ref-Cat	E6 Ref-Pd
2	0.6353	0.3925	-0.2246	0.2428	0.6171	0.8599
4	0.49	0.2698	-0.0665	0.2202	0.3363	0.5565
6	0.4143	0.209	0.032	0.2053	0.177	0.3823
8	0.3678	0.1742	0.0846	0.1936	0.0896	0.2832
10	0.3308	0.1556	0.1204	0.1752	0.0352	0.2104
12	0.3038	0.1446	0.1548	0.1592	-0.0102	0.149
14	0.2775	0.1363	0.1595	0.1412	-0.0232	0.118
16	0.259	0.13	0.1592	0.129	-0.0292	0.0998
18	0.2436	0.123	0.1578	0.1206	-0.0348	0.0858
20	0.2298	0.1178	0.1594	0.112	-0.0416	0.0704
29	0.1949	0.1027	0.1579	0.0922	-0.0552	0.037
32	0.1839	0.1	0.1563	0.0839	-0.0563	0.0276
36	0.1749	0.0967	0.1556	0.0782	-0.0589	0.0193
40	0.1659	0.0927	0.1564	0.0732	-0.0637	0.0095
44	0.1606	0.0902	0.153	0.0704	-0.0628	0.0076
48	0.1532	0.0899	0.1518	0.0633	-0.0619	0.0014
52	0.1514	0.0884	0.1499	0.063	-0.0615	0.0015
56	0.1445	0.086	0.1503	0.0585	-0.0643	-0.0058
60	0.1428	0.0838	0.1485	0.059	-0.0647	-0.0057
64	0.1383	0.0847	0.1496	0.0536	-0.0649	-0.0113
68	0.1361	0.0818	0.1485	0.0543	-0.0667	-0.0124
72	0.1345	0.0799	0.1494	0.0546	-0.0695	-0.0149
76	0.1312	0.0795	0.1464	0.0517	-0.0669	-0.0152
80	0.1285	0.0794	0.1474	0.0491	-0.068	-0.0189
84	0.1272	0.08	0.148	0.0472	-0.068	-0.0208
88	0.123	0.0757	0.1435	0.0473	-0.0678	-0.0205

Appendix D. BCCL Radiolysis Chemistry Computer Code

D.1 BCCLMIT Program Listing

```
      PROGRAM MITIRAD
C
C*************************************************************************
C                        MITIRAD CODE PACKAGE
C*************************************************************************
C
C     VERSION: MIT 5.1                28 FEBRUARY 1990
C     MIT BCCL MITIRAD CODE MODIFICATION
C
C     CODE CUSTODIAN: VERRDON H. MASON
C                     MASSACHUSETTS INSTITUTE OF TECHNOLOGY
C                     138 ALBANY ST. Rm NW12-311
C                     CAMBRIDGE, MA 02139
C                     (617) 253-4204
C
C     ORIGINAL RADIOLYSIS CODE WRITTEN BY: S. A. SIMONSON, 8/05/88
C     BWR MODIFICATION(MIT5.0) WRITTEN BY: J. H. CHUN,  2/05/90
C
C     OPERATING SYSTEM: MICROVMS VERSION 5.0
C     VAX FORTRAN COMPILER VERSION 4.2
C
C*************************************************************************
C
C     VERSION 5.1 NOTE:
C
C     This version modifies version 5.0 for MIT BWR Coolant
C     Corrosion Loop (BCCL) radiolysis chemistry calculations.  Version
C     5.0 was written for a BWR core calculation.  This version
C     divides the BCCL into several sections with two separate sampling
C     points.  This program also allows non-boiling calculations
C     to support parametric evaluation and experimental work.
C     A separate two-phase flow model (Drift Flux) is used for the
C     plenum region to better characterize fluid dynamics.  The output
C     from this program (moles per liter or PPB, user selected by setting
C     the PPBFLAG in the input file) are normalized to liquid
C     density at 1g/cc to provide since the kinetics equations are
C     based on calculating moles per liter at the temperature and
C     fluid density at the actual mesh point.   Inlet concentrations
C     should be specied using the same reference and the program
C     will adjust the inlet concentrations to the actual initial
C     conditions.
C
C     THIS PROGRAM INCLUDES TWO EXPRESSIONS FOR THE SURFACE
C     DECOMPOSITION RATE COEFFICIENT.  ONE FOR THE CORE MATERIAL
C     AND ONE FOR THE BCCL MATERIAL OF CONSTRUCTION.  THESE
C     TWO EQUATIONS MUST REMAIN IN THE SAME ORDER AT THE END OF
C     THE EQUATION LIST FOR PROPER EXECUTION.
C
C     THIS PROGRAM IS BASED ON THE LAYOUT OF THE BCCL WITH THE
C     FOLLOWING SECTION DESCRIPTIONS [NOTE: A SECTION NAME IN THE
C     INPUT FILE TYPICALLY DESCRIBES THE POINT AT THE END OF THE
C     SECTION, THEREFORE, CARE MUST BE TAKEN TO ENSURE THE LENGTH
C     AND DIAMETER SPECIFIED IN THE SECTION ARE FOR THE LOOP UP
C     TO THE POINT DESCRIBED BY THE SECTION NAME]:
C
C     1- DEFINES THE LOOP AT THE CHEMICAL INJECTION POINT
C     2- DEFINES THE LOOP FROM 1 TO THE ZIRCALOY TRANSITION
C     3- DEFINES THE CORE INLET
C     4- DEFINES THE LOOP UP TO AND INCLUDING THE START OF
C        BOILING FOR TWO-PHASE. FOR THE NON-BOILING CASE, THE
```

```
C        LENGTH OF SECTION 4 IS ONLY USED TO CORRECTLY DEFINE
C        THE SUBSEQUENT POSITION VALUES.
C     5- DEFINES THE LOOP FROM SECTION 4 TO THE CORE OUTLET
C     6- DEFINES THE LOOP FROM 5 TO THE ZIRCALOY TRANSITION
C     7- DEFINES THE LOOP FROM 6 TO THE PLENUM INLET
C     8- DEFINES THE LOOP PLENUM AREA. THE LENGTH OF THIS
C        SECTION WOULD BE THE AVERAGE WATER LEVEL IN THE PLENUM
C        IF BOILING.  ALSO, A SEPARATE TWO-PHASE FLOW MODEL IS
C        USED FOR THIS SECTION.
C     9- DEFINES THE LOOP FROM THE PLENUM TO THE SAMPLE TAP.
C    10- DEFINES THE LOOP FROM 9 TO THE INLET TO THE DOWNCOMER
C    11- DEFINES THE DOWNCOMER
C    12- DEFINES THE LOOP FROM 11 TO THE DOWNCOMER SAMPLE TAP.
C
C     VERSION 5.0 NOTE
C
C     This version solves for spatial concentration dC/dx rather than
C     dC/dt which was used in the previous versions.
C     Complete mass balance is
C     implemented including convection and mass transfer terms.  The
C     mass transfer terms are handled differently from the original
C     version by Simonson.
C
C     MITIRAD NOTE
C
C     MITIRAD COMPUTES THE CONCENTRATIONS OF VARIOUS SPECIES
C     PRODUCED BY RADIATION AS A FUNCTION OF TIME USING A
C     VARIATION OF GEAR'S METHOD FOR SOLVING THE STIFF NON-
C     LINEAR SYSTEM OF EQUATIONS.  THE ROUTINES ARE IMPLEMENTED IN
C     DOUBLE PRECISION.
C
C  PROGRAM ELEMENTS:
C
C     READIN:      READS INPUT DATA FROM INPUT FILE.
C     SETUP:       SETS UP REACTION MATRIX FOR RADIOLYSIS CALCULATION.
C     PRINTDATA:   PRINTS INPUT DATA TO OUTPUT FILE.
C     RADIOLYSIS:  CALLS LSODE WHICH IN TURN CALLS FRO AND JACL WHICH
C                  EVALUATES CONCENTRATION PROFILE.
C     LSODE:       LIVERMORE SOLVER OF ORDINARY DIFFERENTIAL
C                  EQUATIONS -  A SET OF SUBROUTINES
C                  PROVIDED BY ALAN HINDMARSH OF LLNL
C                  WHICH SOLVES A GENERAL SET OF ORDINARY
C                  DIFFERENTIAL EQUATIONS USING GEARS METHOD FOR
C                  STIFF NONLINEAR DIFFERENTIAL EQUATIONS THE CURRENT
C                  VERSION MAY HAVE BEEN MODIFIED TO ONLY INCLUDE THE
C                  STIFF OPTION TO SAVE ON SPACE.
C     FRO:         SETS UP THE CONCENTRATION DIFFERENTIAL EQUATION
C                  TO BE SOLVED BY LSODE.
C     JACL:        CONTAINS THE JACOBIAN OF THE DIFFERENTIAL EQUATION
C                  IN FRO.
C     PRINTSTAT:   PRINTS RUN STATISTICS.
C     WRITEPLOT:   GENERATES A PLOT FILE TO BE READ BY RS/1.
C                  THIS FILE IS ALSO USED FOR SENSITIVITY ANALYSIS.
C
C  GLOBAL VARIABLES:
C
C     BOILFLAG:  FLAG TO INDICATE WHETHER TWO-PHASE FLOW PROBLEM
C                [DEFAULT= FALSE, NO BOILING]
C     BOILSTART: POSITION OF ONSET OF BOILING IN TWO PHASE FLOW (cm)
C     CALCSURF:  FLAG USED FOR HYDROGEN PEROXIDE SURFACE DECOMPOSITION
```

```
C                TRUE(DEFAULT)=CONSIDER SURFACE EFFECT,
C                FALSE=DISREGARD SURFACE EFFECT
C     CONC:      SPECIES CONCENTRATION VECTOR (MOLES/L)
C     CONCINIT:  INITIAL CONCENTRATION ARRAY (MOLES/L)
C     CONCOUT:   CONCENTRATION ARRAY FOR OUTPUT (MOLES/L)
C     DENSLIQI:  DENSITY OF LIQUID (g/cc)-INTERPOLATED VALUE AT NODE
C     DENSLIQIN: DENSITY OF LIQUID (g/cc)-INLET LIQUID DENSITY
C     DENSGAS:   DENSITY OF VAPOR (g/cc)
C     DENSLIQ:   DENSITY OF LIQUID (g/cc)-AT OUTLET TEMPERATURE
C     DIAMETER:  EFFECTIVE HYDRAULIC DIAMETER OF THE SECTION(cm)
C     DOWNFLOW:  DOWNCOMER FLOW RATE (g/s)FROM PLENUM
C     DSR:       SECTION GAMMA DOSERATE (CORE*GAMMAMULT)
C     DHR:       SECTION NEUTRON DOSERATE (CORE*NEUTMULT)
C     DVFDX:     d(VOID FRACTION)/dx
C     DVLDX:     d(LIQUID VELOCITY)/dx
C     DVGDX:     d(VAPOR VELOCITY)/dx
C     EA:        ACTIVATION ENERGY (KJ/MOLE-K)
C     FLOWPARA:  FLOW PARAMETER USED IN BANKOFF'S EQUATION
C     FLOWRATE:  MASS FLOWRATE (g/sec)
C     GAMMAMULT: FLUX SCALING MULTIPLIER FOR EACH SECTION (1. = CORE)
C     GAMMARATE: GAMMA DOSE RATE (RAD/S) (CORE AVERAGE)
C     GASCONST:  UNIVERSAL GAS CONSTANT (kJOULES/MOL-K)
C     GCONVERT:  CONVERSION FACTOR FROM # SPECIES/100 eV TO MOL/L-RAD
C     GGAMMA:    GAMMA G-VALUE (# SPECIES/100 ev)
C     GNEUT:     NEUTRON G-VALUE (# SPECIES/100 ev)
C     ID1:       REACTION ARRAY SIZING PARAMETER
C     ID2:       REACTANT ARRAY SIZING PARAMETER
C     ID3:       SECTION ARRAY SIZING PARAMETER
C     ID4:       SECTION ARRAY SIZE INPUT PARAMETER
C     IFLG:      INDEX USED TO SET UP REACTION ORDER
C     INn:       n=1 TO 3; INDICIES ARRAYS FOR CHEMICAL REACTION EVALUATION
C     IND:       INDICIES ARRAYS FOR CHEMICAL REACTION EVALUATION
C     INFILE:    INPUT DATA FILE
C     IP:        PRODUCT ARRAY
C     IR:        REACTANT ARRAY
C     ITER:      ITERATION PERFORMED FOR OUTPUT FOR EACH SECTION
C     ITERSECT:  SECTION ITERATION COUNTER
C     ITERTOTAL: TOTAL OF ITER FOR ALL SECTIONS (FOR OUTPUT USE)
C     IWORK11:   SUMMATION FOR IWORK(11) OUTPUT
C     IWORK12:   SUMMATION FOR IWORK(12) OUTPUT
C     IWORK13:   SUMMATION FOR IWORK(13) OUTPUT
C     JFLAG:     SPECIFIES NUMBER OF OUTER ITERATIONS
C     KOEF:      REACTION COEFFICIENT; + FOR PRODUCT, - FOR REACTANT
C                                      1 FOR FIRST ORDER, 2 FOR SECOND ORDER
C     LENGTH:    LENGTH FOR EACH SECTION (cm)
C     LINLIN:    FLAG FOR PLOTFILE OUTPUT FORMAT
C                TRUE(DEFAULT)=LIN CONC, LIN X; FALSE=LOG CONC, LIN X
C     MASSFLUX:  FLOW RATE PER UNIT AREA FOR PLENUM VOID CALCULATION
C     MOLEWT:    ARRAY FOR SPECIES' MOLECULAR WEIGHTS (FOR PPB CONVERT)
C     NEUTMULT:  NEUTRON FLUX MULTIPLIER FOR EACH SECTION (1.= CORE)
C     NEUTRATE:  NEUTRON DOSE RATE (RAD/S)-(CORE AVERAGED)
C     NJ:        ORIGINAL REACTION COEFFICIENT MATRIX
C     NRX:       NUMBER OF CHEMCAL REACTIONS
C     NSPECIES:  NUMBER OF CHEMICAL SPECIES INCLUDING GAS SPECIES
C     OUTFILE:   OUTPUT FILE
C     PDJ:       COLUMN VECTOR FOR JACOBIAN MATRIX
C     PLOTFILE:  PLOT DATA FILE TO BE READ BY RS/1
C     PPBFLAG:   FLAG FOR GENERATING OUTPUT IN PPB (MASS BASIS) OR
C                MOL/LIT.  TRUE(DEFAULT)=OUTPUT IN PPB (EXCEPT FOR *-
C                WHICH PPB OUTPUT IS MOLE BASIS!)
```

```
C     PPBMULT:    PPB CONVERSION MULTIPLIER
C     PRESSURE:   SYSTEM PRESSURE (atm)
C     QUAL:       STEAM QUALITY AT EACH MESH POINT (FRACTION)
C     QUALEXIT:   CORE EXIT QUALITY (FRACTION)
C     RATECONST:  RATE CONSTANT AT SYSTEM TEMPERATURE (MOL/L-S IN GENERAL)
C     RCINIT:     RATE CONSTANT AT REFERENCE TEMPERATURE (MOL/L-S IN GENERAL)
C     RSOUT:      FLAG FOR PLOTFILE OUTPUT TO BE READ BY RS1
C                 TRUE(DEFAULT)=GENERATE PLOT FILE,FALSE=NO PLOT FILE
C     RXNAME:     ARRAY OF REACTION NAMES
C     SECTNAME:   ARRAY OF SECTION NAMES
C     SLIPRATIO:  TWO-PHASE SLIP RATIO
C     SPECIES:    ARRAY OF SPECIES NAMES
C     SPECIESDUMMY: DUMMY VARIABLE STORAGE TO OFFSET SPECIES(0)
C     STEAMFLOW:  STEAM FLOW RATE EXITING PLENUM (g/s)
C     TEM:        TEMPERATURE ALONG THE FLOW CHANNEL (K)
C     TEMREF:     REFERENCE TEMPERATURE TO BASE ARRHENIUS' LAW UPON (K)
C     TIMEx:      SYSTEM TIME USED IN CALCULATING EXECUTION TIME
C     TINLET:     INLET TEMPERATURE (K)
C     TOUTLET:    OUTLET TEMPERATURE (K)
C     VELINF:     TERMINAL VAPOR BUBBLE VELOCITY FOR DRIFT FLUX MODEL(cm/s)
C     VELINLET:   BOILING SECTION INLET LIQUID VELOCITY (cm/s)
C     VELGAS:     VAPOR VELOCITY ALONG THE CHANNEL (cm/s)
C     VELLIQ:     LIQUID VELOCITY ALONG THE CHANNEL (cm/s)
C     XFINAL:     FINAL POSITION TO EVALUATE RADIOLYSIS (cm)
C     XOUTPUT:    POSITION ARRAY FOR OUTPUT (cm)
C     XSTEP:      POSITION STEP TO BE TAKEN IN OUTPUT (cm)
C     XSUM:       POSITION AT THE END OF THE CURRENT SECTION
C
C     LSODE VARIABLES ARE DEFINED IN THE LSODE WRITE-UP
C
C  NON-STANDARD VAX FORTRAN FUNCTIONS CALLED:
C
C     INCLUDE:    INCLUDES AN EXTERNAL TEXT FILE AS A PART OF THE SOURCE.
C                 'COMMON.BLK' IS USED TO DECLARE GLOBAL VARIABLES.
C     SECNDS:     PASSES SYSTEM CLOCK IN SECONDS TO REAL*4 VARIABLE.
C                 THIS FUNCTION MAY BE OMITTED WITHOUT AFFECTING
C                 THE ESSENTIAL PART OF THE CODE.
C     NAMELIST :  COMPACT WAY OF READING INPUT DATA.  THIS MAY BE REWRITTEN
C                 TO READ INPUT PARAMETERS ONE BY ONE IN STANDARD WAY.
C     DATE:       RETURNS TODAY'S DATE AS FOUND IN THE SYSTEM
C     TIME:       RETURNS CURRENT TIME AS FOUND IN THE SYSTEM
C
C*************************************************************************
C
      INCLUDE 'COMMON.BLK'
C
      TIME1=SECNDS(0.0)    !START CLOCK TO MEASURE EXECUTION TIME
      CALL READIN          !READS ALL INPUT PARAMETERS
      CALL SETUP      !PREPARES INPUT PARAMETERS FOR RADIOLYSIS CALC
      OPEN (6,FILE=OUTFILE,STATUS='NEW')          !OUTPUT FILE
      CALL PRINTDATA       !WRITES INPUT PARAMETERS TO OUTPUT FILE
      CALL RADIOLYSIS      !PROCESS THE DATA
      CALL PRINTSTAT                              !WRITE RUN STATISTICS
      CLOSE (6)
      IF (RSOUT) CALL WRITEPLOT                   !WRITE PLOT FILE
C
      STOP
      END       ! OF MITIRAD
```

```
      SUBROUTINE READIN
C
C*************************************************************************
C     VERSION: MIT 5.1                                  22 FEBRUARY 1990
C     CODE CUSTODIAN: VERRDON H. MASON
C*************************************************************************
C
C     READS LOGICAL UNIT NUMBER 5 FOR THE REACTION MATRIX
C     AND REACTION RATE CONSTANTS.  REACTION RATE CONSTANTS ARE
C     ADJUSTED FOR TEMPERATURE USING AN ARRHENIUS TEMPERATURE
C     DEPENDENCE
C*************************************************************************
C
      INCLUDE 'COMMON.BLK'
C
      NAMELIST /FILENAME/ OUTFILE,PLOTFILE
      NAMELIST /SIZE/ NSPECIES,NRX
      NAMELIST /GEOMETRY/ BOILSTART,XSUM,DIAMETER,LENGTH
      NAMELIST /STATE/ TINLET,TOUTLET,TEMREF,GAMMARATE,NEUTRATE,
     +                 VELINLET,DENSLIQIN,DENSLIQ,DENSGAS,
     +                 PRESSURE,FLOWRATE,QUALEXIT,QUAL
      NAMELIST /CONTROL/ XSTEP,ID4
      NAMELIST /FLAGS/ CALCSURF,RSOUT,LINLIN,BOILFLAG,PPBFLAG
      NAMELIST /LSODEDATA/ IOPT,ITASK,RTOL,ITOL,ATOL,RWORK,IWORK,
     +                     ISTATE,MF
      NAMELIST /NAMES/ SPECIES
C
C     ASSIGN DEFAULT VALUES
C
      DATA NSPECIES/1/,NRX/1/
      DATA TINLET/298./,TOUTLET/298./,TEMREF/298./,GAMMARATE/0./,
     +     NEUTRATE/0./,VELINLET/1./,DENSLIQ/1./,VELINF/1./,
     +     DENSGAS/1./,PRESSURE/14.7/,FLOWRATE/1./,DENSLIQI/0./,
     +     DENSLIQIN/1./,QUALEXIT/0./STEAMFLOW/0./,MASSFLUX/1./,
     +     DOWNFLOW/0./,GCONVERT/1./
      DATA XSTEP/1./,BOILSTART/0./
      DATA CALCSURF/.TRUE./,RSOUT/.TRUE./,LINLIN/.TRUE./,
     +     BOILFLAG/.FALSE./,PPBFLAG/.TRUE./
      DATA ATOL/1.D-15/,MF/21/,ITOL/1/,ISTATE/1/,ITASK/1/,RTOL/1.D-5/
      ID4=ID3  !INITIALIZES SECTION SIZE INPUT PARAMETER
C
      TYPE 10   !GET INPUT FILE NAME FROM TERMINAL
10    FORMAT(' INPUT FILE: '$)
      ACCEPT 20,INFILE
20    FORMAT(A)
C
      OPEN (5,FILE=INFILE,STATUS='OLD') !OPEN INPUT DATA FILE
C
      READ (5,NML=FILENAME)           !READ OUTFILE, PLOTFILE NAMES
      READ (5,NML=SIZE)               !READ NSPECIES,NRX
      READ (5,NML=STATE)   !READ STATE VARIABLES
      READ (5,NML=CONTROL) !READ PROGRAM CONTROL PARAMETERS
      READ (5,NML=FLAGS)   !READ LOGICAL FLAGS FOR PROGRAM CONTROL
      READ (5,NML=LSODEDATA)          !READ LSODE CONTROL VARIABLES
      READ (5,NML=NAMES)   !READ THE SPECIES NAMES
C
      READ (5,*)           !READ A BLANK LINE
      READ (5,*)           !READ A BLANK LINE
      DO 140 I=1,NRX       !READ REACTION INFORMATION
```

```
        READ(5,100) RXNAME(I),(IR(I,K),K=1,3),(IP(I,K),K=1,4)
     +             ,RCINIT(I),EA(I)
140   CONTINUE
100   FORMAT(X,A3,3X,7I3,D18.8,D18.8)
C
      READ (5,*)            !READ A BLANK LINE
      READ (5,*)            !READ A BLANK LINE
      DO 200 I=1,NSPECIES  !READ G-VALUES, INITIAL CONCENTRATIONS
        READ (5,220)  GGAMMA(I),GNEUT(I),CONCINIT(I),MOLEWT(I)
200   CONTINUE
220   FORMAT(9X,D10.3,3(/9X,D10.3))
C
      READ (5,*)            !READ A BLANK LINE
      READ (5,*)            !READ A BLANK LINE
      DO 300 I=1,ID4     !READ SECTION PARAMETERS
        READ (5,*)          !READ A BLANK LINE
        READ (5,*)          !READ A BLANK LINE
        READ (5,320) LENGTH(I),DIAMETER(I),GAMMAMULT(I),NEUTMULT(I)
     +              ,SECTNAME(I)
300   CONTINUE
320   FORMAT (11X,D10.3,3(/11X,D10.3),/11X,A16)
C
      CLOSE (5) !CLOSE INPUT FILE
      RETURN
      END       !OF READIN
```

```
      SUBROUTINE SETUP
C
C*************************************************************************
C     VERSION: MIT 5.1                              22 FEBRUARY 1990
C     CODE CUSTODIAN: VERRDON H. MASON
C*************************************************************************
C
C     PREPARES INPUT DATA FOR RADIOLYSIS CALCULATION.
C*************************************************************************
C
      INCLUDE 'COMMON.BLK'
C
      TEM=TINLET           !INITIALLY USE TINLET TO ADJUST PARAMETERS
C     INITIALIZE THE COEFFICIENT AND ORDER MATRICIES FOR THE FUNCTION
C     EVALUATION SEGMENT OF LSODE
C
      DO 110 I=1,NSPECIES  !INITIALIZE TO ZERO
        DO 105 J=1,NRX
          KOEF(J,I)=0
          NJ(J,I)=0
105     CONTINUE
110   CONTINUE
C
C     WARNING PROMPT IN CASE 2-PHASE CONDITIONS ARE SPECIFIED THAT
C     ARE INCONSISTENT WITH CONSTANTS SPECIFIED IN THE INPUT FILE
C
      IF ((BOILFLAG).AND.(TOUTLET.LT.525)) TYPE 115
115   FORMAT ('GAS STRIPPING/ABSORBTION CONSTANTS SPECIFIED IN THE INPUT
     + FILE MUST BE CONSISTENT FOR SPECIFIED OUTLET TEMPERATURES!')
C
C     SET UP THE COEFFICIENT MATRICIES(KOEF), AND THE REACTION ORDER MATRIX(NJ)
C
      DO 140 I=1,NRX
C
C     LOAD IN INITIAL VALUES FOR RATE CONSTANTS
C
        RATECONST(I)=RCINIT(I)
C
C       CHECK FOR SECOND ORDER REACTANTS
C
        IF(((IR(I,1).EQ.IR(I,2)).OR.(IR(I,2).EQ.IR(I,3)))
     +    .AND.(IR(I,2).NE.0))THEN
          NJ(I,JIABS(IR(I,2)))=-2
          KOEF(I,JIABS(IR(I,2)))=-2
        ENDIF
C
C       CHECK FOR FIRST ORDER REACTANTS
C
        DO 120 K=1,3
          IF((IR(I,K).NE.0).AND.(NJ(I,JIABS(IR(I,K))).NE.-2))THEN
            NJ(I,JIABS(IR(I,K)))=-1
            KOEF(I,JIABS(IR(I,K)))=-1
          ENDIF
120     CONTINUE
C
C       CHECK FOR SECOND ORDER PRODUCTS
C
        IF(((IP(I,1).EQ.IP(I,2)).OR.(IP(I,2).EQ.IP(I,3)))
     +    .AND.(IP(I,2).NE.0))THEN
          KOEF(I,JIABS(IP(I,2)))=2
```

```
          ENDIF
          IF(((IP(I,2).EQ.IP(I,3)).OR.(IP(I,3).EQ.IP(I,4)))
     +      .AND.(IP(I,3).NE.0))THEN
            KOEF(I,JIABS(IP(I,3)))=2
          ENDIF
C
C         FILL UP THE PRODUCTS MATRIX FOR FIRST ORDER PRODUCTS
C
          DO 130 K=1,4
            IF((IP(I,K).NE.0).AND.(KOEF(I,IP(I,K)).NE.2))THEN
              KOEF(I,IP(I,K))=1
            ENDIF
130       CONTINUE
140     CONTINUE
C
C       NORMALIZE REACTANTS IN SELF-CATALYTIC REACTIONS
C
        DO 150 K=1,NSPECIES
          DO 151 I=1,NRX
C
C           ARE THERE PRODUCTS OF SPECIES K AS WELL AS REACTANTS OF SPECIES K?
C
            IF((KOEF(I,K).NE.NJ(I,K)).AND.(NJ(I,K).NE.0))
     +        KOEF(I,K)=KOEF(I,K)+NJ(I,K)
C
C           ARE THERE ONLY PRODUCTS? (FILL NJ AFTER CHECKING FOR CATALYTIC RX
C
            IF((KOEF(I,K).NE.NJ(I,K)).AND.(NJ(I,K).EQ.0))
     +        NJ(I,K)=KOEF(I,K)
C
151       CONTINUE
150     CONTINUE
C
C       SET UP REACTION ORDER INDICIES FOR FAST FUNCTION EVALUATION
C
        CONC(NSPECIES+1)=1.0D0          !SET FOR ZERO-ORDER RX
        DO 180 I=1,NRX
C
C         INITIALIZE ALL REACTANTS TO ZERO ORDER
C
          IN1(I)=NSPECIES+1
          IN2(I)=NSPECIES+1
          IN3(I)=NSPECIES+1
          IND=0
          IFLG=0
          DO 170 J=1,NSPECIES
C
C           ESTABLISH ALL FIRST ORDER REACTANTS
C
            IF((NJ(I,J).EQ.-1).AND.(IND.EQ.0))THEN
              IN1(I)=J
              IFLG=IFLG+1
            ELSE IF ((NJ(I,J).EQ.-1).AND.(IND.EQ.1))THEN
              IN2(I)=J
              IFLG=IFLG+1
            ELSE IF ((NJ(I,J).EQ.-1).AND.(IND.EQ.2))THEN
              IN3(I)=J
              IFLG=IFLG+1
            ENDIF
C
```

```
C         DETERMINE THE SECOND ORDER REACTANTS (EITHER FIRST TWO
C         OR LAST TWO). IND IS NUMBER OF REACTANTS CHOSEN SO FAR
C
          IF ((NJ(I,J).EQ.-2).AND.(IND.EQ.0)) THEN
            IN1(I)=J
            IN2(I)=J
            IFLG=IFLG+2
          ELSE IF ((NJ(I,J).EQ.-2).AND.(IND.EQ.1)) THEN
            IN2(I)=J
            IN3(I)=J
            IFLG=IFLG+2
          ENDIF
          IND=IND+IFLG
          IFLG=0
C
170       CONTINUE
180     CONTINUE
C
        RETURN
        END       !OF SETUP
```

```
      SUBROUTINE PRINTDATA
C
C*********************************************************************
C     VERSION: MIT 5.1                          28 FEBRUARY 1990
C     CODE CUSTODIAN: VERRDON H. MASON
C*********************************************************************
C
C     WRITES PROCESSED INPUT DATA TO OUTPUT FILE.
C
C     CAUTION ON NON-STANDARD USE OF ARRAY SUBSRIPT!
C     AN ELEGANT WAY OF PRINTING BLANK SPACES FOR EMPTY SPECIES NAME IS
C     DANGEROUSLY IMPLEMENTED BY USING SPECIES(0) BELOW.  IN FORTRAN77
C     ACCESSING ZERO SUBSCRIPT IS ILLEGAL BUT VAX FORTRAN DOESN'T SEEM
C     TO CARE.  TO COMPENSATE THIS, A DUMMY ARRAY SPECIESDUMMY IS INSERTED
C     JUST BEFORE SPECIES ARRAY TO ALLOCATE A FEW BYTES OF MEMORY SPACE.
C     IF YOU WISH, YOU MAY MODIFY THIS BY REWRITING IT.
C*********************************************************************
C
      INCLUDE 'COMMON.BLK'
      CHARACTER*9 TODAY,NOW
C
      CALL DATE(TODAY)                  !VAX FUNCTION
      CALL TIME(NOW)
      IF (BOILFLAG) THEN    ! 2-PHASE OPTION FLAG
        BOILSTART=LENGTH(4)+LENGTH(3)+LENGTH(2)+LENGTH(1)
      ELSE
        QUALEXIT=0.D0
      ENDIF
C
      WRITE (6,120) TODAY,NOW
120   FORMAT(
     + 12X,    '_____________________________________________________'
     +,/ ,12X,'|              MITIRAD CODE PACKAGE OUTPUT              |'
     +,/ ,12X,'|               MITIRAD VERSION: MIT  5.1               |'
     +,/ ,12X,'|                 MIT BCCL MODIFICATION                 |'
     +,/ ,12X,'|                                                       |'
     +,/ ,12X,'|',17X,A9,2X,A9,16X,'|'
     +,/ ,12X,'_____________________________________________________')
      WRITE (6,140)
      WRITE (6,150)
      WRITE (6,140)
      WRITE (6,135) INFILE, OUTFILE, PLOTFILE
      WRITE (6,130) NRX,NSPECIES
140   FORMAT(/80(1H_)/)
150   FORMAT(33X,'INPUT PARAMETERS')
135   FORMAT(    5X,36H  INPUT FILE NAME                  = ,A35,/
     +           5X,36H  OUTPUT FILE NAME                 = ,A35,/
     +           5X,36H  PLOT FILE NAME                   = ,A35)
130   FORMAT ( /5X,36H  NUMBER OF CHEMICAL REACTIONS      = ,I8,/,
     +           5X,36H  NUMBER OF SPECIES EVALUATED      = ,I8/)
C
      WRITE(6,105) XSTEP,BOILSTART,QUALEXIT
105   FORMAT (5X,36H  POSITION INCREMENT                = ,F14.5,' cm',
     +       /5X,36H  POSITION AT ONSET OF BOILING      = ,F14.5,' cm',
     +       /5X,36H  CORE EXIT QUALITY (FRACTION)      = ,F14.5,/)
C
      WRITE(6,110) TINLET,TOUTLET,TEMREF
110   FORMAT (5X,36H  INLET TEMPERATURE                 = ,F14.5' K',
     +       /5X,36H  OUTLET TEMPERATURE                = ,F14.5' K',
     +       /5X,36H  REFERENCE TEMPERATURE             = ,F14.5' K')
```

```
C
      WRITE(6,106) DENSLIQIN,DENSLIQ,DENSGAS,PRESSURE
106   FORMAT (5X,36H  INLET WATER DENSITY              = ,F14.5,' g/cc',
     +       /5X,36H  OUTLET WATER DENSITY             = ,F14.5,' g/cc',
     +       /5X,36H  VAPOR DENSITY                    = ,F14.5,' g/cc',
     +       /5X,36H  PRESSURE                         = ,F14.5,' atm')
C
      WRITE(6,107) FLOWRATE
107   FORMAT (5X,36H  MASS FLOWRATE                    = ,D14.5,' g/s'/)
C
      WRITE (6,250) ATOL,RTOL
250   FORMAT (5X,36H  ABSOLUTE TOLERANCE               = ,D14.5,
     +       /5X,36H  RELATIVE TOLERANCE               = ,D14.5/)
C
      WRITE (6,230) GAMMARATE,NEUTRATE
230   FORMAT (5X,36H  GAMMA DOSE RATE (CORE)           = ,D14.5,' Rad/s',
     +       /5X,36H  NEUTRON DOSE RATE (CORE)         = ,D14.5' Rad/s'/)
C
C     THIS BLOCK WRITES SECTION INPUT PARAMETERS
C
      WRITE (6,252)
252   FORMAT ('1',5X,'SECTION PARAMETERS:')
C
      WRITE (6,253)
253   FORMAT (3X,7HSECTION,13X,6HLENGTH,5X,8HDIAMETER,5X,5HGAMMA,
     +        6X,7HNEUTRON,/3X,4HNAME,16X,4H(cm),8x,4H(cm),
     +        5x,2(10HMULTIPLIER,2X))
C
      DHOLD = LENGTH(5)    !TEMPORARY HOLD
      DO 254 I=1,ID4
      IF ((.NOT.(BOILFLAG)).AND.(I.EQ.4)) THEN
        LENGTH(5)=LENGTH(4)+LENGTH(5)
C       CHANGE VALUE FOR PRINTING ONLY
        GO TO 254
      ENDIF
      WRITE (6,255) SECTNAME(I),LENGTH(I),DIAMETER(I),
     +              GAMMAMULT(I),NEUTMULT(I)
254   CONTINUE
      LENGTH(5)=DHOLD  !RESETS VALUE FOR SUBSEQUENT USE
255   FORMAT (1X,A16,3X,F10.3,2X,F10.3,2(2X,D10.3))
C
C
      WRITE (6,256) CALCSURF,RSOUT,LINLIN,BOILFLAG,PPBFLAG
256   FORMAT (/5X,36H  CALCSURF                         = ,L4,
     +       /5X,36H  RSOUT                            = ,L4,
     +       /5X,36H  LINLIN                           = ,L4,
     +       /5X,36H  BOILFLAG                         = ,L4,
     +       /5X,36H  PPBFLAG                          = ,L4)
C
      WRITE (6,190)
190   FORMAT(/1X,/12X,7HLOW LET,3X,8HHIGH LET,6X,7HINITIAL,
     + /       9X,3X,8HG-VALUES,3X,8HG-VALUES,3X,14HCONCENTRATIONS,
     + /       12X,'(#/100eV)',2X,'(#/100eV)',2X,'(MOLES/LITER)'/)
C
      DO 200 I=1,NSPECIES
        WRITE (6,210) SPECIES(I),GGAMMA(I),GNEUT(I),CONCINIT(I)
200   CONTINUE
210   FORMAT (1X,A8,2(2X,F9.2),5X,D9.2)
C
C     PRINT OUT REACTION MATRIX
```

```
C
      WRITE (6,292)
      WRITE (6,10)
      WRITE (6,140)
      WRITE (6,11)
292   FORMAT ('1',80(1H_),/)
10    FORMAT (10X,
     +59HCHEMICAL REACTIONS, RATE CONSTANTS, AND ACTIVATION ENERGIES)
11    FORMAT (/
     +26X,'REACTIONS',30X,'RATE',2X,'ACTIVATION',/63X,'CONSTANT',2X,
     +'ENERGIES'/62X,'          (KJ/MOL-K)'/)
C
      SPECIES(0)='         '           !SUBSCRIPT ZERO IS A DANGER. TAKE CAUTION!!!
      DO 160 I=1,NRX
        WRITE(6,111) RXNAME(I),(SPECIES(JIABS(IR(I,K))),K=1,3),
     +       (SPECIES(IP(I,K)),K=1,4),RATECONST(I),EA(I)
160   CONTINUE
111   FORMAT(1X,A3,1X,3A8,'>',4A8,D9.2,1X,D9.2)
C
      RETURN
      END       !OF PRINTDATA
```

```
      SUBROUTINE RADIOLYSIS
C
C*************************************************************************
C     VERSION: MIT 5.1                              28 FEBRUARY 1990
C     CODE CUSTODIAN: VERRDON H. MASON
C*************************************************************************
C     CALLED BY MITIRAD
C     CALLS LSODE
C
C     ITERATES THROUGH THE FLOW CHANNEL AND CALLS LSODE TO EVALUATE
C     RADIOLYSIS.
C*************************************************************************
C
      INCLUDE 'COMMON.BLK'
      EXTERNAL FRO,JACL
C
C     ASSIGN INITIAL VALUES TO ARRAY CONC.  THE INITIAL CONCENTRATIONS
C     ARE ASSUMED TO BE NORMALIZED TO ROOM TEMPERATURE.
C
      DO 225 I=1,NSPECIES
        CONC(I)=CONCINIT(I)*DENSLIQIN
225   CONTINUE
C
      WRITE (6,292)
      WRITE (6,291)
292   FORMAT ('1',80(1h_),/)
291   FORMAT(31X,'MITIRAD BCCL OUTPUT',/23X,'POSITIONS MEASURED
     + FROM CORE INLET')
C
C     INITIALIZE FOR LSODE
C
      RWORK(1)=LENGTH(1)
      ITASK=4
      IOPT  = 0
      ITER  = 1
      ITERSECT=1
      X     = LENGTH(1)
      XOUT  = X
C
C     INITIALIZE FOR FRO AND JACL
C
      FLOWPARA=0.71D0+0.00143D0*PRESSURE         !P IN ATM
      DENSLIQI= DENSLIQIN
      VELLIQ=FLOWRATE/DENSLIQI/(0.7854D0*DIAMETER(1)**2)
      GCONVERT= 1.038D-9*DENSLIQIN
C
C     BOILSTART IS USED IN TEMPERATURE DETERMINATION AND
C     IS THEREFORE DEFINED AS THE ENTIRE CORE LENGTH FOR
C     THE NON-BOILING CASE
C
      IF (.NOT.BOILFLAG) THEN
          BOILSTART = LENGTH(1)+LENGTH(2)+LENGTH(3)+
     +                LENGTH(4)+LENGTH(5)
      ENDIF
C
C     INITIALIZE SURFACE DECOMPOSITION REACTION
C     CODE ASSUMES THE SURFACE DECOMPOSITION REACTIONS ARE THE LAST
C     EQUATIONS IN THE INPUT EQUATION MATRIX!
C
      IF (CALCSURF) THEN       !EVALUATE SURFACE DECOMPOSITION TERM
```

```
        RCINIT(NRX-1)=RCINIT(NRX-1)/DIAMETER(ITERSECT)
        RCINIT(NRX)=RCINIT(NRX)/DIAMETER(ITERSECT)
      ELSE
        RCINIT(NRX-1)= 0.D0
        RCINIT(NRX)=0.D0       !NO SURFACE DECOMPOSITION REACTION
      ENDIF
C
C
C     OTHER INITIALIZATION
C
      IWORK11=0
      IWORK12=0
      IWORK13=0
      TEM = TINLET
      XFINAL=0.D0
      XSUM=0.D0
      DO 275 I=1,ID4  !ADDS SECTION LENGTHS TO DEFINE XFINAL
        XFINAL=XFINAL+LENGTH(I)
275   CONTINUE
C
C**** MAIN LOOP OF RADIOLYSIS BEGINS
C
280   CALL LSODE(FRO,NSPECIES,CONC,X,XOUT,ITOL,RTOL,ATOL,ITASK,
     +           ISTATE,IOPT,RWORK,LRW,IWORK,LIW,JACL,MF)
C
C     THIS BLOCK PRINTS OUT VALUES AT EACH STEP
C
      WRITE (6,290)
C
C     OUTPUT IS CONVERTED TO PPB AND CONCENTRATIONS ARE
C     NORMALIZED TO WATER WITH 1 G/CC DENSITY.
C     ALSO, CONCENTRATIONS ARE STORED IN CONCOUT FOR PLOTFILE
C
      XOUTPUT(ITERSECT,ITER) = X
      DO 284 I=1,NSPECIES
        IF (PPBFLAG) THEN
           PPBMULT = MOLEWT(I)*1.D+06
        ELSE
           PPBMULT = 1.D+0
        ENDIF
        IC=INDEX(SPECIES(I),'G')
        IF (IC.NE.0) THEN   !FOR GASES
           CONCOUT(ITERSECT,ITER,I)=CONC(I)*PPBMULT/DENSGAS
           IF (ITERSECT.GT.8) CONCOUT(ITERSECT,ITER,I)=0.D+0
        ELSE      !FOR AQUEOUS SPECIES
           CONCOUT(ITERSECT,ITER,I) = CONC(I)*PPBMULT/DENSLIQI
        ENDIF
284   CONTINUE
C
      IF (PPBFLAG) THEN
         IF (ITER .EQ. 1) THEN
           WRITE (6,289) SECTNAME(ITERSECT),X
         ELSE
           WRITE (6,311) X
         ENDIF
      ELSE
         IF (ITER .EQ. 1) THEN
           WRITE (6,285) SECTNAME(ITERSECT),X
         ELSE
           WRITE (6,310) X
```

```
         ENDIF
       ENDIF
C
       WRITE (6,320) (SPECIES(I),CONCOUT(ITERSECT,ITER,I),I=1,NSPECIES)
C
       WRITE (6,300) IWORK(11),VELLIQ
C      QUALity AND VOID fraction ARE ONLY PRINTED IF TWO-PHASE
C
       IF (QUAL.GT.0) WRITE (6,286) QUAL, VOID
       IF ((ITERSECT.LT.5).OR.((ITERSECT.LT.6).AND.(.NOT.
      +    (BOILFLAG)))) WRITE (6,287) TEM
       IF ((ITERSECT.EQ.8).AND.(ITER.EQ.1)) THEN
         WRITE (6,288) STEAMFLOW,DOWNFLOW
       ENDIF
C
285    FORMAT (11X,'CONCENTRATION[mol/lit] AT ',A16,1X,'(',F10.2,'cm)')
286    FORMAT (5X,'QUALITY    =',F10.5,10X,'VOID FRACTION =',F10.5)
287    FORMAT (5X,'TEMPERATURE=',F8.0,1X,'K')
288    FORMAT (5X,'STEAM FLOW RATE = ',4X,F9.2,'g/sec',/5X,'DOWNCOMER
      + FLOW RATE= ',F9.2,1X,'g/sec')
289    FORMAT (11X,'   CONCENTRATION[ppb] AT ',A16,1X,'(',F10.2,'cm)')
290    FORMAT (/80(1h_),/)
310    FORMAT (12X,'CONCENTRATIONS[mol/lit] AT POSITION = ',
      +        F9.2,' cm'/)
311    FORMAT (12X,'   CONCENTRATIONS[ppb] AT POSITION = ',
      +        F9.2,' cm'/)
320    FORMAT (2(5X,A8,' = ',D15.6,' **'))
300    FORMAT (/5X,'NO. STEPS  = ',I7,10X,'LIQUID VELOCITY =',
      +        F10.3,1X,'cm/s')
C
C      WRITE GAS IN PARTIAL PRESSURE
C
C      GAS PARTIAL PRESSURE IS ONLY PRINTED IF VAPOR PHASE EXISTS
C
       IF ((X.LE.BOILSTART).OR.(.NOT.BOILFLAG).OR.(ITERSECT.GE.
      +    9)) GOTO 340
C
       DO 340 I=1,NSPECIES
         IC=INDEX(SPECIES(I),'G')
         IF (IC.NE.0) THEN
        GAS=CONC(I)*0.018D0/DENSGAS*PRESSURE      !ASSUME IDEAL GAS
           CONC(I)=CONC(I)
        WRITE(6,330) SPECIES(I),GAS
         ENDIF
340    CONTINUE
330    FORMAT(5X,'PARTIAL PRESSURE OF ',A5,'  = ',F11.4,'atm')
C
       IF (ISTATE.EQ.-1) THEN
         ISTATE=2           !RESETS LSODE FLAG TO CONTINUE EXECUTION
         GO TO 280          !REITERATES TO FACILITATE CONVERGENCE
       ENDIF
C
C      EXIT LOOP UPON XFINAL OR LSODE ERROR
C
       IF ((X.GE.XFINAL).OR.(ISTATE.LT.0)) GO TO 380
C
C      THE FOLLOWING PREPARES PARAMETERS FOR NEXT ITERATION
C      OF LSODE.
C
       IF ((ITERSECT.EQ.5).AND.(ITER.EQ.1)) THEN
```

```
        STEAMFLOW=VELGAS*VOID*DENSGAS*0.7854D0*DIAMETER(5)**2
        DOWNFLOW =FLOWRATE-STEAMFLOW  !DOWNCOMER FLOW RATE
      ENDIF
C
C     SECTION COUNTER INCREMENT
C
      IF (ITER.EQ.1) THEN
        ITERSECT = ITERSECT +1
        ITASK=4
        RWORK(1)=RWORK(1)+LENGTH(ITERSECT)
        RCINIT(NRX-1)=RCINIT(NRX-1)*DIAMETER(ITERSECT-1)/
     +                DIAMETER(ITERSECT)
        RCINIT(NRX)=RCINIT(NRX)*DIAMETER(ITERSECT-1)/
     +                DIAMETER(ITERSECT)
      ENDIF
C
C     SECTION #4 IS SKIPPED EXCEPT FOR 2-PHASE FLOW CASE
C
      IF ((ITERSECT.EQ.4).AND.(.NOT.(BOILFLAG))) THEN
        ITERSECT = 5
        ITASK=4
        RWORK(1)=RWORK(1)+LENGTH(ITERSECT)
        RCINIT(NRX-1)=RCINIT(NRX-1)*DIAMETER(ITERSECT-2)/
     +                DIAMETER(ITERSECT)
      ENDIF
C

C
C     THIS BLOCK ADJUSTS VELLIQ FOR CHANGING DIAMETER
C
      IF (((ITERSECT.EQ.6).OR.(ITERSECT.EQ.7)).AND.
     +    (ITER.EQ.1)) THEN
        VELLIQ=VELLIQ*(DIAMETER(ITERSECT-1)/
     +          DIAMETER(ITERSECT))**2
        VELGAS=SLIPRATIO*VELLIQ
      ENDIF
C
C     EVALUATE DOSE RATES AS A FUNCTION OF SECTION
C
      DSR = GAMMARATE*GAMMAMULT(ITERSECT)
      DHR = NEUTRATE*NEUTMULT(ITERSECT)
C
C     INCREMENT XOUT AND ITER.  NOTE: THE FIRST ITERATION
C     OF EACH SECTION STARTS WITH '2' AND COUNTS UP THE NEXT TO
C     THE LAST STEP.  THE LAST STEP IS '1'.  THE NET AFFECT RESULTS
C     IN THE SECTION COUNTER (ITERSECT) AND THE ITERATION COUNTER
C     (ITER) BEING OFFSET ONE STEP TO FACILITATE FLAGGING
C     SECTION PARAMETERS FOR UPDATE.
C
      DO 370 I=1,ITERSECT
        XSUM = XSUM + LENGTH(I)  !XSUM DEFINES THE VALUE OF
C       X AT THE END OF THE CURRENT SECTION
C
370   CONTINUE
C
C     THE NEXT STEP MAKES XOUT AN INTEGER VALUE REGARDLESS
C     OF THE LAST ITERATIONS X VALUE.  CONSEQUENTLY, THE MINIMUM
C     EFFECTIVE XSTEP IS 1 CM--REGARDLESS OF USER SPECIFICATION.
C
      XOUT = DNINT(XSTEP*(1+DNINT(XOUT/XSTEP)))
```

```
C
      ITER = ITER+1
      IF (ITER.EQ.2) THEN
       ISTATE=1
       IWORK11=IWORK(11)+IWORK11
       IWORK12=IWORK(12)+IWORK12
       IWORK13=IWORK(13)+IWORK13
      ENDIF
C
      IF (XOUT.GE.XSUM) THEN
        XOUT=XSUM
        CONCOUT(ITERSECT,1,NSPECIES+1) = ITER -1
        ITER=1              !RESETS ITER FOR NEXT SECTION
C
C     NOTE:  THE FIRST ITERATION WITH ITER = 1 IS ACTUALLY
C            FOR THE LAST STEP OF THE PREVIOUS SECTION
      ENDIF
C
      XSUM =0.D0            !RESETS XSUM FOR NEXT ITERATION
C
      GO TO 280
C
C**** END OF THE MAIN LOOP OF RADIOLYSIS
C
380   RETURN
      END       !OF RADIOLYSIS
```

```
      SUBROUTINE FRO (NREACTANT,X,CONCVEC,DCDX)
C
C*************************************************************************
C     VERSION: MIT 5.1                              28 FEBRUARY 1990
C     CODE CUSTODIAN: VERRDON H. MASON
C*************************************************************************
C     CALLED BY LSODE
C
C     FRO CALCULATES THE SPATIAL MASS BALANCE DIFFERENTIAL EQUATION:
C     dC/dx = CHEMICAL GENERATION - CHEMICAL ANNIHILATION
C           + GENERATION BY RADIATION + CONVECTION
C           + MASS TRANSFER BETWEEN GAS AND LIQUID
C*************************************************************************
C
      INCLUDE 'COMMON.BLK'
      DIMENSION CONCVEC(ID2),DCDX(ID2)          !CONCVEC IS EQUIVALENT TO CONC
C
C     INITIALIZES VALUES WHENEVER X IS LESS THAN BOILSTART
C
      IF (X.LE.BOILSTART) THEN
         VOID  = 0.D0
         QUAL  = 0.D0
         DVFDX = 0.D0
         DVLDX = 0.D0
         VELGAS= 0.D0
         DVGDX = 0.D0
      ENDIF
C
C     USE ARRHENIUS LAW TO CORRECT RATE CONSTANTS AT TEM
C     THIS BLOCK CALCULATES THE NEW TEMPERATURE FOR THIS
C     CORRECTION.  LIQUID DENSITY FOR THE ITERATION IS
C     ALSO CALCULATED.  DENSITY AND TEMPERATURE CAN EITHER
C     INCREASE OR DECREASE TO FACILITATE CODE FLEXIBILITY
C
      XTEMP = LENGTH(1)+LENGTH(2)+LENGTH(3)
      IF (XTEMP.GE.X) THEN
        TEM = TINLET
        DENSLIQI=DENSLIQIN
        GO TO 30
      ENDIF
      DENSLIQI = DENSLIQIN-(DENSLIQIN-DENSLIQ)/(BOILSTART
     +             -XTEMP)*(X-XTEMP)
      TEM=(TOUTLET-TINLET)/(BOILSTART-XTEMP)*(X-XTEMP)+TINLET
      IF ((((TEM.GE.TOUTLET).AND.(TOUTLET.GE.TINLET)).OR.((TEM.LT.
     +    TOUTLET).AND.(TOUTLET.LT.TINLET))) THEN
        TEM = TOUTLET
        DENSLIQI = DENSLIQ
      ENDIF
C
30    GCONVERT = 1.038D-9*DENSLIQI
C
C     THE FOLLOWING SECTION PREPARES THE DERIVATIVES AND MESH
C     POINT PARAMETERS FOR USE IN THE FOLLOWING dC/dX CALCULATION.
C
      IF ((.NOT.BOILFLAG).OR.(X.LE.BOILSTART)) THEN
        VELLIQ=FLOWRATE/DENSLIQI/(0.7854D0*DIAMETER(ITERSECT)**2)
        VELGAS=0.D0
        VOID =0.D0
        VELINLET=VELLIQ
        GO TO 50
```

```
      ENDIF
C
C     EVALUATE TWO-PHASE PARAMETERS IF BOILING STARTED
C     PROGRAM ASSUMES QUALITY IS PROPORTIONAL TO DISTANCE
C     THROUGH THE BOILING SECTION.
C
      QUAL = QUALEXIT*(X-BOILSTART)/LENGTH(5)
C
      IF (QUAL.GT.QUALEXIT) QUAL = QUALEXIT
      VOID=FLOWPARA/(1.D0-DENSGAS/DENSLIQ*(1.D0-1.D0/QUAL))
C
      IF (ITERSECT.EQ.5) THEN
        DVFDX=VOID*VOID/FLOWPARA*DENSGAS/DENSLIQ/QUAL/QUAL
     +        *QUALEXIT/LENGTH(ITERSECT)
        SLIPRATIO=(1.D0-VOID)/(FLOWPARA-VOID)
        DSRDX=DVFDX/(FLOWPARA-VOID)*(SLIPRATIO-1.D0)
        VELLIQ=VELINLET/(VOID*(DENSGAS/DENSLIQ*SLIPRATIO-1.D0)+1.D0)
        DVLDX=-VELLIQ*VELLIQ/VELINLET
     +         *(DVFDX*(DENSGAS/DENSLIQ*SLIPRATIO-1.D0)
     +         +VOID*DENSGAS/DENSLIQ*DSRDX)
        VELGAS=SLIPRATIO*VELLIQ
        DVGDX=DSRDX*VELLIQ+SLIPRATIO*DVLDX
        GO TO 50
      ENDIF
C
      IF ((ITERSECT.EQ.6).OR.(ITERSECT.EQ.7)) THEN
        DVLDX =0.D0
        DVGDX =0.D0
        DSRDX =0.D0
        DVFDX =0.D0
        GO TO 50
      ENDIF
C
      IF (ITERSECT.EQ.8) THEN   !THIS DOES PLENUM REGION
C
C               THE ZUBER-FINDLAY DRIFT-FLUX TWO-PHASE FLOW MODEL
C     IS USED FOR BCCL PLENUM VICE THE TUBING FLOW MODEL
C
        VELINF=.35D0*(980.D0*DIAMETER(ITERSECT)*(1-DENSGAS/DENSLIQ)
     +          )**0.5D0
        MASSFLUX=FLOWRATE/(0.7854D0*DIAMETER(ITERSECT)**2.D0)
        VOID=1/(1.2D0*(1+(1/QUAL-1)*DENSGAS/DENSLIQ)+
     +        VELINF*DENSGAS/QUAL/MASSFLUX)
        SLIPRATIO=(1.D0-VOID)/(FLOWPARA-VOID)
        VELLIQ=DOWNFLOW/DENSLIQ/0.7854D0/(DIAMETER(ITERSECT)
     +     **2.D0)/(VOID*(DENSGAS/DENSLIQ*SLIPRATIO-1.D0)+1.D0)
        VELGAS=SLIPRATIO*VELLIQ
      ELSE
        VELGAS=0.D0
        VOID  =0.D0
        QUAL  =0.D0
        VELLIQ=DOWNFLOW/DENSLIQ/0.7854D0/
     +          (DIAMETER(ITERSECT)**2.D0)
      ENDIF
C
C     - - - - - - - - - - - - - - - - - - - - - - - - - - - - -
C     EVALUATE dC/dx.
C     OUTER LOOP ITERATES THROUGH ALL OF THE ODES, AND THE INNER
C     LOOP ITERATES OVER THE APPLICABLE REACTIONS FOR EACH ODE.
C
```

```
50    CONTINUE
C
      DO 110 I=1,NREACTANT
        DCDX(I) = 0.0D0                          !INITIALIZE TO ZERO
        IC=INDEX(SPECIES(I),'G')      !SEE IF THE SPECIES IS GAS
C
C     CALC CHEMICAL REACTIONS AND MASS TRANSFER BETWEEN LIQUID AND GAS
C
        DO 100 J=1,NRX
          IF (KOEF(J,I).EQ.0) GOTO 100
          IF (EA(J).LT.0.D0) THEN     !ADJUST MASS TRANSFER RATE
            RATECONST(J)=RCINIT(J)*VOID/(1.D0-VOID)
            IF ((IC.NE.0).AND.(X.GT.BOILSTART)) THEN
              IF (BOILFLAG) THEN
                RATECONST(J)=RCINIT(J)
              ELSE
                RATECONST(J)=0.D0
              ENDIF
            ENDIF
          ELSE
            RATECONST(J)=RCINIT(J)*DEXP(-EA(J)/GASCONST*
     +                  (1.D0/TEM-1.D0/TEMREF))
          ENDIF
C         THIS SKIPS THE NON-APPLICABLE SURFACE RATE CONSTANT
          IF ((((ITERSECT.GE.3).AND.(ITERSECT.LE.6)).AND.(J.EQ.NRX))
     +       .OR.(((ITERSECT.LT.3).OR.(ITERSECT.GT.6)).AND.
     +       (J.EQ.(NRX-1)))) GO TO 100
C
          DCDX(I)=DCDX(I)+RATECONST(J)*DFLOTJ(KOEF(J,I))*
     +            CONCVEC(IN1(J))*CONCVEC(IN2(J))*CONCVEC(IN3(J))
100     CONTINUE
C
C       CALC IRRADIATION AND CONVECTION TERMS
C
        IF (IC.EQ.0) THEN             !LIQUID
          DCDX(I)=(DCDX(I)+(GGAMMA(I)*DSR+GNEUT(I)*DHR)*GCONVERT
     +            -CONCVEC(I)*(DVLDX-VELLIQ/(1.D0-VOID)*DVFDX))
     +            /VELLIQ
        ELSE IF ((VELGAS.GT.0).AND.(ITERSECT.LT.9)) THEN    !GAS
          DCDX(I)=(DCDX(I)-CONCVEC(I)*(DVGDX+VELGAS/VOID*DVFDX))
     +            /VELGAS
        ELSE IF ((IC.NE.0).AND.(ITERSECT.GE.9)) THEN
          DCDX(I)=0.D0
        ENDIF
110   CONTINUE
C
      RETURN
      END       !OF FRO
```

```
      SUBROUTINE JACL (NREACTANT,X,CONCVEC,ML,MU,PD,NROWPD)
C
C*********************************************************************
C     VERSION: MIT 5.1                          28 FEBRUARY 1990
C     CODE CUSTODIAN: VERRDON H. MASON
C*********************************************************************
C     CALLED BY LSODE
C
C     JACL CALCULATES THE FULL JACOBIAN MATRIX OF dc/dx.
C*********************************************************************
C
      INCLUDE 'COMMON.BLK'
      DIMENSION PD(NROWPD,ID2),CONCVEC(ID2)      !CONCVEC IS EQUIV TO  CONC
C
      DO 100 J=1,NREACTANT            !NREACTANT IS EQUIVALENT TO NSPECIES
C
C       CHEMICAL REACTIONS AND MASS TRANSFER TERMS
C
        PD(I,J)=0.D0
        DO 101 I=1,NREACTANT
          IC=INDEX(SPECIES(I),'G')   !SEE IF THE SPECIES IS GAS
          DO 102 K=1,NRX
            IF((KOEF(K,J).EQ.0).OR.(KOEF(K,I).EQ.0)) GOTO 102
            IF (EA(K).LT.0) THEN      !ADJUST MASS TRANSFER RATE
              RATECONST(K)=RCINIT(K)*VOID/(1.D0-VOID)
              IF ((IC.NE.0).AND.(X.GT.BOILSTART))  THEN
                IF (BOILFLAG)THEN
                  RATECONST(K)=RCINIT(K)
                ELSE
                  RATECONST(K)=0.D0
                ENDIF
           ENDIF
            ELSE
              RATECONST(K)=RCINIT(K)*DEXP(-EA(K)/GASCONST*
     +                    (1.D0/TEM-1.D0/TEMREF))
            ENDIF
C
C           THIS SKIPS THE NON-APPLICABLE SURFACE RATE CONSTANT
            IF ((((ITERSECT.GE.3).AND.(ITERSECT.LE.6)).AND.
     +         (K.EQ.NRX)).OR.(((ITERSECT.LT.3).OR.
     +         (ITERSECT.GT.6)).AND.(K.EQ.(NRX-1)))) GO TO 102
C
            A = RATECONST(K)*DFLOTJ(KOEF(K,I)*JIABS(KOEF(K,J)))
            IM = IN1(K)
            IN = IN2(K)
            IO = IN3(K)
C
C           CATCH SECOND ORDER REACTIONS
C
            IF((IM.EQ.IN.OR.IO.EQ.IN).AND.(IN.EQ.J))THEN
              PD(I,J)=PD(I,J)+A*CONCVEC(IM)*CONCVEC(IO)
           GOTO 102
            ELSE IF (IM.EQ.J) THEN
              PD(I,J)=PD(I,J)+A*CONCVEC(IN)*CONCVEC(IO)
           GOTO 102
            ENDIF
C
C           CATCH FIRST ORDER REACTIONS
C
            IF (IO.EQ.J) THEN
```

```
              PD(I,J) = PD(I,J)+A*CONCVEC(IN)*CONCVEC(IM)
              GOTO 102
            ENDIF
            IF (IN.EQ.J) PD(I,J) = PD(I,J)+A*CONCVEC(IM)*CONCVEC(IO)
102       CONTINUE
C
        PD(I,J)=PD(I,J)/VELLIQ
C
101     CONTINUE
C
C       CONVECTION TERMS
C
        IC=INDEX(SPECIES(J),'G')      !SEE IF THE SPECIES IS GAS
        IF (IC.EQ.0) THEN             !LIQUID
          PD(J,J)=PD(J,J)-DVLDX/VELLIQ+DVFDX/(1.D0-VOID)
        ELSE IF ((VELGAS.GT.0).AND.(ITERSECT.LT.9)) THEN    !GAS
          PD(J,J)=(PD(J,J)*VELLIQ-DVGDX)/VELGAS-DVFDX/VOID
        ELSE IF ((IC.NE.0).AND.(ITERSECT.GE.9)) THEN
          PD(J,J)=0.D0
        ENDIF
C
100   CONTINUE
C
      RETURN
      END       !OF JACL
```

```
      SUBROUTINE PRINTSTAT
C
C*************************************************************************
C     VERSION: MIT 5.0                              22 FEBRUARY 1990
C     CODE CUSTODIAN: VERRDON H. MASON
C*************************************************************************
C     CALLED BY MITIRAD
C
C     PRINTSTAT WRITES RUN STATISTICS TO THE OUTPUT FILE.
C*************************************************************************
C
      INCLUDE 'COMMON.BLK'
C
C     PRINT THE RUN STATISTICS
C
      ET=SECNDS(TIME1)                !ELAPSED TIME
      IWORK11=IWORK11+IWORK(11)
      IWORK12=IWORK12+IWORK(12)
      IWORK13=IWORK13+IWORK(13)
      WRITE (6,290)
      WRITE (6,381)
      WRITE (6,290)
      WRITE (6,390) IWORK(17),IWORK(18),IWORK11,IWORK12,IWORK13,ET
290   FORMAT (/80(1h_),/)
381   FORMAT(29X,'RUN STATISTICS')
390   FORMAT(5X,/25H REQUIRED RWORK SIZE   = ,I7,
     +       5X,/25H IWORK SIZE            = ,I7,
     +       5X,/25H NUMBER OF STEPS       = ,I7,
     +       5X,/25H # OF FUNC.- EVALS.    = ,I7,
     +       5X,/25H # OF JACOB.- EVALS    = ,I7,
     +       5X,/25H TOTAL JOB TIME        = ,F7.2,' seconds')
C
      IF (ISTATE.EQ.2) THEN           !SUCCESS
        WRITE (6,395)
      ELSE                            !FAILURE
        WRITE (6,400) ISTATE
      ENDIF
395   FORMAT (//' COMPLETED SUCCESSFULLY!')
400   FORMAT (//22H ERROR HALT...ISTATE =,I3)
C
      RETURN
      END       !OF PRINTSTAT
```

```
      SUBROUTINE WRITEPLOT
C
C*************************************************************************
C     VERSION: MIT 5.1                              22 FEBRUARY 1990
C     CODE CUSTODIAN: VERRDON H. MASON
C************************************* ***********************************
C     CALLED BY MITIRAD
C
C     WRITEPLOT WRITES THE PLOT FILE TO BE READ BY RS/1.
C     THE FLAG LINLIN CONTROLS OUTPUT FORMAT
C       LINLIN=.TRUE.  ->  LINEAR CONCENTRATION/LINEAR POSITION
C       LINLIN=.FALSE. ->  LOG CONCENTRATION/LINEAR POSITION
C*************************************************************************
C
      INCLUDE 'COMMON.BLK'
C
      OPEN (8,FILE=PLOTFILE,STATUS='NEW')
      IFLAG=0
      ITERTOTAL=0  !INITIALIZE COUNTER
C
      DO 400 I=2,ID4       !DETERMINES TOTAL # OF ITERATIONS
        ITERTOTAL=ITERTOTAL+CONCOUT(I,1,NSPECIES+1)
400   CONTINUE
C
      WRITE (8,410) NSPECIES, ITERTOTAL+1, LINLIN
410   FORMAT (1X,I3)
C
      DO 420 I = 1,NSPECIES
        WRITE (8,430) SPECIES(I)
420   CONTINUE
430   FORMAT (1X,A8)
C
C     THIS BLOCK WRITES INITIAL CONDITIONS IN PLOT FILE
C
      WRITE (8,460) LENGTH(1)                    ! WRITE INITIAL CONDITIONS
      DO 434 I = 1,NSPECIES
        IF (LINLIN) THEN              !LINEAR CONC-LINEAR POSITION
          WRITE (8,460) CONCOUT(1,1,I)
        ELSE IF (CONCOUT(1,1,I).GT.0.0D0) THEN !LOG CONC-LINEAR
          WRITE (8,460) DLOG10(CONCOUT(1,1,I))
        ELSE
          WRITE (8,*)      ! WRITE BLANK FOR ZERO I.C. SINCE LOG(0)=-INFINITE
        ENDIF
434   CONTINUE
C
C     THIS BLOCK WRITES VALUES AT EACH ITERATION
C
      DO 455 I=2,ID4
        IF (1.EQ.CONCOUT(I,1,NSPECIES+1)) GO TO 445
        DO 450 J = 2,CONCOUT(I,1,NSPECIES+1)    !WRITE ITERATIONS
          JJ = J
437       WRITE (8,460) XOUTPUT(I,JJ)
438       DO 440 K = 1,NSPECIES
            IF (LINLIN) THEN                    !LINEAR CONC-LINEAR POSITION
              WRITE (8,460) CONCOUT(I,JJ,K)
            ELSE IF (CONCOUT(I,JJ,K).GT.0.0D0) THEN         !LOG CONC-LINEAR POSITION
              WRITE (8,460) DLOG10(CONCOUT(I,JJ,K))
         ELSE
              WRITE (8,*)  !WRITE BLANK FOR ZERO SINCE LOG(0)=-INFINITE
            ENDIF
```

```
440         CONTINUE
          IF (IFLAG.EQ.1) THEN
         IFLAG=0
         GO TO 455
          ENDIF
          IF (J.EQ.CONCOUT(I,1,NSPECIES+1)) THEN
445         IFLAG=1
            JJ = 1
            GO TO 437
           ENDIF
450       CONTINUE
455     CONTINUE
460     FORMAT (1X,E21.14)
470     CLOSE (8)
C
        RETURN
        END         !OF WRITEPLOT
```

```
C  COMMON.BLK
C
C  THIS MODULE IS INCLUDED IN MITIRAD 5.1 (BCCLMIT) AS A COMMON
C  VARIABLE BLOCK USED BY SUBROUTINES.
C
C  VERRDON H. MASON
C
C  NW12-311
C  MASSACHUSETTS INSTITUTE OF TECHNOLOGY
C  138 ALBANY STREET
C  CAMBRIDGE, MA 02139
C  (617) 253-4204
C
C     ID1=REACTION ARRAY, ID2=REACTANT ARRAY, ID3=SECTION ARRAY
C     LRW=LIW=LSODE WORK ARRAY
C     ADJUST THESE ACCORDING TO WORK SIZE.
C
      PARAMETER (ID1=50,ID2=50,ID3=12,LRW=3000,LIW=200)
      IMPLICIT DOUBLE PRECISION (A-H, O-Z)
      COMMON /FILENAME/ INFILE,OUTFILE,PLOTFILE
      COMMON /SIZE/ NSPECIES,NRX
      COMMON /NAMES/ SPECIESDUMMY,SPECIES,RXNAME,SECTNAME
      COMMON /GEOMETRY/ BOILSTART,XSUM,DIAMETER(ID3),LENGTH
      COMMON /STATE/ TINLET,TOUTLET,TEMREF,GAMMARATE,NEUTRATE,
     +               VELINLET,DENSLIQIN,TEM,VELLIQ,VELGAS,
     +               PRESSURE,DENSLIQ,DENSGAS,FLOWRATE,FLOWPARA,
     +               QUALEXIT,QUAL,DENSLIQI,STEAMFLOW,DOWNFLOW,
     +               MASSFLUX,VOID,SLIPRATIO
      COMMON /GVALUES/ GGAMMA(ID2),GNEUT(ID2),GCONVERT,
     +                 GAMMAMULT(ID3),NEUTMULT,DSR,DHR
      COMMON /DERIVATIVE/ DVFDX,DVLDX,DVGDX
      COMMON /CHEMICAL/ KOEF(ID1,ID2),NJ(ID1,ID2),MOLEWT,
     +                  IN1(ID1),IN2(ID1),IN3(ID1),PPBMULT
      COMMON /CONCENTRATIONS/ CONC(ID2),CONCINIT(ID2)
      COMMON /REACTIONS/ IR(ID1,3),IP(ID1,4),RCINIT(ID1),
     +                   RATECONST(ID1),EA(ID1)
      COMMON /OUTPUT/ ITER,CONCOUT(ID3,2*ID2,ID2),IWORK11,
     +        IWORK12,IWORK13,XOUTPUT(ID3,2*ID2),TIME1,TIME2
      COMMON /CONTROL/ XSTEP,ITERSECT,ID4
      COMMON /FLAGS/ CALCSURF,RSOUT,LINLIN,BOILFLAG,PPBFLAG
      COMMON /LSODEDATA/ IOPT,ITASK,RTOL,ITOL,ATOL,RWORK(LRW),
     +                   IWORK(LIW),ISTATE,MF
C
      REAL*4 TIME1,TIME2
      REAL*8 NEUTRATE,MASSFLUX,LENGTH(ID3),NEUTMULT(ID3),MOLEWT(ID2)
      CHARACTER*3 RXNAME(ID1)
      CHARACTER*16 SECTNAME(ID3)
C
C     SPECIESDUMMY IS USED TO VACATE MEMORY SPACE JUST BEFORE SPECIES
C     SINCE SPECIES ILLEGALLY CHANGES SPECIES(0) ELEMENT.
C
      CHARACTER*8 SPECIESDUMMY(3),SPECIES(ID2)
      CHARACTER*35 INFILE,OUTFILE,PLOTFILE
      LOGICAL*1 CALCSURF,RSOUT,LINLIN,BOILFLAG,PPBFLAG
      PARAMETER GASCONST=8.314D-3
```

D.2 BCCLMIT Sample Output File

```
MITIRAD CODE PACKAGE OUTPUT
MITIRAD VERSION: MIT  5.1
MIT BCCL MODIFICATION

5-APR-90  12:15:25
```

INPUT PARAMETERS

INPUT FILE NAME	=	NELGBH.IN	
OUTPUT FILE NAME	=	NELGBH.OUT	
PLOT FILE NAME	=	NELGBH.PLOT	
NUMBER OF CHEMICAL REACTIONS	=	46	
NUMBER OF SPECIES EVALUATED	=	14	
POSITION INCREMENT	=	10.00000	cm
POSITION AT ONSET OF BOILING	=	42.35000	cm
CORE EXIT QUALITY (FRACTION)	=	0.10000	
INLET TEMPERATURE	=	546.00000	K
OUTLET TEMPERATURE	=	558.00000	K
REFERENCE TEMPERATURE	=	298.00000	K
INLET WATER DENSITY	=	0.80000	g/cc
OUTLET WATER DENSITY	=	0.74100	g/cc
VAPOR DENSITY	=	0.03620	g/cc
PRESSURE	=	68.00000	atm
MASS FLOWRATE	=	0.27000D+02	g/s
ABSOLUTE TOLERANCE	=	0.10000D-14	
RELATIVE TOLERANCE	=	0.10000D-04	
GAMMA DOSE RATE (CORE)	=	0.11100D+06	Rad/s
NEUTRON DOSE RATE (CORE)	=	0.11100D+06	Rad/s

SECTION PARAMETERS:

SECTION NAME	LENGTH (cm)	DIAMETER (cm)	GAMMA MULTIPLIER	NEUTRON MULTIPLIER
CHEM INJECTION	0.000	0.460	0.000D+00	0.000D+00
ZIRC TRANSITION	5.000	0.460	0.100D-01	0.100D-02
CORE INLET	31.000	0.645	0.100D+00	0.300D-01
START OF BOILING	6.350	0.645	0.100D+01	0.100D+01
CORE OUTLET	135.900	0.645	0.100D+01	0.100D+01
ZIRC TRANSITION	31.000	0.645	0.100D+00	0.300D-01
PLENUM INLET	52.100	0.460	0.100D-01	0.500D-02
PLENUM OUTLET	15.240	3.358	0.100D-02	0.100D-05
PLENUM SAMPLE	29.800	0.460	0.100D-01	0.100D-03
DOWNCOMER INLET	12.400	0.460	0.200D-01	0.100D-02
DOWNCOMER OUTLET	14.000	3.160	0.500D-01	0.100D-01
DOWNCOMER SAMPLE	12.100	0.460	0.200D-01	0.100D-02

CALCSURF	=	T
RSOUT	=	T
LINLIN	=	T
BOILFLAG	=	T
PPBFLAG	=	T

	LOW LET G-VALUES (#/100eV)	HIGH LET G-VALUES (#/100eV)	INITIAL CONCENTRATIONS (MOLES/LITER)
e-	3.20	0.80	0.00D+00
OH-	0.00	0.00	0.25D-05
H2	0.44	0.99	0.10D-03
OH	5.30	0.68	0.00D+00
HO2-	0.00	0.00	0.00D+00
H2O2	0.57	1.27	0.00D+00
O2-	0.00	0.00	0.00D+00
O2	0.00	0.00	0.63D-05
H	2.40	0.45	0.00D+00
H+	3.20	0.80	0.25D-05
HO2	0.00	0.00	0.00D+00
O2G	0.00	0.00	0.00D+00
H2G	0.00	0.00	0.00D+00
O	0.00	0.00	0.00D+00

CHEMICAL REACTIONS, RATE CONSTANTS, AND ACTIVATION ENERGIES

	REACTIONS					RATE CONSTANT	ACTIVATION ENERGIES (KJ/MOL-K)
W 1 e-		>H	OH-			0.40D+02	0.13D+02
W 2 e-	H+	>H				0.60D+11	0.13D+02
W 3 e-	OH	>OH-				0.75D+11	0.13D+02
W 4 e-	H2O2	>OH	OH-			0.32D+11	0.13D+02
W 5 H	H	>H2				0.25D+11	0.13D+02
W 6 e-	HO2	>HO2-				0.50D+11	0.13D+02
W 7 e-	O2	>O2-				0.47D+11	0.13D+02
W 8 e-	e-	>OH-	OH-	H2		0.12D+11	0.13D+02
W 9 OH	OH	>H2O2				0.11D+11	0.13D+02
W10 OH-	H	>e-				0.78D+08	0.19D+02
W11 e-	H	>H2	OH-			0.62D+11	0.13D+02
W12 e-	HO2-	>OH	OH-	OH-		0.87D+10	0.13D+02
W13 H	OH	>				0.50D+11	0.13D+02
W14 OH	H2	>H				0.11D+09	0.13D+02
W15 O	O	>O2				0.22D+11	0.13D+02
W16 H	O2	>HO2				0.47D+11	0.13D+02
W17 H	HO2	>H2O2				0.50D+11	0.13D+02
W18 H	O2-	>HO2-				0.50D+11	0.13D+02
W19 e-	O2-	>HO2-	OH-			0.51D+11	0.19D+02
W20 H	H2O2	>OH				0.24D+09	0.14D+02
W21 OH	H2O2	>HO2				0.41D+08	0.14D+02
W22 OH	HO2	>O2				0.30D+11	0.13D+02
W23 OH-	H2O2	>HO2-				0.70D+09	0.19D+02
W24 HO2-		>OH-	H2O2			0.22D+07	0.19D+02
W25 H+	O2-	>HO2				0.12D+12	0.13D+02
W26 HO2		>H+	O2-			0.20D+07	0.13D+02
W27 HO2	O2-	>HO2-	O2			0.58D+08	0.19D+02
W28 O2-	O2-	>H2O2	O2	OH-	OH-	0.66D+08	0.19D+02
W29 HO2	HO2	>H2O2	O2			0.11D+08	0.19D+02
W30 H+	OH-	>				0.15D+13	0.43D+00
W31		>H+	OH-			0.14D-01	0.34D+02
W32 OH	O2-	>O2	OH-			0.30D+11	0.13D+02
W33 H		>H2	OH			0.49D-01	0.85D+02
W34 HO2	O	>O2	OH			0.20D+11	0.13D+02
W35 OH	O	>H	O2			0.10D+00	0.70D+02
W36 O		>OH	OH			0.95D+05	0.41D+02
W37 OH	O	>HO2				0.20D+11	0.13D+02
W38 H2	O	>H	OH			0.48D+04	0.35D+02
W39 H2O2	O	>HO2	OH			0.13D+07	0.18D+02
W40 H	O	>OH				0.20D+11	0.13D+02
AE1 H2		>H2G				0.30D+02	-0.10D+01
AE1 H2G		>H2				0.10D+02	-0.10D+01
AE2 O2		>O2G				0.23D+02	-0.10D+01
AE2 O2G		>O2				0.12D+02	-0.10D+01
COR H2O2		>O				0.53D-06	0.67D+02
CCL H2O2		>O				0.53D-06	0.67D+02

MITIRAD BCCL OUTPUT
POSITIONS MEASURED FROM CORE INLET

CONCENTRATION[ppb] AT CHEM INJECTION (0.00cm)

e-	=	0.000000D+00 **	OH-	=	0.425000D+02 **
H2	=	0.200000D+03 **	OH	=	0.000000D+00 **
HO2-	=	0.000000D+00 **	H2O2	=	0.000000D+00 **
O2-	=	0.000000D+00 **	O2	=	0.200000D+03 **
H	=	0.000000D+00 **	H+	=	0.250000D+01 **
HO2	=	0.000000D+00 **	O2G	=	0.000000D+00 **
H2G	=	0.000000D+00 **	O	=	0.000000D+00 **

NO. STEPS = 0 LIQUID VELOCITY = 203.080 cm/s
TEMPERATURE= 546. K

CONCENTRATION[ppb] AT ZIRC TRANSITION (5.00cm)

e-	=	0.185446D-04 **	OH-	=	0.440938D+02 **
H2	=	0.199769D+03 **	OH	=	0.122563D-02 **
HO2-	=	0.271379D-02 **	H2O2	=	0.423443D+01 **
O2-	=	0.169869D+01 **	O2	=	0.194709D+03 **
H	=	0.401347D-05 **	H+	=	0.264692D+01 **
HO2	=	0.222578D+00 **	O2G	=	0.000000D+00 **
H2G	=	0.000000D+00 **	O	=	0.280001D-08 **

NO. STEPS = 153 LIQUID VELOCITY = 203.080 cm/s
TEMPERATURE= 546. K

CONCENTRATIONS[ppb] AT POSITION = 20.00 cm

e-	=	0.239074D-03 **	OH-	=	0.437229D+02 **
H2	=	0.189124D+03 **	OH	=	0.250481D-01 **
HO2-	=	0.116690D+00 **	H2O2	=	0.183632D+03 **
O2-	=	0.300519D+01 **	O2	=	0.233850D+02 **
H	=	0.271893D-03 **	H+	=	0.266940D+01 **
HO2	=	0.397208D+00 **	O2G	=	0.000000D+00 **
H2G	=	0.000000D+00 **	O	=	0.865981D-07 **

NO. STEPS = 183 LIQUID VELOCITY = 103.291 cm/s
TEMPERATURE= 546. K

CONCENTRATIONS[ppb] AT POSITION = 30.00 cm

e-	=	0.417853D-03 **	OH-	=	0.444146D+02 **
H2	=	0.182743D+03 **	OH	=	0.160154D+00 **
HO2-	=	0.815363D-01 **	H2O2	=	0.126310D+03 **
O2-	=	0.406235D+00 **	O2	=	0.109364D+01 **
H	=	0.253453D-02 **	H+	=	0.262781D+01 **
HO2	=	0.529112D-01 **	O2G	=	0.000000D+00 **
H2G	=	0.000000D+00 **	O	=	0.595661D-07 **

```
NO. STEPS  =     252          LIQUID VELOCITY =   103.291 cm/s
TEMPERATURE=    546. K
```

```
          CONCENTRATION[ppb] AT CORE INLET        (     36.00cm)
e-        =    0.508933D-03 **     OH-       =    0.444552D+02 **
H2        =    0.180384D+03 **     OH        =    0.192146D+00 **
HO2-      =    0.560322D-01 **     H2O2      =    0.867208D+02 **
O2-       =    0.277442D+00 **     O2        =    0.737235D+00 **
H         =    0.306136D-02 **     H+        =    0.262541D+01 **
HO2       =    0.361126D-01 **     O2G       =    0.000000D+00 **
H2G       =    0.000000D+00 **     O         =    0.408961D-07 **

NO. STEPS  =     275          LIQUID VELOCITY =   103.291 cm/s
TEMPERATURE=    546. K
```

```
          CONCENTRATION[ppb] AT START OF BOILING (     42.35cm)
e-        =    0.305100D-02 **     OH-       =    0.518197D+02 **
H2        =    0.201480D+03 **     OH        =    0.743608D+00 **
HO2-      =    0.136781D+00 **     H2O2      =    0.196031D+03 **
O2-       =    0.812366D+00 **     O2        =    0.294987D+01 **
H         =    0.857587D-02 **     H+        =    0.307792D+01 **
HO2       =    0.115185D+00 **     O2G       =    0.000000D+00 **
H2G       =    0.000000D+00 **     O         =    0.104510D-06 **

NO. STEPS  =     161          LIQUID VELOCITY =   111.515 cm/s
TEMPERATURE=    558. K
```

```
          CONCENTRATIONS[ppb] AT POSITION =     50.00 cm

e-        =    0.291241D-02 **     OH-       =    0.517861D+02 **
H2        =    0.189013D+03 **     OH        =    0.716702D+00 **
HO2-      =    0.145879D+00 **     H2O2      =    0.209206D+03 **
O2-       =    0.931312D+00 **     O2        =    0.363802D+01 **
H         =    0.769639D-02 **     H+        =    0.307993D+01 **
HO2       =    0.132104D+00 **     O2G       =    0.338339D+02 **
H2G       =    0.261739D+04 **     O         =    0.111535D-06 **

NO. STEPS  =      66          LIQUID VELOCITY =   121.304 cm/s
QUALITY    =   0.00579          VOID FRACTION =   0.08602
PARTIAL PRESSURE OF O2G    =      0.0000atm
PARTIAL PRESSURE OF H2G    =      0.0016atm
```

```
          CONCENTRATIONS[ppb] AT POSITION =     60.00 cm

e-        =    0.272239D-02 **     OH-       =    0.517132D+02 **
H2        =    0.152894D+03 **     OH        =    0.668854D+00 **
HO2-      =    0.155374D+00 **     H2O2      =    0.223143D+03 **
O2-       =    0.119896D+01 **     O2        =    0.583085D+01 **
H         =    0.573562D-02 **     H+        =    0.308428D+01 **
HO2       =    0.170223D+00 **     O2G       =    0.807112D+02 **
H2G       =    0.410739D+04 **     O         =    0.118965D-06 **
```

```
NO. STEPS  =      76          LIQUID VELOCITY =   133.718 cm/s
QUALITY    =   0.01357          VOID FRACTION =   0.17736
PARTIAL PRESSURE OF O2G    =      0.0000atm
PARTIAL PRESSURE OF H2G    =      0.0025atm
```

```
          CONCENTRATIONS[ppb] AT POSITION =     70.00 cm

e-       =    0.253538D-02 **      OH-       =    0.516149D+02 **
H2       =    0.119419D+03 **      OH        =    0.602772D+00 **
HO2-     =    0.164597D+00 **      H2O2      =    0.236847D+03 **
O2-      =    0.156417D+01 **      O2        =    0.988725D+01 **
H        =    0.394144D-02 **      H+        =    0.309018D+01 **
HO2      =    0.222372D+00 **      O2G       =    0.153486D+03 **
H2G      =    0.438205D+04 **      O         =    0.126271D-06 **

NO. STEPS  =      81          LIQUID VELOCITY =   144.116 cm/s
QUALITY    =   0.02050          VOID FRACTION =   0.24207
PARTIAL PRESSURE OF O2G    =      0.0000atm
PARTIAL PRESSURE OF H2G    =      0.0027atm
```

```
          CONCENTRATIONS[ppb] AT POSITION =     80.00 cm

e-       =    0.238827D-02 **      OH-       =    0.515177D+02 **
H2       =    0.953679D+02 **      OH        =    0.543075D+00 **
HO2-     =    0.171330D+00 **      H2O2      =    0.247009D+03 **
O2-      =    0.192776D+01 **      O2        =    0.155735D+02 **
H        =    0.274644D-02 **      H+        =    0.309602D+01 **
HO2      =    0.274452D+00 **      O2G       =    0.262448D+03 **
H2G      =    0.416962D+04 **      O         =    0.131689D-06 **

NO. STEPS  =      86          LIQUID VELOCITY =   154.593 cm/s
QUALITY    =   0.02791          VOID FRACTION =   0.29878
PARTIAL PRESSURE OF O2G    =      0.0000atm
PARTIAL PRESSURE OF H2G    =      0.0026atm
```

```
          CONCENTRATIONS[ppb] AT POSITION =     90.00 cm

e-       =    0.227303D-02 **      OH-       =    0.514361D+02 **
H2       =    0.792652D+02 **      OH        =    0.498797D+00 **
HO2-     =    0.176396D+00 **      H2O2      =    0.254723D+03 **
O2-      =    0.223413D+01 **      O2        =    0.221899D+02 **
H        =    0.202501D-02 **      H+        =    0.310094D+01 **
HO2      =    0.318473D+00 **      O2G       =    0.404674D+03 **
H2G      =    0.382508D+04 **      O         =    0.135802D-06 **

NO. STEPS  =     114          LIQUID VELOCITY =   165.115 cm/s
QUALITY    =   0.03584          VOID FRACTION =   0.34883
PARTIAL PRESSURE OF O2G    =      0.0000atm
PARTIAL PRESSURE OF H2G    =      0.0023atm
```

```
          CONCENTRATIONS[ppb] AT POSITION =    100.00 cm
```

e-	=	0.217916D-02 **	OH-	=	0.513722D+02 **
H2	=	0.683523D+02 **	OH	=	0.467939D+00 **
HO2-	=	0.180681D+00 **	H2O2	=	0.261239D+03 **
O2-	=	0.247390D+01 **	O2	=	0.290747D+02 **
H	=	0.158421D-02 **	H+	=	0.310480D+01 **
HO2	=	0.353012D+00 **	O2G	=	0.569781D+03 **
H2G	=	0.348430D+04 **	O	=	0.139276D-06 **

NO. STEPS = 120 LIQUID VELOCITY = 174.780 cm/s
QUALITY = 0.04363 VOID FRACTION = 0.38980
PARTIAL PRESSURE OF O2G = 0.0000atm
PARTIAL PRESSURE OF H2G = 0.0021atm

CONCENTRATIONS[ppb] AT POSITION = 110.00 cm

e-	=	0.210047D-02 **	OH-	=	0.513231D+02 **
H2	=	0.606108D+02 **	OH	=	0.446410D+00 **
HO2-	=	0.184558D+00 **	H2O2	=	0.267105D+03 **
O2-	=	0.265792D+01 **	O2	=	0.358487D+02 **
H	=	0.129989D-02 **	H+	=	0.310777D+01 **
HO2	=	0.379573D+00 **	O2G	=	0.747052D+03 **
H2G	=	0.318632D+04 **	O	=	0.142404D-06 **

NO. STEPS = 124 LIQUID VELOCITY = 183.360 cm/s
QUALITY = 0.05100 VOID FRACTION = 0.42284
PARTIAL PRESSURE OF O2G = 0.0000atm
PARTIAL PRESSURE OF H2G = 0.0020atm

CONCENTRATIONS[ppb] AT POSITION = 120.00 cm

e-	=	0.203337D-02 **	OH-	=	0.512852D+02 **
H2	=	0.548435D+02 **	OH	=	0.431089D+00 **
HO2-	=	0.188138D+00 **	H2O2	=	0.272490D+03 **
O2-	=	0.279942D+01 **	O2	=	0.423424D+02 **
H	=	0.110552D-02 **	H+	=	0.311007D+01 **
HO2	=	0.400032D+00 **	O2G	=	0.928555D+03 **
H2G	=	0.293502D+04 **	O	=	0.145275D-06 **

NO. STEPS = 128 LIQUID VELOCITY = 191.420 cm/s
QUALITY = 0.05836 VOID FRACTION = 0.45143
PARTIAL PRESSURE OF O2G = 0.0000atm
PARTIAL PRESSURE OF H2G = 0.0018atm

CONCENTRATIONS[ppb] AT POSITION = 130.00 cm

e-	=	0.197555D-02 **	OH-	=	0.512557D+02 **
H2	=	0.503679D+02 **	OH	=	0.419955D+00 **
HO2-	=	0.191447D+00 **	H2O2	=	0.277445D+03 **
O2-	=	0.290907D+01 **	O2	=	0.484854D+02 **
H	=	0.965955D-03 **	H+	=	0.311186D+01 **
HO2	=	0.415905D+00 **	O2G	=	0.110912D+04 **
H2G	=	0.272453D+04 **	O	=	0.147917D-06 **

NO. STEPS = 132 LIQUID VELOCITY = 198.990 cm/s

```
QUALITY     =   0.06573          VOID FRACTION =   0.47643
PARTIAL PRESSURE OF O2G     =      0.0000atm
PARTIAL PRESSURE OF H2G     =      0.0017atm
```

```
          CONCENTRATIONS[ppb] AT POSITION =    140.00 cm

e-        =    0.192539D-02 **      OH-       =    0.512326D+02 **
H2        =    0.467851D+02 **      OH        =    0.411723D+00 **
HO2-      =    0.194494D+00 **      H2O2      =    0.281990D+03 **
O2-       =    0.299470D+01 **      O2        =    0.542486D+02 **
H         =    0.861791D-03 **      H+        =    0.311327D+01 **
HO2       =    0.428312D+00 **      O2G       =    0.128550D+04 **
H2G       =    0.254747D+04 **      O         =    0.150340D-06 **

NO. STEPS   =      135          LIQUID VELOCITY =   205.468 cm/s
QUALITY     =   0.07243           VOID FRACTION =   0.49657
PARTIAL PRESSURE OF O2G     =      0.0000atm
PARTIAL PRESSURE OF H2G     =      0.0016atm
```

```
          CONCENTRATIONS[ppb] AT POSITION =    150.00 cm

e-        =    0.188165D-02 **      OH-       =    0.512143D+02 **
H2        =    0.438477D+02 **      OH        =    0.405559D+00 **
HO2-      =    0.197287D+00 **      H2O2      =    0.286143D+03 **
O2-       =    0.306202D+01 **      O2        =    0.596250D+02 **
H         =    0.781634D-03 **      H+        =    0.311438D+01 **
HO2       =    0.438074D+00 **      O2G       =    0.145572D+04 **
H2G       =    0.239730D+04 **      O         =    0.152554D-06 **

NO. STEPS   =      138          LIQUID VELOCITY =   212.619 cm/s
QUALITY     =   0.08031           VOID FRACTION =   0.51763
PARTIAL PRESSURE OF O2G     =      0.0001atm
PARTIAL PRESSURE OF H2G     =      0.0015atm
```

```
          CONCENTRATIONS[ppb] AT POSITION =    160.00 cm

e-        =    0.184335D-02 **      OH-       =    0.511998D+02 **
H2        =    0.413922D+02 **      OH        =    0.400905D+00 **
HO2-      =    0.199836D+00 **      H2O2      =    0.289925D+03 **
O2-       =    0.311521D+01 **      O2        =    0.646214D+02 **
H         =    0.718403D-03 **      H+        =    0.311526D+01 **
HO2       =    0.445792D+00 **      O2G       =    0.161858D+04 **
H2G       =    0.226873D+04 **      O         =    0.154570D-06 **

NO. STEPS   =      141          LIQUID VELOCITY =   218.145 cm/s
QUALITY     =   0.08679           VOID FRACTION =   0.53317
PARTIAL PRESSURE OF O2G     =      0.0001atm
PARTIAL PRESSURE OF H2G     =      0.0014atm
```

```
          CONCENTRATIONS[ppb] AT POSITION =    170.00 cm

e-        =    0.180967D-02 **      OH-       =    0.511882D+02 **
```

H2	= 0.393086D+02 **	OH	=	0.397368D+00 **
HO2-	= 0.202157D+00 **	H2O2	=	0.293359D+03 **
O2-	= 0.315743D+01 **	O2	=	0.692531D+02 **
H	= 0.667475D-03 **	H+	=	0.311597D+01 **
HO2	= 0.451922D+00 **	O2G	=	0.177349D+04 **
H2G	= 0.215765D+04 **	O	=	0.156401D-06 **

NO. STEPS = 149 LIQUID VELOCITY = 224.377 cm/s
QUALITY = 0.09458 VOID FRACTION = 0.55000
PARTIAL PRESSURE OF O2G = 0.0001atm
PARTIAL PRESSURE OF H2G = 0.0013atm

CONCENTRATION[ppb] AT CORE OUTLET (178.25cm)

e-	= 0.178489D-02 **	OH-	=	0.511804D+02 **
H2	= 0.378121D+02 **	OH	=	0.395098D+00 **
HO2-	= 0.203911D+00 **	H2O2	=	0.295951D+03 **
O2-	= 0.318568D+01 **	O2	=	0.728135D+02 **
H	= 0.632502D-03 **	H+	=	0.311644D+01 **
HO2	= 0.456024D+00 **	O2G	=	0.189510D+04 **
H2G	= 0.207690D+04 **	O	=	0.157783D-06 **

NO. STEPS = 152 LIQUID VELOCITY = 228.468 cm/s
QUALITY = 0.10000 VOID FRACTION = 0.56071
PARTIAL PRESSURE OF O2G = 0.0001atm
PARTIAL PRESSURE OF H2G = 0.0013atm

CONCENTRATIONS[ppb] AT POSITION = 190.00 cm

e-	= 0.168774D-03 **	OH-	=	0.515118D+02 **
H2	= 0.342540D+02 **	OH	=	0.594660D-01 **
HO2-	= 0.190765D+00 **	H2O2	=	0.275112D+03 **
O2-	= 0.192929D+01 **	O2	=	0.577244D+02 **
H	= 0.825077D-04 **	H+	=	0.309618D+01 **
HO2	= 0.273970D+00 **	O2G	=	0.205885D+04 **
H2G	= 0.210022D+04 **	O	=	0.146676D-06 **

NO. STEPS = 186 LIQUID VELOCITY = 228.468 cm/s
QUALITY = 0.10000 VOID FRACTION = 0.56071
PARTIAL PRESSURE OF O2G = 0.0001atm
PARTIAL PRESSURE OF H2G = 0.0013atm

CONCENTRATIONS[ppb] AT POSITION = 200.00 cm

e-	= 0.175333D-03 **	OH-	=	0.515259D+02 **
H2	= 0.338560D+02 **	OH	=	0.608341D-01 **
HO2-	= 0.178111D+00 **	H2O2	=	0.256793D+03 **
O2-	= 0.188767D+01 **	O2	=	0.560263D+02 **
H	= 0.850611D-04 **	H+	=	0.309533D+01 **
HO2	= 0.267988D+00 **	O2G	=	0.210008D+04 **
H2G	= 0.209750D+04 **	O	=	0.136909D-06 **

NO. STEPS = 196 LIQUID VELOCITY = 228.468 cm/s
QUALITY = 0.10000 VOID FRACTION = 0.56071
PARTIAL PRESSURE OF O2G = 0.0001atm

PARTIAL PRESSURE OF H2G = 0.0013atm

CONCENTRATION[ppb] AT ZIRC TRANSITION (209.25cm)

e-	=	0.180529D-03 **	OH-	=	0.515322D+02 **
H2	=	0.337420D+02 **	OH	=	0.612190D-01 **
HO2-	=	0.167600D+00 **	H2O2	=	0.241609D+03 **
O2-	=	0.187395D+01 **	O2	=	0.556770D+02 **
H	=	0.859718D-04 **	H+	=	0.309496D+01 **
HO2	=	0.266007D+00 **	O2G	=	0.212150D+04 **
H2G	=	0.209293D+04 **	O	=	0.128814D-06 **

NO. STEPS = 202 LIQUID VELOCITY = 228.468 cm/s
QUALITY = 0.10000 VOID FRACTION = 0.56071
PARTIAL PRESSURE OF O2G = 0.0001atm
PARTIAL PRESSURE OF H2G = 0.0013atm

CONCENTRATIONS[ppb] AT POSITION = 220.00 cm

e-	=	0.193119D-04 **	OH-	=	0.517326D+02 **
H2	=	0.338253D+02 **	OH	=	0.119714D-01 **
HO2-	=	0.166977D+00 **	H2O2	=	0.239780D+03 **
O2-	=	0.111329D+01 **	O2	=	0.549889D+02 **
H	=	0.135259D-04 **	H+	=	0.308295D+01 **
HO2	=	0.157380D+00 **	O2G	=	0.212969D+04 **
H2G	=	0.209072D+04 **	O	=	0.179253D-06 **

NO. STEPS = 160 LIQUID VELOCITY = 449.190 cm/s
QUALITY = 0.10000 VOID FRACTION = 0.56071
PARTIAL PRESSURE OF O2G = 0.0001atm
PARTIAL PRESSURE OF H2G = 0.0013atm

CONCENTRATIONS[ppb] AT POSITION = 230.00 cm

e-	=	0.194203D-04 **	OH-	=	0.517339D+02 **
H2	=	0.338391D+02 **	OH	=	0.119945D-01 **
HO2-	=	0.165599D+00 **	H2O2	=	0.237795D+03 **
O2-	=	0.110979D+01 **	O2	=	0.544386D+02 **
H	=	0.136369D-04 **	H+	=	0.308287D+01 **
HO2	=	0.156881D+00 **	O2G	=	0.213183D+04 **
H2G	=	0.208920D+04 **	O	=	0.177769D-06 **

NO. STEPS = 167 LIQUID VELOCITY = 449.190 cm/s
QUALITY = 0.10000 VOID FRACTION = 0.56071
PARTIAL PRESSURE OF O2G = 0.0001atm
PARTIAL PRESSURE OF H2G = 0.0013atm

CONCENTRATIONS[ppb] AT POSITION = 240.00 cm

e-	=	0.195116D-04 **	OH-	=	0.517349D+02 **
H2	=	0.338325D+02 **	OH	=	0.120000D-01 **
HO2-	=	0.164235D+00 **	H2O2	=	0.235832D+03 **
O2-	=	0.110744D+01 **	O2	=	0.541572D+02 **

```
H       =    0.136889D-04 **      H+      =    0.308281D+01 **
HO2     =    0.156545D+00 **      O2G     =    0.213151D+04 **
H2G     =    0.208787D+04 **      O       =    0.176302D-06 **

NO. STEPS  =     170          LIQUID VELOCITY =   449.190 cm/s
QUALITY    =   0.10000          VOID FRACTION =   0.56071
PARTIAL PRESSURE OF O2G    =      0.0001atm
PARTIAL PRESSURE OF H2G    =      0.0013atm
```

```
          CONCENTRATIONS[ppb] AT POSITION =    250.00 cm

e-      =    0.195948D-04 **      OH-     =    0.517357D+02 **
H2      =    0.338183D+02 **      OH      =    0.119976D-01 **
HO2-    =    0.162890D+00 **      H2O2    =    0.233897D+03 **
O2-     =    0.110562D+01 **      O2      =    0.539935D+02 **
H       =    0.137149D-04 **      H+      =    0.308276D+01 **
HO2     =    0.156286D+00 **      O2G     =    0.213008D+04 **
H2G     =    0.208662D+04 **      O       =    0.174855D-06 **

NO. STEPS  =     173          LIQUID VELOCITY =   449.190 cm/s
QUALITY    =   0.10000          VOID FRACTION =   0.56071
PARTIAL PRESSURE OF O2G    =      0.0001atm
PARTIAL PRESSURE OF H2G    =      0.0013atm
```

```
          CONCENTRATIONS[ppb] AT POSITION =    260.00 cm

e-      =    0.196743D-04 **      OH-     =    0.517364D+02 **
H2      =    0.338013D+02 **      OH      =    0.119917D-01 **
HO2-    =    0.161566D+00 **      H2O2    =    0.231992D+03 **
O2-     =    0.110404D+01 **      O2      =    0.538804D+02 **
H       =    0.137298D-04 **      H+      =    0.308272D+01 **
HO2     =    0.156061D+00 **      O2G     =    0.212811D+04 **
H2G     =    0.208539D+04 **      O       =    0.173431D-06 **

NO. STEPS  =     175          LIQUID VELOCITY =   449.190 cm/s
QUALITY    =   0.10000          VOID FRACTION =   0.56071
PARTIAL PRESSURE OF O2G    =      0.0001atm
PARTIAL PRESSURE OF H2G    =      0.0013atm
```

```
          CONCENTRATION[ppb] AT PLENUM INLET      (    261.35cm)
e-      =    0.196849D-04 **      OH-     =    0.517365D+02 **
H2      =    0.337989D+02 **      OH      =    0.119908D-01 **
HO2-    =    0.161389D+00 **      H2O2    =    0.231737D+03 **
O2-     =    0.110384D+01 **      O2      =    0.538671D+02 **
H       =    0.137314D-04 **      H+      =    0.308271D+01 **
HO2     =    0.156032D+00 **      O2G     =    0.212782D+04 **
H2G     =    0.208523D+04 **      O       =    0.173241D-06 **

NO. STEPS  =     175          LIQUID VELOCITY =   449.190 cm/s
QUALITY    =   0.10000          VOID FRACTION =   0.56071
PARTIAL PRESSURE OF O2G    =      0.0001atm
PARTIAL PRESSURE OF H2G    =      0.0013atm
```

CONCENTRATIONS[ppb] AT POSITION = 270.00 cm

e-	=	0.186836D-05 **	OH-	=	0.518976D+02 **
H2	=	0.328488D+02 **	OH	=	0.176840D-02 **
HO2-	=	0.152498D+00 **	H2O2	=	0.218292D+03 **
O2-	=	0.503085D+00 **	O2	=	0.474821D+02 **
H	=	0.189895D-05 **	H+	=	0.307314D+01 **
HO2	=	0.708874D-01 **	O2G	=	0.187812D+04 **
H2G	=	0.202165D+04 **	O	=	0.223547D-07 **

NO. STEPS = 170 LIQUID VELOCITY = 4.812 cm/s
QUALITY = 0.10000 VOID FRACTION = 0.24675
PARTIAL PRESSURE OF O2G = 0.0001atm
PARTIAL PRESSURE OF H2G = 0.0012atm

CONCENTRATION[ppb] AT PLENUM OUTLET (276.59cm)

e-	=	0.194263D-05 **	OH-	=	0.519027D+02 **
H2	=	0.321354D+02 **	OH	=	0.183879D-02 **
HO2-	=	0.145085D+00 **	H2O2	=	0.207660D+03 **
O2-	=	0.491143D+00 **	O2	=	0.429863D+02 **
H	=	0.203768D-05 **	H+	=	0.307284D+01 **
HO2	=	0.691980D-01 **	O2G	=	0.170035D+04 **
H2G	=	0.197760D+04 **	O	=	0.212660D-07 **

NO. STEPS = 172 LIQUID VELOCITY = 4.812 cm/s
QUALITY = 0.10000 VOID FRACTION = 0.24675
STEAM FLOW RATE = 2.70g/sec
DOWNCOMER FLOW RATE= 24.30 g/sec
PARTIAL PRESSURE OF O2G = 0.0001atm
PARTIAL PRESSURE OF H2G = 0.0012atm

CONCENTRATIONS[ppb] AT POSITION = 290.00 cm

e-	=	0.195167D-04 **	OH-	=	0.517750D+02 **
H2	=	0.316845D+02 **	OH	=	0.127498D-01 **
HO2-	=	0.139765D+00 **	H2O2	=	0.200539D+03 **
O2-	=	0.979227D+00 **	O2	=	0.422861D+02 **
H	=	0.154078D-04 **	H+	=	0.308042D+01 **
HO2	=	0.138315D+00 **	O2G	=	0.000000D+00 **
H2G	=	0.000000D+00 **	O	=	0.149918D-06 **

NO. STEPS = 140 LIQUID VELOCITY = 197.325 cm/s

CONCENTRATIONS[ppb] AT POSITION = 300.00 cm

e-	=	0.197460D-04 **	OH-	=	0.517778D+02 **
H2	=	0.313611D+02 **	OH	=	0.128030D-01 **
HO2-	=	0.136292D+00 **	H2O2	=	0.195546D+03 **
O2-	=	0.971752D+00 **	O2	=	0.420377D+02 **
H	=	0.154152D-04 **	H+	=	0.308025D+01 **
HO2	=	0.137251D+00 **	O2G	=	0.000000D+00 **
H2G	=	0.000000D+00 **	O	=	0.146185D-06 **

NO. STEPS = 145 LIQUID VELOCITY = 197.325 cm/s

CONCENTRATION[ppb] AT PLENUM SAMPLE (306.39cm)

e-	=	0.198926D-04 **	OH-	=	0.517796D+02 **
H2	=	0.311579D+02 **	OH	=	0.128387D-01 **
HO2-	=	0.134127D+00 **	H2O2	=	0.192432D+03 **
O2-	=	0.966975D+00 **	O2	=	0.418703D+02 **
H	=	0.154236D-04 **	H+	=	0.308014D+01 **
HO2	=	0.136572D+00 **	O2G	=	0.000000D+00 **
H2G	=	0.000000D+00 **	O	=	0.143857D-06 **

NO. STEPS = 148 LIQUID VELOCITY = 197.325 cm/s

CONCENTRATION[ppb] AT DOWNCOMER INLET (318.79cm)

e-	=	0.406744D-04 **	OH-	=	0.517394D+02 **
H2	=	0.306819D+02 **	OH	=	0.205783D-01 **
HO2-	=	0.128470D+00 **	H2O2	=	0.184459D+03 **
O2-	=	0.112491D+01 **	O2	=	0.416325D+02 **
H	=	0.264407D-04 **	H+	=	0.308254D+01 **
HO2	=	0.159008D+00 **	O2G	=	0.000000D+00 **
H2G	=	0.000000D+00 **	O	=	0.137897D-06 **

NO. STEPS = 120 LIQUID VELOCITY = 197.325 cm/s

CONCENTRATIONS[ppb] AT POSITION = 330.00 cm

e-	=	0.138016D-03 **	OH-	=	0.517696D+02 **
H2	=	0.248032D+02 **	OH	=	0.528076D-01 **
HO2-	=	0.629834D-01 **	H2O2	=	0.903788D+02 **
O2-	=	0.107384D+01 **	O2	=	0.337469D+02 **
H	=	0.695542D-04 **	H+	=	0.308075D+01 **
HO2	=	0.151721D+00 **	O2G	=	0.000000D+00 **
H2G	=	0.000000D+00 **	O	=	0.983537D-08 **

NO. STEPS = 194 LIQUID VELOCITY = 4.181 cm/s

CONCENTRATION[ppb] AT DOWNCOMER OUTLET (332.79cm)

e-	=	0.139039D-03 **	OH-	=	0.517727D+02 **
H2	=	0.248072D+02 **	OH	=	0.533608D-01 **
HO2-	=	0.618946D-01 **	H2O2	=	0.888112D+02 **
O2-	=	0.106327D+01 **	O2	=	0.332347D+02 **
H	=	0.705862D-04 **	H+	=	0.308056D+01 **
HO2	=	0.150219D+00 **	O2G	=	0.000000D+00 **
H2G	=	0.000000D+00 **	O	=	0.966477D-08 **

NO. STEPS = 197 LIQUID VELOCITY = 4.181 cm/s

CONCENTRATIONS[ppb] AT POSITION = 340.00 cm

e-	=	0.542595D-04 **	OH-	=	0.518179D+02 **

```
H2        =    0.246862D+02 **      OH        =    0.255744D-01 **
HO2-      =    0.610827D-01 **      H2O2      =    0.875703D+02 **
O2-       =    0.893133D+00 **      O2        =    0.329814D+02 **
H         =    0.312324D-04 **      H+        =    0.307787D+01 **
HO2       =    0.126056D+00 **      O2G       =    0.000000D+00 **
H2G       =    0.000000D+00 **      O         =    0.654653D-07 **

NO. STEPS  =     129          LIQUID VELOCITY =   197.325 cm/s
```

```
          CONCENTRATION(ppb) AT DOWNCOMER SAMPLE (    344.89cm)
e-        =    0.544753D-04 **      OH-       =    0.518194D+02 **
H2        =    0.246053D+02 **      OH        =    0.257379D-01 **
HO2-      =    0.604846D-01 **      H2O2      =    0.867104D+02 **
O2-       =    0.887913D+00 **      O2        =    0.327246D+02 **
H         =    0.314297D-04 **      H+        =    0.307778D+01 **
HO2       =    0.125316D+00 **      O2G       =    0.000000D+00 **
H2G       =    0.000000D+00 **      O         =    0.648224D-07 **

NO. STEPS  =     132          LIQUID VELOCITY =   197.325 cm/s
```

RUN STATISTICS

```
REQUIRED RWORK SIZE   =      344
IWORK SIZE            =       34
NUMBER OF STEPS       =     1887
# OF FUNC.- EVALS.    =     2471
# OF JACOB.- EVALS    =      368
TOTAL JOB TIME        =    88.88 seconds

COMPLETED SUCCESSFULLY!
```

D.3 BCCLMIT Sample Input File

```
$FILENAME
OUTFILE  = 'NELGBH.OUT',
PLOTFILE = 'NELGBH.PLOT',
$END

$SIZE
NSPECIES =          14,
NRX      =          46,
$END

$STATE
TINLET   =   546.000000000000     ,
TOUTLET  =   558.0,
TEMREF   =   298.000000000000     ,
GAMMARATE=   1.11E5,
NEUTRATE =   1.11E5,
DENSLIQIN=   0.800,
DENSLIQ  =   0.741,
DENSGAS  =   3.62D-2,
PRESSURE =  68.00,
FLOWRATE =  2.7E1,
QUALEXIT =  0.10E0,
$END

$CONTROL
XSTEP    = 1.0E1,
$END

$FLAGS
CALCSURF = TRUE,
RSOUT    = T,
LINLIN   = T,
BOILFLAG = T,
PPBFLAG  = T,
$END

$LSODEDATA
$END

$NAMES
SPECIES  = 'e- ',          'OH-',        'H2 ',      'OH ', 'HO2-',    'H2O2 ',
       'O2- ', 'O2 ',       'H ',        'H+ ', 'HO2 ',    'O2G',     'H2G',
    'O ',
$END

REACTION NAME, REACTION, RATE CONSTANT AND ACTIVATION ENERGY
W 1      1  0  0  9  2  0  0   0.400000E+02   0.126000E+02
W 2      1 10  0  9  0  0  0   0.600000E+11   0.126000E+02
W 3      1  4  0  2  0  0  0   0.750000E+11   0.126000E+02
W 4      1  6  0  4  2  0  0   0.320000E+11   0.126000E+02
W 5      9  9  0  3  0  0  0   0.250000E+11   0.126000E+02
W 6      1 11  0  5  0  0  0   0.500000E+11   0.126000E+02
W 7      1  8  0  7  0  0  0   0.470000E+11   0.126000E+02
W 8      1  1  0  2  2  3  0   0.120000E+11   0.126000E+02
W 9      4  4  0  6  0  0  0   0.110000E+11   0.126000E+02
W10      2  9  0  1  0  0  0   0.780000E+08   0.188000E+02
W11      1  9  0  3  2  0  0   6.200000E+10   0.126000E+02
W12      1  5  0  4  2  2  0   8.700000E+09   0.126000E+02
W13      9  4  0  0  0  0  0   0.500000E+11   0.126000E+02
W14      4  3  0  9  0  0  0   1.100000E+08   0.126000E+02
```

W15	14	14	0	8	0	0	0	2.200000E+10	0.130000E+02
W16	9	8	0	11	0	0	0	0.470000E+11	0.126000E+02
W17	9	11	0	6	0	0	0	0.500000E+11	0.126000E+02
W18	9	7	0	5	0	0	0	0.500000E+11	0.126000E+02
W19	1	7	0	5	2	0	0	0.510000E+11	0.188000E+02
W20	9	6	0	4	0	0	0	2.400000E+08	0.136000E+02
W21	4	6	0	11	0	0	0	0.410000E+08	1.400000E+01
W22	4	11	0	8	0	0	0	0.300000E+11	0.126000E+02
W23	2	6	0	5	0	0	0	0.700000E+09	0.188000E+02
W24	5	0	0	2	6	0	0	0.220000E+07	0.188000E+02
W25	10	7	0	11	0	0	0	0.120000E+12	0.126000E+02
W26	11	0	0	10	7	0	0	0.200000E+07	0.126000E+02
W27	11	7	0	5	8	0	0	0.580000E+08	0.188000E+02
W28	7	7	0	6	8	2	2	6.600000E+07	0.188000E+02
W29	11	11	0	6	8	0	0	1.100000E+07	0.188000E+02
W30	10	2	0	0	0	0	0	1.500000E+12	0.430000E+00
W31	0	0	0	10	2	0	0	0.140000E-01	0.340000E+02
W32	4	7	0	8	2	0	0	0.300000E+11	0.126000E+02
W33	9	0	0	3	4	0	0	4.900000E-02	0.850000E+02
W34	11	14	0	8	4	0	0	2.000000E+10	0.130000E+02
W35	4	14	0	9	8	0	0	1.000000E-01	0.700000E+02
W36	14	0	0	4	4	0	0	9.500000E+04	0.410000E+02
W37	4	14	0	11	0	0	0	2.000000E+10	0.13000E+02
W38	3	14	0	9	4	0	0	4.800000E+03	0.350000E+02
W39	6	14	0	11	4	0	0	1.300000E+06	0.180000E+02
W40	9	14	0	4	0	0	0	2.000000E+10	0.130000E+02
AE1	3	0	0	13	0	0	0	30.D0	-1.D0
AE1	13	0	0	3	0	0	0	10.D0	-1.D0
AE2	8	0	0	12	0	0	0	23.D0	-1.D0
AE2	12	0	0	8	0	0	0	12.D0	-1.D0
COR	6	0	0	14	0	0	0	5.322000E-07	66.90E0
CCL	6	0	0	14	0	0	0	5.322000E-07	66.90E0

GAMMA AND NEUTRON G-VALUES AND INITIAL CONCENTRATIONS

e-	3.2000
	0.800D+00
	0.000D+00
	0.180D+02
OH-	0.0000
	0.000D+00
	2.500D-06
	0.170D+02
H2	0.4400
	0.990D+00
	0.100D-03
	0.200D+01
OH	5.3000
	0.680D+00
	0.000D+00
	0.170D+02
HO2-	0.0000
	0.000D+00
	0.000D+00
	0.330D+02
H2O2	0.5700
	1.270D+00
	0.000D-00
	0.340D+02
O2-	0.0000
	0.000D+00

```
          0.000D+00
          0.320D+02
O2           0.0000
          0.000D+00
          6.250D-06
          0.320D+02
H            2.4000
          0.450D+00
          0.000D+00
          0.100D+01
H+           3.2000
          0.800D+00
          2.500D-06
          0.100D+01
HO2          0.0000
          0.000D-00
          0.000D+00
          0.330D+02
O2G          0.0000
          0.000D+00
          0.000D+00
          0.320D+02
H2G          0.0000
          0.000D+00
          0.000D+00
          0.200D+01
O            0.0000
          0.000D+00
          0.000D+00
          0.160D+02

    SECTION PARAMETERS:

SECTION #1
LENGTH     0.000D+00
DIAMETER   0.460D+0
GAMMAMULT  0.000D0
NEUTMULT   0.000D0
NAME       CHEM INJECTION

SECTION #2
LENGTH     5.000D0
DIAMETER   0.460D0
GAMMAMULT  1.000D-2
NEUTMULT   1.000D-3
NAME       ZIRC TRANSITION

SECTION #3
LENGTH     3.100D+01
DIAMETER   0.645D0
GAMMAMULT  1.000D-1
NEUTMULT   3.000D-2
NAME       CORE INLET

SECTION #4
LENGTH     6.350D+0
DIAMETER   0.645D+0
GAMMAMULT  1.000D0
NEUTMULT   1.000D0
NAME       START OF BOILING
```

```
SECTION #5
LENGTH     1.359D+02
DIAMETER   0.645D+00
GAMMAMULT  1.000D+00
NEUTMULT   1.000D-00
NAME       CORE OUTLET

SECTION #6
LENGTH     3.100D+01
DIAMETER   0.645D+00
GAMMAMULT  1.000D-1
NEUTMULT   3.000D-2
NAME       ZIRC TRANSITION

SECTION #7
LENGTH     5.210D1
DIAMETER   0.460D0
GAMMAMULT  1.000D-2
NEUTMULT   5.000D-3
NAME       PLENUM INLET

SECTION #8
LENGTH     1.524D+01
DIAMETER   3.358D0
GAMMAMULT  1.000D-3
NEUTMULT   0.100D-5
NAME       PLENUM OUTLET

SECTION #9
LENGTH     2.980D+01
DIAMETER   0.460D0
GAMMAMULT  1.000D-2
NEUTMULT   1.000D-4
NAME       PLENUM SAMPLE

SECTION #10
LENGTH     1.240D+1
DIAMETER   0.460D0
GAMMAMULT  2.00D-2
NEUTMULT   1.00D-3
NAME       DOWNCOMER INLET

SECTION #11
LENGTH     1.400D+1
DIAMETER   3.160D0
GAMMAMULT  5.000D-2
NEUTMULT   1.000D-2
NAME       DOWNCOMER OUTLET

SECTION #12
LENGTH     1.210D+1
DIAMETER   0.460D0
GAMMAMULT  2.000D-2
NEUTMULT   1.000D-3
NAME       DOWNCOMER SAMPLE
```

D.4 Modified Notre Dame Reaction Equation Set

CHEMICAL REACTIONS, RATE CONSTANTS, AND ACTIVATION ENERGIES

	REACTIONS					RATE CONSTANT	ACTIVATION ENERGIES (KJ/MOL-K)
W 1	e-		>H	OH-		0.40D+02	0.13D+02
W 2	e-	H+	>H			0.60D+11	0.13D+02
W 3	e-	OH	>OH-			0.75D+11	0.13D+02
W 4	e-	H2O2	>OH	OH-		0.32D+11	0.13D+02
W 5	H	H	>H2			0.25D+11	0.13D+02
W 6	e-	HO2	>HO2-			0.50D+11	0.13D+02
W 7	e-	O2	>O2-			0.47D+11	0.13D+02
W 8	e-	e-	>OH-	OH-	H2	0.12D+11	0.13D+02
W 9	OH	OH	>H2O2			0.11D+11	0.13D+02
W10	OH-	H	>e-			0.78D+08	0.19D+02
W11	e-	H	>H2	OH-		0.62D+11	0.13D+02
W12	e-	HO2-	>OH	OH-	OH-	0.87D+10	0.13D+02
W13	H	OH	>			0.50D+11	0.13D+02
W14	OH	H2	>H			0.11D+09	0.13D+02
W15	O	O	>O2			0.22D+11	0.13D+02
W16	H	O2	>HO2			0.47D+11	0.13D+02
W17	H	HO2	>H2O2			0.50D+11	0.13D+02
W18	H	O2-	>HO2-			0.50D+11	0.13D+02
W19	e-	O2-	>HO2-	OH-		0.51D+11	0.19D+02
W20	H	H2O2	>OH			0.24D+09	0.14D+02
W21	OH	H2O2	>HO2			0.41D+08	0.14D+02
W22	OH	HO2	>O2			0.30D+11	0.13D+02
W23	OH-	H2O2	>HO2-			0.70D+09	0.19D+02
W24	HO2-		>OH-	H2O2		0.22D+07	0.19D+02
W25	H+	O2-	>HO2			0.12D+12	0.13D+02
W26	HO2		>H+	O2-		0.20D+07	0.13D+02
W27	HO2	O2-	>HO2-	O2		0.58D+08	0.19D+02
W28	O2-	O2-	>H2O2	O2	OH- OH-	0.66D+08	0.19D+02
W29	HO2	HO2	>H2O2	O2		0.11D+08	0.19D+02
W30	H+	OH-	>			0.15D+13	0.43D+00
W31			>H+	OH-		0.14D-01	0.34D+02
W32	OH	O2-	>O2	OH-		0.30D+11	0.13D+02
W33	H		>H2	OH		0.49D-01	0.85D+02
W34	HO2	O	>O2	OH		0.20D+11	0.13D+02
W35	OH	O	>H	O2		0.10D+00	0.70D+02
W36	O		>OH	OH		0.95D+05	0.41D+02
W37	OH	O	>HO2			0.20D+11	0.13D+02
W38	H2	O	>H	OH		0.48D+04	0.35D+02
W39	H2O2	O	>HO2	OH		0.13D+07	0.18D+02
W40	H	Q	>OH			0.20D+11	0.13D+02
AE1	H2		>H2G			0.30D+02	-0.10D+01
AE1	H2G		>H2			0.10D+02	-0.10D+01
AE2	O2		>O2G			0.23D+02	-0.10D+01
AE2	O2G		>O2			0.12D+02	-0.10D+01
COR	H2O2		>O			0.53D-06	0.67D+02
CCL	H2O2		>O			0.53D-06	0.67D+02

D.5 Modified Burns and Marsh Reaction Equation Set

CHEMICAL REACTIONS, RATE CONSTANTS, AND ACTIVATION ENERGIES

	REACTIONS					RATE CONSTANT	ACTIVATION ENERGIES (KJ/MOL-K)
W 1	e-		>H	OH-		0.66D+03	0.13D+02
W 2	e-	H+	>H			0.24D+11	0.13D+02
W 3	e-	OH	>OH-			0.24D+11	0.13D+02
W 4	e-	H2O2	>OH	OH-		0.13D+11	0.13D+02
W 5	H	H	>H2			0.10D+11	0.13D+02
W 6	e-	HO2	>HO2-			0.20D+11	0.13D+02
W 7	e-	O2	>O2-			0.19D+11	0.13D+02
W 8	e-	e-	>OH-	OH-	H2	0.28D+10	0.13D+02
W 9	OH	OH	>H2O2			0.45D+10	0.13D+02
W10	OH-	H	>e-			0.20D+08	0.19D+02
W11	e-	H	>H2	OH-		0.10D+13	0.13D+02
W12	e-	HO2-	>OH	OH-	OH-	0.14D+12	0.13D+02
W13	H	OH	>			0.20D+11	0.13D+02
W14	OH	H2	>H			0.34D+08	0.19D+02
W15	O	O	>O2			0.22D+11	0.13D+02
W16	H	O2	>HO2			0.19D+11	0.13D+02
W17	H	HO2	>H2O2			0.20D+11	0.13D+02
W18	H	O2-	>HO2-			0.20D+11	0.13D+02
W19	e-	O2-	>HO2-	OH-		0.53D+12	0.19D+02
W20	H	H2O2	>OH			0.90D+08	0.14D+02
W21	OH	H2O2	>HO2			0.27D+08	0.14D+02
W22	OH	HO2	>O2			0.12D+11	0.13D+02
W23	OH-	H2O2	>HO2-			0.50D+09	0.19D+02
W24	HO2-		>OH-	H2O2		0.23D+08	0.19D+02
W25	H+	O2-	>HO2			0.50D+11	0.13D+02
W26	HO2		>H+	O2-		0.80D+06	0.13D+02
W27	HO2	O2-	>HO2-	O2		0.15D+08	0.19D+02
W28	O2-	O2-	>H2O2	O2	OH- OH-	0.29D+11	0.19D+02
W29	HO2	HO2	>H2O2	O2		0.27D+07	0.19D+02
W30	H+	OH-	>			0.15D+13	0.43D+00
W31			>H+	OH-		0.12D-01	0.34D+02
W32	OH	O2-	>O2	OH-		0.12D+11	0.13D+02
W33	H		>H2	OH		0.33D+05	0.85D+02
W34	HO2	O	>O2	OH		0.20D+11	0.13D+02
W35	OH	O	>H	O2		0.10D+00	0.70D+02
W36	O		>OH	OH		0.78D+05	0.41D+02
W37	OH	O	>HO2			0.20D+11	0.13D+02
W38	H2	O	>H	OH		0.48D+04	0.35D+02
W39	H2O2	O	>HO2	OH		0.13D+07	0.18D+02
W40	H	O	>OH			0.20D+11	0.13D+02
AE1	H2		>H2G			0.30D+02	-0.10D+01
AE1	H2G		>H2			0.10D+02	-0.10D+01
AE2	O2		>O2G			0.23D+02	-0.10D+01
AE2	O2G		>O2			0.12D+02	-0.10D+01
COR	H2O2		>O			0.53D-06	0.67D+02
CCL	H2O2		>O			0.53D-06	0.67D+02

Appendix E. References

1. M. Ullberg, T. Rooth and B. Persson, "Hydrogen Peroxide in BWRs", in Water Chemistry of Nuclear Reactor Systems 4 (Proc. 4th Int. Conf. London, 1986) Vol. 2, BNES, London, (1986) 67.

2. R. L. Cowan et al., "Experience with Hydrogen Water Chemistry in Boiling Water Reactors" in Water Chemistry of Nuclear Reactor Systems 4 (Proc. 4th Int. Conf. London, 1986) Vol. 1, BNES, London, (1986) 26.

3. EPRI Report NP-5800M, "Hydrogen Water Chemistry to Mitigate Intergranular Stress Corrosion Cracking: In-Reactor Tests", (1988).

4. D. R. McCracken, J. B. Rasewych, and W. R. Shorter, "Coolant Radiolysis & Boiling in Water-Cooled Reactors", in Water Chemistry in Nuclear Power Plants 5 (Proc. 5th Int. Conf. Tokyo, 1989) Vol. 1, JAIF, Tokyo (1989) 36.

5. EPRI Report NP-3779, "Automated Nuclear Power Plant Maintenance", (1983).

6. M. J. Driscoll, O. K. Harling, G. E. Kohse, and R. G. Ballinger, "The MIT In-Pile Loops for Coolant Chemistry and Corrosion Studies", in Water Chemistry in Nuclear Power Plants (Proc. 5th Int. Conf. Tokyo, 1989) Vol. 1, JAIF, Tokyo (1989).

7. M. J. Driscoll and C. R. L. Oliveira, "Prospectus for BWR Coolant Chemistry Experiments to be Carried Out Using the BWR In-Pile Loop Facility at the MIT Research Reactor," MITNRL-023, August 1987

8. M. J. Driscoll and G. E. Kohse, "Revised Prospectus for BWR Loop Radiolysis Chemistry Studies", (As of 15 December 1989), MIT Nuclear Reactor Laboratory

9. M. J. Driscoll and G. E. Kohse, "Revised Prospectus for N^{16} Scoping Studies", (As of 1 December 1989), MIT Nuclear Reactor Laboratory

10. C. Oliveira, "Design and Proof-of-Principle Testing of an In-Pile Loop to Simulate BWR Coolant Chemistry", Nuclear Engineer and SM Thesis, Department of Nuclear Engineering, MIT, (December 1987)

11. J. L. Baeza, "Refinement of an In-Pile Loop Design for BWR Chemistry Studies", SM Thesis, Department of Nuclear Engineering, MIT, (January 1989).

12. J. Outwater III, "Design, Construction and Operation of an In-Pile Loop for BWR Chemistry Studies", Prospectus for ScD Thesis, Department of Nuclear Engineering, MIT, (March 1988).

13. J. Outwater, MIT Doctoral Seminar Presentation, Dept. of Nuclear Engineering, MIT, 7 March 1990.

14. S. Simonson, "Modeling of Radiation Effects on Nuclear Waste Package Materials", PhD Thesis, Department of Nuclear Engineering, MIT, (September 1988).

15. J. H. Chun, "Modeling of BWR Water Chemistry", SM Thesis, Dept. of Nucl. Eng., MIT, (expected 1990).

16. C. C. Lin et al., "Decomposition of Hydrogen Peroxide in Aqueous Solutions at Elevated Temperatures", in Water Chemistry in Nuclear Power Plants 5 (Proc. 5th Int. Conf. Tokyo, 1989) Vol. 1, JAIF, Tokyo (1989) 145.

17. J. Takagi, N. Ichikawa, Y. Hemmi, and H. Nagao, "Study on Radiolysis Behavior and ECP Measurement under BWR Primary Loop Condition", in Water Chemistry in Nuclear Power Plants 5 (Proc. 5th Int. Conf. Tokyo, 1989) Vol. 1, JAIF, Tokyo (1989) 35.

18. CHEMetrics, Inc. product information supplied with the K-5503 H_2O_2 Vacu-vials.

19. EPRI Report NP-2806, "Monitoring Techniques for pH, Hydrogen and Redox Potential in Nuclear Reactor Circuits", (January 1983).

20. M. J. Driscoll, "Reference Electrodes for the MIT BWR Loop", MIT Nuclear Reactor Laboratory Technical Note, 15 January 1990.

21. J. V. Dobson, "Potentials of the Palladium Hydride Reference Electrode Between 25°C and 195°C", J. Electroanal. Chem., Vol. 35, (1972) 129.

22. J. V. Dobson, M. N. Dagless and H. R. Thirsk, "Some Experimental Factors which Govern the Potential of the Palladium Hydride Electrode at 25°C and 195°C", J. Chem. Soc. Faraday Trans., 1, Vol. 68, (1972) 749.

23. M. Fleischmann and J. N. Hiddleston, "A Palladium-Hydrogen Probe Electrode for Use as a Microreference Electrode", J. Scien. Instr. (J. Physics E), Series 2, Vol. 1 (1968) 667.

24. M. J. Driscoll, "Some Conceptual Designs for ECP Electrode Configurations", MIT Nuclear Reactor Laboratory Technical Note, 24 December 1989.

25. M. J. Driscoll, "An Alternative Reference Electrode", MIT Nuclear Reactor Laboratory Technical Note, 8 September 1989.

26. J. Takagi, N. Ichikawa and Y. Hemmi, "Evaluation of Corrosion Environment in BWR Primary Circuit by Water Radiolysis Model", in Water Chemistry in Nuclear Power Plants 5 (Proc. 5th Int. Conf. Tokyo, 1989) Vol. 1, JAIF, Tokyo (1989).

27. M. Ashraf-Knorassami and R. D. Braun, "A Tungsten Reference Electrode for Use in Corrosive Media - A Comparative Study with Other Reference Electrodes", Corrosion, Vol. 43, No. 1, 32, (January 1987).

28. E. Ibe and S. Uchida, "A Water Radiolysis Model in a Circulating Flow System with a Boiling Region and Its Application to Hydrogen Alternate Water Chemistry of Boiling Water Reactors", Nuclear Science and Engineering, 90, 140-157, (January 1985).

29. E. Ibe, M. Sakagami and S. Uchida, "Theoretical Model Analyses for Effects of Hydrogen Injection on Radiolysis of Coolant Water in BWR", Journal of Nuclear Science and Technology, Vol. 23, 11-28, (January 1986).

30. S. R. Lukac, "Modelling of Coolant Radiolysis in the Primary Heat Transport System of CANDU Reactors - Effect of Coolant Boiling", Nuclear Materials, 158, 240-252, (January 1988).

31. A. C. Hindmarsh, "ODEPACK, A Systematized Collection of ODE Solvers," Scientific Computing, North-Holland Publishing Co, (1983).

32. H. Bateman, in Proc. Cambridge Phil. Soc., 78:211 (1910).

33. D. Edelson, "The New Look in Chemical Kinetics", J. Chem. Ed., Vol. 52, 642-644, (1975).

34. S. Gordon, K. H. Schmidt and J. R. Honekamp, "An Analysis of the Hydrogen Bubble Concerns in the Three-Mile Island Unit-2 Reactor Vessel", Radiat. Phys. Chem., Vol. 21(3), 247-258, (1983).

35. A. K. Pikeav, S. A. Kabakchi and G. F. Egorov, "Some Radiation Chemical Aspects of Nuclear Engineering", Radiat. Phys. Chem., Vol. 31(4-6), 789-803, (1988).

36. S. G. Bankoff, Trans. ASME, Ser. E265 (1960) 82.

37. A. J. Elliot, D. R. McCracken, G. V. Buxton and N. D. Wood, "Estimation of Rate Constants for Near Diffusion-Controlled Reactions in Water at High Temperatures", To be published in J. Faraday Soc., (1989).

38. N. E. Todreas and M. S. Kazimi, Nuclear Systems I: Thermal-Hydraulic Fundamentals, Hemisphere Publishing Corp., New York, 1990.

39. "RELAP-5 MOD1 Code Manual", EGG-270, (Discussed in Todreas and Kazimi, Ref. 38), (1980).

40. G. F. Hewitt and D. N. Roberts, "Studies of Two-Phase Flow Patterns by Simultaneous X-Ray and Flash Photography", AERE-M2159, (1969).

41. W. G. Burns and W. R. Marsh, "Radiation Chemistry of High-Temperature Water", J. Chem. Soc., Faraday Trans. 1, Vol. 77, 197-215, (1981).

42. A. J. Elliot et al., "The G-Values of the Primary Species in 0.4 mol dm^{-3} H_2SO_4 Irradiated at 300°C", Radiat. Phys. Chem., Vol. 34, No. 5, 747-751, (1989).

43. A. J. Elliot, M. P. Chenier and Denis C. Ouellette, "G-Values for Gamma-Irradiated Water as a Function of Temperature", to be published, (1990).

44. EPRI Report NP-6386, "Modeling Hydrogen Water Chemistry for BWR Applications", June 1989.

45. Y. Katsumura et al., "Water Radiolysis at High Temperatures", Radiat. Phys. Chem., Vol. 33, 299, (1989).

46. A. Appleby and H. A. Schwarz, "Radical and Molecular Yields in Water Irradiated by Gamma Rays and Heavy Ions", J. Phys. Chem., Vol. 75(6), 1937, (1969).

47. Radiation Chemistry Data Center, Radiation Laboratory, University of Notre Dame, Notre Dame, IN 46556.

48. EPRI Report NP-2400, "High Temperature Thermodynamic Data for Species in Aqueous Solution", June 1989.

49. H. Christensen, K. Sehested and H. Corfitzen, "Reactions of Hydroxyl Radicals with Hydrogen Peroxide at Ambient and Elevated Temperatures", J. Phys. Chem., Vol. 86, 1588-1590, (1982).

50. G. Wikmark, "Problems in Monitoring Oxidizing Conditions", paper presented at EPRI workshop: LWR Radiation Water Chemistry and Its Influence on In-Core Structural Materials Behavior, Palo Alto, CA, 14-15 November 1989.

51. F. P. Ford and P. L. Andresen, "Prediction of Stress Corrosion Cracking of 304 Stainless Steel under Irradiation Conditions", reported in EPRI workshop: LWR Radiation Water Chemistry and Its Influence on In-Core Structural Materials, Palo Alto, Ca, 14-15 November 1989.

52. J. J. Carberry, Chemical and Catalytic Reaction Engineering, McGraw-Hill, New York, 1976.

53. I. S. Hwang, personal communication, MIT Department of Materials Science and Engineering and Nuclear Engineering Department, (April 1990).

54. E. Ibe et al., "Chemistry of Radioactive Nitrogen in BWR Primary System", Journal of Nuclear Science and Technology, Vol. 26, No. 8, (August 1989).

55. E. Ibe et al., "Behavior of Nitrogen-Compounds in Radiation-Field and Nuclear-Reactor System", Journal of Nuclear Science and Technology, Vol. 26, No. 9, (September 1989).

DUDLEY KNOX LIBRARY
NAVAL POSTGRADUATE SCHOOL
MONTEREY, CALIFORNIA 93943-5002

Thesis
M36285 Mason
c.1 Chemical characterization of simulated boiling water reactor coolant.

Thesis
M36285 Mason
c.1 Chemical characterization of simulated boiling water reactor coolant.

AMERICAN BINDERY
TOPEKA KANSAS

thesM36285
Chemical characterization of simulated b
3 2768 000 89276 4
DUDLEY KNOX LIBRARY